SISSA
SCUOLA INTERNAZIONALE SUPERIORE DI STUDI AVANZATI
PHD COURSE IN STATISTICAL PHYSICS
ELEVENTH CYCLE

DOCTORAL THESIS

SCALING PROPERTIES AND FLOQUET ENGINEERING FOR LOW DIMENSIONAL BOSE GASES

AUTHOR
ANDREA COLCELLI

SUPERVISORS
PROF. ANDREA TROMBETTONI
AND
PROF. GIUSEPPE MUSSARDO

ACADEMIC YEAR 2019/2020

A Diletta,
che ha rimescolato le carte del mio destino.

DECLARATION

I, *Andrea Colcelli*, confirm that the research included within this Thesis is my own work or that where it has been carried out in collaboration with, or supported by others, that this is duly acknowledged below and my contribution indicated.
I confirm that this Thesis has not been previously submitted for the award of a degree by this or any other university.

DETAILS OF PUBLICATIONS

[1] A. Colcelli, G. Mussardo, and A. Trombettoni, *Deviations from off-diagonal long-range order in one-dimensional quantum systems*, Europhys. Lett. **122**, 50006 (2018).

Abstract: A quantum system exhibits off-diagonal long-range order (ODLRO) when the largest eigenvalue λ_0 of the one-body-density matrix scales as $\lambda_0 \sim N$, where N is the total number of particles. Putting $\lambda_0 \sim N^{\mathcal{C}}$ to define the scaling exponent $\mathcal{C}$, then $\mathcal{C} = 1$ corresponds to ODLRO and $\mathcal{C} = 0$ to the single-particle occupation of the density matrix orbitals. When $0 < \mathcal{C} < 1$, $\mathcal{C}$ can be used to quantify deviations from ODLRO. In this paper we study the exponent $\mathcal{C}$ in a variety of one-dimensional bosonic and anyonic quantum systems at $T = 0$. For the $1D$ Lieb-Liniger Bose gas we find that for small interactions $\mathcal{C}$ is close to 1, implying a mesoscopic condensation, *i.e.* a value of the zero temperature "condensate" fraction λ_0/N appreciable at finite values of N (as the ones in experiments with $1D$ ultracold atoms). $1D$ anyons provide the possibility to fully interpolate between $\mathcal{C} = 1$ and 0. The behaviour of $\mathcal{C}$ for these systems is found to be non-monotonic both with respect to the coupling constant and the statistical parameter.

[2] A. Colcelli, J. Viti, G. Mussardo, and A. Trombettoni, *Universal off-diagonal long-range-order behavior for a trapped Tonks-Girardeau gas*, Phys. Rev. A **98**, 063633 (2018).

Abstract: The scaling of the largest eigenvalue λ_0 of the one–body density matrix of a system with respect to its particle number N defines an exponent $\mathcal{C}$ and a coefficient $\mathcal{B}$ via the asymptotic relation $\lambda_0 \sim \mathcal{B}\, N^{\mathcal{C}}$. The case $\mathcal{C} = 1$ corresponds to off–diagonal long–range order. For a one–dimensional homogeneous Tonks–Girardeau gas, a well known result also confirmed by bosonization gives instead $\mathcal{C} = 1/2$. Here we investigate the inhomogeneous case, initially addressing the behaviour of $\mathcal{C}$ in presence of a general external trapping potential V. We argue that the value $\mathcal{C} = 1/2$ characterises the hard–core system independently of the nature of the potential V. We then define the exponents γ and β which describe the scaling with N of the peak of the momentum distribution and the natural orbital corresponding to λ_0 respectively, and we derive the scaling relation $\gamma + 2\beta = \mathcal{C}$. Taking as a specific case the power–law potential $V(x) \propto x^{2n}$, we give analytical formulas for γ and β as functions of n. Analytical predictions for the coefficient $\mathcal{B}$ are also obtained.

These formulas are derived exploiting a recent field theoretical formulation and checked against numerical results. The agreement is excellent.

[3] A. Colcelli, G. Mussardo, G. Sierra, and A. Trombettoni, *Integrable Floquet Hamiltonian for a Periodically Tilted 1D Gas*, Phys. Rev. Lett. **123**, 130401 (2019).

Abstract: An integrable model subjected to a periodic driving gives rise generally to a non-integrable Floquet Hamiltonian. Here we show that the Floquet Hamiltonian of the integrable Lieb–Liniger model in presence of a linear potential with a periodic time–dependent strength is instead integrable and its quasi-energies can be determined using the Bethe ansatz approach. We discuss various aspects of the dynamics of the system at stroboscopic times and we also propose a possible experimental realization of the periodically driven tilting in terms of a shaken rotated ring potential.

[4] A. Colcelli, G. Mussardo, G. Sierra, and A. Trombettoni, *Dynamics of one-dimensional quantum many-body systems in time-periodic linear potentials*, Phys. Rev. A **102**, 033310 (2020).

Abstract: We study a system of one–dimensional interacting quantum particles subjected to a time–periodic potential linear in space. After discussing the cases of driven one- and two-particles systems, we derive the analogous results for the many-particles case in presence of a general interaction two-body potential and the corresponding Floquet Hamiltonian. When the undriven model is integrable, the Floquet Hamiltonian is shown to be integrable too. We determine the micro-motion operator and the expression for a generic time evolved state of the system. We discuss various aspects of the dynamics of the system both at stroboscopic and intermediate times, in particular the motion of the center of mass of a generic wavepacket and its spreading over time. We also discuss the case of accelerated motion of the center of mass, obtained when the integral of the coefficient strength of the linear potential on a time period is non-vanishing, and we show that the Floquet Hamiltonian gets in this case an additional static linear potential. We also discuss the application of the obtained results to the Lieb–Liniger model.

[5] A. Colcelli, N. Defenu, G. Mussardo, and A. Trombettoni, *Finite temperature off-diagonal long-range order for interacting bosons*, `arXiv:2007.01403`, accepted for publication in Phys. Rev. B.

Abstract: Characterizing the scaling with the total particle number (N) of the largest eigenvalue of the one–body density matrix (λ_0), provides informations on the occurrence of the off-diagonal long-range order (ODLRO) according to the Penrose-Onsager criterion. Setting $\lambda_0 \sim N^{\mathcal{C}_0}$, then $\mathcal{C}_0 = 1$ corresponds to ODLRO. The intermediate case, $0 < \mathcal{C}_0 < 1$, corresponds for translational invariant systems to the power-law decaying of (non-connected) correlation functions and it can be seen as identifying quasi-long-range order. The goal of the present paper is to characterize the ODLRO properties encoded in $\mathcal{C}_0$ [and in the corresponding quantities $\mathcal{C}_{k\neq 0}$ for excited natural orbitals] exhibited by homogeneous interacting bosonic systems at finite temperature for different dimensions. We show that $\mathcal{C}_{k\neq 0} = 0$ in the thermodynamic limit. In $1D$ it is $\mathcal{C}_0 = 0$ for non-vanishing temperature, while in $3D$ $\mathcal{C}_0 = 1$ ($\mathcal{C}_0 = 0$) for temperatures smaller (larger) than the Bose-Einstein critical temperature. We then focus our attention to $D = 2$, studying the XY and the Villain models, and the weakly interacting Bose gas. The universal value of

$\mathcal{C}_0$ near the Berezinskii–Kosterlitz–Thouless temperature T_{BKT} is $7/8$. The dependence of $\mathcal{C}_0$ on temperatures between $T = 0$ (at which $\mathcal{C}_0 = 1$) and T_{BKT} is studied in the different models. An estimate for the (non-perturbative) parameter ξ entering the equation of state of the $2D$ Bose gases, is obtained using low temperature expansions and compared with the Monte Carlo result. We finally discuss a double jump behaviour for $\mathcal{C}_0$, and correspondingly of the anomalous dimension η, right below T_{BKT} in the limit of vanishing interactions.

[6] A. Colcelli, G. Mussardo, G. Sierra, and A. Trombettoni, *Free Fall of a Quantum Many-Body System*, `arXiv:2009.03744`, submitted to Am. J. Phys.

Abstract: The quantum version of the free fall problem is a topic usually skipped in undergraduate Quantum Mechanics courses because its discussion would require to deal with wavepackets built on the Airy functions – a notoriously difficult computation. Here, on the contrary, we show that the problem can be nicely simplified both for a single particle and for general many–body systems making use of a gauge transformation of the wavefunction corresponding to a change of the reference frame, from the laboratory frame of reference to the one comoving with the falling system. Within this approach, the quantum mechanics problem of a particle in an external gravitational potential – counterpart of the free fall of a particle in Classical Mechanics each student is used to see from high-school – reduces to a much simpler one where there is no longer gravitational potential in the Schrödinger equation. It is instructive to see that the same procedure applies also to many–body systems subjected to a two–body interparticle potential, function of the relative distances between the particles. This topic provides then a handful and pedagogical example of a quantum many–body system whose dynamics can be analytically described in simple terms.

CONTENTS

INTRODUCTION

Out of all the interesting properties that a physical system exhibits on the quantum world level, certainly the ordering properties of the particles constituting the apparatus is one of the most fascinating. From the study of the ordering properties, one can really appreciate the fermionic or bosonic quantum natures of the systems, which nowadays can be observed in realistic experiments. Playing with the dimensionality of the underlying space where the system lives, also the possibility to analyse "intermediate" statistics (anyonic statistics), between the Bose–Einstein and Fermi–Dirac ones, triggers our minds.

Off-diagonal long-range order in the one–body density matrix of Bose particles signals the appearance of Bose-Einstein condensation (BEC) in quantum systems. This relation is established by the Penrose-Onsager criterion [7] which applies in all dimensions D and at any temperature T, irrespectively of the presence of confining potentials. For its versatility, it constitutes a simple way to determine whether a quantum Bose gas exhibits condensation and coherence effects [8–10]. A major example of detection of ODLRO is provided by the measurement of the momentum distribution $n(k)$ in ultracold atom experiments, with a clear peak around zero momentum forming at the BEC critical temperature [11].

For $D \leq 2$ the Mermin-Wagner theorem [12, 13] ensures that, for translational invariant systems with continuous symmetry such as interacting bosons or $O(N)$ spin models with $N \geq 2$, no long-range order can be found at finite temperature. Indeed, the theorem forbids the occurrence of spontaneous symmetry breaking for $T > 0$ in low dimensional systems, where the symmetry of the Hamiltonian is always restored by the proliferation of long–wavelength fluctuations, often called Goldstone modes. For a Bose gas the Goldstone modes are represented by the phonons, which in $D = 2$ destroy long-range order, leaving low temperature superfluidity intact. In such a case, due to the persistence of $U(1)$ symmetry, the equilibrium finite-temperature average of the bosonic field operator $\hat{\Psi}$ vanishes, due to the lack of phase coherence [9]. It is worth noting that a similar effect occurs in a wide range of systems, even if the Mermin-Wagner theorem does not strictly apply, when the scaling dimension of the bosonic order parameter $\hat{\Psi}$ becomes zero [14–16]. A position space version of the Mermin-Wagner theorem, where a relation between the size of a condensate and the coherence properties of the gas is established, is discussed in [17].

A compact way to define off-diagonal long-range order (ODLRO) is to introduce the one–body density matrix (1BDM) [18]

$$\rho(\mathbf{x}, \mathbf{y}) \, = \, \left\langle \hat{\Psi}^{\dagger}(\mathbf{x}) \hat{\Psi}(\mathbf{y}) \right\rangle \, ,$$

where the field operator $\hat{\Psi}(\mathbf{x})$ destroys a particle at the point identified by the D–dimensional vector $\mathbf{x}$. The 1BDM, as an Hermitian matrix, satisfies the eigenvalue equation:

$$\int \rho(\mathbf{x}, \mathbf{y}) \, \phi_i(\mathbf{y}) \, d\mathbf{y} \, = \, \lambda_i \, \phi_i(\mathbf{x}) \, ,$$

with the eigenvalues λ_i being real. They denote the occupation number of the i-th natural orbital eigenfunction ϕ_i, with $\sum_i \lambda_i = N$, where N is the total number of particles. The

occurrence of ODLRO (and therefore of BEC) is characterized by a linear scaling of the largest eigenvalue λ_0 with respect to the total number of particles N in the system [7,19]: $\lambda_0 \sim N$.

For a translational invariant system, the indices i in Eq. (3.2) are wavevectors, which are conventionally denoted by the vector $\mathbf{k}$. Introducing the scaling formula:

$$\lambda_0 \sim N^{\mathcal{C}_0(T)} ,$$

the Mermin-Wagner theorem implies that $\mathcal{C}_0(T) < 1$ for $T > 0$ and $D \leq 2$, so there is no ODLRO at finite temperature. One can show as well that $\mathcal{C}_0(T = 0) = 1$ for $D = 2$ and $\mathcal{C}_0(T = 0) < 1$ in $D = 1$ (for the interacting case), see [20]. For a translational invariant system, the absence of ODLRO, or equivalently of BEC, in $D = 2$ at finite temperature amounts to the following behaviour of the 1BDM at large distances:

$$\left\langle \hat{\Psi}^\dagger(\mathbf{x})\hat{\Psi}(\mathbf{y}) \right\rangle \xrightarrow{|\mathbf{x}-\mathbf{y}|\to\infty} \left\langle \hat{\Psi}(\mathbf{x}) \right\rangle^* \left\langle \hat{\Psi}(\mathbf{y}) \right\rangle = 0 .$$

The existence and regimes for BEC, *i.e.* whether $\mathcal{C}_0 = 1$ or not, in various physical systems has been the subject of a remarkable amount of work. It would be therefore desirable to complete such analysis with a systematic study of when $\mathcal{C}_0$ is smaller than 1: In this case there is no ODLRO/BEC but nevertheless the condition $0 < \mathcal{C}_0 < 1$ implies that, in translational invariant systems, the correlation function $\langle \hat{\Psi}^\dagger(\mathbf{x})\hat{\Psi}(\mathbf{y}) \rangle$ has a power-law decay. One may refer to this situation as *quasi-long-range order*. The relation between the scaling behaviour of density matrices of any order (including the one–body density matrix considered in the present work) and the types of order characterizing the physical system were analysed in [21, 22], where the so-called order indices were introduced and studied both for certain fermionic and bosonic systems. Since the order index for the nth order reduced density matrix is defined as: $\alpha^{(n)} = \lim_{N\to\infty} \ln \lambda_0^{(n)} / \ln N$, where $\lambda_0^{(n)}$ is the largest eigenvalue of the nth order density matrix, then we can identify the order index $\alpha^{(1)}$ of the 1BDM as the exponent $\mathcal{C}_0(T)$ defined from the scaling of $\lambda_0 \equiv \lambda_0^{(1)}$. The concept of order indices can be extended to arbitrary matrices (see [23] for a discussion), while the relation between order indices and entanglement production is presented in [24].

In the first Chapters of this Thesis, we will study ODLRO properties in terms of the scaling with the particles number N of the eigenvalues λ_k of the 1BDM, both of the largest eigenvalue λ_0 and of the others $\lambda_{k\neq 0}$. Let us stress that, for a system of interacting bosons, the index $\mathcal{C}_0$ may also depend on the interaction strength and, moreover, one may expect that increasing the repulsion among the bosons, $\mathcal{C}_0$ gets dampened with respect to the weak interacting case.

In this work, we are going to characterize ODLRO, in translational invariant bosonic systems interacting via short-range potential in 1-, 2- and 3-dimensions both at zero and finite temperatures. Thanks to integrability properties, for the case of $D = 1$ we will be able to obtain the scaling exponent and prefactor of λ_j for the Lieb–Liniger model with generic anyonic statistics. For the case $\kappa = 0$, *i.e.* Bose statistics, we will construct an interpolation scheme which allows to evaluate the 1BDM for any interactions and particles number. Later on, we will also focus on confining effects, *i.e.* the effects that an external trapping potential exhibits on the system, and for this particular case we will deal with one–dimensional systems only, both with contact and long–range interactions at zero temperature. We will also generalize the analysis of trapping effects to anyonic statistics, where we will deal with the trapped Lieb–Liniger anyon gas at zero temperature.

Obviously there is an interest also to characterize ODLRO and possible deviations from it, in confined systems at finite temperatures (and possibly in more than one dimension), but this goes beyond the scope of the present Thesis, even though future works on this direction are in our mind. With "possible deviations" from ODLRO, we mean a study of the behaviour of the index $\mathcal{C}_k(T)$, defined as:

$$\lambda_k \sim N^{\mathcal{C}_k(T)} ,$$

where $k \neq 0$. The study of $\mathcal{C}_{k\neq 0}(T)$ gives an insight about the possible *quasi-fragmentation* of the system, *i.e.* how the particles occupy the other, $k \neq 0$, states. Notice that in literature usually one refers to fragmentation when more than one eigenvalue of the 1BDM scales with N. So, one can refer to the case in which at least two $\mathcal{C}_k$ are larger than zero (and at least one is smaller than 1) as a quasi-fragmentation.

The power-law behaviour of λ_0 determines the leading scaling of the largest eigenvalue of the 1BDM and, according to the Penrose-Onsager criterion, there is a BEC/ODLRO, *i.e.* a macroscopic occupation of the lowest energy state, if $\mathcal{C}_0(T) = 1$. There will be instead a mesoscopic condensate (i.e. quasi-long-range order), with a finite value for the condensate fraction $\frac{\lambda_0}{N}$ for finite values of N, if $0 < \mathcal{C}_0(T) < 1$. In this case the condensate fraction of course vanishes for $N \to \infty$ but, even though the system is not a true BEC, one would observe nevertheless a clear peak in the momentum distribution in an experiment with ultracold gases: The reason is that the number of particles which are typically used in these apparatus are of order $N \sim 10^3 - 10^5$, and therefore the condensate fraction $\frac{\lambda_0}{N} \sim \frac{N^{\mathcal{C}_0(T)}}{N}$ could be very close to the unity for $\mathcal{C}_0(T)$ close to 1. For $\mathcal{C}_0(T) = 0$ there will be no order at all, and in these cases the system may behave like a Fermi gas where for all the eigenvalues we have $\lambda_i = 1$, because of the Pauli principle. When $\mathcal{C}_0(T) = 0$ it may also happen that the scaling of the largest eigenvalue is logarithmic in N, still signaling an absence of ODLRO.

Nonetheless, all of these concepts are introduced in a static formalism, where the system is in an equilibrium situation. Interesting effects will arise when we consider dynamical properties, studying the system under the action of an external time varying potential. In this Thesis we will focus on the effects of a time–dependent gravitational potential, linear in the position variable, both in one– and three–dimensional spaces. For $D = 3$ we will construct an exact solution of the time–dependent Schrödinger equation of a quantum many–body system in free fall. While, for $D = 1$, the possible integrability features of the system together with the Floquet formalism (when the time variation of the linear potential is periodic), allows to make wonderful predictions for the many–body wavefunction both at stroboscopic and intermediate times. Time–periodic driven quantum systems have become recently the subject of an intense research activity. These out of equilibrium systems give rise to interesting novel physical properties as, for instance, dynamic localization effects [25], suppression of tunneling subjected to a strongly driven optical lattice [26–32] (see [33] for more references), topological Floquet phases [34, 35], time crystals [36–43], dynamics in driven systems [44–46] and Floquet prethermalization [47, 48]. All these concepts and phenomena can be collected together under the heading of "Floquet engineering" [33, 49], a very active field both from experimental and theoretical points of view.

The name itself came from a famous paper by Floquet [50], who was interested in the study of differential equations with coefficients given by time–periodic functions. The

formalism he developed turns out to be very helpful in dealing with the Schrödinger equation of a Quantum Mechanical system with a time–periodic Hamiltonian [51, 52]. Preparing the system in an initial state $\chi(t=0)$ and letting the periodic driving act on it, the Floquet Hamiltonian $\hat{H}_F$ is the operator that formally gives the state of the system at multiples of the period T:

$$\chi(t=nT) = e^{-i\frac{nT}{\hbar}\hat{H}_F}\,\chi(t=0)\,.$$

In other words, the Floquet Hamiltonian $\hat{H}_F$ determines the stroboscopic evolution of the system. It depends on the parameters of the original undriven Hamiltonian, $\hat{H}_0$, and on the time–dependent perturbation. $\hat{H}_F$ is a hermitian operator whose eigenvalues are the so called quasi-energies $\mathcal{E}_F$. On the other hand, the evolution of the state $\chi(t=0)$ at generic times $t \in (0,T)$ is determined by the *micro-motion operator* $\hat{U}_F(t,0)$, defined by the following decomposition of the time evolution operator of the system $\hat{U}(t,0)$:

$$\hat{U}(t,0) = \hat{U}_F(t,0)\,e^{-i\frac{t}{\hbar}\hat{H}_F}\,.$$

Applying the micro-motion operator $\hat{U}_F(t,0)$ on the eigenstates of the Floquet Hamiltonian and multiplying by a complex exponential containing the quasi-energies, one obtains the *Floquet states* $|\psi_F(t)\rangle$. They form a complete and orthonormal set of functions and therefore any solution of the original time–dependent Schrödinger equation can be written as a superposition in terms of them

$$\chi(t) = \int dk\, A(k)\ |\psi_F(t)\rangle\ ,$$

where k is a momentum variable, related to the energy of the system ($k \propto \sqrt{E}$), and the $A(k)$'s are time–independent coefficients. Therefore finding $\hat{H}_F$ and $\hat{U}_F(t,0)$ gives access to the full quantum dynamics of the system.

Finding the Floquet Hamiltonian and the micro-motion operator for an interacting many-body system in the presence of a time–dependent driving is in general a challenging and highly interesting task, relevant for a variety of applications in the field of Floquet engineering. Tuning the form and the parameters of the undriven system and of the periodic perturbation, one aims at controlling the (desired) effective Hamiltonian of the quantum dynamics of the system itself.

In general, even if the undriven model is integrable, when we subject it to a time–periodic potential, we end up in a non-integrable Floquet Hamiltonian. We will address the question whether it would be possible to have an integrable Floquet Hamiltonian by perturbing an integrable $1D$ bosonic model with a time–periodic perturbation, and we will find a positive answer. Namely, we will consider the integrable Hamiltonian that describes a one–dimensional gas of bosons with contact interactions, *i.e.* the Lieb–Liniger Hamiltonian [53], in the presence of a linear in space, time–periodic one-body potential of the form:

$$V(x,t) = f(t)\,x\ ,$$

with a driving function $f(t)$ with period T: $f(t) = f(t+T)$. Despite the fact that other exactly solvable time–dependent Hamiltonians can be constructed using different approaches [54, 55], the problem of finding an integrable Floquet Hamiltonian from an undriven interacting one is in general a difficult task. It is also worth to underline that,

in general, one of the difficulties in identifying integrable Floquet Hamiltonians is that the integrability of these Hamiltonians is not at all guaranteed by the integrability of the original time–independent undriven model (see, for instance, [56] where starting from the original BCS model the corresponding BCS gap equation in the presence of a periodic driving is derived and solved numerically). For the class of one–dimensional interacting many-particles systems considered here, we show instead that it is not the case, as far as the periodic driving is a linear function on the position variables.

In later Chapters we will first discuss the effects of the linear external potential on a system with a general two-body interaction term, and then we will focus on the paradigmatic and experimentally relevant case where the particles interact with contact interactions, *i.e.* the Lieb–Liniger model. This model constitutes an ideal playground for integrable models in one–dimensional continuous space. It is indeed exactly solvable using Bethe ansatz techniques [53, 57–59], related to the non-relativistic limit of the Sinh-Gordon model [60] and routinely used to describe (quasi-) one–dimensional bosonic gases realized in ultracold atoms experiments (see the reviews [61–63]). These properties will guarantee the possibility to build a generalized Gross–Pitaevskii equation which describes the dynamic and static properties of the Lieb–Liniger gas at $T = 0$, for which, in particular, we will be able to construct dark soliton solutions and find the ground state density profiles in presence of an external harmonic confinement.

1

ONE–DIMENSIONAL HOMOGENEOUS GASES

Exactly solvable models constitute an ideal playground for a theoretical physicist. Referring to quantum systems, we say that a model is exactly solvable when a solution to the corresponding Schrödinger equation can be provided. In the context of quantum many–body systems, because of the interactions among particles, in general the Schrödinger equation cannot be exactly solved, and one has to rely on approximation methods in order to find the many–body wavefunction. Nevertheless, there exist a paradigmatic model which can be treated exactly and for which, therefore, many physical properties were subjects of interest: A one–dimensional gas of Dirac–delta interacting particles. We will refer to it, in general, as the Lieb–Liniger model [53]. Even though in the original paper of Lieb and Liniger, they were dealing with the case of particles having Bose statistic, in later years it was proved that also contact interacting gases respecting other statistics can be exactly solved [64,65]. The interest on this peculiar model stems also from the fact that it can be proven that every homogeneous exactly solvable one–dimensional systems reduces to the case of a Lieb–Liniger model [59]. On top of that, the Lieb–Liniger model is also experimentally relevant, since it can describe dilute 1D gases confined on waveguides in real world experiments.

Let us introduce the model, first focusing on the case of Bose statistics, and later we will extend the study to quantum particles with a generalized statistics with contact interactions. In this Chapter we will deal with the ground state $T = 0$ temperature situation, leaving the discussion of temperature effects on the system for later.

1.1 THE LIEB–LINIGER MODEL

The Lieb–Liniger (LL) model [53] consists of a homogeneous one–dimensional system of N bosons of mass m, interacting via a two-body repulsive δ–potential in a ring of circumference L. The wavefunctions $\psi_B(x_1, \dots, x_N)$ of this system are invariant under permutations of any pair of its variables

$$\psi_B(\dots, x_i, \dots, x_j, \dots) = \psi_B(\dots, x_j, \dots, x_i, \dots) \ ,$$

and satisfy the stationary Schrödinger equation:

$$H_B \, \psi_B(x_1, \dots, x_N) = E \, \psi_B(x_1, \dots, x_N) \, , \tag{1.1}$$

with the Hamiltonian given by

$$H_B = -\frac{\hbar^2}{2m} \sum_{i=1}^{N} \frac{\partial^2}{\partial x_i^2} + \frac{\hbar^2 c_B}{m} \sum_{i<j} \delta(x_i - x_j) \, . \tag{1.2}$$

In second quantized formalism the non-relativistic field theory describing bosons interacting via a delta-potential is defined by the Gross–Pitaevskii Hamiltonian [58]

$$\mathcal{H}_B \,=\, \int_0^L \mathrm{d}x \left[\frac{\hbar^2}{2m} \frac{\partial \Psi^\dagger}{\partial x} \frac{\partial \Psi}{\partial x} + \frac{\hbar^2 c_B}{2m} \Psi^\dagger(x) \Psi^\dagger(x) \Psi(x) \Psi(x) \right] , \tag{1.3}$$

where the complex Bose field $\Psi(x,t)$ satisfies the canonical commutation relations

$$[\Psi(x,t), \Psi^\dagger(x',t)] \,=\, \delta(x-x') \;, \quad [\Psi(x,t), \Psi(x',t)] = 0 \;. \tag{1.4}$$

The quantity $c_B > 0$ can be determined in terms of the parameters of the three-dimensional Bose gas in the quasi-one–dimensional limit, and it has dimension of an inverse of a length. In particular, one can write [66]:

$$c_B = \frac{a_\perp^2}{2a_s} \left[1 - C \frac{a_s}{a_\perp} \right] , \tag{1.5}$$

which is the definition of the one–dimensional scattering length, where $a_\perp = \sqrt{2\hbar/m\omega_\perp}$, a_s is the three–dimensional scattering length and $C \simeq 1.4603$. Here $\omega_\perp$ refers to the perpendicular trap frequency necessary in order to reduce the system to live in a one–dimensional space, giving the shape of a cigar to the external trapping potential which confines the system.

However, the effective coupling constant which characterizes many properties of the LL model is given by the dimensionless quantity:

$$\gamma = \frac{c_B}{n_B} \;, \tag{1.6}$$

where $n_B = N/L$ is the density of the gas. Notice that the coupling constant γ increases when the particle density decreases, and this is a peculiarity of one–dimensional systems. The weak interactions regime is reached in the limit $\gamma \ll 1$: It can be successfully studied in terms of the Bogoliubov approximation (obtained by linearizing the Gross–Pitaevskii equation) which gives indeed an accurate estimate of the ground state energy of the system [53]. The strong limit regime is reached instead for $\gamma \gg 1$, and in particular for $\gamma \to \infty$ one reaches the Tonks–Girardeau limit [67]. An interesting question is to study the crossover between these two regimes, a topic recently approached also from an experimental point of view [61].

From the theoretical point of view, there is no difficulty in ranging between strong and weak interactions. Indeed, as well known, the model is exactly solvable by Bethe ansatz technique [53, 57, 58, 68] which provides the exact expression of the many–body wavefunction:

$$\psi_B(x_1, \ldots, x_N) \,=\, \mathcal{N} \, \det[e^{ik_j x_m}]_{j,m=1,\ldots,N} \prod_{1 \le n < l \le N} [k_l - k_n - i\, c_B \, \mathrm{sgn}(x_l - x_n)] \,, \tag{1.7}$$

where $\mathcal{N}$ is the normalization constant [69], $\mathrm{sgn}(x)$ is the sign function and k_j are the pseudorapidities determined by the Bethe equations:

$$k_j + \frac{2}{L} \sum_{m=1}^{N} \arctan\left(\frac{k_j - k_m}{c_B} \right) \,=\, \frac{2\pi}{L} \left(n_j - \frac{N+1}{2} \right) , \quad \forall j = 1, \ldots, N \,, \tag{1.8}$$

where periodic boundary conditions have been imposed:

$$\psi_B(\ldots, x_j, \ldots) \,=\, \psi_B(\ldots, x_j + L, \ldots) \,, \quad \forall j = 1, \ldots, N \,. \tag{1.9}$$

At $T = 0$, we are only interested in the ground state of the system whose corresponding wavefunction is obtained by choosing the integer numbers n_j, in (1.8), equal to the indicies j. In the thermodynamic limit, the values of the k_j's become dense and therefore described by the density of pseudorapidities $f(k)$. This function $f(k)$ can be directly computed by solving the linear integral equation:

$$f(k) \;=\; \frac{1}{2\pi} + \frac{1}{2\pi}\int_{-B_B}^{B_B} \mathcal{K}_B(\lambda-\lambda')f(\lambda)\,d\lambda\,, \tag{1.10}$$

where the LL kernel is defined as:

$$\mathcal{K}_B(\lambda-\lambda') \;=\; \frac{2c_B}{c_B^2+(\lambda-\lambda')^2}\,.$$

In Eq. (1.10), B_B represents the upper limit for the pseudorapidities, a quantity which is determined by the normalization condition of $f(k)$ to the total number of particles per unit length, which reads:

$$n_B \;=\; \int_{-B_B}^{B_B} f(k)\,dk \;\;. \tag{1.11}$$

In terms of the density of pseudorapidities, the ground state energy of the system is expressed as:

$$E \;=\; \frac{\hbar^2}{2m}\,L\int_{-B_B}^{B_B} f(\lambda)\,\lambda^2\,d\lambda \;\;. \tag{1.12}$$

We will call these set of three equations, the Lieb equations.

It is convenient to define a dimensionless ground state energy density function as:

$$e_B(\gamma) = \frac{2m}{\hbar^2}\,\frac{E}{L}\,n_B^{-3}\,. \tag{1.13}$$

Let us now study two limiting behaviors of these equations which will be useful for our future analysis.

a) $\gamma \to 0$, *i.e.* the Bogoliubov weakly interacting regime. In this limit the energy of the system can be calculated from perturbation theory: At the first order, using for the many–body wavefunction the simple form for N particle belonging to the state $k = 0$, *i.e.* $\psi_0 = 1/\sqrt{L^N}$, one finds that

$$e_B^{Bog}(\gamma) \;\simeq\; \gamma\,.$$

b) $\gamma \to \infty$, *i.e.* the Tonks–Girardeau limit. The solution of (1.11) in this case has the simple expression:

$$f(k) \;=\; \frac{1}{2\pi} \;\;,$$

and it follows that:

$$e_B(\infty) \;=\; \frac{\pi^2}{3} \;\;.$$

For a generic fixed value of γ, one can use the Lieb equations to find numerically the function $f(k)$ and then use it to find the single-particle energy function $e_B(\gamma)$ once it is imposed the normalization condition (1.11). One can then use these quantities to calculate some other thermodynamic variables of interest, such as the sound velocity s associated to the system. In fact, s^2 is determined by taking the derivative of the pressure with respect to the density and then dividing by the mass of the particle. Since, in turn we have [70]:

$$p \equiv -\left(\frac{\partial E}{\partial L}\right)_N = \frac{\hbar^2}{m} n_B^3 \left[e_B(\gamma) - \frac{\gamma}{2} e_B'(\gamma)\right], \tag{1.14}$$

then

$$s^2 = \frac{\hbar^2}{m^2} n_B^2 \left[3\, e_B(\gamma) - 2\,\gamma\, e_B'(\gamma) + \frac{\gamma^2}{2} e_B''(\gamma)\right]. \tag{1.15}$$

Similarly we can evaluate the chemical potential: It is defined as the derivative of the energy with respect to N with fixed L and hence it can be written as [70]:

$$\mu = \frac{\hbar^2}{m} n_B^2 \left[\frac{3}{2} e_B(\gamma) - \frac{\gamma}{2} e_B'(\gamma)\right]. \tag{1.16}$$

A dimensionless parameter which will be useful in subsequent Sections, is the so called *Luttinger parameter* K, a quantity introduced in the bosonization formalism valid for one–dimensional quantum systems [71,72]. It must be stressed that, in general, the determination of this parameter is quite difficult but fortunately this is not the case for the LL model: In this case one can use the results coming from the thermodynamic studies [cfr (1.15)] and the Galilean invariance of the system, in order to obtain the Luttinger parameter which reads:

$$K = \frac{v_F}{s}, \tag{1.17}$$

where v_F is the Fermi velocity which, in our notation, is given by $v_F = \hbar\pi n_B/m$. Therefore, solving the Lieb equations one has access both to the sound velocity and the Luttinger parameter for any values of the coupling constant γ (see, for instance, [63]). Let us present here the weak and strong coupling limit of both the sound velocity and the Luttinger parameter: Using the weak interaction result for the ground state energy density in Eq. (1.15), in the Bogoliubov limit the sound velocity is given by:

$$s_{Bog} \simeq \frac{\hbar}{m} n_B \sqrt{\gamma},$$

which means that for $\gamma \to 0$

$$K_{Bog} \simeq \frac{\pi}{\sqrt{\gamma}}. \tag{1.18}$$

In the Tonks–Girardeau (TG) limit we have instead:

$$s_{TG} = \frac{\hbar\pi n_B}{m} = v_F,$$

as expected, and this implies that for $\gamma \to \infty$ the Luttinger parameter simly reads:

$$K_{TG} = 1. \tag{1.19}$$

In summary, the Luttinger parameter for a homogeneous system of δ–repulsive bosons ranges from ∞ (for $\gamma \to 0$) to 1 (for $\gamma \to \infty$).

For generic interactions, in order to determine all these interesting quantities, ideally one should numerically solve the Lieb equations, as we already said. This is sometime a very long procedure, especially when one needs immediately functions like $e_B(\gamma)$ for a certain value of γ, as it happens in order to evaluate the liquid sound velocity, pressure, chemical potential, Luttinger parameter, etc. With the aim of obtaining an expression for the ground state energy density valid in all regimes of interactions, we now discuss how we deal with this problem, first recognizing that Eq. (1.10) is a notorious type of Fredholm integral equation: The Love's integral equation [73] describing the electrostatic problem of a condenser with parallel, circular, coaxial disks.

1.2 LOVE'S INTEGRAL EQUATION

When E. R. Love first studied the problem of describing the electrostatic field produced by a condenser consisting of two parallel circular plates [73], he surely couldn't realize how wide would have been the applicability in physical problems of his integral equation. In the classical original problem of a condenser with parallel, circular, coaxial disks, studied by Love, he was able to write an equation to describe the electrostatic potential which reads:

$$V(\rho,\xi,\xi') = \frac{V_0}{\pi}\int_{-1}^{1}\left\{\frac{1}{\sqrt{\rho^2+(\xi+it)^2}} \pm \frac{1}{\sqrt{\rho^2+(\xi'+it)^2}}\right\} f(t)\,dt\,, \tag{1.20}$$

written in terms of dimensionless coordinates, and normalized to the radius of the plates (assumed to be equal). Here ρ is the radial distance, ξ and ξ' are the axial distances from the two plates, while V_0 is the magnitude of the potential in each plate. Finally, $f(t)$ is the solution to the Fredholm integral equation:

$$f(x) \pm \frac{1}{\pi}\int_{-1}^{1}\frac{\kappa}{\kappa^2+(x-t)^2} f(t)dt = 1\,, \quad -1 \le x \le 1\,, \tag{1.21}$$

where κ is the spacing parameter. The upper sign in Eqs. (1.20) and (1.21) refers to the case of equally charged plates, while the lower one refers to the case of oppositely charged disks. In what follows, we will refer, for convenience, to the 'Love's equation of the first (second) kind' for Eq. (1.21) obtained by the lower (upper) sign.

As we will see in more detail in the following Sections, Eqs. (1.21), known as the Love's integral equations, have the same form of the equations which describe the densities of pseudorapidities in one–dimensional models. In particular, for the LL model the equation for the densities has the same form as the Love's equation of the first kind. This fascinating parallelism is of a great interest since if one finds the solution of the Love's equation, then one is also able to extract other important physical properties of the system, and we will discuss some applications.

Another interesting one–dimensional system which is exactly solvable, and whose density of pseudorapidities satisfies a Love's integral equation of the second kind, is the Gaudin–Yang (GY) model, which describes 1D spin Fermi gases with Dirac–delta attractive interactions [74]. We will discuss the GY model and its integral equations later, in more detail.

Let us now come back to the electrostatic problem, and let us discuss it in more details. A condenser with parallel, circular, coaxial disks with equal radii but different potentials V_1 and V_2, has its electrostatic potential described by two different weight functions $f_j(t)$, for $j = 1$ and 2, for the two plates. In particular one has [75]:

$$f_1(x) + \frac{1}{\pi}\int_{-1}^{1} \frac{\kappa}{\kappa^2 + (x-t)^2} f_2(t)dt = \frac{2}{\pi} V_1\,, \tag{1.22}$$

for one plate with charge $Q_1 = \int_0^1 f_1(t)dt$, while:

$$f_2(x) + \frac{1}{\pi}\int_{-1}^{1} \frac{\kappa}{\kappa^2 + (x-t)^2} f_1(t)dt = \frac{2}{\pi} V_2\,, \tag{1.23}$$

for the other plate with charge $Q_2 = \int_0^1 f_2(t)dt$. Writing: $V_2 = \mathcal{Z}V_1$, assuming $\mathcal{Z} > 0$, from the above two equations one can write a single Fredholm integral equation for the weight function $\bar{f}(x) = \frac{f_1+f_2}{2}$, which reads

$$\bar{f}(x) + \frac{1}{\pi}\int_{-1}^{1} \frac{\kappa}{\kappa^2 + (x-t)^2} \bar{f}(t)dt = \frac{2}{\pi}\left(\frac{1+\mathcal{Z}}{2}\right) V_1\,. \tag{1.24}$$

If we instead write: $V_2 = -\mathcal{Z}V_1$, with $\mathcal{Z} > 0$, taking: $\tilde{f}(x) = \frac{f_1-f_2}{2}$, we have:

$$\tilde{f}(x) - \frac{1}{\pi}\int_{-1}^{1} \frac{\kappa}{\kappa^2 + (x-t)^2} \tilde{f}(t)dt = \frac{2}{\pi}\left(\frac{1+\mathcal{Z}}{2}\right) V_1\,. \tag{1.25}$$

Therefore if one is interested in finding the weight function solution of a condenser with two plates with charges equal (opposite) in sign but different in intensity, then one simply has to compute the $f(x)$ function from Eq. (1.21) with the plus (minus) sign and then, after normalizing with $2V_1/\pi$, multiply the weight function by $2/(\mathcal{Z}+1)$ to get the solution $\bar{f}(x)$ [$\tilde{f}(x)$]. Finally notice that from Eq. (1.24) if we take $\mathcal{Z} = 1$ one gets back Eq. (1.21) with the plus sign [once $f(x)$ has been normalized with $2V_1/\pi$], while from taking $\mathcal{Z} = 1$ from (1.25) we obtain the same equation in (1.21) with the minus sign (again after normalizing the weight function with the constant potential), as it should. From the knowledge of the weight function, one can also determine the capacitance of the parallel plate capacitor as:

$$C = \frac{1}{\pi}\int_{-1}^{1} f(t)\,dt\,.$$

While the Love's equation of the first (second) kind is the same equation which describes the density of pseudorapidities of the LL (GY) model as we are going to see in detail, another interesting case is the one in which $V_1 = V$ and $V_2 = 0$. In that case, indeed, Eqs. (1.22) and (1.23) describe the densities of pseudorapidities of one–dimensional Bose–Fermi mixture [76]. The Love's equation of the second kind is also found to describe the density of pseudorapidities and the dressed charge function of a Lieb–Liniger gas of anyons [77], where the distance among plates is replaced by the renormalized coupling constant which encloses information about the statistic properties of the particles; in a later Section we will study the effects of anyonic statistic in more detail. Now that we know something more about the broad applicability of Love's integral equations, let us come back to one–dimensional exactly solvable physical systems whose wavefunction depends on the solution of Love's equation. We will now discuss how to deal and solve the integral equations for these systems, and in particular for the GY and LL models.

1.2.1 LOVE'S EQUATION OF THE FIRST AND SECOND KIND

While the Lieb–Liniger model has been already presented, we now briefly introduce the Gaudin–Yang model and then we set some notations. The Gaudin–Yang model describes a 1D fermionic gas of two spin-components with attractive interactions. In the second quantization formalism, the Hamiltonian reads [74]:

$$H_F = \int_0^L dx \left[\frac{\hbar^2}{2m_F} \left(\frac{\partial \Psi_\downarrow^\dagger}{\partial x} \frac{\partial \Psi_\downarrow}{\partial x} + \frac{\partial \Psi_\uparrow^\dagger}{\partial x} \frac{\partial \Psi_\uparrow}{\partial x} \right) + \frac{\hbar^2 c_F}{2m_F} \Psi_\downarrow^\dagger(x) \Psi_\uparrow^\dagger(x) \Psi_\uparrow(x) \Psi_\downarrow(x) \right] , \quad (1.26)$$

where m_F is the mass of the fermions, c_F is the coupling and $\Psi_\downarrow(x)$ and $\Psi_\uparrow(x)$ are the fermionic matter-field for the two spin-components. In this case the matter-fields of the systems obey to the constraint:

$$\int_0^L \left[\Psi_\downarrow^\dagger(x) \Psi_\downarrow(x) + \Psi_\uparrow^\dagger(x) \Psi_\uparrow(x) \right] dx = N_F \, , \quad (1.27)$$

where N_F is the total number of fermions. We note that the contact interaction here is possible thanks to the presence of two spin-components. As we did for the bosonic system, it is convenient to define a dimensionless interaction parameter, which we denote by γ_F, and reads:

$$\gamma_F = -\frac{c_F}{n_F} \, , \quad (1.28)$$

where $n_F = N_F/L$ is the total particle density for the fermionic model. From now on, we will drop the subscripts B and F if the equations are valid for both the LL and GY models.

For these two models, the Bethe ansatz technique allows to find an exact expression for the many–body wavefunction which reads [58, 78]:

$$\psi(x_1, \ldots, x_N) = \sum_P [P, Q] \, e^{i\left(k_{P_1} x_{Q_1} + \cdots + k_{P_N} x_{Q_N}\right)} \, ,$$

where P and Q are permutations of the integers $\{1, 2, \ldots, N\}$, while k_j's are the pseudo-rapidities of the system. It can be shown that for $\gamma \to \infty$, where the LL model approaches the Tonks-Girardeau limit, the bosonic and fermionic models are identified by the same set of Bethe equations if the conditions [79, 80]:

$$N_F \leftrightarrow \frac{N_B}{2} \, , \quad c_F \leftrightarrow -2c_B \, , \quad \gamma_F \leftrightarrow \frac{\gamma_B}{4} \, , \quad m_F \leftrightarrow \frac{m}{2} \, ,$$

hold.

For the LL model, we have seen that in the thermodynamic limit one can write an integral equation for the density of pseudorapidities, $f_B(x)$, and it is given by [53]:

$$\frac{f_B(x)}{2} - \frac{1}{2\pi} \int_{-B_B}^{B_B} \frac{f_B(y)}{1 + (y - x)^2} \, dy = 1 \, , \quad (1.29)$$

where we have changed the notations, in order to render the comparison between the GY and LL models more fluid. We redefined the pseudorapidities density function as: $f_B(x) = f(k)/4\pi$. The dimensionless coupling constant is then given by:

$$\frac{1}{\gamma_B} = \frac{1}{4\pi} \int_{-B_B}^{B_B} f_B(x) \, dx \, , \quad (1.30)$$

The (dimensionless) ground state energy density $e(\gamma) = \frac{2m}{\hbar^2}\left(\frac{E}{L}\right) n^{-3}$, is then related to the weight function $f_B(x)$ as:

$$e_B(\gamma_B) = \frac{\gamma_B^3}{4\pi}\int_{-B_B}^{B_B} x^2 f_B(x)\, dx\,. \tag{1.31}$$

Similarly, one can write analogous equations for the GY model. In particular, the density of pseudorapidities, here denoted by $f_F(x)$, is given by:

$$\frac{f_F(x)}{2} + \frac{1}{2\pi}\int_{-B_F}^{B_F} \frac{f_F(y)}{1+(y-x)^2}\, dy = 1\,, \tag{1.32}$$

while the dimensionless coupling reads:

$$\frac{1}{\gamma_F} = \frac{1}{\pi}\int_{-B_F}^{B_F} f_F(x)\, dx\,. \tag{1.33}$$

From these two equations, we can find the dimensionless ground state energy as:

$$e_F(\gamma_F) = -\frac{\gamma_F^2}{4} + \frac{\gamma_F^3}{\pi}\int_{-B_F}^{B_F} x^2 f_F(x)\, dx\,. \tag{1.34}$$

Notice that in the weak coupling limit, $\gamma \to 0$, the integral equations for the weight functions are singular and the solution for a weakly interacting dilute gas is rather a difficult task, both analytically and numerically [81,82] (for the LL model we used before the perturbation theory results, but in order to get higher orders of approximation, one should follow different approaches).

These three set of equations, one for the density of pseudorapidities, one for the cut-off of pseudorapidities and another one for the dimensionless ground state energy, for each models, has to be solved numerically for a fixed generic coupling strength and there no exist an expression for each of the physical variables which hold in all the regime of interactions. Let us now discuss how to solve them numerically.

1.2.2 NUMERICAL SOLUTION

First of all, let us define, for convenience, the parameter: $\lambda = 1/B$. Eqs. (1.30) and (1.33) will then be expressed as:

$$\lambda_B = \frac{\gamma_B}{4\pi}\int_{-1}^{1} f_B(B_B t)\, dt\,, \tag{1.35}$$

and

$$\lambda_F = \frac{\gamma_F}{\pi}\int_{-1}^{1} f_F(B_F t)\, dt\,, \tag{1.36}$$

where $t = x/B$ are the normalized pseudorapidities. Then, rewriting the density functions:

$$g_B(t) = f_B(B_B t)\,,$$
$$g_F(t) = f_F(B_F t)\,,$$

for the LL model and the GY model, respectively, we can rewrite Eqs. (1.29) – (1.31), for the LL model, as:

$$g_B(t) - \frac{\lambda_B}{\pi}\int_{-1}^{1}\frac{g_B(t')}{\lambda_B^2+(t'-t)^2}\,dt' = 2\,,$$
$$\lambda_B = \frac{\gamma_B}{4\pi}\int_{-1}^{1} g_B(t)\,dt\,,$$
$$e_B(\gamma_B) = \frac{\gamma_B^3}{4\pi\lambda_B^3}\int_{-1}^{1} t^2 g_B(t)\,dt\,,$$

while Eqs. (1.32) – (1.34) of the GY model, as:

$$g_F(t) + \frac{\lambda_F}{\pi}\int_{-1}^{1}\frac{g_F(t')}{\lambda_F^2+(t'-t)^2}\,dt' = 2\,,$$
$$\lambda_F = \frac{\gamma_F}{\pi}\int_{-1}^{1} g_F(t)\,dt\,,$$
$$e_F(\gamma_F) = -\frac{\gamma_F^2}{4} + \frac{\gamma_F^3}{\pi\lambda_F^3}\int_{-1}^{1} t^2 g_F(t)\,dt\,.$$

Now, this set of equations can be solved in several ways. One method is more direct, and it consists in solving these equations by using the Chebyshev quadrature method with $M = 100$ points. Briefly, denoting by $h(t)$ a generic function and by M the number of quadrature points, one relies on the following approximation [83]:

$$\int_{-1}^{1} h(t)\,dt \simeq \sum_{j=1}^{M} h(t_j) w_j \sqrt{1-t_j^2}\,,$$

where $t_j = \cos\left(\frac{2j-1}{2M}\right)$, and the weights for the Chebyshev quadrature reads: $w_j = \frac{\pi}{M}$, $\forall j$. In this case the first two equations for each model, has to be solved iteratively.

Another method was proposed by Love, in his original work [73]. He showed that, for fixed λ, the weight function can be written as:

$$g_{B/F}(t) = 1 + \sum_{n=1}^{\infty}(\pm 1)^n \int_{-1}^{1} K_n(t',t)\,dt'\,, \tag{1.37}$$

where:

$$K_1(t',t) = \frac{1}{\pi}\frac{\lambda}{\lambda^2+(t'-t)^2}\,,$$
$$K_n(t',t) = \int_{-1}^{1} K_{n-1}(t,s)K_1(s,t')ds\,,$$

where, again, we used the Chebyshev quadrature to compute the integrals. We truncated the series when the terms had an absolute value below 10^{-40}. The comparison with the previous "direct" method was very good, with errors at most of the order of 10^{-10}.

Anyway, from these numerical solutions we are able to study the γ dependence of the normalized λ's parameters. In Fig. 1.1 we plot the behaviour for $\ln(\lambda_F)$ in orange line, while $\ln(\lambda_B)$ is reported in blue solid line. Notice that the two cut-off pseudorapidities coincide for very large interactions, *i.e.* $\gamma \to \infty$, where the hard–core interactions wash away the statistic properties of the gases and the two models coincide.

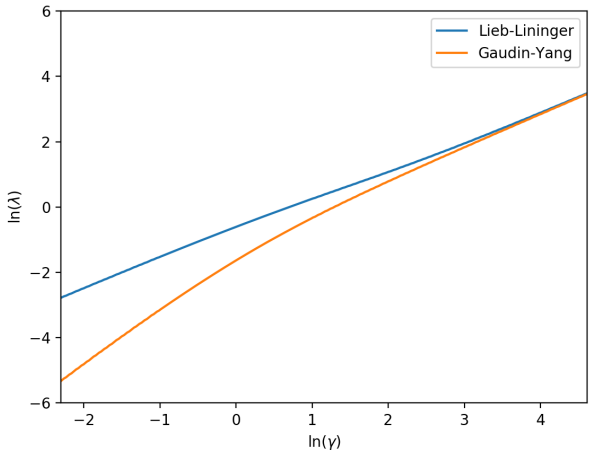

Figure 1.1: Natural logarithm of the inverse of the cut-off of the pseudorapidities, $\lambda = 1/B$, vs the logarithm of the dimensionless coupling, γ, for the Gaudin–Yang (orange line) and Lieb–Liniger (blue line) models.

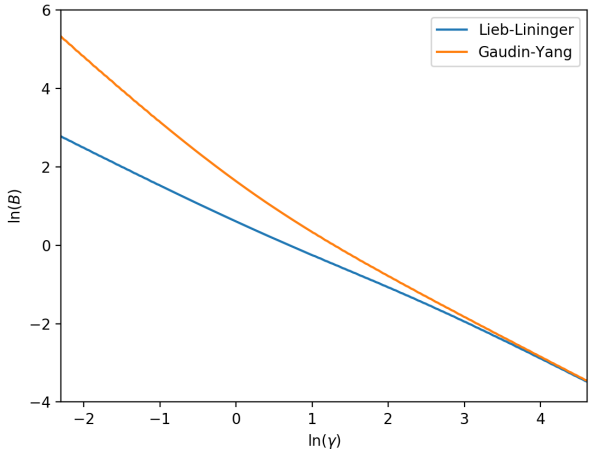

Figure 1.2: Logarithm of the cut-off of the pseudorapidities, B, vs the logarithm of the dimensionless coupling, γ, for the Gaudin–Yang (orange line) and Lieb–Liniger (blue line) models.

We plot in Fig. 1.2 the behaviour of the cut-off pseudorapidities B_B and B_F against the dimensionless coupling strength.

To further proceed with our studies, we find convenient to define a normalized density of pseudorapidities, denoted by $\tilde{f}(t)$, which reads:

$$\tilde{f}_B(t) = \frac{1}{4\pi}\frac{\gamma_B}{\lambda_B} f_B(B_B t)\,, \tag{1.38}$$

for the LL model, whereas for the GY model:

$$\tilde{f}_F(t) = \frac{1}{\pi}\frac{\gamma_F}{\lambda_F} f_F(B_F t)\,. \tag{1.39}$$

With these notations, Eqs. (1.30) and (1.33) become the condition of normalization, valid in both cases:

$$\int_{-1}^{1} \tilde{f}(t)\, dt = 1\,. \tag{1.40}$$

On the other hand, for the LL model Eqs. (1.29) and (1.31) become, respectively:

$$\tilde{f}_B(t) - \frac{\lambda_B}{\pi} \int_{-1}^{1} \frac{\tilde{f}_B(t')}{\lambda_B^2 + (t'-t)^2}\, dt' = \frac{1}{2\pi} \frac{\gamma_B}{\lambda_B}\,, \tag{1.41}$$

and:

$$e_B(\gamma_B) = \left(\frac{\gamma_B}{\lambda_B}\right)^2 \int_{-1}^{1} t^2 \tilde{f}_B(t)\, dt\,, \tag{1.42}$$

while for the GY model we get that Eqs (1.32) and (1.34) transform into:

$$\tilde{f}_F(t) + \frac{\lambda_F}{\pi} \int_{-1}^{1} \frac{\tilde{f}_F(t')}{\lambda_F^2 + (t'-t)^2}\, dt' = \frac{2}{\pi} \frac{\gamma_F}{\lambda_F}\,, \tag{1.43}$$

and for the dimensionless ground state energy density:

$$e_F(\gamma_F) = -\frac{\gamma_F^2}{4} + \left(\frac{\gamma_F}{\lambda_F}\right)^2 \int_{-1}^{1} t^2 \tilde{f}_F(t)\, dt\,. \tag{1.44}$$

We pause here to appreciate, once again, the similarities between Eqs. (1.41) and (1.43), with the Love's equations for the condenser problem in (1.25) and (1.24) [once $\mathcal{Z} = 1$ has been chosen and once normalized by $2V_1/\pi$], respectively. They are integral equations of the same type, but where the distance between the plates and the capacitance are substituted with the coupling strength parameter and the cut-off of the pseudorapidities of the systems. As stated previously, these equations cannot be solved analytically in the entire regime of interactions, and one has to rely on numerical approaches which can take several time for certain computation, above all when one needs the function $e(\gamma)$ for different couplings. With the aim of obtaining an expression for the ground state energy density valid in all regimes of interactions, we will now build an interpolation scheme in order to write the density of pseudorapidities as power series with coefficients determined from Chebyshev points. This will be the basis from which one can then construct an Hermite interpolation also for the function $e(\gamma)$, which has to be compared with the numerical solution, therefore used for quality checks.

1.2.3 CHEBYSHEV INTERPOLATION FOR THE SOLUTION

In order to find an analytical approximate expressions for the normalized solution to the Love's equations (1.41) and (1.43), we propose to use a Hermite interpolation via Chebyshev points. The Chebyshev polynomials in the closed interval: $x \in [-1, 1]$, are defined as:

$$T_n(x) = \cos\left[n \cos^{-1}(x)\right]\,, \qquad n \in \mathbb{N}\,.$$

The extrema of the Chebyshev polynomials are usually called as Chebyshev points and are important in approximation theory, since they are used as matching points for optimizing the polynomial interpolation [84]. The first M Chebyshev points for the polynomial $T_{2M}(x)$ are located at positions:

$$t_i = \cos\left(i\, \frac{\pi}{2M}\right)\,, \qquad i = 0, 1, 2, \ldots, M-1\,.$$

With Hermite interpolation we mean that in addition to interpolating the values of the function at the Chebyshev points, we are also interested in interpolating the derivatives of the function at, in general, some other points.

In our specific case, for a certain fixed γ, the interpolation procedure will be the same for the solutions of both kinds of Love's equations. Let us discuss our method: First of all, we notice that $\tilde{f}(t)$ is an even function in t, hence we can interpolate it with a polynomial with even powers of t. This property also allow us to consider only the interval: $t \in [0, 1]$. To find a good approximation, we selected the first M extrema greater or equal to 0 of the Chebyshev polynomial of degree $2M$. Then, in order to fix the values of the function at the interpolating points, we used the results of $\tilde{f}$ obtained numerically with the methods seen in the previous Section, in each t_i and the value of the derivatives of $\tilde{f}$ with respect to t for two of these points, far from $t = 1$. The two points where we fixed the derivatives, which we call Hermite points, have been chosen in such a way that the errors of the function are minimized in the intermediate range $t \in [0, 1]$. Finally, we approximated the solutions of the Love's equations as:

$$\tilde{f}(t) = \sum_{i=0}^{M+1} \tilde{C}_i t^{2i} \,, \tag{1.45}$$

where M coefficients are fixed for $\tilde{f}(t_i)$, while 2 other coefficients are fixed in the Hermite points for the derivatives of the weight functions.

We have chosen $M = 17$, therefore with 19 constraints, and the interpolation is then done with a polynomial of maximum degree of 36. One can easily go to more points in the interpolation scheme, but we checked that already from 16 the interpolation formula gives very good results, as we are going to see. In Fig. 1.3 we plotted the solutions of the Love's equations of the first and second kind on the left and right side plot respectively, with respect to the parameter γ, obtained by the Hermite interpolation described above. They are solutions of Eqs. (1.41) and (1.43), having Eq. (1.40) satisfied. Notice that the two weight functions coincide in the limit of strong interactions, and are simply constants equal to $1/2$, while in the weakly interacting limit the LL density of pseudorapidities follows the well known semi-circle law [53]. In Fig. 1.4 we plot the logarithm of the absolute value of the relative percentage errors of the interpolation scheme with respect to the numerical estimates, denoted by $\log_{10}\left|\Delta_{\%}\tilde{f}(t)\right|$.

1.2.4 CHEBYSHEV PARAMETRIZATION FOR THE MOMENTA

Also the momenta of the Love's integral equations are of fundamental importance. As we saw for the LL and GY model, for example, the second momenta of the weight functions of the models are related to the dimensionless ground state energy density, which in turn will determine other important properties of the system, such as the sound velocity, chemical potential and Luttinger parameter. With this aim, we proceed to find an analytical approximation via Chebyshev Hermite interpolation also for the second, fourth and sixth momenta of the Love's equations of both kinds, in a certain interval of the coupling constant. Let us denote the momenta by σ_i^B, for the Love's equation of the first kind, and σ_i^F, for the Love's equation of the second kind, with $i = 2$, 4 and 6, *i.e.*

$$\sigma_i = \int_{-1}^{1} t^i \, \tilde{f}(t) \, dt \,. \tag{1.46}$$

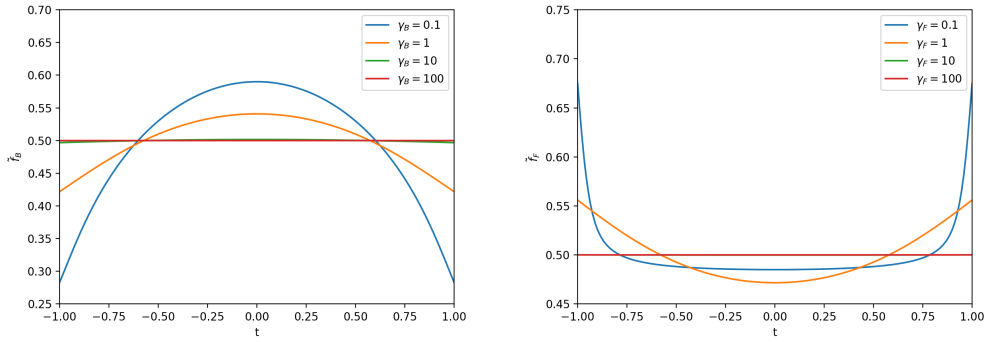

Figure 1.3: The weight function $\tilde{f}(t)$, normalized solution to the Love's equation of the first kind (left) and second kind (right), given by the Chebyshev interpolation, for different values of the interaction parameter γ. These figures are the results from using only 17(+2) points for the interpolation.

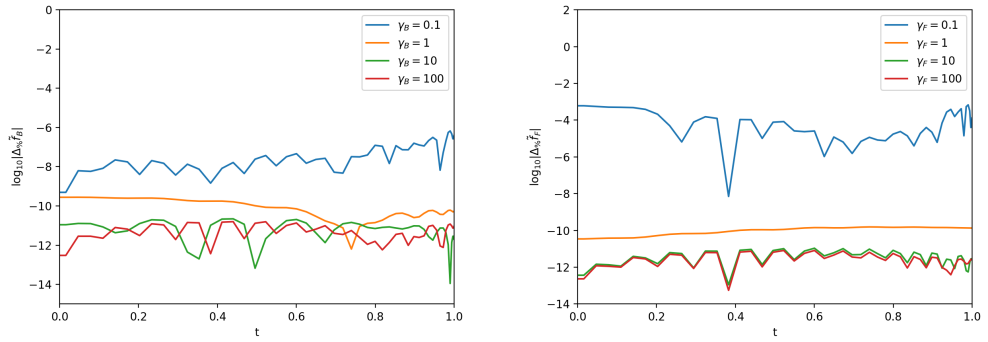

Figure 1.4: Logarithmic behaviour of the absolute value of the relative percentage error of the solutions of the Love's equation of the first kind (left) and the second kind (right) with respect to t, plotted at different values of the interaction parameter γ. The errors are evaluated from an interpolating scheme which uses only 17(+2) points.

In order to proceed with the Hermite interpolation via Chebyshev points, we need to introduce an auxiliary variable $\xi \in [-1, 1]$, related to γ as:

$$\gamma = 2\,\frac{A+\xi}{B-\xi}\,, \tag{1.47}$$

where A and B are numbers to be fixed once the interval of the coupling γ that has to be mapped between $[-1, 1]$ is fixed. As a first attempt, let us try to study an interpolation scheme for the range of coupling strengths: $\gamma \in [0.1, 100]$. Notice that going to lower values, $\gamma < 0.1$, is a very difficult task from the numerical solution point of view. With the methods at our hands, indeed, one does not reach convergence for very small values of the coupling, where instead we will rely on analytical exact equations, as we are going to see in a while.

In order to map the γ interval $[0.1, 100]$ into the ξ interval $[-1, 1]$, one has to choose: $A = \frac{3367}{3333}$ and $B = \frac{3467}{3333}$, which can be found from Eq. (1.47). In this case, since the momenta $\sigma_i(\xi)$ are not even functions of ξ, we will interpolate with both odd and even

powers and we will consider the set of points given by the maxima of the Chebyshev polynomials $T_M(\xi)$:

$$\xi_k = \cos(k\pi/M)\,, \qquad k = 0, 1, 2..., M\,, \tag{1.48}$$

in order to set the interpolation points. Then the Hermite interpolation is done by finding the coefficients $\tilde{C}_k$ of

$$\sigma_i(\xi) = \sum_{k=0}^{M+1} \tilde{C}^i_k \xi^k\,, \tag{1.49}$$

once we fix numerically the values of the momenta at the Chebyshev points, $\sigma_j(\xi_k)$, and once also the first derivatives of the momenta at the end points of the interval, $\sigma'_j(\xi = \pm 1)$, are fixed and obtained numerically.

Using only 17(+2) points, *i.e.* $M = 17$, we obtained the results reported in Fig. 1.5 for the second momentum function of the Love's integral equations of both kinds and the behaviour of the interpolation relative percentage error estimated with respect to the numerical solution. In Figs. 1.6 and 1.7 we plotted the behaviours of the fourth and sixth momenta for both kinds of the Love's equations, together with their relative percentage errors. In conclusion, this interpolation scheme allows to find expression for the second momenta with errors of about $10^{-2}\%$, while for the fourth and sixth momenta the errors accumulation is more evident, and one finds that the maximum relative percentage error of the Chebyshev parametrization is of about 5%.

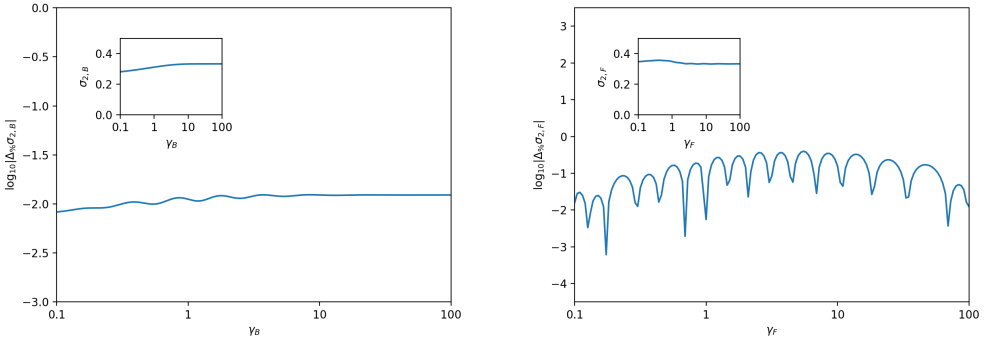

Figure 1.5: Logarithm of the absolute value of the percentage error for the second momentum function of the Love's equation of the first (left) and second kind (right) with respect to the coupling strength, γ, which is reported in log scale. The errors are obtained by comparing the results obtained via Chebyshev interpolation with the numerical outcomes. In the insets there are reported σ_2 vs γ in linear- log scale. These results are obtained from the Chebyshev Hermite interpolation scheme with $M = 17$.

In this explanatory example we have showed how to deal with the case: $\gamma \in [0.1, 100]$, but one may think to extend the interval on a wider range of couplings. Beside the problem of non-convergence of the numerical algorithm for very weak couplings, the final results for the momentum functions will not be outstandingly good. The relative percentage errors will run between $10^{-2}\%$ and 10%, making this rather simple interpolation procedure not really useful.

Here comes our intuition: What if we divide the space of coupling strength in three domains in each of which we rely on either numerical or analytical exact (if presents)

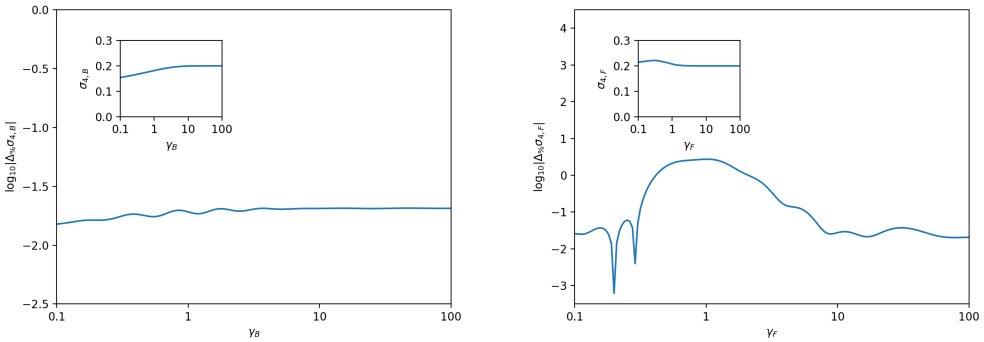

Figure 1.6: Logarithm of the absolute value of the percentage error for the fourth momentum function of the Love's equation of the first (left) and second kind (right) with respect to the coupling strength, γ, again reported in log scale. The errors are evaluated by comparing the results obtained via Chebyshev interpolation with the numerical outcomes. In the insets we report the behaviour of σ_4 vs γ in linear- log scale. These results are obtained from the Chebyshev Hermite interpolation scheme with $M = 17$.

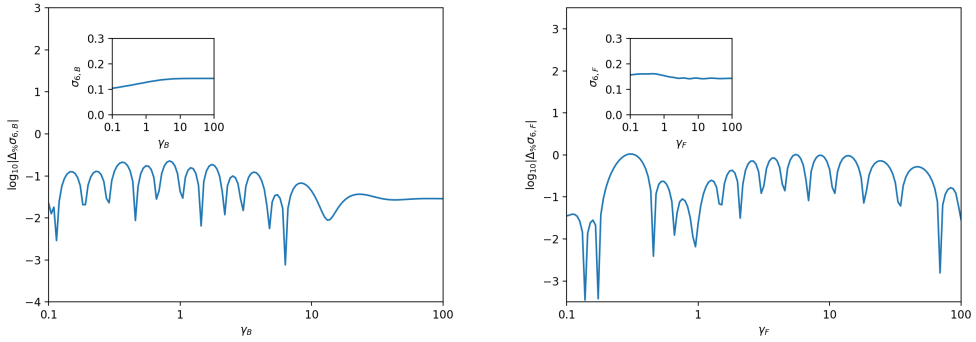

Figure 1.7: Logarithm of the absolute value of the percentage error for the sixth momentum function of the Love's equation of the first (left) and second kind (right) with respect to the coupling strength, γ, in log scale. As usual, the errors are computed by comparing the results obtained via Chebyshev interpolation with the numerical outcomes. In the insets there are reported σ_2 vs γ in linear- log scale. These results are obtained from the Chebyshev Hermite interpolation scheme with $M = 17$.

results? It is indeed well known in the literature [79, 80, 82, 85, 86] that there exist expressions valid in the weak and strong coupling regimes for the weight functions and the second momenta of Love's equations of both kinds. We will focus on the dimensionless energy density function of the LL model, which is related to the second momenta of the Love's equation of the first kind, as we have seen previously. The same approach could be extended to the Love's equation of the second kind, *i.e.* to the energy density function of the GY model. Our idea is then to rely on analytical expressions in the regime of weak couplings (where the numerical approach fails) and strong couplings, while we build the above mentioned Chebyshev Hermite interpolation scheme for $e_B(\gamma_B)$ in the intermediate region of interaction strengths. In order to get a smooth and complete form of the energy density function, we will need to first determine the optimal amplitudes of the three coupling regions, and then match the behaviour of $e_B(\gamma_B)$ and its first derivatives at the matching points of the different coupling regions.

1.3 CHEBYSHEV PARAMETRIZATION FOR THE $e_B(\gamma_B)$ FUNCTION

Coming back in discussing the LL model, exact expressions for the second momentum functions valid at high or low couplings are available in the literature. In the regime of weak interactions, the dimensionless energy density can be written as [86]:

$$\begin{aligned} e_B^w(\gamma_B) &= \gamma_B - \frac{4\gamma_B^{3/2}}{3\pi} + \left(\frac{1}{6} - \frac{1}{\pi^2}\right)\gamma_B^2 + \frac{3\zeta(3)-4}{8\pi^3}\gamma_B^{5/2} + \frac{3\zeta(3)-4}{24\pi^4}\gamma_B^3 + \\ &+ \frac{60\zeta(3) - 45\zeta(5) - 32}{1024\pi^5}\gamma_B^{7/2} + \frac{3[4\zeta(3) + 6\zeta(3)^2 - 15\zeta(5)]}{2048\pi^6}\gamma_B^4 + \\ &+ \frac{-4368\zeta(3) + 6048\zeta(3)^2 + 2520\zeta(5) - 8505\zeta(7) + 1024}{786432\pi^7}\gamma_B^{9/2} + \\ &+ O(\gamma_B^5)\,, \end{aligned} \tag{1.50}$$

where $\zeta(x)$ is the Riemann zeta function, and the superscript w in $e_B^w(\gamma_B)$ stands for "*weak*". Notice that at the lowest level we recover the result of Bogoliubov approximation: $e_B^{Bog}(\gamma_B) = \gamma_B$. By comparing the above analytical expression with the numerical results, we were able to fix the limit of the first region of the coupling strength (the weak coupling region) at:

$$\gamma_B^w = 0.33\,. \tag{1.51}$$

This was fixed by noting that at this value of the coupling, the absolute percentage error between the numerical estimate and the one obtained by the aforementioned power-series expansion in γ_B reaches a value of: $\Delta_{\%}(e_B(\gamma_B^w)) \simeq 1.55 \cdot 10^{-6}$, which is the minimum error value.

For strong couplings, *i.e.* large values of γ_B, there is a power-series of $1/\gamma_B$ which descries the behaviour of the energy density function for the LL model [82]:

$$e_B^s(\gamma_B) = \frac{\pi^2}{3} - \frac{4\pi^2}{3}\frac{1}{\gamma_B} + 4\pi^2\frac{1}{\gamma_B^2} + \left(\frac{32\pi^4}{45} - \frac{32\pi^2}{3}\right)\frac{1}{\gamma_B^3} + O(\gamma_B^{-4})\,, \tag{1.52}$$

where the superscript s in $e_B^s(\gamma_B)$ stands for "*strong*". Next we proceed in finding the upper limit of γ_B from which the analytical expression in Eq. (1.52) will be used in our three-range interpolation scheme. We fixed an upper value of:

$$\gamma_B^s = 1010\,, \tag{1.53}$$

by noting that an optimal, *i.e.* minimum, value of the error $\Delta_{\%}(e_B(\gamma_B^s)) \simeq 1.61 \cdot 10^{-6}$ evaluated between the numerical computation and the power-series result (1.52), is reached.

To further check the reliability of the coupling strength intervals between γ_B^w and γ_B^s, we computed also the errors between the derivatives with the respect to γ_B of the numerical and the analytical results of the energy density function. In particular, we found that the absolute percentage error is given by:
$\Delta_{\%}(\frac{de_B}{d\gamma_B}) \simeq 1.25 \cdot 10^{-7}$, for $\gamma_B = \gamma_B^w$, and:
$\Delta_{\%}(\frac{de_B}{d\gamma_B}) \simeq 1.40 \cdot 10^{-3}$, for $\gamma_B = \gamma_B^s$.

In the intermediate region of couplings, *i.e.* for $\gamma_B \in [\gamma_B^w, \gamma_B^s]$, we will build our Hermite interpolation scheme using Chebyshev points as we did previously in the example $\gamma_B \in$

$[0.1, 100]$. First of all we introduce the variable ξ which ranges in $[-1, 1]$, and is related to γ_B as stated in Eq. (1.47). From this equation, fixing $\xi = -1$ for $\gamma_B = \gamma_B^w$, and $\xi = 1$ for $\gamma_B = \gamma_B^s$, we find that the parameters A and B are equal to: $A = \frac{134363}{100967}$, and $B = \frac{101433}{100967}$. The mapping between ξ and γ_B is now completely defined and we can write the interpolation formula for the dimensionless ground state energy as:

$$e_B^i(\xi) = \sum_{k=0}^{M+1} C_k \xi^k \,, \tag{1.54}$$

where the superscript i stands for "*interpolation*". While M coefficients C_k are determined by fixing the values of $e_B(\xi)$ at the Chebyshev points (1.48) to be the numerical resulting values [which come from solving Eq. (1.42) using the interpolation scheme results for the density of pseudorapidities], the other two coefficients are fixed by requiring a continuity of the first order derivative of $e_B(\gamma_B)$ at the limiting region points γ_B^w and γ_B^s, making such an interpolation one of the Hermite kind.

Therefore, finally we can write a complete expression for the dimensionless ground state energy density function for the Lieb–Liniger model as:

$$e_B^{3r}(\gamma_B) = \begin{cases} e_B^w(\gamma_B) & \gamma_B < \gamma_B^w \\ e_B^i(\gamma_B) & \gamma_B \in [\gamma_B^w, \gamma_B^s] \\ e_B^s(\gamma_B) & \gamma_B > \gamma_B^s \end{cases} , \tag{1.55}$$

where the superscript $3r$ stands for "$three-ranges$". We stress that the remarkable feature of this expression is that it is an analytical estimate for $e_B(\gamma_B)$ for all values of γ_B, making very fast to immediately get a value for the ground state energy density function for a certain fixed γ_B. We refer to Appendix 1.1.A for the coefficients C_k of Eq. (1.54).

In Fig. 1.8 we report the behaviour of the ground state energy density function using $M = 17$ points, Eq. (1.55), for a certain range of couplings. The blue solid line is the $e_B^i(\gamma_B)$ function, while the orange and red dashed lines represent the analytical behaviour at weak (1.50) and strong (1.52) couplings, respectively. In the insets there are shown the matching of the functions and their first order derivatives around the limiting regions points.

Finally, in Fig. 1.9, we plotted the relative percentage errors of this procedure from using only $17(+2)$ interpolation points. The error of the interpolation is computed with respect to the numerical results coming from directly solving Eq. (1.42), together with Eqs. (1.41) and (1.40). Note that we report the relative percentage error behaviour only in the region: $\gamma_B \in [\gamma_B^w, \gamma_B^s]$, since outside these regions we rely on the analytical forms of the dimensionless ground state energy density, where we proved that they well describes the true numerical results.

Notice that the errors are surprisingly small, even though we are using only $M = 17$ for the interpolation scheme, and the error reaches a maximum of about $10^{-6}\%$ for weak couplings. This "three-range" interpolation procedure is then much better than the simple single-range one, that we saw in the previous section, for the case $\gamma_B \in [0.1, 100]$. With these vanishingly small percentage errors, we find safe to use our resulting formula (1.55) to compute interesting physical properties of the Lieb–Liniger model. We will focus on the calculation of the chemical potential, pressure, sound velocity and local two-particles correlation function. Other interesting applications, like finding black and grey solitons

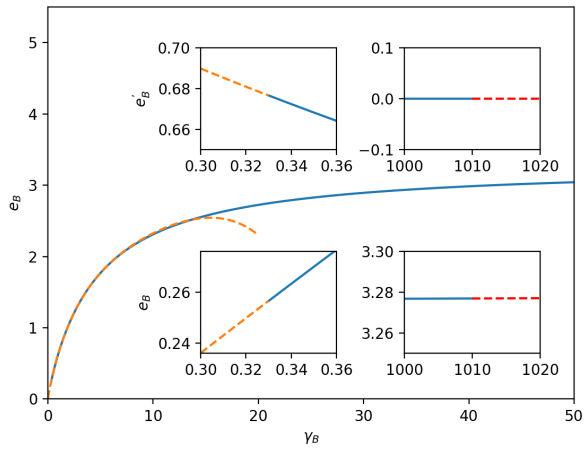

Figure 1.8: Dimensionless ground state energy density function $e_B^{3r}(\gamma_B)$. The blue solid line refers to the interpolation scheme results, while the orange dashed line to e_B^w, *i.e.* the power-series in γ_B valid for low values of coupling strengths, and finally the red dashed line to e_B^s, *i.e.* the power-series in $1/\gamma_B$ valid for strong interactions. In the main plot we can see that e_B^l becomes less reliable as γ_B increases, as we expect. In the lower-left inset and upper-left inset, we plot, respectively, the interpolation results and e_B^w and their derivatives around $\gamma_B = \gamma_B^w$. Instead, in the lower-right and upper-right inset, we plot, respectively, the interpolation results and e_B^s and their derivatives around $\gamma_B = \gamma_B^s$.

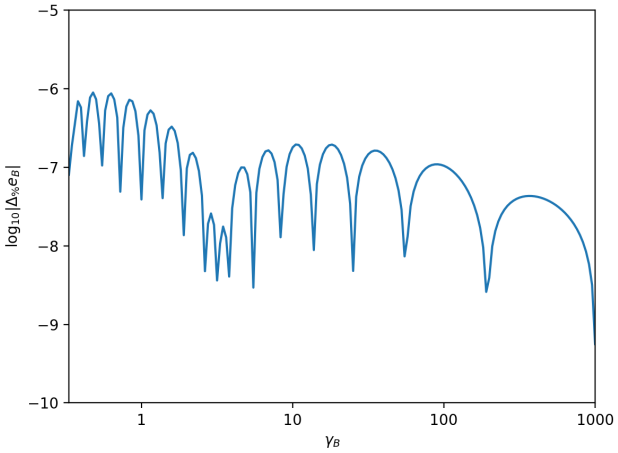

Figure 1.9: Logarithm of the absolute value of the percentage error of e_B^i, with the respect to the dimensionless coupling, $\gamma_B \in [\gamma_B^w, \gamma_B^s]$, which is reported in log scale. These are the results coming from using $17(+2)$ points for the interpolation.

solutions, or even the effects of a trapping potential on the density profile of the system, will be discussed in a subsequent Chapter.

Henceforth, for convenience, we will drop the subscript B after the interaction parameter γ.

1.3.1 APPLICATIONS ON INTERESTING PHYSICAL VARIABLES

As we already saw in Section 1.1.1, the dimensionless ground state energy density enters in a variety of expressions of physical variables. For example, the $e_B(\gamma)$ function and its derivatives, enter in the equations for the pressure, sound velocity and chemical potential, given by Eqs. (1.14), (1.15) and (1.16), respectively. From the results of the sound velocity, one could then determine the Luttinger parameter of the system, whose value can be used to determine in which range of interaction we are. In Figs. 1.10, 1.11 and 1.12, we report the results for the calculation of the aforementioned physical variables obtained from using $e_B^{3r}(\gamma)$. In dashed lines there are reported the analytical results for small and large values of interactions, where Eqs. (1.50) and (1.52) have been used for the energy density function in those regions.

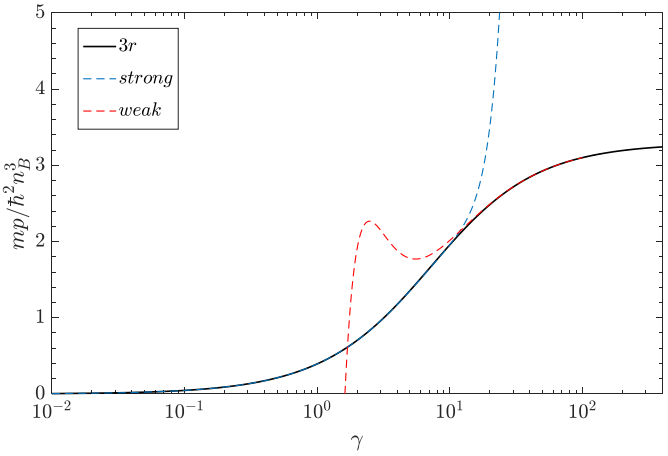

Figure 1.10: Dimensionless pressure function of the Lieb–Liniger Bose gas against the coupling strength γ. The black solid line has been obtained from using Eq. (1.55) in Eq. (1.14), while blue and red dashed lines are the low and high limits of the pressure function obtained from using the power series (1.50) and (1.52), respectively.

Finally let us discuss another application which concerns a correlation function of the Lieb–Liniger model which can be written in terms of the ground state energy density: The local two-particles correlation function. This correlator is defined as:

$$\frac{g_2(x,x')}{(n_B)^2} = \langle \Psi^\dagger(x)\Psi(x)\Psi^\dagger(x')\Psi(x')\rangle\,, \tag{1.56}$$

where we have indicated with $\Psi(x)$ the bosonic matter-field in second quantization formalism. Using the Hellmann–Feynman theorem, one can prove that there exists a relation between the diagonal part of the local two-particles correlation function, $g_2(0,0)$, and the dimensionless ground state energy density, which reads [60, 70, 87]:

$$\frac{g_2(0,0)}{(n_B)^2} = \frac{de_B(\gamma)}{d\gamma}\,. \tag{1.57}$$

We can then compute the function $g_2(0,0)$ by deriving with the respect to γ the results given by $e_B^{3r}(\gamma)$ of Eq. (1.55). In the inset of Fig. 1.13 we report the behaviour of $g_2(0,0)/(n_B)^2$ evaluated in this way, against the coupling strength. In the main plot we report the relative percentage error results coming from comparing the outcomes of

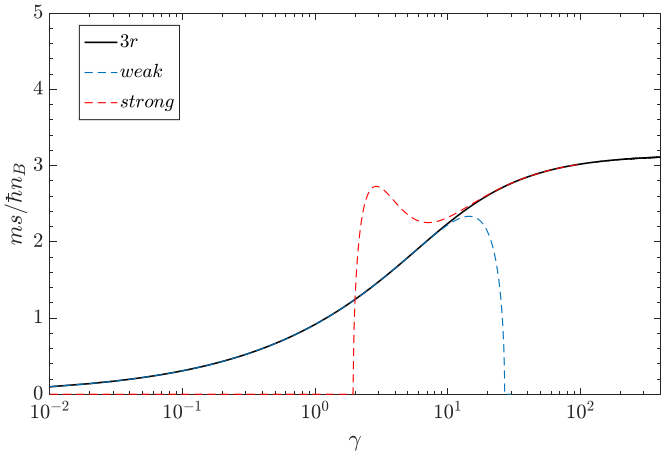

Figure 1.11: Dimensionless sound velocity of the Lieb–Liniger Bose gas against the coupling strength γ. The black solid line has been obtained from using Eq. (1.55) in Eq. (1.15) and taking the square root, while blue and red dashed lines are the low and high limits of the sound velocity function obtained from using the power series (1.50) and (1.52), respectively.

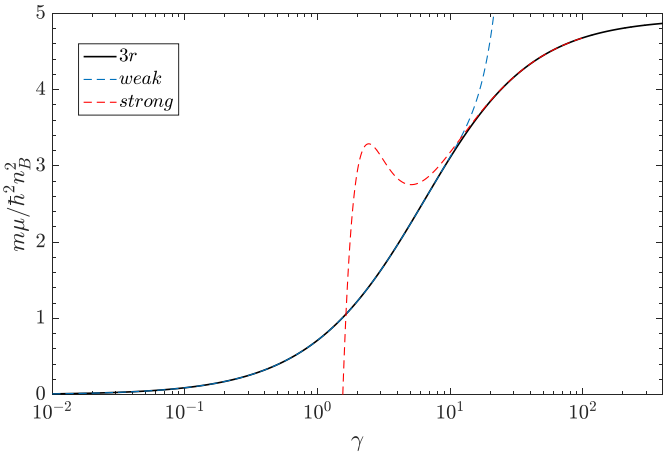

Figure 1.12: Dimensionless chemical potential of the Lieb–Liniger Bose gas against the coupling strength γ. Once again, the black solid line has been obtained from using Eq. (1.55) in Eq. (1.16), while blue and red dashed lines are the low and high limits of the sound velocity function obtained from using the power series (1.50) and (1.52), respectively.

$g_2(0,0)$ using $e^{3r}(\gamma)$ with the numerical exact one [*i.e.* the results obtained from calculating directly the ground state energy density from Eq. (1.42) and evaluating its first order derivative]. The maximum value of the relative percentage error is below $10^{-4}\%$, which is quite good.

Among the many interesting physical properties that one can study for an exactly solvable contact interacting many–body system (apart from those just discussed), we find that the characterization of ordering properties of the system has a relevant importance since it determines quantum coherence effects and occurrence of Bose–Einstein condensation phenomena in the system, or more generally it describes how particles occupy the available quantum states. For this reason, in the next Section we will discuss about deviations from off–diagonal long–range order in the Lieb–Liniger model at zero temperature.

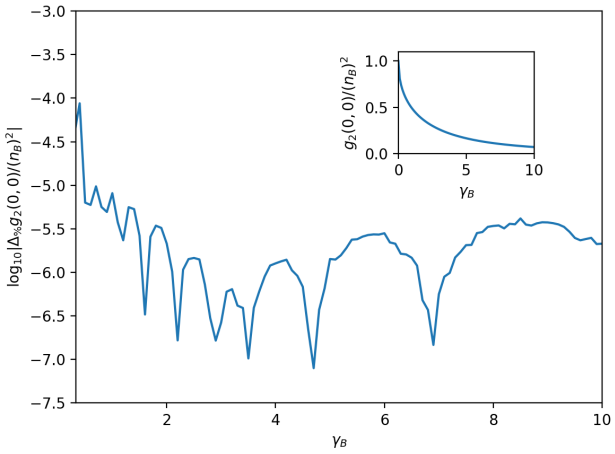

Figure 1.13: Logarithm of the absolute value of the relative percentage error of the computation of the dimensionless diagonal local two-particle correlation function for the Lieb–Liniger model, with respect to the dimensionless coupling, γ_B. The error is evaluated from comparing the results for $g_2(0,0)/(n_B)^2$ from using $e^{3r}(\gamma_B)$ with the numerical exact outcomes. In the inset there is shown the behaviour of the function $g_2(0,0)/(n_B)^2$ with respect to the dimensionless coupling, γ_B, obtained from using our interpolation scheme for the ground state energy density function.

1.4 ODLRO IN THE LIEB–LINIGER GAS

The Penrose–Onsager criterion for the presence of off–diagonal long–range order (ODLRO) is the cornerstone of the present understanding of quantum coherence and Bose–Einstein condensation (BEC) [7]. It is simply related to the occurrence of BEC and it is based on the study of the scaling with the number of particles of the eigenvalues of the one–body density matrix (1BDM) $\rho(x,y)$, defined as [18]:

$$\rho(x,y) = \langle \hat{\Psi}^\dagger(x)\hat{\Psi}(y)\rangle\,, \tag{1.58}$$

where $\hat{\Psi}^\dagger(x)$ is the field operator creating a particle at the point x. Denoting by λ_i the eigenvalues of this matrix, we have

$$\int dy\,\rho(x,y)\,\varphi_i(y) = \lambda_i\,\varphi_i(x)\,, \tag{1.59}$$

where the φ_i's are the corresponding eigenfunctions. There is ODLRO and BEC when the largest eigenvalue λ_0 scales as the total number of particles N of the system [7, 19]. The occurrence of ODLRO implies phase coherence, as shown by a simple argument due to Anderson [8] and reviewed in [9].

The Penrose–Onsager criterion relates, altogether, the occurrence of BEC and quantum coherence to the behaviour of correlation functions. Its power and elegance stem from the fact that it applies at zero and finite temperatures and as well in any dimensions, so that in Eqs. (1.58)-(1.59), the coordinates x, y may denote space vectors with D components, and we are going to deal with these cases in a subsequent Chapter. Moreover, the system may also be subjected to a generic one–body external potential, case which will be studied as well in a following Chapter.

When the system is homogeneous and the thermodynamic limit is taken in the usual way by keeping fixed the density $n \equiv N/L$, then $\rho(x,y)$ tends to the condensate density λ_0/L when $|x-y| \to \infty$ [18]. This definition makes transparent the analogy of the condensate fraction λ_0/N with the magnetization M in magnetic spin systems, where the analog of the 1BDM (1.58) is the correlation function $\langle S_i S_j \rangle$ which, in the homogeneous case, tends to M^2 for $|i-j| \to \infty$ (see, for instance, [59]).

Given that in presence of ODLRO the largest eigenvalue λ_0 scales as N, we can conveniently quantify deviations from ODLRO in terms of the exponent $\mathcal{C}$ of a scaling law as:

$$\lambda_0 \sim N^{\mathcal{C}} . \tag{1.60}$$

Clearly, when $\mathcal{C} = 1$ we are back to the ODLRO and BEC, according to the Penrose-Onsager criterion. On the other hand, when $\mathcal{C} = 0$, we are typically in a situation which is fermionic-like: think, for instance, at the ideal Fermi gas, where for all eigenvalues (including λ_0) we have $\lambda_i = 1$, in view of the Pauli principle. As additional example, consider a system made of two species of fermions with attractive interactions where there may be ODLRO but this manifests in the two-body density matrix, while for the scaling law of the eigenvalues of the 1BDM one still has $\mathcal{C} = 0$. Despite one can imagine more general, non-power-law, dependence of λ_0 on N, it is reasonable to assume a power-law form like the one introduced in Eq. (1.60). The explicit computations presented below on one–dimensional systems are in agreement with the definition (1.60).

One–dimensional quantum systems provide an ideal playground to investigate deviations from ODLRO since there is no BEC in the interacting case. In other words, one expects $\mathcal{C} = 1$ only for the 1D noninteracting Bose gas, which may be regarded, however, as a very delicate, if not pathological, limit. In the homogeneous case, in fact, any infinitesimal repulsive interaction, no matter how small, in 1D destroys ODLRO also at $T = 0$, unlike the $3D$ case. This means that, in 1D interacting systems, $\mathcal{C}$ must be strictly smaller than 1 for any finite value of the interaction. Therefore one may lead to conclude that no clear peak of the momentum distribution should be observed, also at $T = 0$, in experiments with ultracold atoms in one–dimensional confined geometries.

However, when $\mathcal{C}$ is close to 1, for finite N the ratio λ_0/N can be rather large (even though λ_0/N tends to 0 for $N \to \infty$). When this happens, we say that we are in presence of what we can refer to as a mesoscopic condensation at $T = 0$. With this we refer to a phenomenon that, for all practical purposes, can be considered as an ordinary condensation: *e.g.*, for $\mathcal{C} \approx 0.99$ and $N \approx 10^3$ one has $N^{\mathcal{C}}/N \approx 0.9$. Let us remark that $\mathcal{C}$ being close to 1 for small interactions gives reason to the fact that in the weakly interacting limit the mean-field description works reasonably well, despite the absence of a proper BEC.

Let us then proceed to identify and quantify deviations from ODLRO in 1D quantum systems at $T = 0$. We are interested in this subject of study because, first of all, the computation of correlation functions and 1BDM is a quite difficult and often formidable task. For 1D systems, however, the situation is generally better and a huge variety of techniques has been developed for this aim [63,72], ranging from bosonization [71] and density matrix renormalization group [88], to Bethe ansatz and integrability techniques [58,68]. Secondly, ultracold atoms provide an ideal setting to simulate different 1D quantum systems by acting on tunable external parameters [61, 63]. For instance, the coupling constant γ in

1D ultracold bosonic gases can be adjusted by tuning the transverse confinement of the waveguides in which the atoms are trapped [66], and in such an experiment one can explore both the regimes of small γ, as small as $10^{-4} - 10^{-3}$ (the weakly interacting limit), and large γ (the Tonks-Girardeau limit [67]), with numbers of particles N going from few tens to thousands, see the reviews [61–63].

1.4.1 ANALYTICAL PREDICTIONS FOR $\mathcal{C}$

A simple evaluation of the exponent $\mathcal{C}$ can be done using bosonization as follows. The eigenvalues λ_i and the orbitals $\varphi_i(x)$ in Eq. (1.59), for (1.3), are labeled by a quantum number which is evidently the momentum k. From translational invariance, we know that [18]:

$$\varphi_k(x) = \frac{1}{\sqrt{L}} e^{ikx} ,$$

and therefore λ_k simply equals the momentum distribution $n(k) = \langle \hat{\Psi}^\dagger(k)\hat{\Psi}(k)\rangle$, where the operator $\hat{\Psi}(k)$ is the Fourier transform of the field operator $\hat{\Psi}(x)$ [18]. It follows:

$$n(k) = \frac{L}{2\pi} \int_0^L dx\, \rho(x) e^{ikx} , \tag{1.61}$$

where, using translational invariance, we have set $y = 0$ and $\rho(x, 0) \equiv \rho(x)$. From Luttinger liquid theory for large x we have that $\rho(x) \propto x^{-1/2K}$ and therefore $n(k) \propto \frac{1}{k^{1-1/2K}}$ for $k \to 0$. The bosonization then gives the large distance behaviour of ρ, which then fixes the exponent $\mathcal{C}$. Indeed, since the smallest momentum is $k_{min} \propto 2\pi/L$ and $n_B = N/L$, one gets $\lambda_0 \propto N^{1-1/2K}$, *i*.e. finally:

$$\mathcal{C}(K) = 1 - \frac{1}{2K} . \tag{1.62}$$

Notice that $\mathcal{C}$ is then expected to depend on γ, *i*.e. on the ratio c_B/n_B, and not on c_B and n_B separately.

An accurate, high-precision check of such a prediction is not easy to obtain, since one should determine λ_0 as a function of N and then fit $\mathcal{C}$ from the scaling. It is clear that the larger is the maximum value of N considered, the better the estimate of $\mathcal{C}$, but from exact computations is not straightforward to reach large values of N, especially for intermediate values of γ. Of course, one could think to use the Bethe ansatz expression for the wavefunction of the ground state, but, in practice, even for small number of particles, such an expression is difficult to handle. One way to get around this difficulty consists, *e*.g., in using a numerical approach as ABACUS [89,90], in which the sum on the corresponding Bethe eigenfunctions can be efficiently truncated. In [91] such a method was used for the approximate computation of the 1BDM up to 150 particles and for any values of γ. In the following we introduce a new method based on an interpolation of the 1BDM between large and short distance asymptotic expansions, and which can be used to larger number of particles for all values of γ. Hereafter we present the results obtained with the interpolated $\rho(x)$ till $N = 10^3$ (there is however no major problem to extend such a computation to larger values of N). For $N = 10^3$ we found that the error in $\mathcal{C}$ is, *e*.g., at the fifth significant figure for $\gamma = 1$ and such an error can be further decreased since larger the value of N,

smaller the error in $\mathcal{C}$. Our results with $N = 10^3$ confirm that the $\mathcal{C}$ depends only on γ and not separately on n_B and c_B.

To conveniently set up such an interpolation formula we have built upon several known behaviors of the 1BDM $\rho(x)$ as a function of distance x, and in particular on its short-distance behaviour $\rho^{SD}(x)$ [87] and on the large-distance one, $\rho^{LD}(x)$ [92,93]. The limits of weak and strong interactions, valid for any values of x, have been extensively investigated [94–98] (see more Refs. in [61, 63]).

1.4.2 DENSITY MATRIX INTERPOLATION SCHEME AND ITS EIGENVALUES

Now we discuss, systematically, how to evaluate the one–body reduced density matrix for LL repulsive interacting bosons in a ring for an arbitrary number of particles in different limits for the coupling constant.

Strong coupling. Let us start by analysing the strong coupling case. At fixed and finite values of N and L, in the regime when $z = N\gamma \gg 1$, one can expand the Bethe eigenfunctions in inverse powers of z and then in this way getting for the 1BDM the asymptotic expansion [94]

$$\frac{\rho^{SI}(x)}{n_B} \;=\; \rho_N^{(0)}(x) + \frac{1}{N\gamma}\,\rho_N^{(1)}(x) + \mathcal{O}\left(\frac{1}{N\gamma}\right)^2 \;, \tag{1.63}$$

where $\rho_N^{(0)}$ and $\rho_N^{(1)}$ are expressed in terms of the determinant of some complex matrices (see the cited article for the details). For $\gamma \to \infty$ one obtains the well known Lenard's formula [99] for the 1BDM of a Tonks–Girardeau gas of N particles in a ring of circumference L:

$$\frac{\rho^{TG}(\alpha)}{n_B} \;=\; \frac{1}{N}\det\left[c_{n-m}(\alpha)\right]_{n,m\,=\,1,\ldots,N-1} \;, \tag{1.64}$$

where $\alpha = 2\pi x/L \in [0, 2\pi]$, and:

$$c_i(\alpha) \;=\; 2\delta_{i,0}\cos(\alpha) - \delta_{n,1} - \delta_{n,-1} + \frac{2}{\pi}\Big\{\frac{\sin\left[\alpha(i+1)/2\right]}{i+1} + \frac{\sin\left[\alpha(i-1)/2\right]}{i-1} + \\ + 2i\cos(\alpha/2)\sin(i\alpha/2)\Big\}\,,$$

where δ_{ab} is the Kronecker delta function.

Weak coupling. Let us now analyse the weak coupling regime. If the Luttinger parameter satisfies the inequality $K \ll 1$ (which, using the results of the previous Sections, simply means $\gamma \lesssim 0.1$), then we can write the 1BDM as [95]

$$\frac{\rho^{Bog}(x)}{n_B} \;=\; \exp\left\{-\frac{\hbar}{K\sqrt{m\mu}}\int_0^\infty dk\;\left[1-\cos(k\,x)\right](v_k)^2\right\} \;, \tag{1.65}$$

where:

$$v_k \;=\; \frac{1}{2}\left(\sqrt[4]{\frac{k^2}{k^2+4\hbar^2/m\mu}} - \sqrt[4]{\frac{k^2+4\hbar^2/m\mu}{k^2}}\right) \;,$$

and the chemical potential μ calculated via (1.16). Notice, however, that this expression for $\rho^{Bog}(x)$ is manifestly non–periodic in x: indeed it was originally derived only in the

thermodynamic limit where $L, N \to \infty$, as stressed in [95]. To solve this issue we decide to use a "brute force" approach, namely to evaluate $\rho^{Bog}(x)$ for $x \in [0, L/2]$ and to get all other values of the density matrix for $x \in [L/2, L]$ by "reflection" as:

$$\rho(x = L/2 + \delta) = \rho(x = L/2 - \delta) \ , \tag{1.66}$$

where $\delta \in (0, L/2]$, so that it also holds $\rho(x = L) = \rho(x = 0)$. This turns out to be a good way to approximate $\rho(x)$ since we are interested in studying how the largest eigenvalue of the 1BDM scales with respect to N when the number of particles becomes very large. This topic is discussed in more detail in the following.

Arbitrary coupling. To study the behaviour of the 1BDM for an arbitrary value of the coupling constant γ, we need to follow a different procedure since an explicit closed formula is not known. First of all, we can use known expressions for $\rho(x)$ at short distance and large distance which are valid for any γ.

- At short distances, *i.e.* $\mid x\, n_B \mid \ll 1$, in the thermodynamic limit the behaviour of the 1BDM is expressed by a Taylor expansion around the origin as [87]

$$\frac{\rho^{SD}(x)}{n_B} = 1 + \sum_{k=1}^{\infty} p_k \mid n_B\, x \mid^k , \tag{1.67}$$

  where p_k are the Taylor coefficients:

$$p_1 = 0 \ , \ p_2 = \frac{\gamma e'(\gamma) - e(\gamma)}{2} \ , \ p_3 = \frac{\gamma^2}{12} e'(\gamma) \ , \ \dots \tag{1.68}$$

  where for $e(\gamma)$ we can use either our Chebyshev interpolated formula, Eq. (1.55), or numerically solve the Lieb equations. In the following we will use only the first three coefficients of this expansion, so that the error associated to the truncation is of order $O(x^4)$. We have checked the validity of such an approximation for $\rho(x)$ at small distance by comparing the results of Eq. (1.67) versus the results for the density matrix at small and large values of the coupling (in particular for $\gamma = 0.01$ and $\gamma = 100$) from (1.65) and (1.63) and also versus the results coming from the Tonks–Girardeau expression (1.64). As a result of these checks, the relative percentage errors between the effective $\rho(x)$ at those γ for small x and its prediction from (1.67) are well below 1% for: $x\, n_B \lesssim 1$.

- At large distances, *i.e.* $x\, n_B \gg 1$, in the thermodynamic limit the 1BDM can be written as an infinite sum [93]

$$\frac{\rho^{LD}(x)}{n_B} = \sum_{m \geq 0} \frac{B_m \cos(2m k_F x)}{(n_B x)^{2m^2 K + 1/2K}} , \tag{1.69}$$

  where K is the Luttinger parameter, m is the mass of the particle, k_F is the Fermi–momentum and B_m are numerical coefficients which can be determined numerically once a value of γ is fixed. It is remarkable that one can get already a good approximation of the large distance behavior of the 1BDM by just taking the leading term of this sum, *i.e.* $m = 0$:

$$\frac{\rho^{LD}(x)}{n_B} = \frac{B_0}{(n_B x)^{1/2K}} \ . \tag{1.70}$$

Also is this case we have compared the values of the 1BDM obtained by this expression versus those relative to weak and strong coupling constants and also those coming from the Tonk–Girardeau limit: In all these cases, the relative percentage errors remain always below 1% for: $x\, n_B \gtrsim 20$.

Interpolation Formula. With both the expressions of the 1BDM at small and large distance under control, it is natural to think of an interpolation between these two limiting regimes in such a way to be able to compute the 1BDM at any value of the coupling constant γ. But what kind of interpolation? In order to select a valid interpolation scheme, the fact that we know $\rho(x)\ \forall x$, for large and small values of the coupling constant γ comes in help. Indeed, using eqs. (1.65) and (1.63) for $\gamma = 0.01$ and $\gamma = 100$ respectively, and matching their shapes with the ones obtained by implementing a "*cut–off interpolation*" with (1.67) and (1.70) for the same couplings, we are able to set up a very efficient interpolation formula for the density matrix at any distance x, and it reads:

$$\frac{\rho(x)}{n_B} = \frac{\rho^{SD}(x)}{n_B}\left[1-\tanh\left(\frac{x}{\alpha}\right)\right]\left[1-\tanh\left(\frac{\sqrt{x^3}}{\beta}\right)\right]+\frac{\rho^{LD}(x)}{n_B}\tanh\left(\frac{x}{\eta}\right)\tanh\left(\frac{x}{\omega}\right). \tag{1.71}$$

In this formula α, β, η and ω are coefficients that need to be fixed as γ and N vary. The best choice of these parameters are obtained by minimising the χ^2 in a chi-squared test made for small and large values of x of $\rho(x)$, since only in these regions we know how the density matrix behaves. Once these parameters are fixed, the values assumed by $\rho(x)$ in formula in (1.71) are in good agreement (*i.e.* relative percentage errors $\simeq 1\%$) with those obtained for large and small couplings at any x.

There is a further fact to take into account, namely that the interpolation formula (1.71) is not periodic in x with period L. Anyway, this problem can be solved using the same approach sketched before for the small coupling case implemented by Eq. (1.66). Once this aspect has also been cured, we are then able to compute numerically the density matrix $\rho(x)$ for a LL boson gas at any value of the coupling constant and its eigenvalues.

In order to study the eigenvalues of the density matrix of our system, we have first to build up the matrix itself. A way to construct a computationally efficient one–body reduced density matrix for a LL gas of bosons with periodic boundary conditions (PBC) is the following:

$$\rho(x) = \begin{pmatrix} \rho(0) & \rho(\delta) & \cdots & \rho(L) \\ \rho(\delta) & \rho(0) & & \vdots \\ \vdots & & \ddots & \vdots \\ \vdots & & & \\ & & & \rho(L-(N_I-1)\delta) \\ \rho(L) & \cdots & \rho(L-(N_I-1)\delta) & \rho(0) \end{pmatrix} \tag{1.72}$$

where we've implemented the translational invariance of the system and δ is the interval in terms of which we have divided the length of the system N_I times, *i.e.* $L = N_I\delta$. In this way $\rho(x)$ becomes a Toeplitz matrix having dimensions of $(N_I+1)\times(N_I+1)$. Hence

the number of its eigenvalues λ_i is equal to $N_I + 1$ and, being the occupation numbers of the system, we must require that

$$\sum_{i=0}^{N_I} \lambda_i \xrightarrow{N_I \to \infty} N \,. \tag{1.73}$$

The discrepancy of the sum from N at finite values of N_I provides an indication of how good is our approximation of the density matrix for a certain finite value of N_I. It is clear, though, that if we want to satisfy the condition (1.73) using as input our interpolation formula (1.71), we have to use a different normalization for the density matrix: Rather than having $\rho(x) \propto n_B$, as done so far, we must impose instead $\rho(x) \propto N/(1+N_I)$, which means that we have to multiply our previous $\rho(x)$ by $L/(1+N_I)$. In this way the sum of the eigenvalues of the 1BDM is equal to the number of particles and how λ_0 scales with respect to N is independent on the density of the system n_B.

In summary, the procedure that we have used to study the scaling behavior of the eigevalues of the density matrix consists of the following steps:

1. Once the particle number and the interaction parameter γ are fixed, find the optimal values for the coefficients in (1.71);
2. Enforce the periodicity of $\rho(x)$ via eq. (1.66), with the density matrix values given by the interpolation formula;
3. Build up the density matrix through eq. (1.72);
4. Compute the eigenvalues of this Toeplitz matrix, which can be done in two ways: Directly diagonalizing the matrix in (1.72) or evaluating the integral in (1.59) using $\varphi_0(x) = 1/\sqrt{L}$;
5. Finally, fit all the data for the largest eigenvalue λ_0 coming from using different values for the number of particles N, with a power law of the form

$$\lambda_0 = \mathcal{A} + \mathcal{B}\, N^{\mathcal{C}} \,, \tag{1.74}$$

in such a way that the coefficient of determination r^2 of the fitting is close to 1.

Here the possibility of varying N up to large values is important: *e.g.,* we get $\mathcal{C} = 0.8540614(5)$ for $\gamma = 1$. In the Tonks–Girardeau case we get $\mathcal{C} = 0.50001(3)$ in agreement with the exact result [99,100]. The Tonks–Girardeau result, $\mathcal{C} = 1/2$, confirms the different nature of (non-local) correlation functions of hard-core bosons and ideal fermions, and our outcomes illustrate the crossover from the ideal BEC case to the hard-core limit. Let us also mention that for $\gamma \sim 10^{-4} - 10^{-3}$, realistic for experimentally relevant situations, we get $\mathcal{C} \sim 0.99$, which is very close to 1. Our results for the behavior of $\mathcal{C}$ versus γ are summarised in Fig. 1.14.

Our results are strictly valid at $T = 0$ in the regime of large N and finite density, and they provide the zero temperature counterpart of the well known quasi-1D condensation phenomenon [62,101–103], signaled by a temperature below which the correlations decay on distances larger than the size of the system.

Our results implies that even in absence of BEC, if $\mathcal{C}$ is rather close to 1, one would observe a clear peak in the momentum distribution, especially because typically in experiments with $1D$ ultracold gases the number of particle is $N \sim 10^2 - 10^3$.

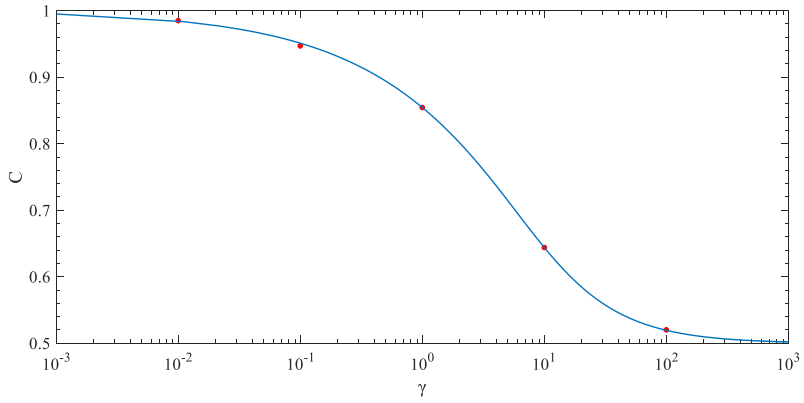

Figure 1.14: Exponent $\mathcal{C}$ *vs* γ: Bosonization predictions are reported in blue solid line while numerical results for $\gamma = 0.01, 0.1, 1, 10, 100$ are reported with red dots.

1.5 1D ANYONS

Let us now turn the attention to the case where the system is made of anyons rather than bosons. Some of the previous considerations will remain the same but there will be nevertheless some important changes in the properties of the gas. It is obvious the motivation of our interest in extending our studies also for anyon gases: One–dimensional anyonic gases, indeed, set a non-trivial interpolation between Bose and Fermi statistics, and have the further advantage to be Bethe solvable [105, 106] as we are going to discuss.

For a system of N anyons of mass m with contact interactions, their Schrödinger equation looks as the one for a Lieb–Liniger Bose gas:

$$H_B\,\psi_A(x_1,\dots,x_N) \;=\; E\,\psi_A(x_1,\dots,x_N)\,, \tag{1.75}$$

with H_B and c_B given in (1.2) and (1.6) respectively. This time, however, the solutions have to be found in the class of wavefunctions which exhibit a generalised symmetry under the exchange of any pair of particles:

$$\psi_A(\dots,x_i,x_{i+1},\dots) \;=\; e^{i\pi\kappa\,\mathrm{sgn}(x_{i+1}-x_i)}\psi_A(\dots,x_{i+1},x_i,\dots)\,, \tag{1.76}$$

where κ is the so called *statistical parameter* which runs from 0 (corresponding to bosons) to 1 (fermions). The boundary conditions on the wavefunctions has to be taken with care, because it is well known that periodic boundary conditions for anyons correspond to twisted boundary conditions for bosons and viceversa [77]. Since we want to compare the LL model for anyons with the one for bosons having implemented (1.9), we will impose the following twisted boundary conditions for the anyonic wavefunctions:

$$\psi_A(x_1,\dots,x_j+L,\dots,x_N) \;=\; e^{i\pi(1-\kappa)(N-1)-2i\pi(1-\kappa)(j-1)}\psi_A(x_1,\dots,x_j,\dots,x_N)\,, \tag{1.77}$$

where we have assumed that $0 < x_1 < x_2 < \cdots < x_N < L$.

As before, one can employ the coordinate Bethe ansatz to find the eigenfunctions of the system, with the final result expressed as [65]

$$\psi_A(x_1,\dots,x_N) \;=\; \mathcal{N}' e^{-i\frac{\pi\kappa}{2}\sum_{j<k} sgn(x_j-x_k)}\det[e^{ik_j x_m}]_{j,m=1,\dots,N} \prod_{1\le n<l\le N}[k_l-k_n-ic'\mathrm{sgn}(x_l-x_n)]\,, \tag{1.78}$$

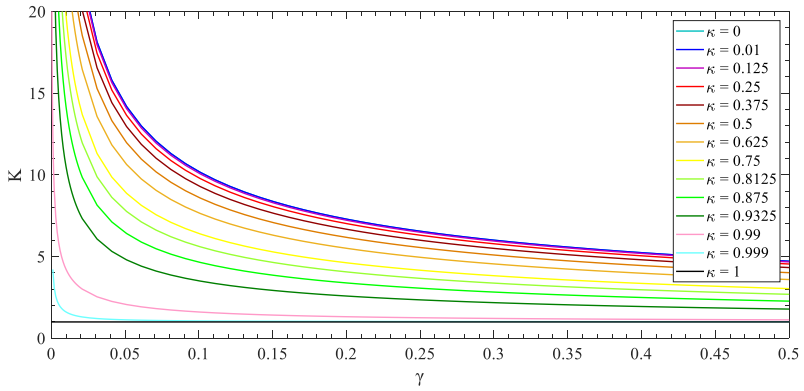

Figure 1.15: Luttinger parameter $K(\gamma)$ for LL anyons at different values of the statistical parameter. The results in the figure are obtained using (1.81) together with (1.82) and (1.83), for γ ranging from 10^{-3} to 0.5.

in which $\mathcal{N}'$ is a normalization factor while c' is the renormalized coupling constant given by:

$$c' \;=\; \frac{c_B}{\cos(\pi\kappa/2)}\,. \tag{1.79}$$

At $T = 0$, the only state which matter is the ground state, whose corresponding pseudomomenta k_j's can be determined from the Bethe equations (1.8) with $n_j = j$ and substituting c_B with c'. Following the same arguments of the previous Sections, we can then find the density of pseudorapidities of the system, its pressure, its sound velocity and so on and so forth. Their expression is similar to those of the Lieb–Liniger Bose gas, with the only differences that c_B has to be substituted by c' and γ by γ', where:

$$\gamma' \;=\; \frac{\gamma}{\cos(\pi\kappa/2)}\,. \tag{1.80}$$

Moreover, using the same steps as before, we can also compute the analogous Luttinger parameter (1.17) for the anyonic system. In this case, however, the task can be fulfilled more conveniently by using the approach suggested in [77]: Instead of computing the sound velocity through (1.15), one can prove in fact that:

$$K \;=\; \mathcal{Z}^2\,, \tag{1.81}$$

where $\mathcal{Z}$ is related to the concept of *dressed charge* $Z(\lambda)$. This quantity is expressed by:

$$\mathcal{Z} \;\equiv\; Z(q)\,, \tag{1.82}$$

where $Z(\lambda)$ is the solution of the linear integral equation:

$$Z(\lambda) \;=\; 1 + \frac{c'}{\pi}\int_{-q}^{q} \frac{Z(\mu)}{(c')^2 + (\lambda-\mu)^2}\,d\mu\,, \tag{1.83}$$

with q fixed by the Lieb equation for the density of state relative to the anyonic system. Adopting this approach, we are able to compute the Luttinger parameter for different values of the coupling constant γ' and the statistical parameter κ. The results are reported in Fig. 1.15 where we have rescaled all quantities in terms of γ. It is easy to see that Eqs. (1.18) and (1.19) hold for $\kappa = 0$, and similar expressions can be also found for $K_{\kappa\neq 0}$. Notice that the corresponding anyonic Luttinger parameter diverges for $\gamma' \to 0$, and goes to 1 for $\gamma' \to \infty$ (a result which is simple to check given all the previous definitions). Finally, for $\kappa = 1$, $K(\gamma) = 1, \forall\gamma$, *i.e.* the Luttinger parameter for free fermions is always equal to 1, as expected from Eq. (1.17), since: $s = v_F$.

1.5.1 HARD–CORE ANYONS

For anyons in homogeneous system of length L with twisted periodic boundary condition, a complete expression for the one–body density matrix is known only in the hard–core limit [107, 108], *i.e.* $\gamma' \to \infty$. The ground state wavefunction of the system can be written via a mapping between the hard-core anyons and fermions (see [100, 109]). For the boundary conditions (1.77), the density matrix for N anyons reads:

$$\rho^{\kappa}(x,y) \;=\; N \int_0^L dx_2 \cdots \int_0^L dx_N \, \psi_A^*(x,x_2,\ldots,x_N)\, \psi_A(y,x_2,\ldots,x_N)\,. \tag{1.84}$$

For a generic statistical parameter κ and N it is not periodic in x with period L, but instead satisfies:

$$\rho^{\kappa}(x+L) \;=\; e^{i\pi(1-\kappa)(N-1)}\, \rho^{\kappa}(x)\,. \tag{1.85}$$

This condition implies that we can make $\rho^{\kappa}(x)$ periodic if $N = 1 + \frac{2n}{\kappa}$, with $n \in \mathbb{N}$. Since N must be an integer, this forces the statistical parameter κ to be a rational number $\kappa = 2n/m$ with $n, m \in \mathbb{N}$. In this case we can build up the density matrix of the system using (1.72). As a consequence of this reasoning, notice that the number N of the particles of the system has to be always odd.

Using [108], the 1BDM in this case is given by:

$$\rho^{\kappa}(t) \;=\; \det\left[\phi^{\kappa}_{j,l}\right]_{j,l=1,\ldots,N-1}\;, \tag{1.86}$$

with $t \in [0, 2\pi]$, and:

$$\phi^{\kappa}_{j,l} \;=\; \frac{2}{\pi}\int_0^{2\pi} d\tau\, e^{i(j-l)\tau} A(\tau - t) \sin\left(\frac{\tau - t}{2}\right) \sin\left(\frac{\tau}{2}\right)\,, \tag{1.87}$$

where the function $A(\tau - t)$ satisfies:

$$A(\tau - t) \;=\; \begin{cases} e^{i\pi(1-\kappa)} & \text{for } \tau < t \\ 1 & \text{for } \tau > t \end{cases}\,. \tag{1.88}$$

At this point we can follow the procedures described in Section 1.1.4.2 to construct a matrix analogous to the one in eq. (1.72), this time being a Toeplitz matrix of complex numbers, with (1.86) that has to be normalized in order to fullfil (1.73). This can be done multiplying the right hand side of the formula of $\rho^{\kappa}(t)$ by $1/(1 + N_I)$. We computed the largest eigenvalue λ_0 of the density matrix for different values of the statistical parameter κ and number of particles N (up to $N = 241$), in such a way that aforementioned relations between the two are satisfied. By fitting the resulting λ_0's to a power law: $N^{\mathcal{C}(\kappa)}$, we obtained the results reported in Fig. 1.16, where we also check the validity of the prediction (1.93), which will be obtained later.

For $\kappa = 0$ (hard–core bosons) one has $\mathcal{C} = 1/2$, while for $\kappa = 1$ (fermions) one has $\mathcal{C} = 0$, and for all other values the curve monotonically interpolates as expected between $1/2$ and 0 when κ increases.

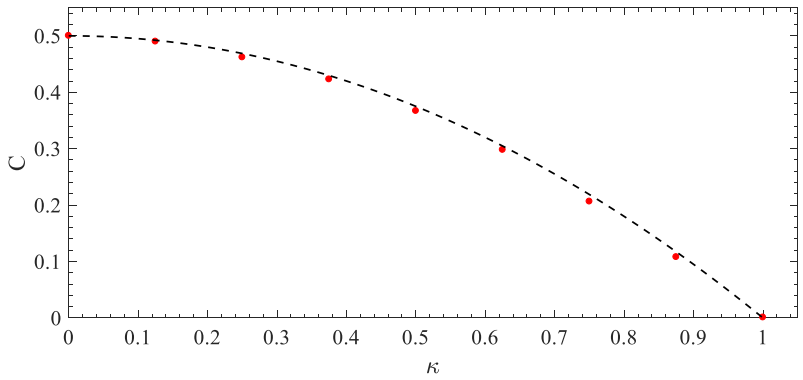

Figure 1.16: $\mathcal{C}$ vs. κ. Numerical values from the diagonalization of the 1BDM of hard-core anyons are reported in red dots, while bosonization results are represented in black dashed line: Excellent agreement is found, and the small differences between the two will disappear by including in the fit procedure also data coming from using higher number of particles (*i.e.* $N > 241$).

1.5.2 LIEB–LINIGER ANYONS

For a finite, soft-core energy coupling γ [110] one has the possibility to fully interpolate between $\mathcal{C} = 0$ and 1: When $\kappa = 0$, then the LL Bose gas at the coupling constant γ is retrieved. To study how $\mathcal{C}$ depends on γ and κ, we resort to the bosonization approach, in light of its successful estimates of $\mathcal{C}$ for the LL Bose gas. For LL anyons, $\rho(x)$ at large distances is given by [111]:

$$\rho(x) = n \sum_{m=-\infty}^{\infty} b_m \frac{e^{2i\left(m+\frac{\kappa}{2}\right)k_F x} e^{-\pi i\left(m+\frac{\kappa}{2}\right)\mathrm{sgn}(x)}}{\left[nL\sin(\pi x/L)\right]^{\left(m+\frac{\kappa}{2}\right)^2 2K+\frac{1}{2K}}}\,, \tag{1.89}$$

where b_m are non–universal amplitudes. From (1.89) one gets for small k and in the thermodynamic limit:

$$n(k) \propto n \sum_{m=-\infty}^{\infty} b_m \frac{(n\pi)^{-\frac{1}{2K}-\left(m+\frac{\kappa}{2}\right)^2 2K}}{\left[k+2k_F\left(m+\frac{\kappa}{2}\right)\right]^{1-\frac{1}{2K}-2K\left(m+\frac{\kappa}{2}\right)^2}}\,. \tag{1.90}$$

As a general consequence of this expression, the momentum distribution in general does not have the maximum at $k = 0$: There is in fact rather a shift due to the imaginary terms of the 1BDM [111]. In Fig. 1.17 we report the behaviour of the momentum distribution for an hard–core anyon gas made up of 153 particles, for different values of the statistical parameter. For growing κ the momentum distribution peak shifts to the left and it is always located around: $kL = -\kappa\pi(N-1)$, as we were expecting. For $\kappa = 0$ we get back the Fermi–Dirac distribution, as should happen.

The leading term of $n(k)$ is the one relative to $m = 0$ for any κ (for $\kappa = 1$, also the term $m = -1$ has the same power law behaviour). Hence, we conclude that: $\lambda_0 \propto N^{1-\frac{1}{2K}-\frac{K\kappa^2}{2}}$, and therefore the scaling coefficient $\mathcal{C}$ for the LL anyons is expressed by:

$$\mathcal{C}(\kappa, K) = 1 - \frac{1}{2K} - \frac{K\kappa^2}{2}\,. \tag{1.91}$$

For $\kappa = 0$ we obtain the result (1.62) for the LL Bose gas, while for $\kappa = 1$ (the fermionic limit) one gets $\mathcal{C} = 0$ since $K = 1$ for all γ, in both cases the correct values. In Fig.1.18

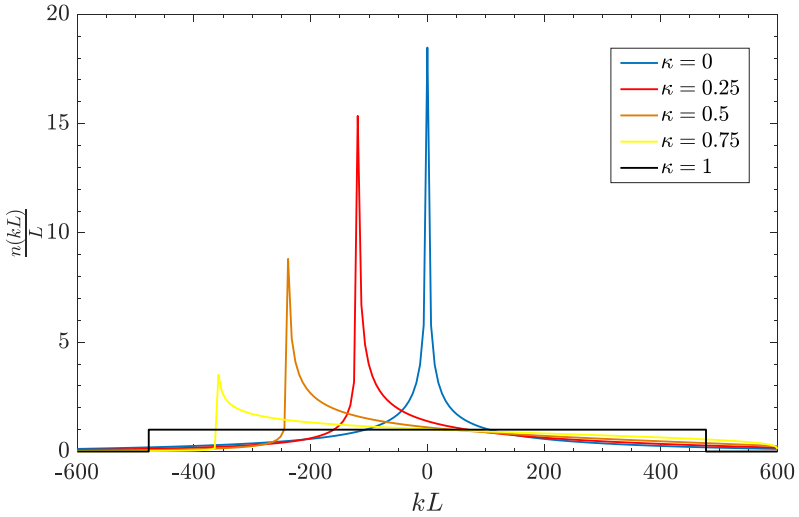

Figure 1.17: Dimensionless momentum distribution of hard–core anyons for different statistical parameter κ, evaluated using the exact expression for the 1BDM in Eq. (1.86), with $N = 153$. The momentum distribution peak shifts for growing κ, and it is located around: $kL = -\kappa\pi(N-1)$.

we plot $\mathcal{C}$ *vs* γ' for different κ: It is evident that $\mathcal{C}$ is always less than one, as it should be. In Fig.1.18 we do not report of course the negative values of $\mathcal{C}(\kappa)$ because there the expression (1.90) for the Fourier transform of the 1BDM is not valid since the power of $1/x$ in (1.89) is greater than 1. Let us underline that this time $\mathcal{C}$ is not a monotonic function of γ. Moreover, it is different from 0 only for γ larger than a critical value γ_c. This result shows once again the singularity related to the bosonic noninteracting limit. A plot of γ_c as a function of κ is shown in Fig.1.19, where it is also evident the non-monotonic behavior in κ, with a maximum around $\kappa \approx 0.9$.

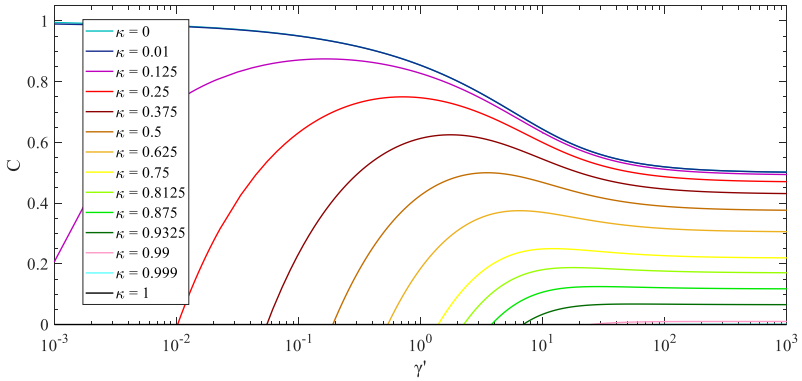

Figure 1.18: $\mathcal{C}$ for Lieb–Liniger anyons *vs* γ', for varying statistical parameter κ.

Let us focus on the hard–core limit: Using Eq. (1.89) for $K = 1$ one gets the following expression for the leading term of the 1BDM of hard–core anyons with contact interactions and PBC:

$$\rho(r) \simeq n\, b_0^1\, \frac{e^{i\kappa k_F r} e^{-\frac{\pi}{2} i\kappa \mathrm{sgn}(r)}}{\left[nL \sin(\pi r/L)\right]^{\frac{\kappa^2}{2}+\frac{1}{2}}}\,, \tag{1.92}$$

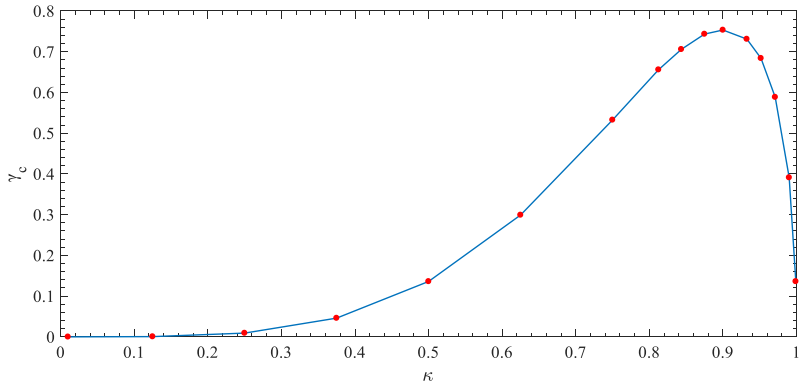

Figure 1.19: Critical value of γ, for which: $\mathcal{C}(\gamma_c) = 0$, as a function of the statistical parameter.

where $b_0^{K=1} = (2\pi)^{-\frac{1+\kappa^2}{4}} G\left(\frac{3+\kappa}{2}\right) G\left(\frac{3-\kappa}{2}\right)$ is the leading amplitude coefficient evaluated thanks to the Fisher-Hartwig conjecture [107, 108, 112]. Eq. (1.92) is valid for $\kappa < 1$, and in the limit of fermions ($\kappa = 1$) one has to take into account also the $m = -1$ term of Eq. (1.89). Therefore, for $\kappa < 1$, one firstly compute the Fourier transform of $\rho(r)$ writing $k = \frac{2\pi}{L} j$, and since the momentum distribution peak is located in: $k = -\kappa\left(k_F - \frac{\pi}{L}\right)$ [108], then in order to get an expression for the largest eigenvalue, one impose: $j = -\kappa\frac{N-1}{2}$. By doing so we get the following parameters for the scaling of the largest eigenvalue of the 1BDM of a anyonic Tonks–Girardeau gas:

$$\mathcal{C}(\kappa, K = 1) \;=\; \frac{1}{2}\left(1 - \kappa^2\right) , \tag{1.93}$$

whose behaviour is reported in Fig. 1.16 against the numerical estimated values for $\mathcal{C}$, and:

$$\begin{aligned}\mathcal{B}(\kappa, K = 1) \;=\; & G^2\left(\frac{3}{2} - \frac{\kappa}{2}\right) G^2\left(\frac{3}{2} + \frac{\kappa}{2}\right) \Gamma\left(\frac{1}{4}(1+\kappa)^2\right) \\ & \sec\left(\frac{\kappa^2\pi}{2}\right) \frac{\cos\left(\frac{\pi}{4}\kappa(2+\kappa)\right) + \sin\left(\frac{\pi}{4}\kappa(2+\kappa)\right)}{\sqrt{2}\,\Gamma\left(\frac{1}{4}(\kappa-3)(\kappa+1)\right)\Gamma\left(\frac{1}{2}(1+\kappa^2)\right)} ,\end{aligned} \tag{1.94}$$

for the prefactor in the scaling: $\lambda_0 \sim \mathcal{B}(\kappa, K) N^{\mathcal{C}(\kappa,K)}$. In Fig. 1.20 we show the comparison between the analytical prediction of Eq. (1.94) with our numerical results coming from the direct diagonalization of the 1BDM for a Tonks–Girardeau anyonic gas with periodic boundary conditions as given by Eq. (1.86).

For the case of $K \neq 1$ an analytical expression for the prefactors $b_0(K)$ is not known, therefore one has to rely on numerical methods such as the one proposed in [112].

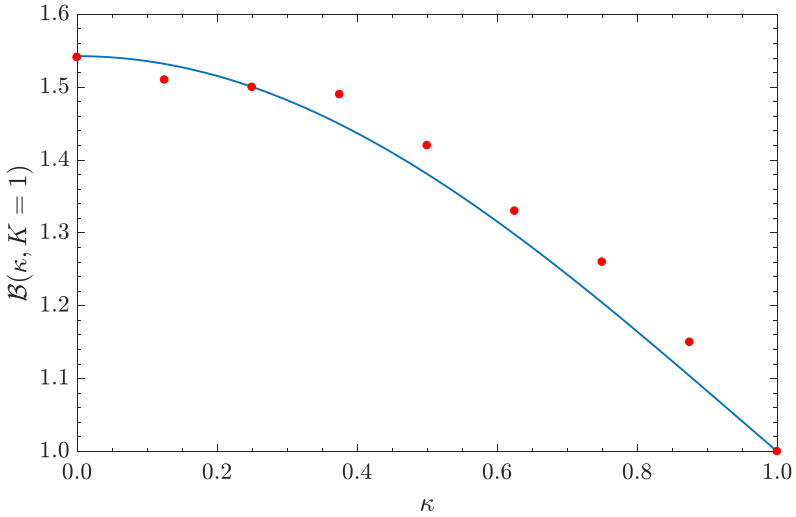

Figure 1.20: Numerical prefactor $\mathcal{B}$ for the scaling of the largest eigenvalue of the 1BDM for the hard–core anyon gas at different values of the statistical parameter κ. Numerical results (red dots) coming from the direct diagonalization, show fairly good agreement with the analytical results of Eq. (1.94) reported in blue solid line. The discrepancies between the numerics and analytical results, are due to the fact that for the direct diagonalization we arrived at a number of particles yet not too much large, $N = 241$, and therefore one should proceed with calculations to larger values of N.

APPENDIX

1.A LIST OF CHEBYSHEV COEFFICIENTS

The coefficients of the polynomial used for the proposed estimate of $e_B(\gamma_B)$ Table 1.1.

Table 1.1: Chebyshev coefficients of the proposed estimate of the dimensionless ground state energy, $e_B(\gamma_B)$, for $\gamma_B \in [0.33, 1010]$

C_0^2	1.25564891735811
C_1^2	1.3334354402797963
C_2^2	0.4860354572947664
C_3^2	−0.051984903874499507
C_4^2	0.04904971501072371
C_5^2	−0.001179939149676739
C_6^2	−0.016280129473601624
C_7^2	−0.013913030793665338
C_8^2	−0.008138388523767335
C_9^2	−0.0031840948669939976
C_{10}^2	−0.0017175103845688048
C_{11}^2	0.0002441458897381856
C_{12}^2	0.0029410626430055585
C_{13}^2	0.0014935402670359808
C_{14}^2	−0.001372595919119918
C_{15}^2	−0.0003179930299544679
C_{16}^2	0.0007911621229777253
C_{17}^2	−0.00003224993093157114
C_{18}^2	−0.0002418397997916562

2

ODLRO IN ONE–DIMENSIONAL TRAPPED SYSTEMS

Up to now we considered systems which were enclosed in a ring geometry, or more general they were studied in a homogeneous space, where translational invariance simplifies the theoretical approach. The study of the effect of external trapping potentials in coherence properties and, more general, in correlation functions of one–dimensional quantum systems is in general an interesting problem. The fascination comes from theoretical as well as experimental reasons. In experiments, such as with ultracold atoms, typically an harmonic trapping potential is used to confine the system giving more control on the apparatus. From the theoretical perspective instead, there are models which are known to be integrable, *i.e.* exactly solvable, in absence of an external potential but integrability is broken once inhomogeneities are introduced, as it happens for the Lieb–Liniger model [53]. This is not the case for two systems: Hard–core interacting particles and long–range $(x_i - x_j)^{-2}$ interacting systems, for which one can then study the effect of inhomogeneity in correlation properties. While we have seen that the Tonks–Girardeau gas describes system with contact hard–core interactions, the Calogero–Sutherland model (CSM) describes a system of long–range inverse squared interacting particles (either bosonic or fermionic) enclosed in a ring of circumference L, and it is known to be solvable via asymptotic Bethe ansatz [113–115]. The presence of an harmonic potential doesn't break the integrability of these systems and the ground state many–body wavefunction can be written in a simple product form [115–119]. Henceforth we will denote the long–range model in presence of harmonic trap as the Calogero model (CM).

In this Chapter we will characterize ODLRO properties of trapped systems, by studying the behaviour of the exponent $\mathcal{C}$ with which the largest eigenvalue of the 1BDM scales. The definition of ODLRO, related to the long–distance behaviours of the 1BDM, is of course valid both for homogeneous $[V(x) = 0]$ and inhomogeneous $[V(x) \neq 0]$ systems, as we already said. However, beside the inherent difficulty of dealing with interacting systems (which is also present for the homogeneous systems), the study of the large-N limit in presence of an external trapping potential shows several additional difficulties due to the lack of translational invariance. For instance: *i)* numerical methods working at small N may not be able to give the correct large-N behaviour; *ii)* the presence of the potential V may spoil the validity of methods which explicitly exploit the translational invariance of the system, such as the perturbative expansions done in terms of Feynman diagrams in momentum space; *iii)* for 1D systems, the external trapping potential typically also breaks the integrability of the homogeneous limit. Although one could derive useful information from approaches based on local density approximation, a complete study of the ODLRO behaviour of strongly correlated quantum systems in presence of external trapping potentials remains a challenging task.

We will begin our studies with the inhomogeneous Tonks–Girardeau Bose gas. Then we will extend our treatment to hard–core anyon gases and finally to the Calogero model,

which reduce to the TG gas when the coupling parameter λ equals the unity. We remark here that also in this Chapter we are assuming $T = 0$, while the study of ODLRO at finite temperatures will be dealt in a subsequent Chapter, focusing on homogeneous systems.

2.1 TRAPPED TONKS–GIRARDEAU GAS

Let us focus on the characterization of ODLRO in a Tonks–Girardeau gas at $T = 0$. The interest in such a study relies both on experimental and theoretical sides. Indeed, several progresses have been done in realising the TG gas with ultracold atoms and characterising its properties, such as momentum distribution and ground state energy [120,121]. For the TG gas, one can also study the confinement of induced resonances as well as the crossover to the so-called super-TG gas [122]; in presence of a periodic potential, one can also address the quantum phase transition which induces to a Mott insulating state [123,124]. From a theoretical perspective, one is able to work out analytical results for this system thanks to its integrability [58,68] and the Bose–Fermi equivalence [125,126], which permits to map the TG gas into a system of non–interacting spinless fermions. It is also known that for a trapped TG gas one can write a closed expression for the 1BDM [127]. For all these reasons there is a broad interest in the study of correlation functions of the TG gas in different potentials, such as harmonic traps [100, 128–133], optical lattices [134–140], disordered potentials [141–143], or also of the super-TG state [144–148] (see [149] for additional references). The effects of an harmonic confinement was studied also for hard-core anyons, whose limit of vanishing statistical parameter gives the TG gas [150, 151].

In presence of a trapping potential, there are two ways in which one can take the large-N limit: *a)* increasing N and at the same time varying the parameters of the external potential V (*e.g.*, the harmonic oscillator length for the harmonic potential) in such a way to keep fixed the density at the center of the trap, for instance; *b)* or fixing the parameters of the external potential V and simply increasing N. It turns out that the scaling of the largest eigenvalue of the 1BDM is the same in both cases.

The influence of a trapping potential on an interacting system was studied by a renormalization group approach in [152], where the effects of the trap inhomogeneity on the critical behaviour can be cast in the form of a trap-size scaling and used this to characterize trapped systems undergoing quantum phase transitions [153]. The TG gas does not at variance exhibit phase transitions and our goal is to study the effects at zero temperature of the varying trapping potential increasing the particle number or fixing the density at the center of the trap.

2.1.1 ONE–BODY DENSITY MATRIX

As we already know, in the limit of infinite coupling, the Lieb–Liniger model reduces to a system of N impenetrable bosons of mass m called the Tonks–Girardeau gas. It is described by the Schrödinger equation [67]

$$H\,\psi(x_1,\ldots,x_N) \;=\; E\,\psi(x_1,\ldots,x_N)\,, \tag{2.1}$$

where the Hamiltonian is written as a sum of single–particle Hamiltonians:

$$H = \sum_{i=1}^{N} \left[-\frac{\hbar^2}{2m}\frac{\partial^2}{\partial x_i^2} + V(x_i) \right] . \tag{2.2}$$

In (2.1) the many–body wavefunctions ψ are symmetric in the exchange of two coordinates due to the bosonic statistics, although they vanish when two arguments have the same value for the hard–core interactions:

$$\psi|_{x_i=x_j} \,=\, 0\,, \quad \forall i \neq j = 1, \ldots, N. \tag{2.3}$$

The many–body wavefunctions of the system can then be written in a Slater determinant form by adding sign functions to ensure the correct symmetry under coordinate exchange:

$$\psi(x_1, \ldots, x_N) \,=\, \frac{1}{\sqrt{N!}} \det\left[\phi_k(x_l)\right]_{\substack{k=0,\ldots,N-1,\\ l=1,\ldots,N}} \prod_{1\leq i<j\leq N} \mathrm{sgn}(x_i - x_j)\,. \tag{2.4}$$

This is the content of the well known Fermi–Bose equivalence [125, 126], where $\phi_k(x)$ denotes the k-th eigenfunction of the single–particle Schrödinger equation ($k = 0, \ldots, N-1$):

$$\left[-\frac{\hbar^2}{2m}\frac{d^2}{dx^2} + V(x) \right] \phi_k(x) \,=\, \varepsilon_k \phi_k(x)\,, \tag{2.5}$$

and ε_k is the corresponding single–particle energy.

We recall that the Hermitian 1BDM $\rho(x, y)$ of the 1D quantum gas is defined as:

$$\rho(x, y) \,=\, N \int \prod_{i=2}^{N} dx_i \; \psi^*(x, x_2, \ldots, x_N)\, \psi(y, x_2, \ldots, x_N)\,. \tag{2.6}$$

In the following, the integrals are meant to be between $-\infty$ and $+\infty$ each time that their extremes are not explicitly written.

The solutions of the eigenvalue equation for the 1BDM, *i.e.* Eq. (1.59), involve the natural orbitals $\varphi_j(x)$: They represent the effective single–particle states of the system, while the $\phi_k(x)$ can be viewed as the natural orbitals for the ideal fermionic gas [154]. The natural orbitals are chosen to be orthonormal, $\int dx\, \varphi_i^*(x)\varphi_j(x) \,=\, \delta_{ij}$. The occupation numbers of the levels j, expressed by λ_j, satisfy the normalization condition:

$$\sum_j \lambda_j \,=\, N\,, \tag{2.7}$$

that is a consequence of $\int dx\; \rho(x, x) \,=\, N$. Substituting Eq. (2.4) into Eq. (2.6) and expanding the Slater determinants along the first column, we obtain:

$$\rho(x, y) \,=\, \frac{1}{(N-1)!} \sum_{i,j=0}^{N-1} (-1)^{i+j}\, \phi_i(y)\, \phi_j^*(x) \int dx_2 \ldots \int dx_N \det[f_k(x_r)]_{\substack{k=0,\ldots,N-1, k\neq i\\ r=2,\ldots,N}} \times \det[g_l(x_r)]_{\substack{l=0,\ldots,N-1, l\neq j\\ r=2,\ldots,N}}\,, \tag{2.8}$$

where $f_k(x_r) = \phi_k(x_r)\,\mathrm{sign}(x - x_r)$, $g_l(x_r) = \phi_l^*(x_r)\,\mathrm{sign}(y - x_r)$, with the index $k \neq i$ in the first determinant while $l \neq j$ in the second. It is worth to recall *Andréief formula* (see [155] for a nice recent historical note):

$$\int dx_1 \cdots \int dx_N \det[f_j(x_k)]_{j,k=1}^N \det[g_j(x_k)]_{j,k=1}^N = N! \det\left[\int dx\ f_j(x) g_k(x)\right]_{j,k=1,\ldots N}, \tag{2.9}$$

to transform the product of two determinants in Eq. (2.8) into the determinant of the product. It follows:

$$\rho(x,y) = \sum_{i,j=0}^{N-1} (-1)^{i+j}\, \phi_i(y)\, \phi_j^*(x) \det\left[\int dt\ f_k(t) g_l(t)\right]_{k\neq i, l\neq j}. \tag{2.10}$$

We then substitute back in Eq. (2.10) the form for the functions f_k and g_l in terms of the single–particle wavefunctions ϕ_k which are solutions of Eq. (2.5). Assuming $x > y$, and using the orthonormality condition $\int dt\, \phi_l(t)\, \phi_k^*(t) = \delta_{k,l}$, we obtain a compact form for the 1BDM of a TG gas in a generic external potential $V(x)$, which reads:

$$\rho(x,y) = \sum_{i,j=0}^{N-1} (-1)^{i+j}\, \phi_i(y)\, \phi_j^*(x) \det\left[\delta_{k,l} - 2\int_y^x dt\, \phi_l(t)\, \phi_k^*(t)\right]_{k\neq i, l\neq j}. \tag{2.11}$$

Consider now the matrix P with entries $P_{ij} = \delta_{i,j} - 2\int_y^x dt\, \phi_j(t)\, \phi_i^*(t)$, for $i, j = 0, \ldots, N-1$. From Cramer theorem, one can check that Eq. (2.11) is actually equivalent to [127]

$$\rho(x,y) = \det(P) \sum_{i,j=0}^{N-1} \phi_i^*(x)\, [P^{-1}]_{ji}\, \phi_j(y), \tag{2.12}$$

having again assumed $x > y$ without loss of generality.

In the following, for numerical computations involving the 1BDM, we find simpler to use its expression given in Eq. (2.11), which does not require explicitly the inverse of the matrix P. This expression also provides a non-trivial check of the large-N limit derived in [156] as we are now going to illustrate.

2.1.2 SCALING OF λ_0 AND THE MOMENTUM DISTRIBUTION PEAK

In this Section we derive our predictions for the scaling of the largest eigenvalue of the 1BDM and the momentum distribution peak of a TG gas in a generic external potential by using Conformal Field Theory (CFT) within a semiclassical framework. In this Section we consider a generic trapping potential, assuming that its single–particle wavefunctions $\phi_j(x)$ and its natural orbitals $\varphi_j(x)$ decay fast enough at large distances.

ONE–BODY DENSITY MATRIX IN THE SEMICLASSICAL (CFT) LIMIT

In the recent article [156], Brun and Dubail studied the large distance behaviour of the 1BDM of a TG gas in a generic trapping potential and in the semiclassical limit $\hbar \to 0$, by using CFT arguments coming from a previous analysis [157]. The results of [156] were then extended in [158] to study the large distance behaviour of correlation functions of a Lieb–Liniger gas in a trap for arbitrary values of the coupling strength. Let us first briefly

remind the framework and the main results of [156]. The semiclassical limit for the TG gas considered in [156] is defined as:

$$\hbar \to 0, \qquad \text{with } m,\ V(x),\ \mu \text{ fixed}, \tag{2.13}$$

where μ is the chemical potential. In the limit (2.13), the inhomogeneous particle density can be obtained exactly within a local density approximation as:

$$\rho(x) \;=\; \frac{1}{\pi\hbar}\sqrt{2m\,[\mu - V(x)]}. \tag{2.14}$$

In the following we denote by x_1 and x_2 (with $x_2 > x_1$) the two solutions of the equation $\mu - V(x) = 0$ and we assume that these are the only two solutions of this equation. For $x > x_2$ or $x < x_1$, the gas density is zero and the latter is effectively confined in a spatial region $x \in [x_1, x_2]$. The total number of particles in the system is:

$$N \;=\; \int_{x_1}^{x_2} \rho(x)\,dx \;=\; \frac{1}{\pi\hbar}\int_{x_1}^{x_2} \sqrt{2m\,[\mu - V(x)]}\,dx\,. \tag{2.15}$$

It follows that the $\hbar \to 0$ limit is actually the thermodynamic limit $N \to \infty$ and this gives rise to the Thomas-Fermi approximation [70]. To keep track of the leading N-dependence in the limit (2.13), it is sufficient to observe that Eq. (2.15) implies:

$$N\hbar = \text{const}, \tag{2.16}$$

i.e. $N = O(\hbar^{-1})$. The main result of [156] is an expression for the 1BDM of the TG gas in Eq. (2.11) in the limit (2.13) that is valid as long as $|x-y|\rho_{\max} \gg 1$, where $\rho_{\max}$ is the maximum density in the trap. Such an expression is:

$$\rho_{\rm cft}(\tilde{x},\tilde{y}) \;=\; \sqrt{\frac{m}{2\hbar\widetilde{L}}}\,\frac{|C|^2\left|\sin\left(\frac{\pi\widetilde{x}}{\widetilde{L}}\right)\right|^{\frac{1}{4}}\left|\sin\left(\frac{\pi\widetilde{y}}{\widetilde{L}}\right)\right|^{\frac{1}{4}}}{\left|\sin\left(\frac{\pi}{\widetilde{L}}\frac{\widetilde{x}-\widetilde{y}}{2}\right)\right|^{\frac{1}{2}}\left|\sin\left(\frac{\pi}{\widetilde{L}}\frac{\widetilde{x}+\widetilde{y}}{2}\right)\right|^{\frac{1}{2}}}\,, \tag{2.17}$$

where $|C|^2$ is a numerical coefficient which can be expressed in terms of Barnes function $G(z)$ as $|C|^2 = \frac{G^4(3/2)}{\sqrt{2\pi}}$, $\widetilde{L}$ is the time needed by a signal travelling with velocity v to cover the interval $[x_1, x_2]$. The signal velocity $v(x)$ depends on the position x as:

$$v(x) \;=\; \sqrt{\frac{2}{m}\,[\mu - V(x)]}\,. \tag{2.18}$$

One has then:

$$\widetilde{L} \;=\; \int_{x_1}^{x_2} \frac{du}{v(u)}\,. \tag{2.19}$$

In Eq. (2.17) $\widetilde{x}(x)$ represents the time needed to a signal emitted in x_1, with velocity (2.18), to reach x, *i.e.*

$$\widetilde{x}(x) \;=\; \int_{x_1}^{x} \frac{du}{v(u)}\,. \tag{2.20}$$

It should be noticed that in the limit (2.13) the condition $|x-y|\rho_{\max} \gg 1$ is satisfied up to distances $|x-y| = O(N^{-1})$. To analyse Eq. (1.59) in the $\hbar \to 0$ limit, we can then safely replace $\rho(x,y)$ with Eq. (2.17) and restrict the integration domain to $y \in [x_1, x_2]$.

Changing integration variable to $\tilde{y}(y)$ through Eq. (2.20), we obtain the semiclassical limit of Eq. (1.59) for the largest eigenvalue of the 1BDM:

$$\int_0^{\tilde{L}} d\tilde{y}\; w(\tilde{y})\rho_{\rm cft}(\tilde{x},\tilde{y})\varphi_0(\tilde{y}) = \lambda_0\varphi_0(\tilde{x}), \tag{2.21}$$

with $w(\tilde{y}) = 1/v(y(\tilde{y}))$. Plugging Eq. (2.17) into Eq. (2.21), we observe that the limit $\hbar \to 0$ is consistent on both sides only if $\lambda_0 = O(\hbar^{-1/2})$. Recalling Eq. (2.16), immediately we conclude that for $N \to \infty$:

$$\lambda_0 \sim \mathcal{B}N^{1/2}, \tag{2.22}$$

namely, in the limit (2.13), the scaling exponent $\mathcal{C}$ is $1/2$, independently on the shape of the potential. The result $\mathcal{C} = 1/2$, was found in the specific case of the harmonic potential in [100]. Notice that it also the value that we found in the homogeneous case. The numerical prefactor $\mathcal{B}$, is instead potential-dependent and can be also explicitly calculated; we will provide an example of such a computation in a following Section.

Eq. (2.22) is intended to describe the scaling of λ_0 when the shape of the external potential is fixed and one varies N. We will see from numerical calculations that the same power–law scaling for λ_0 emerges when the density of particles in the external potential is fixed and one varies N and the trap parameters accordingly.

MOMENTUM DISTRIBUTION

We consider here the small–k behaviour of the momentum distribution $n(k)$ of the system, defined as:

$$n(k) \;=\; \frac{1}{2\pi}\int dx \int dy\, \rho(x,y) e^{-i\,k\,(x-y)}\,. \tag{2.23}$$

From (1.59) we have the eigendecomposition:

$$\rho(x,y) \;=\; \sum_j \lambda_j\, \varphi_j^*(y)\, \varphi_j(x)\,, \tag{2.24}$$

that, substituted into Eq. (3.5), gives:

$$n(k) \;=\; \sum_j \lambda_j |\tilde{\varphi}_j(k)|^2\,, \tag{2.25}$$

where $\tilde{\varphi}_j(k) = \frac{1}{\sqrt{2\pi}}\int dx\; e^{-ikx}\varphi_j(x)$ is the Fourier transform of the natural orbital. Hence the zero-momentum distribution $n_{\rm peak} \equiv n(k=0)$ is given by:

$$n_{\rm peak} \;=\; \frac{1}{2\pi}\sum_j \lambda_j\, M_j\,. \tag{2.26}$$

where the quantities $M_j \equiv |\int dx\; \varphi_j(x)|^2$ involve the natural orbitals.

Notice that $\rho(x,y) = \rho(-x,-y)$ if the trapping potential $V(x)$ is an even function, therefore in such a case the natural orbitals can be chosen to have definite parity. It turns out that they have the same parity as the single–particle wavefunctions, *i.e.* $\varphi_j(-x) = (-1)^j\varphi_j(x)$. Then the sum in Eq. (2.26) is restricted only to even j. For even j the integrals form a decreasing sequence:

$$M_0 \;>\; M_2 \;>\; M_4 \;>\; \dots\,, \tag{2.27}$$

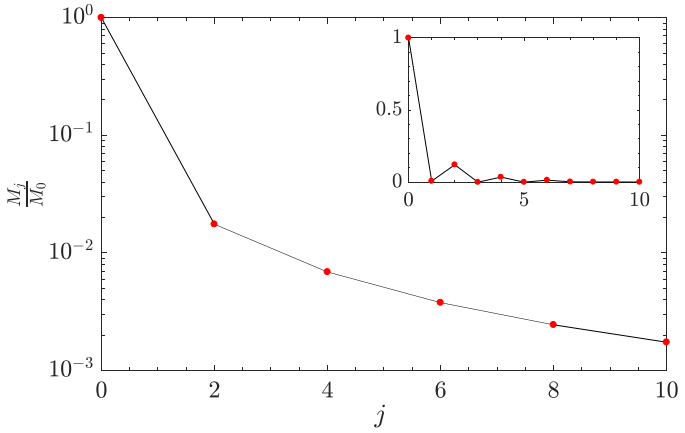

Figure 2.1: Ratio M_j/M_0 *vs* j, for the x^4 potential with $N = 25$, for the first 10 even values of j. The plot is in log–scale. In the inset there is found the same ratio evaluated for the half harmonic oscillator, for every j, with $N = 25$ in linear–scale.

where the $j = 0$ term is typically an order of magnitude greater than $j = 2$, which is in turn an order of magnitude greater than $j = 4$ term and so on (from hereafter the differences are not that big, but there is still an ordering). In Fig. 2.1 we plot, as an example, the ratios $\frac{M_j}{M_0}$ for the quartic potential and even values of $j = 2, 4, \ldots$. In the inset there is the plot done for the half harmonic oscillator for every j (note the different scales of the two plots). From these figures one can argue that the ordering in (2.27) is indeed valid.

To further support this argument, we have also performed an analysis of the coefficients $c_{i,j}$ entering the expansion of the natural orbitals in terms of the single–particle eigenfunctions:

$$\varphi_i(x) \;=\; \sum_j c_{i,j}\,\phi_j(x). \tag{2.28}$$

Since both the sets are orthonormal, the coefficients above have to satisfy:

$$\sum_j |c_{i,j}|^2 \;=\; 1\,. \tag{2.29}$$

In Fig. 2.2 we plot, as an example, the results for the square of the absolute value of the first Fourier coefficients weighting the first 20 eigenfunctions for the $V(x) \propto x^4$ potential.

We conclude that one can write:

$$n_{\rm peak} \;\approx\; \frac{\lambda_0}{2\pi} M_0\,. \tag{2.30}$$

SCALING LAWS

In this Section we aim to determine a relation between the scaling of the largest eigenvalue of the 1BDM and the momentum distribution peak. For this purpose, we have studied the behaviour of the natural orbitals $\varphi_j(x)$ for a variety of potentials, including the (even) power–law potentials $V(x) \propto x^{2n}$ and the (non-even) half harmonic potential $V_{hho}(x)$ defined by $V_{hho}(x) \propto x^2$ for $x > 0$ and $V_{hho}(x) = \infty$ for $x \leq 0$. Due to their normalization, the natural orbitals converge for large values of N to certain functions when the position coordinate x is rescaled by a quantity which depends on (and scale with) N.

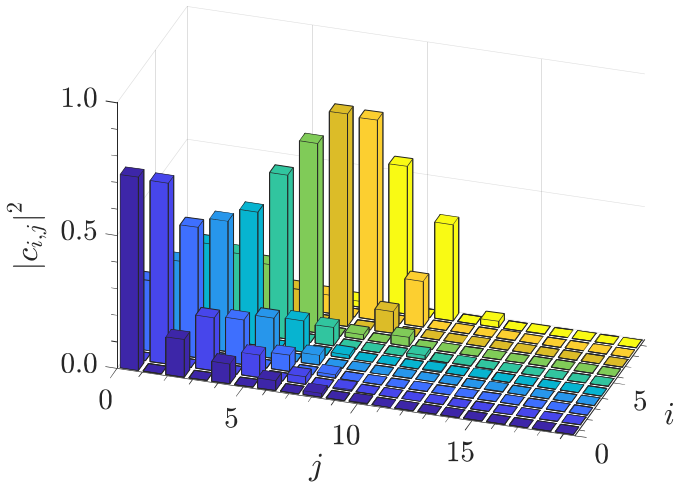

Figure 2.2: First 10 absolute value squared Fourier coefficients $c_{i,j}$ from (2.28) weighting the first 20 eigenfunctions for the x^4 potential case, *i.e.* $i = 0, \ldots, 9$ and $j = 0, \ldots, 19$ ($N = 8$). We have explicitly checked that (2.29) is satisfied up to 1% error.

More precisely, we start by rescaling the position coordinate x in terms of a unit length ξ as:

$$\eta \equiv \frac{x}{\xi}\,. \tag{2.31}$$

We then define the dimensionless ground state natural orbital $\hat{\varphi}_0(\eta)$ such that:

$$\int |\hat{\varphi}_0(\eta)|^2 \, d\eta = 1. \tag{2.32}$$

It follows that $\hat{\varphi}_0(\eta) \equiv \varphi_0(x)\,\sqrt{\xi}$. We denote by β the exponent with which $\hat{\varphi}_0(\eta)$ scales with $\hbar$, *i.e.* $\hat{\varphi}_0(\eta) \sim \hbar^{-\beta}$; in the semiclassical limit this is equivalent (see Eq. (2.16)) to:

$$\hat{\varphi}_0(\eta) \sim N^{\beta}\,. \tag{2.33}$$

We have verified that, plotting $\hat{\varphi}_0(\eta)/N^{\beta}$ as a function of $\eta N^{2\beta}$, for $N \to \infty$ the curves converge to a smooth function. In Fig. 2.3 we plot $\hat{\varphi}_0(\eta)/N^{\beta}$ with respect to $\eta N^{2\beta}$, for the cases of the harmonic potential (top plot) and quartic potential (bottom plot) for different values of the particles number. The convergence to a limiting curve for large N is evident from the figures.

We can also similarly define the dimensionless momentum distribution n_{peak}/ξ and the exponent γ of its scaling with N (or equivalently $\hbar^{-1}$):

$$\frac{n_{\text{peak}}}{\xi} \sim N^{\gamma}. \tag{2.34}$$

From Eq. (2.33), it should be clear that $\int d\eta\, \hat{\varphi}_0(\eta)$ must scale as $N^{-\beta}$ for large N, in such a way that the normalization condition in Eq. (2.32) continues to hold. In other words, the support of the function $\hat{\varphi}_0(\eta)$ should scale as $N^{-2\beta}$ (see again Fig. 2.3). From Eqs. (2.30) and (2.22) we conclude:

$$\frac{n_{\text{peak}}}{\xi} \sim N^{1/2\,-\,2\,\beta}\,. \tag{2.35}$$

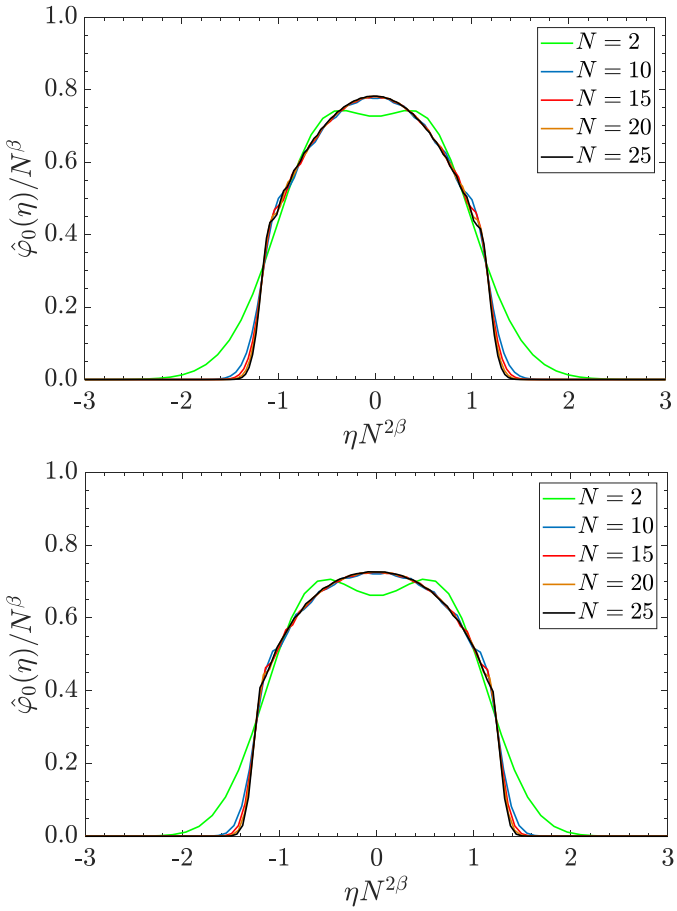

Figure 2.3: $\hat{\varphi}_0(\eta)/N^\beta$ *vs* $\eta N^{2\beta}$ for the harmonic potential ($n = 1$) on the top, and the quartic potential ($n = 2$) on the bottom. From the external curve towards the center of both figures, we consider $N = 2, 10, 15, 20, 25$.

In particular, from Eq. (2.35) it follows a scaling law among the exponents γ (defined in Eq. (2.34)), β (defined in Eq. (2.33)) and $\mathcal{C}$ (given in Eq. (1.62)):

$$\gamma + 2\beta = \mathcal{C}\,. \tag{2.36}$$

We will present a numerical check of these results , in particular the scaling law (2.36) for polynomial potentials $V(x) = \Lambda x^{2n}$ with different values of n. Moreover we will try to get a prediction for γ and β for such external trapping potentials. For the harmonic potential ($n = 1$), from analytical calculations it is already known [100, 135] that $\mathcal{C} = \frac{1}{2}$, $\beta = -\frac{1}{4}$ and $\gamma = 1$, which indeed satisfy both Eq. (2.22) and Eq. (2.36).

2.1.3 RESULTS FOR POWER LAW POTENTIALS

In the previous Section, we have derived an expression for the 1BDM of a TG gas in a generic external potential which leads to Eq. (2.11). In the following, we are going to study the scaling with the particle number of the 1BDM maximum eigenvalue λ_0. For simplicity, we are going to analyse a TG gas at zero temperature trapped by a potential of the form:

$$V(x) = \Lambda\, x^{2n}, \tag{2.37}$$

with n a positive integer and Λ a positive coefficient.

Substituting Eq. (2.37) into Eq. (2.5), one gets a single–particle Hamiltonian with discrete spectrum, and in particular:

$$\left(-\frac{\hbar^2}{2m}\frac{\partial^2}{\partial x^2}+\Lambda\, x^{2n}\right)\phi_k(x) \;=\; \varepsilon_k\phi_k(x)\,, \tag{2.38}$$

for $k = 0,\ldots,N-1$. It is useful to introduce a length scale ξ through:

$$\xi=\left(\frac{\hbar^2 b_n}{m\Lambda}\right)^{\frac{1}{2(n+1)}}\,, \tag{2.39}$$

where b_n is a numerical constant that we will fix later. Analogously we define the energy scale $\epsilon \equiv \hbar^2/(m\xi^2)$ and $\eta = \frac{x}{\xi}$ [see Eq. (2.31)] and then rewrite the single–particle Schrödinger equation as:

$$\left[-\frac{1}{2}\frac{\partial^2}{\partial\eta^2}+b_n\,\eta^{2n}\right]\hat{\phi}_k(\eta) \;=\; \frac{\varepsilon_k}{\epsilon}\hat{\phi}_k(\eta)\,. \tag{2.40}$$

To evaluate the 1BDM it is needed to determine the single–particle wavefunctions, solutions of Eq. (2.40), and substitute their expressions into Eq. (2.11). The exact analytical solution of the Schrödinger equation (2.40) is available only for two cases: $n = 1$ and $n = \infty$ that correspond to the harmonic potential and the hard wall, respectively. For intermediate values of n, one has to rely either on numerical methods or semiclassical WKB approximation and, as a matter of fact, we have implemented both methods.

We used the lowest order WKB approximation, WKB_0 according to the notation of [159]. One gets then the following estimate for the energy levels of the potential (2.37) directly from the Bohr–Sommerfeld quantization condition:

$$\varepsilon_k^{wkb} \;=\; \left[\sqrt{\frac{\pi}{2m}}\,\frac{\Gamma\left(\frac{3}{2}+\frac{1}{2n}\right)}{\Gamma\left(1+\frac{1}{2n}\right)}\,\hbar\,\Lambda^{1/2n}\right]^{\frac{2n}{n+1}}\left(k+\frac{1}{2}\right)^{\frac{2n}{n+1}}\,, \tag{2.41}$$

where $\Gamma(z)$ is the Euler Gamma function. From Eq. (2.39), recalling the definition of the length scale ξ, we obtain:

$$\epsilon \;=\; \left[\frac{\hbar}{\sqrt{m}}\left(\frac{\Lambda}{b_n}\right)^{\frac{1}{2n}}\right]^{\frac{2n}{n+1}}\,. \tag{2.42}$$

We choose then b_n in Eq. (2.39) in such a way that the energy scale in Eq. (2.42) matches with the first factor of Eq. (2.41), namely:

$$b_n \;=\; \left[\sqrt{\frac{2}{\pi}}\,\frac{\Gamma\left(1+\frac{1}{2n}\right)}{\Gamma\left(\frac{3}{2}+\frac{1}{2n}\right)}\right]^{2n}\,. \tag{2.43}$$

We have checked (2.41) for different values of n, comparing the semiclassical results with numerical outcomes obtained with the routine `Chebfun` [160] (and also with direct diagonalization of the single–particle Hamiltonian). As one can see from Tab. 2.1 and as expected, the WKB formula (Eq. (2.41)) approaches the numerical results in the limit of large k (apart of course the harmonic potential case where it is exact). The WKB approximation also provides a form for the single–particle wavefunctions $\hat{\phi}_k(\eta)$ along the full real

	$n=2$		$n=3$		$n=4$	
k	ε_k^{wkb}	ε_k^{num}	ε_k^{wkb}	ε_k^{num}	ε_k^{wkb}	ε_k^{num}
0	0.397	0.485	0.353	0.505	0.330	0.530
1	1.717	1.739	1.837	1.915	1.913	2.059
2	3.393	3.412	3.953	4.006	4.332	4.435
3	5.314	5.329	6.548	6.593	7.421	7.509
4	7.429	7.442	9.546	9.586	11.09	11.17
5	9.708	9.720	12.89	12.93	15.30	15.37
6	12.13	12.14	16.57	16.61	19.98	20.05
7	14.68	14.69	20.54	20.57	25.12	25.19
8	17.35	17.35	24.78	24.81	30.69	30.75
9	20.12	20.13	29.28	29.31	36.67	36.73
10	22.99	23.00	34.02	34.05	43.04	43.10

Table 2.1: Semiclassical energy levels obtained from (2.41) and the corresponding numerical results for ε_k for $n = 2, 3, 4$ and $V(\eta) = b_n\,\eta^{2n}$, with b_n fixed by (2.43). Energies are in units of ϵ.

line. Near the turning points of the potential, one has to use a standard Airy function approximation.

Since the WKB approximation works better for higher energy levels, as one may check comparing the differences $\varepsilon_k^{wkb} - \varepsilon_k^{num}$ for different values of k, we expect that the value of $\mathcal{C}^{wkb}$ may be be different from the one obtained by numerically computing the single–particle wavefunctions if N is not very large. Moreover, since the ground state and first excited states energies computed with the WKB method, for $n \neq 1$, are smaller than the one computed numerically, we expect that the WKB ground state will be more populated by the particles with respect to the exact occupation. Therefore a larger value of $\mathcal{C}^{wkb}$ may be obtained for the values of N we consider ($N \lesssim 30$), which is indeed what we find below.

After determining the single–particle wavefunctions either numerically or within the WKB approximation, we have generated the 1BDM (2.11) for the potentials in Eq. (2.37). For $n = 1$ and $n = \infty$ exact form of the wavefunctions are of course available and the task simplifies. Finally, we are left with the eigenvalue problem:

$$\int \rho(x,y)\,\varphi_j(y)\,dy \;=\; \lambda_j\,\varphi_j(x)\,, \tag{2.44}$$

that we have solved by discretizing the integral; for finite n, for instance, one can employ a Gauss–Hermite quadrature [83] (see Appendix 2.2.A for the details). To be sure that the method works accurately for different potentials and particles number, we have verified whether the results converge increasing the number of nodes (points) of the quadrature.

We are interested in the study of deviations from ODLRO and therefore we focus our attention on the behaviour of λ_0 for different number of particles in the system. To

characterise and quantify these deviations in the TG gas, we have fitted the large N asymptotic of the maximum eigenvalue of the 1BDM with a power–law [100]:

$$\lambda_0 \,=\, \mathcal{A} + \mathcal{B}\, N^{\mathcal{C}} + \frac{\mathcal{D}}{N^{\mathcal{E}}}\,, \tag{2.45}$$

where in principle all the parameters $\mathcal{A}, \ldots, \mathcal{E}$ are potential-dependent (*i.e.* n-dependent). Since the number of particles N typically goes from 2 to 25, sub-leading finite-size corrections are taken into account by the exponent $\mathcal{E}$ (and the pref-actor $\mathcal{D}$) in Eq. (2.45).

As discussed previously, it is possible to define two different scalings of λ_0 with respect to the particle number. In the first case (case (b)), we could fix the external potential and increase N. In the second case (case (a)) we could fix instead the density of particles in the trap and vary N and Λ accordingly. For example, for the harmonic potential we can write $\Lambda \,=\, \frac{1}{2}\, m\, \omega^2$, and, using the length scale $\xi \,\equiv\, \sqrt{\hbar/m\omega}$, we can define the average density $\rho \,=\, N/\sqrt{\hbar/m\omega}$. We are going to approach the problem in both ways.

A power–law scaling similar to Eq. (2.45) can be also argued for the dimensionless momentum distribution peak:

$$\frac{n_{\rm peak}}{\xi} \,=\, \mathcal{F} + \mathcal{G}\, N^{\gamma} + \frac{\mathcal{H}}{N^{\mathcal{I}}}\,. \tag{2.46}$$

To obtain β defined in (2.33), we proceed in the following way. First we evaluate $\hat{\varphi}_0(\eta)$ for two different values of the particle number, N_1 and N_2. To have an estimate of β, we impose that:

$$\hat{\varphi}_0^{(N_1)}(\eta)\, N_1^{-\beta} \,=\, \hat{\varphi}_0^{(N_2)}(\eta)\, N_2^{-\beta}\,, \tag{2.47}$$

near the origin, from which it follows that:

$$\beta \,=\, \frac{\ln\left[\hat{\varphi}_0^{(N_2)}(\eta)\,\Big/\,\hat{\varphi}_0^{(N_1)}(\eta)\right]}{\ln\Big(N_2\Big/N_1\Big)}\,. \tag{2.48}$$

Once the value of β is found, we have checked that the scaled natural orbitals, *i.e.* $\hat{\varphi}_0(\eta)\, N^{-\beta}$, converge by increasing N.

SEMICLASSICAL (CFT) DETERMINATION OF THE PREFACTOR $\mathcal{B}$

Let us now show how it is possible to use the asymptotic form in Eq. (2.17) for the 1BDM to extract directly the potential-dependent coefficient $\mathcal{B}$ in Eq. (2.45) for $N \to \infty$ [see Eq. (2.22)]. Once again we focus on power-law potentials given in Eq. (2.37). In the semiclassical limit defined in Eq. (2.13), the following dimensionful quantities (μ, Λ, m) do not scale with $\hbar$, and we replace them with $(R, \tilde{L}, m)$ where $R \equiv \left(\frac{\mu}{\Lambda}\right)^{1/2n}$ is a length scale and $\tilde{L}$ the time scale in Eq. (2.19). For the power-law potentials:

$$\tilde{L} = \Xi R \sqrt{\frac{m}{2\mu}}, \tag{2.49}$$

where Ξ a numerical constant given by:

$$\Xi = \int_{-1}^{1} \frac{du}{\sqrt{1-u^{2n}}} = 2\sqrt{\pi}\frac{\Gamma\left(\frac{2n+1}{2n}\right)}{\Gamma\left(\frac{n+1}{2n}\right)}. \tag{2.50}$$

In the semiclassical approximation $\hbar$ can be replaced by N according to Eq. (2.16) which in our case reads:

$$N\hbar = \frac{mR^2}{\tilde{L}}\left(\frac{\alpha\Xi}{\pi}\right). \tag{2.51}$$

In Eq. (2.51), α is another numerical constant given by:

$$\alpha = \int_{-1}^{1} du\ \sqrt{1-u^{2n}} = \sqrt{\pi}\frac{\Gamma\left(\frac{2n+1}{2n}\right)}{\Gamma\left(\frac{3n+1}{2n}\right)}. \tag{2.52}$$

The 1BDM in Eq. (2.17) is expressed in terms of a variable $\tilde{x}(x) \equiv \tilde{L}F(x/R)$. Again for the potentials in Eq. (2.37), F is given by:

$$F(\eta) \;=\; \frac{1}{\Xi}\int_{-1}^{\eta} du\ \frac{1}{\sqrt{1-u^{2n}}}. \tag{2.53}$$

However, it is actually more convenient to introduce $G(\eta)$ in such a way that $F(\eta) \equiv \frac{1}{2} + G(\eta)$ and it turns out:

$$G(\eta) \;=\; \mathrm{sign}(\eta)\frac{B_{\eta^{2n}}\left(\frac{1}{2n},\frac{1}{2}\right)}{2n\Xi}, \tag{2.54}$$

where the function $B_z(a,b)$ is the incomplete Beta function [161]. The function $G(\eta)$ simplifies in the limit $n=1$ (harmonic oscillator) where we have $G(\eta)|_{n=1} = \frac{1}{\pi}\arcsin(\eta)$ and also in the limit $n\to\infty$ (hard wall) where $G(\eta)|_{n=\infty} = \frac{1}{2}\eta$. Taking into account all of this, we can rewrite the eigenvalue equation (1.59) for the semiclassical 1BDM as:

$$\sqrt{N}|C|^2\sqrt{\frac{\pi}{\alpha\Xi}}\int_{-1}^{1} d\eta'\ K(\eta,\eta')\varphi_j(\eta') = \lambda_j\varphi_j(\eta)\,, \tag{2.55}$$

where $K(\eta,\eta')$ is the kernel:

$$K(\eta,\eta') \;=\; \frac{\left|1-\sin^2(\pi G(\eta))\right|^{\frac{1}{8}}\ \left|1-\sin^2(\pi G(\eta'))\right|^{\frac{1}{8}}}{\left|\sin(\pi G(\eta)) - \sin(\pi G(\eta'))\right|^{\frac{1}{2}}}\,. \tag{2.56}$$

As already anticipated, the existence of the limit (2.13) requires $\lambda_j \sim \mathcal{B}_j\sqrt{N}$, *i.e.* $\mathcal{C} = 1/2$ [see Eq. (2.45)]. The numerical prefactors $\mathcal{B}_j$ can be calculated from the knowledge of the eigenvalues $\bar{\lambda}_j$ of Eq. (2.56). Indeed from (2.55) one has:

$$\mathcal{B}_j \equiv |C|^2\sqrt{\frac{\pi}{\alpha\Xi}}\bar{\lambda}_j. \tag{2.57}$$

In the following we only focus on the scaling of largest eigenvalue λ_0 and then define $\mathcal{B} \equiv \mathcal{B}_0$.

The largest eigenvalue of the kernel in Eq. (2.56) can be obtained with a numerical procedure similar to the one outlined at the end of the previous Section. Notice that the kernel in Eq. (2.56) is singular for $\eta = \eta'$ and its diagonal elements have to be regularized with a cut-off δ. The physical origin of the cut-off can be traced back to the validity of Eq. (2.17) up to distances $|x-y| \simeq \rho_{\max}^{-1}$. In the dimensionless variable η, therefore the cut-off is $\delta \simeq \frac{\rho_{\max}^{-1}}{R} \ll 1$. This condition, determining the validity of the CFT approach, already appears in [156]. From this perspective the semiclassical limit $\hbar \to 0$ in Eq. (2.13)

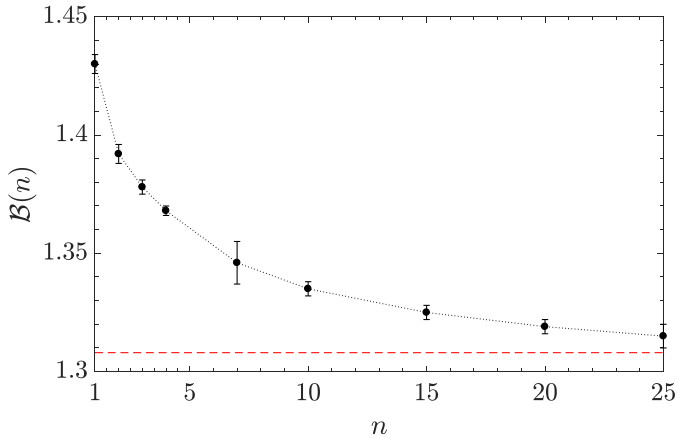

Figure 2.4: $\mathcal{B}(n)$ *vs* n obtained from solving Eq. (2.55) with kernel given by Eq. (2.56). $\mathcal{B}$ monotonically decreases from 1.430(4) for $n = 1$ to 1.308(3) for $n = \infty$ which is represented by the red dashed line. The black dotted line is a guide for the eye.

it is actually a convenient way to take the continuum limit to a field theory. Such a field theory describes the gas density fluctuations on intermediate length scales much larger than $\rho_{\max}^{-1}$ and much smaller than the effective length R of the system [156–158]. A non-trivial consequence is that the two procedures (a) and (b) to implement the large-N limit should reproduce the same results. Indeed fixing the external potential and varying the density is equivalent to consider $\rho_{\max}^{-1} \to 0$ while keeping R fixed; on the other hand fixing the density and varying the potential corresponds to $R \to \infty$ while keeping $\rho_{\max}$ fixed. In both cases $\delta \ll 1$ and the gas is described by a CFT.

Numerical estimations for $\mathcal{B}$ in Eq. (2.57) obtained with a Gauss-Legendre quadrature up to $Z = 20000$ nodes are given in Tab. 2.2 and Fig. 2.4. Z is the number of points of the grid in which the interval $[-1, 1]$ is divided. The error is estimated by extrapolating the value of $\mathcal{B}$ in the limit $\delta \to 0$ by increasing Z. Then the obtained values for varying Z are fitted with a function of the form $\mathcal{B} + \mathcal{M}/Z^{\zeta}$. We observe that Refs. [100, 162] also provide a numerical evaluation of $\mathcal{B}$ for the harmonic potential ($n = 1$) and the hard wall ($n = \infty$). Our results fully confirm and generalize these predictions.

The CFT predictions for $\mathcal{B}$ are compared in Tab. 2.2 with $\mathcal{B}_{\text{fit}}$, which is the value of $\mathcal{B}$ obtained from the fit (2.45) using the numerical results for the 1BDM $\rho(x, y)$ directly computed. The large-N limit is implemented here fixing the potential and varying the density (case (b)). Notice that in doing the fit one could either fix $\mathcal{C}$ to the value $1/2$ or re-fit as well $\mathcal{C}$ according to (2.45). Since the value $\mathcal{C} = 1/2$ has been independently established and checked, we present our results for $\mathcal{B}_{\text{fit}}$ with the former procedure. When instead $\mathcal{C}$ is re-fitted, substantial agreement for $\mathcal{B}_{\text{fit}}$ is found, except for $n \sim 2 - 4$ where we obtained a discrepancy of order 1%. To check which procedure is better, we performed both with N up to 30, and then we compared their predictions with the value for λ_0 obtained for $N = 35$ directly from the numerical diagonalization of the ODBM. We found that the procedure in which $\mathcal{C}$ is fixed gives slightly better results. Finally we also verified that the scaling of the largest eigenvalue obtained fixing the density in the trap and varying the potential (case (a)) is also consistent with the CFT predictions; see Table 2.6, for fits without fixing $\mathcal{C} = 1/2$ and Table 2.7 for fits with $\mathcal{C} = 1/2$. Compare in particular the results in Table 2.7 with those collected in Table 2.3.

n	$\mathcal{B}_{\rm fit}$	$\mathcal{B}$
1	1.4304(2)	1.430(4)
2	1.400(4)	1.392(4)
3	1.380(4)	1.378(3)
4	1.372(5)	1.368(2)
∞	1.31(1)	1.308(3)

Table 2.2: Estimation of the prefactor $\mathcal{B}$ in Eq. (2.45). The values $\mathcal{B}_{\rm fit}$ are obtained fitting the finite-N results for the largest eigenvalue of Eq. (2.11) with Eq. (2.45). The fit for λ_0 is done fixing the potential and varying the density by increasing the number of particles. The numerical error in the last digit is reported in brackets. In the second column are given the values of $\mathcal{B}$ obtained from Eq. (2.57), after determining numerically the largest eigenvalue $\bar{\lambda}_0$ of the kernel in Eq. (2.56).

n	$\mathcal{A}_{\rm fit}$	$\mathcal{B}_{\rm fit}$	$\mathcal{D}_{\rm fit}$	$\mathcal{E}_{\rm fit}$
1	$-0.554(2)$	1.4304(2)	0.122(1)	0.60(1)
2	$-0.55(4)$	1.400(4)	0.141(8)	0.79(6)
3	$-0.53(3)$	1.380(4)	0.16(2)	1.1(5)
4	$-0.56(3)$	1.372(5)	0.20(1)	0.9(3)
∞	$-0.6(1)$	1.31(1)	0.31(9)	0.3(1)

Table 2.3: Results for the parameters entering Eq. (2.45) for different values of n by fixing the trapping potential and varying the density at the center of the trap. The numerical error in the last digit is reported in brackets.

In conclusion, the agreement between the predictions obtained from the CFT formula (2.17) and the numerical values for $\mathcal{B}_{\rm fit}$ is very satisfactory.

NUMERICAL RESULTS

Let us now describe the outcome of the numerical analysis, based on Eq. (2.45) and Eq. (2.46), for the large-N behaviour of λ_0, $n_{\rm peak}/\xi$ and $\hat{\varphi}_0(\eta)$. Such a study strongly corroborates the validity of Eq. (2.22) and Eq. (2.36). To obtain the results in Tab. 2.3, Tab. 2.4 and Tab 2.5, we have varied the density of particles in the system (by increasing N typically up to $25-30$) for different power-law potentials in Eq. (2.37). In particular:

- In Tab. 2.3 are collected the results obtained for the parameters of the scaling of λ_0 according to Eq. (2.45).
- In Tab. 2.4 we report the results for the dimensionless momentum distribution peak according to Eq. (2.46).
- In Tab. 2.5 we summarise the values of $\mathcal{C}$, β and γ obtained as a function of n.

Our findings for λ_0 as a function of N using Eq. (2.45) are plotted for different values of n in Fig. 2.5. The inset of Fig. 2.5 shows the WKB approximation results, where it is

n	$\mathcal{F}_{\rm fit}$	$\mathcal{G}_{\rm fit}$	$\mathcal{H}_{\rm fit}$	$\mathcal{I}_{\rm fit}$
1	0.002(2)	0.561(6)		
2	−0.046(8)	0.5001(3)	0.025(6)	0.6(3)
3	−0.15(8)	0.491(2)	0.10(8)	0.3(3)
4	−0.21(1)	0.500(5)	0.015(5)	0.41(3)
∞	−0.752(3)	0.1994(2)	0.0048(1)	1.09(5)

Table 2.4: Results for the parameters in the dimensionless momentum distribution peak (2.46) for different values of n. Note that for $n = 1$ the correction term $\propto 1/N$ in the fitting is not necessary.

called λ_0^{wkb}. The exponent $\mathcal{C}$ is approaching $1/2$ within the numerical error. Also notice from Tab. 2.5 that $\mathcal{C}^{wkb}$ is greater than $\mathcal{C}_{\rm fit}$ for $n \neq 1$, as expected, and $\mathcal{C} = 1/2$ is within the estimated error for $\mathcal{C}^{wkb}$ (but $n = 2$).

By studying the system by fixing the density and varying Λ, we have collected the data reported in Table 2.6 for different values of n of the polynomial trapping potential. From these results is evident that $\mathcal{C} = 1/2$ is also found in this case. For this reason we then fitted the data via Eq. (2.45) with $\mathcal{C}$ fixed to the value $1/2$ and we obtained the results reported in Table 2.7. Consistently with the discussion in Sec. 2.2.1.3, the values estimated for the parameter $\mathcal{B}$ (actually for all the fit parameters) are consistent within the error bar with the ones in Table 2.3.

We have also done calculations for a potential $V_{hho}(x) = \Lambda x^2$ for $x > 0$ and zero otherwise, *i.e.* half of the harmonic potential: By varying the density in the system we get:

$$\begin{aligned} &\mathcal{A}_{\rm fit} = -0.37(1);\ \ \mathcal{B}_{\rm fit} = 1.267(3);\ \ \mathcal{C}_{\rm fit} = 0.51(2); \\ &\mathcal{D}_{\rm fit} = 0.103(1);\ \ \mathcal{E}_{\rm fit} = 0.58(1)\,. \end{aligned} \tag{2.58}$$

n	$\mathcal{C}_{\rm fit}$	$\mathcal{C}^{wkb}$	$\beta_{\rm fit}$	$\gamma_{\rm fit}$	β	γ
1	0.500(2)	0.496(8)	−0.25(1)	1.02(4)	$-\frac{1}{4}$	1
2	0.501(1)	0.54(3)	−0.16(1)	0.85(2)	$-\frac{1}{6}$	$\frac{5}{6}$
3	0.501(2)	0.54(7)	−0.12(2)	0.76(1)	$-\frac{1}{8}$	$\frac{3}{4}$
4	0.500(3)	0.54(9)	−0.10(1)	0.70(1)	$-\frac{1}{10}$	$\frac{7}{10}$
∞	0.500(1)		0.00(1)	0.502(2)	0	$\frac{1}{2}$

Table 2.5: From the second to the fifth columns are gathered numerical results for the parameters ruling the scaling with N of λ_0, λ_0^{wkb}, $\hat{\varphi}_0(\eta)$ and $n_{\rm peak}/\xi$. The value for $\mathcal{C}$, within the numerical precision, appears to be independent on the potential and equal to $1/2$. Last two columns: Exact values for β and γ coming from Eq. (2.61) and Eq. (2.62) respectively.

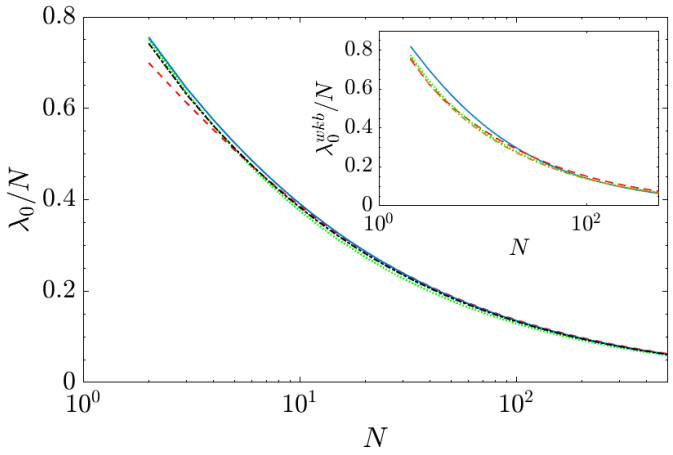

Figure 2.5: λ_0 *vs* N obtained for $n = 1$ (in solid blue), $n = 2$ (in dashed red), $n = 3$ (in dotted green) and $n = \infty$ (in dotted-dashed black), up to 500 particles. In the inset is shown the behaviour of λ_0^{wkb} vs N obtained with the WKB approximation, for $n = 1$ (in solid blue), $n = 2$ (in dashed red), $n = 3$ (in dotted green) and $n = 4$ (in dotted-dashed orange).

n	$\mathcal{A}_{\rm fit}$	$\mathcal{B}_{\rm fit}$	$\mathcal{C}_{\rm fit}$	$\mathcal{D}_{\rm fit}$	$\mathcal{E}_{\rm fit}$
1	−0.58(2)	1.45(3)	0.4995(8)	0.36(5)	2.00(1)
2	−0.56(3)	1.418(2)	0.498(5)	0.16(4)	1.2(3)
3	−0.56(2)	1.391(1)	0.500(3)	0.18(2)	1.0(1)
4	−0.52(7)	1.34(4)	0.503(6)	0.21(1)	0.30(5)

Table 2.6: Results for the parameters entering Eq. (2.45) for different values of n by fixing the density at the center of the traps and varying N and Λ accordingly. The numerical error in the last digit is reported in brackets.

n	$\mathcal{A}_{\rm fit}$	$\mathcal{B}_{\rm fit}$	$\mathcal{D}_{\rm fit}$	$\mathcal{E}_{\rm fit}$
1	−0.56(3)	1.432(4)	0.13(3)	0.57(2)
2	−0.55(2)	1.407(4)	0.15(3)	1.0(2)
3	−0.56(2)	1.391(1)	0.18(2)	1.0(1)
4	−0.56(1)	1.38(2)	0.18(4)	0.8(1)

Table 2.7: Results for the parameters entering Eq. (2.45) with $\mathcal{C}$ fixed to $1/2$, for different values of n by fixing the density at the center of the traps and varying N and Λ accordingly. The numerical error in the last digit is reported in brackets.

ANALYTICAL PREDICTIONS FOR β AND γ

All previous results are compatible (within the numerical error) with an exponent $\mathcal{C}$, characterising deviations from ODLRO in the thermodynamic limit, equal to $1/2$. For very large number of particles we therefore confirm the validity of Eq. (2.22), independently of the external potential. It is also interesting to observe that not only Eq. (2.36) is satisfied for the different power–law potentials analysed, but also that it is possible to work out

predictions for β and γ as a function of n. For β one can observe that, recalling the definition of length scale ξ in Eq. (2.39), the support of the dimensionless ground state natural orbit scales as: ξ^{-1}, *i.e.*

$$\int d\eta \propto \frac{1}{\xi} \propto \hbar^{-\frac{1}{n+1}} . \tag{2.59}$$

Since: $\int d\eta \propto N^{-2\beta}$, and in the semiclassical limit $\hbar \propto N^{-1}$, then we have:

$$N^{-2\beta} \propto N^{\frac{1}{n+1}} , \tag{2.60}$$

from which:

$$\beta = -\frac{1}{2n+2} . \tag{2.61}$$

From the universal relation (2.36) it also follows a prediction for γ:

$$\gamma = \frac{n+3}{2(n+1)} . \tag{2.62}$$

The main results for the exponents $\mathcal{C}$, γ and β for different power–law potentials are reported in Tab. 2.5. Hence, the predictions (2.61) and (2.62) are in excellent agreement with the numerical results.

Finally observe that the result $\gamma = 1$ for $n_{\rm peak}/\xi$ in the case of harmonic potential does not imply at all that in an experiment one would see a BEC, (*i.e.* a macroscopic occupation of the lowest energy state). Indeed, also ξ has a dependence on N. In experiments where $\tilde{\rho}(k)$ is measured, from Eq. (2.59) one would have:

$$n_{\rm peak} \sim N^{1/2} . \tag{2.63}$$

The same behaviour is obtained for all values of n. This shows that for a TG gas the condensate *fraction* is $1/\sqrt{N}$ independently of the external trapping potential used to confine the system.

Now we wonder if we can extend the above analysis to the case of hard–core anyon gases. Following the same reasoning just seen for the bosonic case, we expect to find that the exponent $\mathcal{C}(\kappa)$, will be the same as in the homogeneous case, *i.e.* Eq. (1.93). In order to prove that, we will rely once again on a theoretical field approach valid in the semiclassical (thermodynamic) limit.

2.2 TRAPPED HARD–CORE ANYON GAS

The Bose–Fermi mapping which allowed us to write the many–body wavefunction of the bosonic Tonks–Girardeau gas in terms of the wavefunction of a spinless noninteracting fermions, cfr Eq. (2.4), can be generalized also for hard–core anyons [163]. The many–body wavefunction for hard–core anyon gas can be written as:

$$\psi^{\kappa}(x_1, \ldots, x_N) = \frac{1}{\sqrt{N!}} \det \left[\phi_k(x_l)\right]_{\substack{k=0,\ldots,N-1,\\ l=1,\ldots,N}} \prod_{1\le i<j\le N} e^{i\pi(1-\kappa)\theta(x_j-x_i)} , \tag{2.64}$$

where $\theta(x)$ is the Heaviside step function. For $\kappa = 0$ one can easily observe that this equation reduces to Eq. (2.4), as it should. Thanks to this mapping, in [164] they were

able to obtain a closed expression for the 1BDM of a trapped hard–core anyon gas written in terms of the natural orbitals for the ideal Fermi gas, *i.e.* eigenvectors of Eq. (2.5), and therefore valid for any trapping potential. The expression reads:

$$\rho^{\kappa}(x,x') \;=\; \sum_{i,j=0}^{N-1} (-1)^{i+j}\, \phi_i(x')\, \phi_j^*(x)\, \det\left\{ \int_{-\infty}^{\infty} dt\, e^{i\pi(1-\kappa)[\theta(t-x')-\theta(t-x)]}\, \phi_l(t)\, \phi_k^*(t) \right\}_{k\neq i, l\neq j} . \tag{2.65}$$

and we want to recast this expression in a form similar to Eq. (2.11). Assuming $x > x'$, separating the integral as:

$$\int_{-\infty}^{\infty} dt\, e^{i\pi(1-\kappa)[\theta(t-x')-\theta(t-x)]}\, \phi_l(t)\, \phi_k^*(t) = \int_{-\infty}^{x'} dt\, \phi_l(t)\, \phi_k^*(t) + \\ + e^{i\pi(1-\kappa)} \int_{x'}^{x} dt\, \phi_l(t)\, \phi_k^*(t) + \int_{x}^{\infty} dt\, \phi_l(t)\, \phi_k^*(t)\,,$$

by using the orthonormality condition $\int_{-\infty}^{\infty} dt\, \phi_l(t)\, \phi_k^*(t) \;=\; \delta_{k,l}$, we finally arrive at:

$$\rho^{\kappa}(x,x') \;=\; \sum_{i,j=0}^{N-1} (-1)^{i+j}\, \phi_i(x')\, \phi_j^*(x)\, \det\left\{ \delta_{k,l} + \left[e^{i\pi(1-\kappa)} - 1 \right] \int_{y}^{x} dt\, \phi_l(t)\, \phi_k^*(t) \right\}_{k\neq i, l\neq j} . \tag{2.66}$$

Therefore for a generic trapping potential $V(x)$, one has to solve Eq. (2.5) in order to find the single-particle eigenfunctions $\phi_k(x)$ and plug them in Eq. (2.66) for a fixed statistical parameter, κ, and number of particles, N. Notice that for $\kappa = 1$ one gets back Eq. (2.11) for the 1BDM of a bosonic Tonks–Girardeau gas, while for $\kappa = 0$ one has the well known expression for the density matrix of a one–dimensional spinless Fermi gas.

2.2.1 1BDM IN THE SEMICLASSICAL LIMIT

In the same way as we did for the bosonic Tonks–Girardeau gas, we can study if and how the external trapping potential affects the scaling for growing number of particles of the largest eigenvalue of the density matrix, *i.e.* how the momentum distribution peak grows with N for a trapped hard–core anyon gas. This study can be done starting from the Conformal Field Theory results of [112], where using the inhomogeneous Luttinger liquid theory they were able to obtain an expression for a trapped Lieb–Liniger anyon gas. We remark that within this approach, the semiclassical limit, $\hbar \to 0$, is equivalent to the thermodynamic limit, $N \to \infty$, therefore it turns out to be very useful to study the N-dependence of the largest eigenvalue of the 1BDM of the system. The leading order behaviour of the density matrix for a trapped hard–core anyon gas reads for $x > x'$ [112]:

$$\rho^{\kappa}_{\mathrm{cft}}(x,x') \;=\; \left(b_0^1\right)^2\, e^{i\pi\kappa \int_{x'}^{x} \rho(y)\, dy} \sqrt{\rho(x)\, \rho(x')}\, \left[\rho(x)\, v(x)\, \rho(x')\, v(x')\right]^{-\frac{1}{4}(\kappa^2+1)} \cdot \\ \cdot \left\langle \hat{A}_{\kappa,-1}\left(\tilde{x}\right)\,,\, \hat{A}_{-\kappa,1}\left(\tilde{x}'\right) \right\rangle_{\mathrm{obc}}^{[1]}\,, \tag{2.67}$$

where the sound velocity $v(x)$ can be read from the expression of the Luttinger parameter $K(x) \;=\; 1 \;=\; \frac{v(x)}{v_F(x)}$, where in turn $v_F(x) \;=\; \frac{\pi\hbar}{m}\rho(x)$, is the Fermi velocity and $\rho(x)$ the density profile of the gas. The prefactor b_0^1 are the same of the prefactors for the

homogeneous case, *i.e.* $b_0^{K=1} = (2\pi)^{-\frac{1+\kappa^2}{4}}\, G\left(\frac{3+\kappa}{2}\right)\, G\left(\frac{3-\kappa}{2}\right)$, while the vertex correlation function reads:

$$\left\langle \hat{A}_{\kappa,-1}\left(\tilde{x}\right)\,,\,\hat{A}_{-\kappa,1}\left(\tilde{x}'\right)\right\rangle_{\text{obc}}^{[1]} \;=\; e^{-i\pi\kappa\,\text{sgn}(\tilde{x}-\tilde{x}')/2}\,\left[d\left(2\tilde{x}\,,\,2\tilde{L}\right)\,d\left(2\tilde{x}'\,,\,2\tilde{L}\right)\right]^{\frac{1}{4}(1-\kappa^2)}\cdot \\ \cdot\,\frac{\left[d\left(\tilde{x}+\tilde{x}'\,,\,2\tilde{L}\right)\right]^{\frac{1}{2}(\kappa^2-1)}}{\left[d\left(\tilde{x}-\tilde{x}'\,,\,2\tilde{L}\right)\right]^{\frac{1}{2}(\kappa^2+1)}}\,,$$

where: $d\left(\tilde{x}\,,\,\tilde{L}\right) = \frac{\tilde{L}}{\pi}\left|\sin\left(\frac{\pi\tilde{x}}{\tilde{L}}\right)\right|$, and where $\tilde{L}$ and $\tilde{x}$ are the usual variables which represent the time needed to a signal to travel from point x_1 to x_2 and from x_1 to x respectively, and where x_1 and x_2 are the boundary points solutions of the equation: $\mu - V(x) = 0$. We remark here that this expression is valid in the intermediate range of coordinates between the interparticle distance and the system size.

Notice also that the complex exponential in Eq. (2.67) (by plugging also the complex exponential coming from the vertex correlation function), is the one responsible for the shift of the location of the momentum distribution peak for the hard–core anyon gas. In the homogeneous case, for example, where: $\rho(x) = \rho = N/L$, the complex exponential does indeed reduce to: $e^{i\kappa k_F r}e^{-\frac{\pi}{2}i\kappa\text{sgn}(r)}$, which we saw in Eq. (1.89) and shift the momentum distribution peak around the position: $kL = -\kappa\pi\,(N-1)$. In the case of presence of a trapping potential, a closed analytical expression for the intensity of the shift is a difficult task because of the inhomogeneity, but it can be evaluated numerically for a fixed potential.

Now let us turn our attention to the scaling with the particles number. The density profile $\rho(x)$ scales as $O(N)$, therefore the sound velocity has no N-dependence and the same is true for the vertex correlation function. As we did for the bosonic case, we can study the eigenequation (2.44) in the semiclassical limit, by substituting $\rho(x,x')$ with Eq. (2.67) and restrict the integration domain to $x' \in [x_1, x_2]$. Changing integration variable to $\tilde{x}'$, we obtain the semiclassical limit of Eq. (2.44) for the largest eigenvalue of the 1BDM

$$\int_0^{\tilde{L}} d\tilde{x}'\, w(\tilde{x}')\,\rho_{\text{cft}}^{\kappa}(\tilde{x},\tilde{x}')\,\varphi_0(\tilde{x}') \;=\; \lambda_0\,\varphi_0(\tilde{x}), \tag{2.68}$$

with $w(\tilde{x}') = 1/v(x'(\tilde{x}'))$. Plugging Eq. (2.67) into Eq. (2.68), we observe that the limit $\hbar \to 0$ is consistent on both sides only if $\lambda_0 = O\left(\hbar^{-\left(1-\kappa^2\right)/2}\right)$. Recalling that within this approach: $N\,\hbar = \text{const}$, we finally conclude that in the thermodynamic limit:

$$\lambda_0(\kappa) \;\sim\; \mathcal{B}(\kappa) N^{\frac{1}{2}\left(1-\kappa^2\right)}, \tag{2.69}$$

therefore the scaling exponent $\mathcal{C}(\kappa)$ for the largest eigenvalue of the 1BDM is:

$$\mathcal{C}(\kappa) \;=\; \frac{1}{2}\left(1-\kappa^2\right)\,, \tag{2.70}$$

independently on the shape of the potential and in particular notice that it coincides with the result of the homogeneous case, cfr Eq. (1.93). To get the numerical prefactor $\mathcal{B}(\kappa)$ once the trapping potential is fixed, one should evaluate the eigenvalues of the kernel coming from Eq. (2.68) from using (2.67), within the same procedure that we used for the hard–core Bose gas.

Now that we deeply studied the effects of a trapping potential on a hard–core interacting system with general quantum statistic properties, we wonder what will happen when one considers different kind of interactions. For example how long–range repulsive interactions modify the results and analysis? And what if we introduce an external trapping potential for the long–range system? We will now deal with such problem, introducing the Calogero and Calogero–Sutherland models.

2.3 CALOGERO MODEL

We will introduce the Calogero and Calogero Sutherland models (CM and CSM, respectively) which are systems made up of interacting particles with long–range $(x_i - x_j)^{-2}$ interactions. While the CSM refers to a system enclosed in a ring geometry, the CM encodes the effects of inhomogeneity with an external harmonic trapping potential. The Hamiltonian of the Calogero–Sutherland model in a ring of circumference L reads:

$$\hat{H}_{\mathrm{CSM}} = \frac{\hbar^2}{2m}\left\{-\sum_{i=1}^{N}\frac{\partial^2}{\partial x_i^2} + 2\lambda(\lambda-1)\sum_{i\neq j}\frac{\pi^2/L^2}{\sin^2[\pi(x_i-x_j)/L]}\right\}, \tag{2.71}$$

where the interaction among two particles is inversely proportional to the square of the chord distance between them. Its ground state wavefunction is known and can be written in product form as [113]:

$$\psi^{B,F}_{\mathrm{CSM}}(x_1,\ldots,x_N) = \prod_{l>k}\left|e^{2\pi i x_k/L} - e^{2\pi i x_l/L}\right|^{\lambda} S_{B,F}\,, \tag{2.72}$$

apart from a normalization constant. The factor $S_{B,F}$ depends on the quantum statistics: $S_B = 1$ for bosons, while $S_F = (-1)^P$ with P the parity of the permutation, for fermions. The corresponding energy per particle is:

$$\frac{E_{\mathrm{CSM}}}{N} = \frac{\pi^2}{3}\frac{\lambda^2(N^2-1)}{L^2}\,. \tag{2.73}$$

When an external harmonic potential is introduced, we deal with the Calogero model whose Hamiltonian is written as:

$$\hat{H}_{\mathrm{CM}} = -\frac{\hbar^2}{2m}\sum_{i=1}^{N}\frac{\partial^2}{\partial x_i^2} + \frac{m\omega^2}{2}\sum_{i=1}^{N}x_i^2 + \frac{\lambda(\lambda-1)\hbar^2}{m}\sum_{i>j}\frac{1}{(x_i-x_j)^2}\,. \tag{2.74}$$

It is convenient to choose oscillator length $a_{ho} = \sqrt{\hbar/m\omega}$ as unit of length and $\hbar\omega$ as unit of energy. In this case we can recover the limits of vanishing interaction potential $\lambda \to 0$. The Hamiltonian in dimensionless units reads as:

$$\frac{\hat{H}_{\mathrm{CM}}}{\hbar\omega} = -\frac{1}{2}\sum_{i=1}^{N}\frac{\partial^2}{\partial\eta_i^2} + \frac{1}{2}\sum_{i=1}^{N}\eta_i^2 + \sum_{i>j}\frac{\lambda(\lambda-1)}{(\eta_i-\eta_j)^2}\,, \tag{2.75}$$

where we defined with $\eta_j = x_j/a_{ho}$ the dimensionless coordinates of the particles. Also in this case the wavefunction of the ground state can be written explicitly [118] and apart from a normalization constant it reads:

$$\psi^{B,F}_{\mathrm{CM}}(\eta_1,\ldots,\eta_N) = \prod_k e^{-\frac{1}{2}\eta_k^2}\prod_{i>j}|\eta_i-\eta_j|^{\lambda} S_{B,F}\,, \tag{2.76}$$

where the parity factor $S_{B,F}$ was previously defined. The corresponding ground state energy per particle is:

$$\frac{E_{\rm CM}}{N} = \frac{1}{2}[1 + (N-1)\lambda]\,\hbar\omega. \tag{2.77}$$

For the particular choice $\lambda = 1$, it leads to a system of trapped ideal fermions, for fermionic statistics, and a system of Tonks-Girardeau particles for bosonic statistics. For $\lambda = 0$ instead, one finds the result of the ideal Bose gas.

Let us now introduce the study of the correlation functions for these systems. The correlation properties of the CSM were thoroughly studied in the past. The relation between the ground state probability of the CSM and the probability distribution of the eigenvalues of Gaussian unitary random matrices [165–167], allows to write explicit expression for static density correlations of the CSM for certain values of the interaction parameter λ (which corresponds, apart from a factor 2, to the Dyson index in Random Matrix Theory). The analogy with Random Matrix ensambles allows also the calculation of dynamical density correlations [168, 169] and dynamical Green's function [170, 171]. Later on, for integer [172, 173] and rational [174–176] values of the interaction parameter, the method of Jack polynomial has been applied to find exact and asymptotic behaviours for several correlation functions. The replica method was used in [177] to obtain the density-density correlation functions of the CSM for arbitrary values of λ. The same method was used in [178] to study also the large and short distance behaviour of the one–body density matrix and momentum distribution with bosonic and fermionic statistics.

2.3.1 CORRELATION FUNCTIONS AND SCALING PROPERTIES FOR THE CSM

The long–range asymptotics of the ground state wavefunction in a homogeneous system can be inferred from the hydrodynamic theory. It was shown by Reatto and Chester in 1967 that for large separation between particles $x_i - x_j$, the many–body wavefunction can be factorized in a pair-product form:

$$\psi(x_1, ..., x_N) = \prod_{i<j}^{N} |\sin[\pi(x_j - x_i)/L]|^{1/K}. \tag{2.78}$$

There are some interesting observations: (i) this wavefunction is compatible with Luttinger Liquid model. (ii) The parameter $K = v_{\rm F}/s$ is the Luttinger parameter, directly related to the Fermi velocity $v_{\rm F}$ and the speed of sound s. The Fermi velocity $v_{\rm F}$ is completely fixed by the density while the speed of sound s depends on the many–body interactions between particles. (iii) The wavefunction (2.78) is an exact eigenstate of the Calogero–Sutherland model with $\lambda = 1/K$, so the particle separation does no longer need to be large. The interaction potential scales as $1/x^2$ similarly to the kinetic energy, so that there is no any new length scale introduced.

In order to not confuse the 1BDM with the density profile of the gas $\rho(x)$, in this Section we will denote the one–body density matrix as: $g_1(x, y)$, and we remind that, if the system is homogeneous, we can write $g_1(x, y) = g_1(x - y) \equiv g_1(x)$. For bosons in

the Luttinger liquid formalism it has a dominant slow power-law decay, while subleading terms oscillate:

$$g_1^B(x) = \langle \Psi_B^\dagger(x)\Psi_B(0)\rangle = \rho \left[\frac{1}{\rho x}\right]^{\frac{1}{2K}} \left\{ B_0 + \sum_{m=1}^{+\infty} B_m \left[\frac{1}{\rho x}\right]^{2m^2 K} \cos\left(2mk_F x\right)\right\},$$

decaying to zero, resulting in absence of Bose-Einstein condensation even at zero temperature, as we already saw in the previous Chapter. In case of fermions, already the dominant term contains oscillations:

$$g_1^F(x) = \langle \Psi_F^\dagger(x)\Psi_F(0)\rangle = \rho \sum_{m=0}^{+\infty} f_m \left[\frac{1}{\rho x}\right]^{2(m+\frac{1}{2})^2 K + \frac{1}{2K}} \sin\left|2(m+\frac{1}{2})k_F x\right|.$$

In these expressions the *dimensionless* coefficients B_m and f_m are non-universal and depend on the details of the interaction. In the particular case of the Calogero–Sutherland model, it was found:

$$\frac{g_1^B(x)}{\rho} \simeq \frac{A^2(\lambda)}{|2k_F x|^{\lambda/2}} \left[1 + 2\sum_{m=1}^{\infty} (-1)^m \frac{D_m^2(\lambda)\cos 2mk_F x}{|2k_F x|^{2m^2/\lambda}}\right], \tag{2.79}$$

$$\frac{g_1^F(x)}{\rho} \simeq \frac{C^2(\lambda)}{|2k_F x|^{\frac{\lambda}{2}+\frac{1}{2\lambda}-1}} \frac{1}{k_F x} \sum_{m=1}^{\infty} (-1)^{m-1} \frac{F_m^2(\lambda)\sin(2m-1)k_F x}{(2k_F x)^{2m(m-1)/\lambda}}, \tag{2.80}$$

where [178]:

$$A(\lambda) = \frac{\Gamma^{1/2}(1+\lambda)}{\Gamma\left(1+\lambda/2\right)} \exp\left\{\int_0^\infty \frac{dt}{t} e^{-t}\left[\frac{\lambda}{4} - \frac{2\left(\cosh\frac{t}{2}-1\right)}{\left(1-e^{-t}\right)\left(e^{t/\lambda}-1\right)}\right]\right\}, \tag{2.81}$$

$$D_k(\lambda) = \prod_{a=1}^{k} \frac{\Gamma\left(\frac{1}{2}+\frac{a}{\lambda}\right)}{\Gamma\left(\frac{1}{2}+\frac{1}{\lambda}-\frac{a}{\lambda}\right)}, \tag{2.82}$$

$$C(\lambda) = \Gamma^{1/2}(\lambda) \frac{\Gamma(1/2+1/2\lambda)}{\Gamma(1/2+\lambda/2)} \exp\left\{\int_0^\infty \frac{dt}{t} e^{-t}\left[\frac{\lambda}{4} - \frac{1}{4\lambda} + \frac{2e^{t/2\lambda}\left(\cosh\frac{t}{2\lambda} - \cosh\frac{t}{2}\right)}{\left(1-e^{-t}\right)\left(e^{t/\lambda}-1\right)}\right]\right\}, \tag{2.83}$$

$$F_k(\lambda) = \left[\frac{\lambda^2-(2k-1)^2}{\lambda^2-1}\right]^{\frac{1}{2}} \prod_{a=1}^{k-1} \frac{\Gamma\left(1+\frac{1+2a}{\lambda}\right)}{\Gamma\left(1+\frac{1-2a}{\lambda}\right)}. \tag{2.84}$$

These expressions will be useful in order to determine the ODLRO properties of the system, in analogous way as the large distance behaviour of the 1BDM were used to compute the exponent $\mathcal{C}$ in the case of a homogeneous Lieb–Liniger Bose gas. Let us start this analysis by reminding that the Fourier transform of the 1BDM for a homogeneous system is the momentum distribution:

$$n(k) = \frac{L}{2\pi} \int_0^L e^{-ikx} g_1(x)\, dx, \tag{2.85}$$

and once multiplied by $\frac{2\pi}{L}$, it is equivalent to the eigenvalue equation of the 1BDM (1.59). This follows from the fact that for a homogeneous system a good quantum number which labels the occupation numbers and natural orbitals is the momentum quantum number $k = \frac{2\pi}{L} j$, and one can write the effective single-particle states as $\varphi_j(x) = \frac{1}{\sqrt{L}} e^{2\pi i x j/L}$. Therefore the dimensionless momentum distribution peak for bosonic homogeneous system will coincide with the largest eigenvalue of the 1BDM:

$$\frac{n(k=0)}{L} 2\pi = \lambda_0 = \int_0^L g_1(x)\, dx\,. \tag{2.86}$$

For large number of particles, it is convenient to define a power law scaling for the largest eigenvalue of the 1BDM with respect to N, as:

$$\lambda_0 \sim \mathcal{B}_0 N^{\mathcal{C}}\,, \tag{2.87}$$

as we already saw for several different models. In a completely similar way to the scheme followed so far, we can then use the leading behaviour of the asymptotic expressions of the 1BDM for bosonic and fermionic Calogero–Sutherland models to get access to the prefactor $\mathcal{B}_0$ and the power $\mathcal{C}$. In order to do so, we first have to make the one–body density matrices periodic functions of period L so that we construct a circulant matrix whose eigenvalues are known to be real, as it should be since they represent the occupation numbers of the system. From Eqs. (2.79)-(2.80) we symmetrize the leading terms of the density matrices in the following way:

$$\frac{g_1^B(x)}{\rho} \simeq \frac{A^2(\lambda)}{(2\pi\rho)^{\lambda/2}} \left(\frac{L}{\pi} \sin\frac{\pi x}{L}\right)^{-\lambda/2}\,, \tag{2.88}$$

$$\frac{g_1^F(x)}{\rho} \simeq \frac{C^2(\lambda)}{\left|2\pi\rho\left(\frac{L}{\pi}\sin\frac{\pi x}{L}\right)\right|^{\frac{\lambda}{2}+\frac{1}{2\lambda}-1}} \frac{\sin\left[\pi\rho\left(\frac{L}{\pi}\sin\frac{\pi x}{L}\right)\right]}{\pi\rho\left(\frac{L}{\pi}\sin\frac{\pi x}{L}\right)}\,, \tag{2.89}$$

where we substituted the distance x with the chord distance $\frac{L}{\pi}\sin\frac{\pi x}{L}$. Using these expressions in the equation for λ_0, *i.e.* Eq. (2.86), we get respectively:

$$\begin{aligned}
\lambda_0^B &= \frac{2^{-\lambda/2}\,\Gamma\left[\frac{1}{2}\left(1-\frac{\lambda}{2}\right)\right]}{\sqrt{\pi}\,\Gamma\left(1-\frac{\lambda}{4}\right)} A^2(\lambda)\, N^{1-\frac{\lambda}{2}}\,, \qquad (2.90)\\
\lambda_0^F &= 2^{-\frac{1+\lambda^2}{2\lambda}}\,\Gamma\left(1-\frac{1+\lambda^2}{4\lambda}\right)\,{}_1\tilde{F}_2\left(1-\frac{1+\lambda^2}{4\lambda};\frac{3}{2},\frac{1}{4}\left(6-\lambda-\frac{1}{\lambda}\right);-\frac{N^2}{4}\right) C^2(\lambda)\, N^{2-\frac{1+\lambda^2}{2\lambda}}\,,
\end{aligned}$$

where the first equation is valid for $\lambda \in (0,2)$, while the second equation is valid for $\lambda \in (2-\sqrt{3}, 2+\sqrt{3})$, and ${}_1\tilde{F}_2(a;b_1,b_2;c)$ is the regularized generalized hypergeometric function. Finally expanding the hypergeometric function for large N and keeping only the leading term, one obtains:

$$\lambda_0^F = \frac{2^{2-\frac{1+\lambda^2}{2\lambda}}}{\pi} \cos\left[\frac{\pi}{4\lambda}\left(1+\lambda^2\right)\right] \Gamma\left[-\frac{(\lambda-1)^2}{2\lambda}\right] C^2(\lambda)\, N^0\,. \tag{2.91}$$

Let us now discuss the results. For the fermionic Calogero–Sutherland model, from Eq. (2.91) we obtain:

$$\begin{aligned}
\mathcal{B}_0^F(\lambda) &= \tfrac{2^{2-\frac{1+\lambda^2}{2\lambda}}}{\pi} \cos\left[\tfrac{\pi}{4\lambda}\left(1+\lambda^2\right)\right] \Gamma\left[-\tfrac{(\lambda-1)^2}{2\lambda}\right] C^2(\lambda) \qquad \text{for } \lambda \in (2-\sqrt{3}, 2+\sqrt{3}) \quad (2.92)\\
\mathcal{C}^F(\lambda) &= 0
\end{aligned}$$

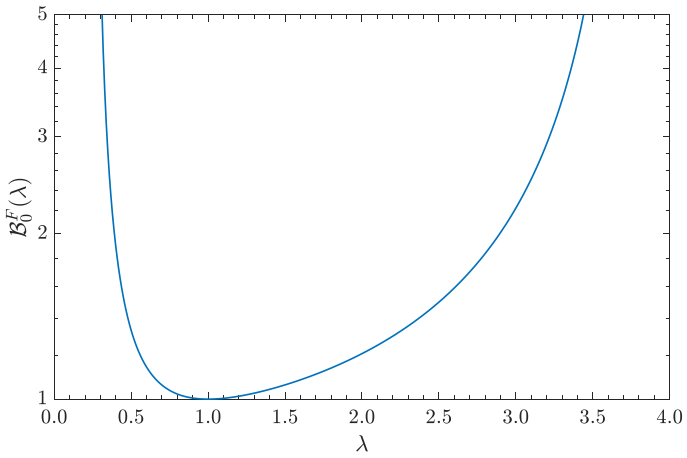

Figure 2.6: Numerical prefactor $\mathcal{B}_0^F(\lambda)$ for the scaling $\lambda_0^F \sim \mathcal{B}_0^F N^{\mathcal{C}^{\mathcal{F}}}$ for the fermionic Calogero–Sutherland model in semi-log scale.

from which we can infer that there is absence of ordering since $\mathcal{C}^F$ is always zero. Notice also that for $\lambda = 1$, *i.e.* free fermions, we get that $\mathcal{B}_0^F(1) = 1$ as expected from the Fermi–Dirac distribution. We report the behaviour of the prefactor $\mathcal{B}_0^F$ of the largest eigenvalue of the fermionic CSM in Fig. 2.6 for different values of the interaction. One should not be surprised by the fact that the prefactor $\mathcal{B}_0^F$ is greater than 1 for $\lambda \neq 1$, since this expression was obtained only by retaining the leading order term from the Luttinger predictions of $g_1^F(x)$, and we expect that the other terms will generate negative corrections on the eigenvalue scaling.

For the bosonic Calogero–Sutherland model the situation is completely different. The power law scaling of the one–body density matrix generates a non-vanishing power $\mathcal{C}^B \neq 1$, which indicates that some particles want to occupy the lowest energy state of the system in the thermodynamic limit, but not everyone of them (*i.e.* no Bose–Einstein condensation occurs). When $0 < \mathcal{C} < 1$ we say that we are in presence of a mesoscopic condensate, which consists of having a finite value for the "condensate" fraction $\frac{\lambda_0}{N}$ in the system. In particular, from Eq. (2.90) we get:

$$\begin{aligned} \mathcal{B}_0^B(\lambda) &= \frac{2^{-\lambda/2}\,\Gamma\left[\frac{1}{2}\left(1-\frac{\lambda}{2}\right)\right]}{\sqrt{\pi}\,\Gamma\left(1-\frac{\lambda}{4}\right)}\,A^2(\lambda) \\ \mathcal{C}^B(\lambda) &= 1-\frac{\lambda}{2} \end{aligned} \qquad \text{for } \lambda \in (0,2)\,. \tag{2.93}$$

For $\lambda = 1$ one should obtain the known results for the Tonks–Girardeau gas [100], indeed from our equations one has $\mathcal{C}^B = 1/2$, and $\mathcal{B}_0^B(1) = \frac{\Gamma(1/4)}{\sqrt{2\pi}\Gamma(3/4)}\,A^2(1) = \frac{\sqrt{e\pi}\,\Gamma(1/4)}{2^{1/3}A^6\,\Gamma(3/4)} \approx 1.54269$, where $A \approx 1.2824271$ is the Glaisher's constant. Notice that since $\lambda = 1/K$, the power $\mathcal{C}^B$ can be rewritten also as $\mathcal{C}^B = 1 - \frac{1}{2K}$, which is a known results valid for the Lieb–Liniger Bose gas as well (and in general for Luttinger liquids, as we are noting).

We were also able to compute the scaling for the other eigenvalues λ_j. In order to do so, one needs to compute the Fourier transform of the symmetrized 1BDM $g_1^B(x)$ and set $k = \frac{2\pi}{L}j$, with $j \in \mathbb{N}$. Imposing $\lambda_j^B \sim \mathcal{B}_j^B \mathcal{C}^B$, we obtained the following results:

$$\begin{aligned} \mathcal{B}_j^B(\lambda) &= \frac{\sin\left(\frac{\pi\lambda}{4}\right)}{\pi}\,\frac{\Gamma\left(1-\frac{\lambda}{2}\right)\Gamma\left(j+\frac{\lambda}{4}\right)}{\Gamma\left(1+j-\frac{\lambda}{4}\right)}\,A^2(\lambda) \\ \mathcal{C}^B(\lambda) &= 1-\frac{\lambda}{2} \end{aligned} \qquad \text{for } \lambda \in (0,2)\,. \tag{2.94}$$

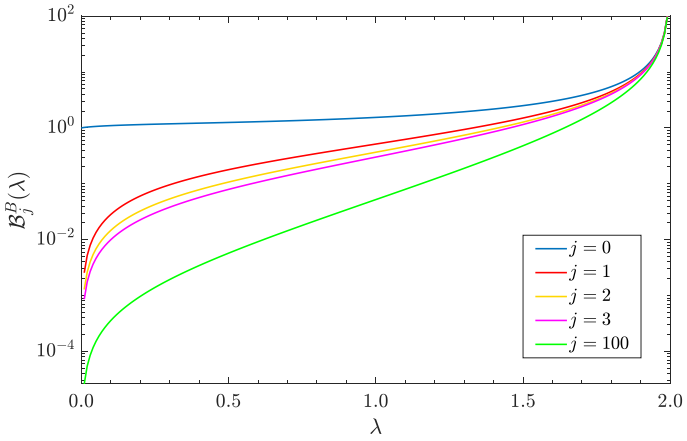

Figure 2.7: Numerical prefactor $\mathcal{B}_j^B(\lambda)$ for the scaling $\lambda_j^B \sim \mathcal{B}_j^B N^{\mathcal{C}^B}$ in semi-log scale for the bosonic Calogero–Sutherland model for different values of the index j.

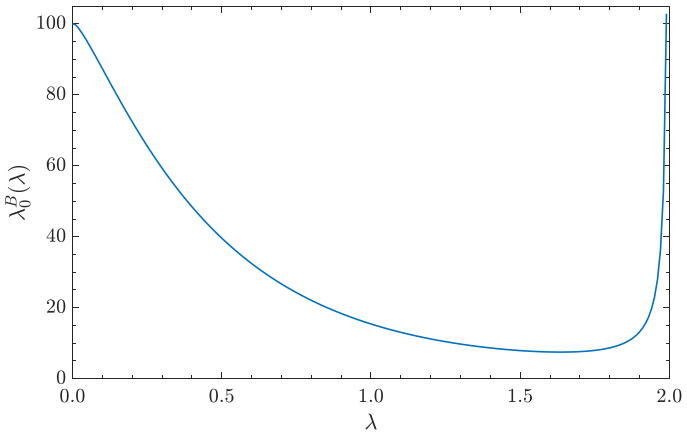

Figure 2.8: Largest eigenvalue of the 1BDM for the bosonic CSM according to $\lambda_0^B \sim \mathcal{B}_0^B N^{\mathcal{C}^B}$ for $N = 100$ for different values of the interaction. For $\lambda = 1.99$ one gets that: $\lambda_0^B \sim \mathcal{B}_0^B N^{\mathcal{C}^B} \approx 103 > N$, and we expect that there will be corrective (negative) subleading terms in the actual expression for λ_0.

Also in this case, for $\lambda = 1$ one obtains the known results of the impenetrable bosons system [100]: $\mathcal{B}_j^B(1) = \frac{\sqrt{e\pi}\,\Gamma\left(j+\frac{1}{4}\right)}{2^{1/3}A^6\,\Gamma\left(j+\frac{3}{4}\right)}$, as it should be. For $\lambda = 0$, one ideally has $\mathcal{C}^B = 1$, $\mathcal{B}_0^B(0) = 1$ and $\mathcal{B}_j^B(0) = 0$ for all other j, which is correct since the occupation numbers should be normalized such that: $\sum_j \lambda_j = N$. In Fig. 2.7 we report the behaviour for the prefactors $\mathcal{B}_j^B(\lambda)$ for $j = 0, 1, 2, 3$ and 100 for different values of the interaction parameter. It has to be stressed that the above equations are valid for j fixed when the thermodynamic limit is taken into account.

In Fig. 2.8 and 2.9 we report respectively the behaviour of the largest eigenvalue and the ratio $\lambda_j(\lambda)/\lambda_0(\lambda)$, of the 1BDM for the CSM fixing $N = 100$, according to the law $\lambda_j^B \sim \mathcal{B}_j^B N^{\mathcal{C}^B}$ using (2.94).

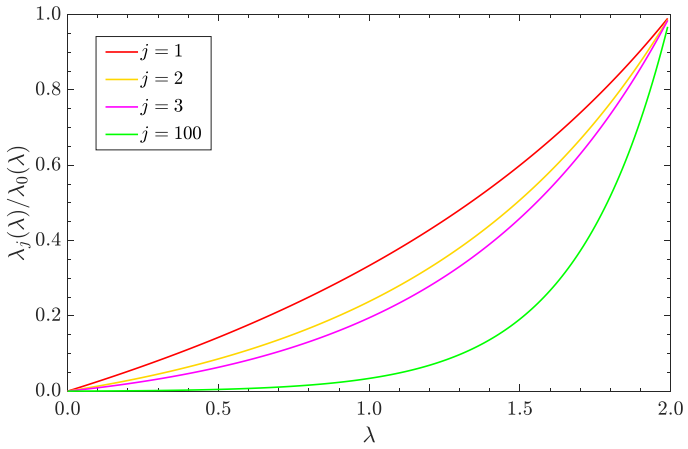

Figure 2.9: Occupation numbers of the bosonic CSM for $N = 100$, normalized with respect to the largest eigenvalue λ_0 for different values of the interaction. We see that for λ approaching the critical value 2, the leading terms of the eigenvalues of the 1BDM tend to originate a behaviour similar to a fragmentation phenomena.

For $\lambda = 2$, one has $\mathcal{C}^B = 0$, and indeed the momentum distribution is known to have a logarithmic scaling with k. Let us discuss this case in more detail: For $\lambda = 2$ the 1BDM is known to be [113]:

$$\frac{g_1^B(x)}{\rho} = \frac{Si(2k_F x)}{2k_F x}\,, \tag{2.95}$$

where $Si(x) = \int_0^x \frac{\sin(y)}{y} dy$ is the sine integral function. From this one finds for the momentum distribution:

$$n_k^B = \begin{cases} \frac{L}{4\pi} \ln \frac{2k_F}{|k|}, & |k| < 2k_F \\ 0, & |k| \geq 2k_F \end{cases}\,. \tag{2.96}$$

Symmetrizing $g_1^B(x)$ by replacing the x variable with the chord distance, we can get an expression for the largest eigenvalue of the system, which reads:

$$\lambda_0^B = \int_0^L \frac{Si\left(2\pi\rho\left(\frac{L}{\pi}\sin\frac{\pi x}{L}\right)\right)}{2\pi\left(\frac{L}{\pi}\sin\frac{\pi x}{L}\right)} dx = N\,{}_2F_3\left(\frac{1}{2},\frac{1}{2};1,\frac{3}{2},\frac{3}{2};-N^2\right)\,, \tag{2.97}$$

where ${}_2F_3(a_1,a_2;b_1,b_2,b_3;c)$ is the generalized hypergeometric function. By expanding ${}_2F_3$ for large N and keeping only the leading terms, one finally gets for the bosonic Calogero–Sutherland model with $\lambda = 2$:

$$\lambda_0^B = \frac{\gamma + \ln(4)}{2} + \frac{1}{2}\ln N\,, \tag{2.98}$$

where $\gamma \approx 0.577216$ is the Euler's constant. Therefore $\mathcal{B}_0^B(\lambda = 2) = \frac{\gamma+\ln(4)}{2} \approx 0.981755$ and $\mathcal{C}^B(\lambda = 2) = 0$, and there is a discontinuity on the prefactor $\mathcal{B}_0^B(\lambda)$ which diverges for λ approaching 2 from the left, but gets a finite value for λ exactly equal to 2. It is also

possible to obtain the scaling of the other eigenvalues λ_j^B also for $\lambda = 2$. The procedure is the same, and after some algebras we obtain:

$$\lambda_1^B = \frac{\gamma + \ln(4)}{2} - 1 + \frac{1}{2}\ln N\,, \tag{2.99}$$

$$\lambda_2^B = \frac{\gamma + \ln(4)}{2} - \frac{4}{3} + \frac{1}{2}\ln N\,, \tag{2.100}$$

$$\lambda_3^B = \frac{\gamma + \ln(4)}{2} - \frac{23}{15} + \frac{1}{2}\ln N\,, \tag{2.101}$$

$$\vdots$$

Therefore we note that $\lambda = 2$ is the critical value beyond which the quasi-condensation disappears. The formation of a quasi-crystal happens around $\lambda = 2$, as nicely characterized in [178].

2.3.2 1BDM AND λ_0 SCALING FOR THE CM

When a trapping potential is introduced, the Galilean invariance of the system is lost and the natural orbitals are not anymore plane waves. Therefore the identification (2.86) does no longer hold and one has to assign, in general, two different power law scalings for λ_0 and $n(k=0)/a_{ho}$.

The expression for the one–body density matrix of a Luttinger liquid in inhomogeneous space in the semiclassical limit $\hbar \to 0$, was obtained in [158] by using Conformal Field Theory arguments. Notice that for a generic system the effect of the trap gives rise to a spatial dependence on some fundamental parameters of the specific model, such as the Luttinger parameter $K \to K(x)$. In the limit $|x-y|\,\rho_{\max} \gg 1$, where $\rho_{\max}$ is the maximum density in the trap, the Luttinger liquid density matrix reads:

$$g_1^{\rm cft}(x,y) \;=\; \frac{\rho_{\rm LDA}(x)^{\frac{2K(x)-1}{4K(x)}}}{v(x)^{\frac{1}{4K(x)}}}\,\frac{\rho_{\rm LDA}(y)^{\frac{2K(y)-1}{4K(y)}}}{v(y)^{\frac{1}{4K(y)}}}\,b(\gamma(x))\,b(\gamma(y))\,\frac{e^{\frac{1}{2}\left[G^N_{[1/4K]}(x)+G^N_{[1/4K]}(y)\right]}}{e^{G^N_{[1/4K]}(x,y)}}\,, \tag{2.102}$$

where $\rho_{\rm LDA}(x)$ is the inhomogeneous particle density in Local Density Approximation (LDA), $v(x)$ is the velocity of gapless excitations in the system, $b(\gamma(x))$ are numerical prefactors that can be obtained using a form factors approach and which in general depends on the spatial coordinate because of the x-dependence of the dimensionless interaction parameter γ (in the case of the Lieb–Liniger model for example) in presence of a trap. Finally the $G^N_{[1/4K]}$ are Green's functions satisfying the Poisson's equation with Neumann boundary conditions on the Euclidean spacetime Ω:

$$\nabla_x \cdot 4K(x)\nabla_x G^N_{[1/4K]}(x,y) \;=\; 4\pi\delta^2(x-y) - \frac{4\pi}{{\rm Vol}(\Omega)}\,, \tag{2.103}$$

and with:

$$\int_\Omega d^2x\, G^N_{[1/4K]}(x,y) \;=\; 0\,,$$

$$\hat{n}_x \cdot \nabla_y G^N_{[1/4K]}(x,y) \;=\; 0 \qquad \text{for } y \in \partial\Omega\,,$$

where $\hat{n}_x$ is the unit vector normal to the boundary at $x \in \partial\Omega$. The so called regularized Green's function is defined as:

$$G^N_{[K]}(x) \;=\; \lim_{y\to x}\left[G^N_{[K]}(x,y) - K(x)\ln|x-y|^2\right]\,. \tag{2.104}$$

Now we're going to apply these formalisms and solutions to the bosonic Calogero model in harmonic potential of Eq. (2.74). From the long–range asymptotic behaviour of the ground state wavefunction in the homogeneous case ($\omega = 0$) in Eq. (2.78), one can infer that the Luttinger parameter K is simply $K = 1/\lambda$ for the Calogero model. Since the presence of a harmonic trap doesn't change the dimensionless interaction parameter λ (notice that this is not true for other models such as the Lieb–Liniger, where the presence of the trap change the density of the particles and therefore also the interaction parameter γ will depend on the spatial coordinate, as stated previously), the case of long–range interactions $(x_i - x_j)^{-2}$ is particularly simple since the Luttinger parameter remains constant, *i.e.* doesn't depend on x. Therefore, from the relation between the Luttinger parameter and the sound and Fermi velocities in the homogeneous case: $K = \frac{v_F}{v}$, we know that the same relation will hold for the Calogero model, and in particular:

$$v(x) \;=\; \lambda\, v_F(x) \;=\; \frac{\lambda\pi\hbar}{m}\rho(x)\,, \tag{2.105}$$

where now we have an x dependence on the Fermi velocity because of the trapping potential, and in the last equality we've written v_F in terms of the particle density. The particle density for the CM within LDA can be written as [118]:

$$\rho(x) \;=\; \frac{1}{\pi}\sqrt{\frac{2Nm\omega}{\lambda\hbar} - \left(\frac{m\omega}{\lambda\hbar}\right)^2 x^2}\,, \tag{2.106}$$

which is valid for any λ's and for $x \in [x_1, x_2]$, with $x_1 = -\sqrt{\frac{2N\lambda\hbar}{m\omega}}$ and $x_2 = -x_1$, while vanishes elsewhere. Notice that since:

$$\int_{x_1}^{x_2} \rho(x)\,dx \;=\; N\,, \tag{2.107}$$

then substituting (2.106), it follows that the $\hbar \to 0$ limit is actually equivalent to the thermodynamic limit $N \to \infty$, as we already saw for the field theoretical treatment of a trapped Tonks–Girardeau gas. In particular we refer to Eq. (2.16).

In [158] they also found an expression for the first terms of the expansion of the density operator. The expansion reads:

$$\rho(x) \;=\; \rho_{\mathrm{LDA}}(x) + 2\,\mathcal{A}(x)\,\cos\left[2\pi\int_0^x \rho_{\mathrm{LDA}}(t)\,dt - \pi\right]\frac{\rho_{\mathrm{LDA}}(x)^{1-K(x)}}{v(x)^{K(x)}}\,e^{\frac{1}{2}G^D_K(x)}\,. \tag{2.108}$$

Such terms, in the Lieb–Liniger model, provide a good comparison with the exact results coming from DMRG, *i.e.* they are able to reproduce correctly also the Friedel oscillations. The density will then read (in dimensionless units):

$$\begin{aligned}
&\rho_{\mathrm{Friedel}}(\eta) \;\equiv\; \rho(\eta)\cdot C_{\mathrm{Friedel}}(\eta) \;=\\
&=\; \rho(\eta)\cdot\Bigg\{1 - \mathcal{A}(\lambda)\,2^{1-\frac{1}{2\lambda}}\pi^{\frac{1}{\lambda}}\lambda^{-\frac{3}{2\lambda}}N^{\frac{1}{2\lambda}}\\
&\qquad\cos\left[\eta\sqrt{\frac{2N}{\lambda} - \left(\frac{\eta}{\lambda}\right)^2} - 2N\arccos\left(\frac{\eta}{\sqrt{2N\lambda}}\right)\right]\left[\frac{2N}{\lambda} - \left(\frac{\eta}{\lambda}\right)^2\right]^{-\frac{3}{2\lambda}}\Bigg\}\,,
\end{aligned} \tag{2.109}$$

where $\rho(\eta)$ is given by (2.106), while $\mathcal{A}(\lambda) = \frac{\Gamma\left(1+\frac{1}{\lambda}\right)}{(2\pi)^{1/\lambda}}$ [93, 178]. We report in Fig. 2.10 the density profiles in Local Density Approximation ρ_{LDA} and with Friedel corrections ρ_{Friedel}, for different values of the interaction parameter λ and number of particles. For $\lambda = 1$, *i.e.* in the Tonks–Girardeau case, we also report the exact analytical value for $\rho(\eta)$ which reads $\rho(\eta) = \sum_{j=0}^{N-1} |\phi_j(\eta)|^2$, where:

$$\phi_j(\eta) \;=\; \frac{1}{\sqrt{2^j j!}} \frac{\exp -\eta^2/2}{\pi^{1/4}} \, H_j(\eta)$$

is the j-th eigenstate of the harmonic oscillator problem. From Fig. 2.10 we can see that the Friedel oscillations are well captured up to $\lambda \simeq 2$, where the quasi-cristallization phenomenon [178] starts to play an important role in the system, and after that value for λ our predictions for the Friedel oscillations of density profiles are not in good agreement with the Monte Carlo results. Nevertheless the LDA approximation captures the scaling of the density profile and we expect that for large N, where Friedel oscillations are less relevant, LDA describes reasonably well the effective behaviour of the system.

Let us now pass to the discussion of the Green's functions entering in the expression of the 1BDM: Defining $\tilde{G}^N_{[\lambda/4]}(x,y) \equiv \frac{1}{\lambda} G^N_{[1/4K]}(x,y)$, one can easily obtain the expressions for the Green's function of the CM solving Eq. (2.103) with $K = 1$ [156], *i.e.* for the Tonks–Girardeau gas, and then multiplying the solutions by λ. It is found:

$$G^N_{[\lambda/4]}(x,y) \;=\; \ln\left[2\left|\sin\left(\frac{\tilde{x}-\tilde{y}}{2}\right)\right|^{\frac{1}{2}}\left|\sin\left(\frac{\tilde{x}+\tilde{y}}{2}\right)\right|^{\frac{1}{2}}\right]^{\lambda}, \tag{2.110}$$

$$G^N_{[\lambda/4]}(x) \;=\; \ln\left[|2\sin(\tilde{x})|^{\frac{1}{2}}\right]^{\lambda}, \tag{2.111}$$

where the coordinate $\tilde{x}$ represents the time needed by a signal traveling with velocity $v(x)$ to go from the origin to the x position, *i.e.*

$$\tilde{x} \;=\; \int_0^x \frac{du}{v(u)} \;=\; \frac{1}{\omega}\left[\arcsin\left(x\sqrt{\frac{m\omega}{2N\lambda\hbar}}\right) + \frac{\pi}{2}\right], \tag{2.112}$$

where in the last equality we used (2.105) and (2.106), and the integration has been performed.

The numerical prefactors $b(\gamma(x))$ now depends solely on λ, *i.e.* the dimensionless interaction parameter of the CM, and their expressions will be the same of the homogeneous case since λ doesn't change in presence of a trap. For the Calogero model with $\omega = 0$ the numerical prefactors can be written as [178]

$$[b(\lambda)]^2 \;=\; \frac{[A(\lambda)]^2}{(2\pi)^{\lambda/2}}, \tag{2.113}$$

with $A(\lambda)$ given by (2.81).

Defining the harmonic oscillator length scale $a_{ho} = \sqrt{\frac{\hbar}{m\omega}}$, we can conveniently describe the system in terms of a dimensionless position variable $\eta = x/a_{ho}$. Plugging all the above results into (2.102), we have an expression for the large distance behaviour of the 1BDM for the CM which reads:

$$g_1^{\text{cft}}(\eta,\eta') \;=\; \frac{1}{a_{ho}} \frac{[b(\lambda)]^2}{\sqrt{\lambda\pi}} \left(\frac{2N}{\pi}\right)^{\frac{1-\lambda}{2}} \frac{\left|1-\frac{\eta^2}{2N\lambda}\right|^{\frac{1}{4}\left(1-\frac{\lambda}{2}\right)} \left|1-\frac{(\eta')^2}{2N\lambda}\right|^{\frac{1}{4}\left(1-\frac{\lambda}{2}\right)}}{\left|\frac{\eta}{\sqrt{2N\lambda}}-\frac{\eta'}{\sqrt{2N\lambda}}\right|^{\frac{\lambda}{2}}}, \tag{2.114}$$

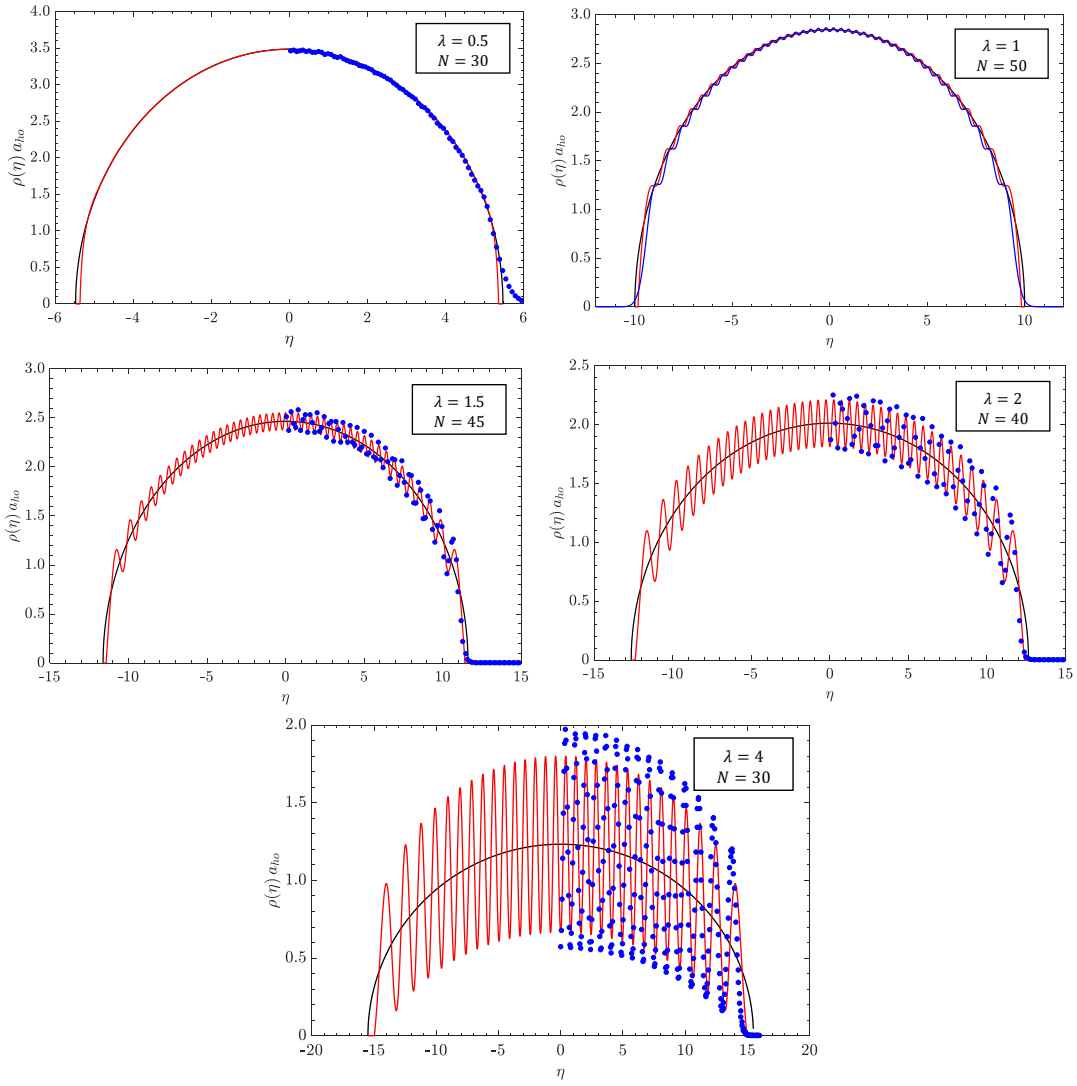

Figure 2.10: Density profiles for the harmonically trapped Calogero model for different number of particles and interaction strengths. The LDA results from Eq. (2.106) are reported in black solid lines, while the results coming from (2.109) by using [158] are reported in red solid lines. The blue dots represent the Monte Carlo results, while for $\lambda = 1$ the exact form for the density profile is reported in blue solid line.

for $\eta \in \left(-\sqrt{2N\lambda}, +\sqrt{2N\lambda}\right)$, and vanishes elsewhere because of (2.106). We report in Fig. 2.11 the one–body density matrices for the harmonically trapped Calogero model for fixed $N = 16$ and for several different values of the interaction parameter λ. Since N is rather small, the Friedel oscillations are present and evident for $\lambda = 2$ and $\lambda = 4$, where they become of "crystal type". Nevertheless the scaling behaviour of the 1BDM is well captured by our prediction in Eq. (2.114) and we expect that for growing N, where Friedel oscillations fade out, the numerical Monte Carlo results will agree even better with our expression.

Let us turn our attention to the scaling of the largest eigenvalue of the 1BDM. From the eigenvalue equation (1.59), in the semiclassical and thermodynamic limit we can then replace $g_1(x, y)$ with Eq. (2.114) after we passed from x to the dimensionless positions η

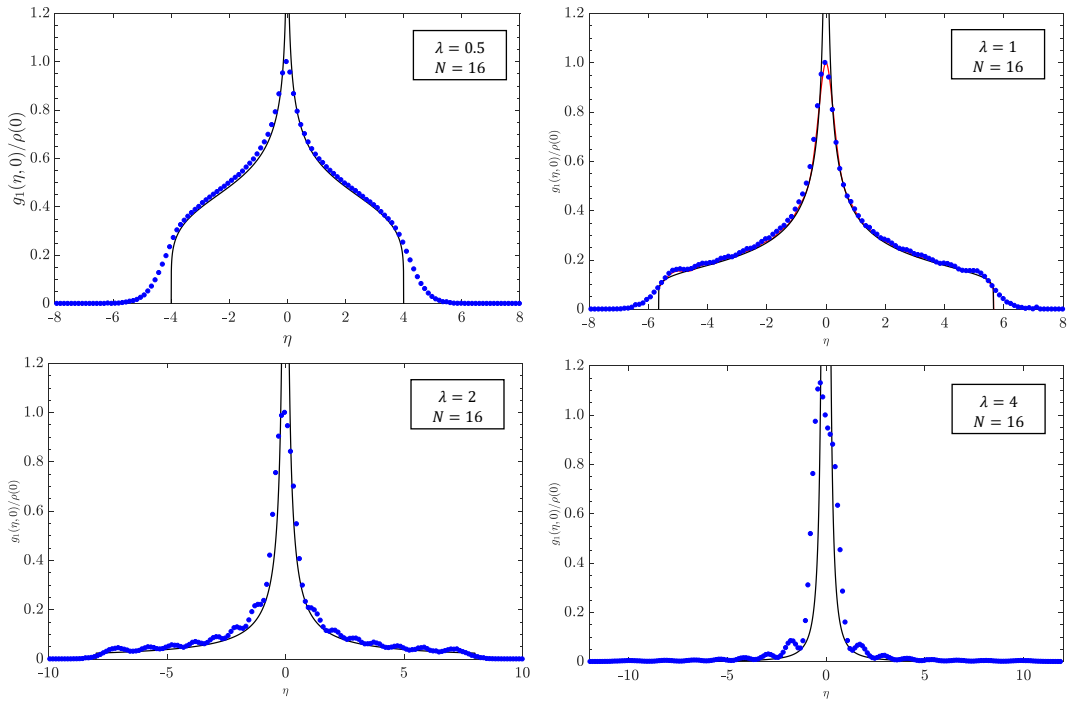

Figure 2.11: Trapped Calogero normalized one–body density matrices predictions with one coordinate fixed in the center of the trap for $\lambda = 0.5$, 1, 2 and 4 from top to bottom, all plots are with fixed $N = 16$. Black solid lines are the results of (2.114), while blue points are the results coming from Monte Carlo calculations. In red solid line for $\lambda = 1$ there is reported the exact result of the harmonically trapped Tonks–Girardeau gas.

and η'. The integration domain is therefore restricted to $y \in [y_1, y_2]$ with $y_1 = -a_{ho}\sqrt{2N\lambda}$ and $y_2 = -y_1$. Focusing only on the largest eigenvalue term $j = 0$, we have:

$$\int_{y_1}^{y_2} g_1^{\rm cft}(x,y)\,\varphi_0(y)\,dy \;=\; \lambda_0\,\varphi_0(x)\,. \tag{2.115}$$

Writing $\lambda_0 \sim \mathcal{B}_0(\lambda)\,N^{\mathcal{C}(\lambda)}$, which will be a good choice for describing the behaviour of the largest eigenvalue of the 1BDM in the large N limit for $\lambda < 2$, from the eigenvalue equation we then have:

$$[B(\lambda)]^2\left(\frac{2}{\pi}\right)^{1-\frac{\lambda}{2}} N^{1-\frac{\lambda}{2}} \int_{-1}^{1} K\left(\tilde\eta,\tilde\eta'\right)\,\varphi_0(\tilde\eta')\,d\tilde\eta' \;=\; \mathcal{B}_0(\lambda)\,N^{\mathcal{C}(\lambda)}\,\varphi_0(\tilde\eta)\,, \tag{2.116}$$

where we passed from x to $\eta = x/a_{ho}$ and then from η to $\tilde\eta = \frac{\eta}{\sqrt{2N\lambda}}$. $K\left(\tilde\eta,\tilde\eta'\right)$ is the kernel:

$$K\left(\tilde\eta,\tilde\eta'\right) \;=\; \frac{\left|1-\tilde\eta^2\right|^{\frac{1}{4}\left(1-\frac{\lambda}{2}\right)}\,\left|1-(\tilde\eta')^2\right|^{\frac{1}{4}\left(1-\frac{\lambda}{2}\right)}}{\left|\tilde\eta-\tilde\eta'\right|^{\frac{\lambda}{2}}}\,, \tag{2.117}$$

and denoting its largest eigenvalue as σ_0, from the equivalence between the left and right hand side of Eq. (2.116) we have an expression for the prefactor of λ_0:

$$\mathcal{B}_0(\lambda) \;=\; [B(\lambda)]^2\left(\frac{2}{\pi}\right)^{1-\frac{\lambda}{2}}\sigma_0\,, \tag{2.118}$$

and for the power with which λ_0 scales with the number of particles:

$$\mathcal{C}(\lambda) \;=\; 1-\frac{\lambda}{2}\,. \tag{2.119}$$

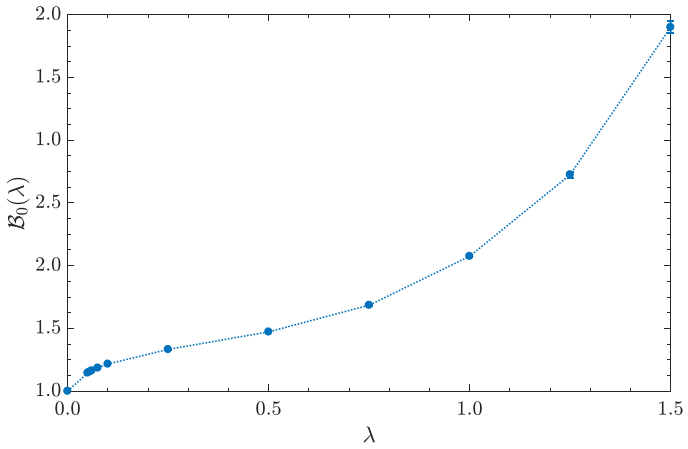

Figure 2.12: Numerical values for the prefactor $\mathcal{B}_0(\lambda)$ for the Calogero model for different values of the interaction parameter.

Notice that the kernel in (2.117) is singular for $\tilde{\eta} = \tilde{\eta}'$ and its diagonal elements have to be regularized with a cutoff ϵ [156], as we did also with the trapped Tonks–Girardeau gas. Numerical estimations for $\mathcal{B}_0(\lambda)$ are obtained with a Gauss-Legendre quadrature up to $Z = 20000$ nodes (see Appendix 2.2.A). Z is the number of points in which the grid the integration interval $[-1, 1]$ is divided. The error is estimated by extrapolating the value of $\mathcal{B}_0(\lambda)$ in the limit $\epsilon \to 0$ by increasing Z. Then the obtained values for varying Z are fitted with a function of the form $\mathcal{B}_0(\lambda) + M/Z^{\xi}$. In Fig. 2.12 we report the behaviour of $\mathcal{B}_0(\lambda)$ for the Calogero model for different values of the interaction parameter. Some values for the λ_0 prefactor are reported below for convenience:

$$
\begin{aligned}
\mathcal{B}_0\left(\lambda = \frac{1}{4}\right) &= 1.133 \pm 0.001\,, \\
\mathcal{B}_0\left(\lambda = \frac{1}{2}\right) &= 1.189 \pm 0.001\,, \\
\mathcal{B}_0\left(\lambda = \frac{3}{4}\right) &= 1.274 \pm 0.002\,, \\
\mathcal{B}_0\left(\lambda = 1\right) &= 1.430 \pm 0.004\,, \\
\mathcal{B}_0\left(\lambda = \frac{5}{4}\right) &= 1.69 \pm 0.01\,, \\
\mathcal{B}_0\left(\lambda = \frac{3}{2}\right) &= 2.16 \pm 0.02\,.
\end{aligned}
$$

Notice that for $\lambda = 1$ we get back the known results of the harmonically trapped Tonks–Girardeau gas, *i.e.* $\mathcal{B}_0(1) = 1.43$ and $\mathcal{C}(1) = 1/2$ [100]. Unfortunately for $\lambda \geq 2$ we do not reach a convergent result for the prefactor $\mathcal{B}_0$.

Another important result to take into account is that we found a universal behaviour for the power $\mathcal{C}(\lambda)$, which assumes the same values of the homogeneous bosonic Calogero–Sutherland model, cfr (2.93). Moreover we recall that in presence of a trapping potential, there are two ways with which the large-N limit can be taken: (a) Increasing N and at the same time varying the frequency parameter ω of the external potential V in such a way to keep the density at the center of the trap fixed; (b) or fixing ω and simply increasing N. Nevertheless since Eq. (2.116) does not depend on the trapping frequency ω, the two ways with which the large-N limit can be taken are equivalent and the scaling of the largest eigenvalue of the 1BDM is the same.

Following the same reasoning used for the trapped Tonks–Girardeau gas, we can make predictions also for the scaling of the dimensionless ground state natural orbital and momentum distribution peak. We define the dimensionless ground state natural orbital $\hat{\varphi}_0(\eta)$ such that:

$$\int_{-\infty}^{\infty} |\hat{\varphi}_0(\eta)|^2 \, d\eta \, = \, 1 \, , \tag{2.120}$$

from which follows that $\tilde{\varphi}_0(\eta) \equiv \varphi_0(x)\sqrt{a_{ho}}$. Since $a_{ho} \propto \sqrt{\hbar} \sim N^{-1/2}$, then we can write:

$$\hat{\varphi}_0(\eta) \sim N^{\beta} \sim N^{-1/4} \, , \tag{2.121}$$

in the semiclassical limit. This is the exact same scaling that we obtained in the harmonically trapped Tonks–Girardeau case, and should be valid for generic λ.

If we now consider the momentum distribution of the system, defined as:

$$n(k) \, = \, \frac{1}{2\pi} \int_{-\infty}^{\infty} dx \, \int_{-\infty}^{\infty} dy \, \rho(x,y) \, e^{-i\,k\,(x-y)} \, , \tag{2.122}$$

then from Eq. (1.59), we have the eigendecomposition:

$$g_1(x,y) \, = \, \sum_j \lambda_j \, \varphi_j^*(y) \, \varphi_j(x) \, , \tag{2.123}$$

which, substituted into the momentum distribution definition, gives:

$$n(k) \, = \, \sum_j \lambda_j \left| \tilde{\varphi}_j(k) \right|^2 \, , \tag{2.124}$$

where we defined the Fourier transform of the natural orbital as

$$\tilde{\varphi}_j(k) = \frac{1}{\sqrt{2\pi}} \int_{-\infty}^{\infty} \varphi_j(x) \, e^{-ikx} \, dx \, .$$

Then for the $k = 0$ term of the momentum distribution we expect that:

$$n(k=0) \approx \frac{\lambda_0}{2\pi} \left| \int_{-\infty}^{\infty} \varphi_0(x) \, dx \right|^2 \, , \tag{2.125}$$

since λ_0 is the largest eigenvalue and will give the largest contribution to the $\sum_j$ in (2.124). From the scaling of the largest eigenvalue of the 1BDM (2.119) and the scaling for the ground state natural orbital (2.121), we can write that the dimensionless momentum distribution peak scales as:

$$\frac{n(k=0)}{a_{ho}} \sim N^{\gamma} \sim N^{\frac{3-\lambda}{2}} \, , \tag{2.126}$$

for any $\lambda < 2$. Notice that $\gamma \geq 1$ doesn't imply formation of BEC, since also a_{ho} has a dependence on N. In experiments where $n(k)$ is measured, from (2.126) and since $a_{ho} \sim N^{-1/2}$, then:

$$n(k=0) \sim N^{1-\frac{\lambda}{2}} \, , \tag{2.127}$$

and only for $\lambda = 0$ (ideal Bose gas) one expects a macroscopic occupation of the $k = 0$ state, *i.e.* a Bose–Einstein condensate.

2.3.3 PAIR DISTRIBUTION

From the results of [158] we are able to extract the behaviour of the pair distribution function for the Calogero model in harmonic trapping potential for distances large with respect to the interparticle distance, and small compared with the total effective length of the system. The pair distribution function is defined as:

$$\nu(x,y) \;=\; \langle \rho(x)\rho(y)\rangle \;, \tag{2.128}$$

and for a Luttinger liquid it can be written as [158]:

$$\begin{aligned}
\nu_c^{\mathrm{cft}}(x,y) \;=\; & -\frac{1}{4\pi^2}\left[v(x)v(y)\right]^{-1}\partial_{\tilde{x}}\partial_{\tilde{y}}G^D_{[K]}(x,y) + \frac{1}{\pi}v(x)^{-1}\left[\partial_{\tilde{x}}G^D_{[K]}(x,y)\right]\sin\left[2\theta(y)\right] \\
& \frac{\rho_{\mathrm{LDA}}(y)^{1-K(y)}}{v(y)^{K(y)}}A(y)e^{\frac{1}{2}G^D_{[K]}(y)} + \frac{1}{\pi}v(y)^{-1}\left[\partial_{\tilde{y}}G^D_{[K]}(x,y)\right]\sin\left[2\theta(x)\right]\frac{\rho_{\mathrm{LDA}}(x)^{1-K(x)}}{v(x)^{K(x)}}\cdot \\
& \cdot A(x)e^{\frac{1}{2}G^D_{[K]}(x)} + 2\,\frac{\rho_{\mathrm{LDA}}(x)^{1-K(x)}}{v(x)^{K(x)}}\frac{\rho_{\mathrm{LDA}}(y)^{1-K(y)}}{v(y)^{K(y)}}A(x)A(y)\,e^{\frac{1}{2}\left[G^D_{[K]}(x)+G^D_{[K]}(y)\right]}. \\
& \cdot\left\{\left[e^{G^D_{[K]}(x,y)}-1\right]\cos\left[2\theta(x)+2\theta(y)\right] + \left[e^{-G^D_{[K]}(x,y)}-1\right]\cos\left[2\theta(x)-2\theta(y)\right]\right\}\;,
\end{aligned} \tag{2.129}$$

where the subscript c stands for the connected part of the distribution function, while:

$$\theta(x) \;=\; -\frac{\pi}{2} + \pi\int_0^x \rho_{\mathrm{LDA}}(t)\,dt\,. \tag{2.130}$$

Defining the pair correlation function as:

$$g_2(x,y) \;=\; \nu_c(x,y) + \rho(x)\rho(y)\,, \tag{2.131}$$

by using the recipes and formulas given in the previous section we are able to write an expression for the pair correlation function of the Calogero model from Eq. (2.129). After a lengthy but straightforward calculation one arrives at the following equation:

$$
\begin{aligned}
g_2^{\mathrm{cft}}(\eta,\eta') \;=\; & \frac{1}{a_{ho}^2}\Bigg\{ \frac{1}{2\pi^2\lambda}\,\frac{\eta\eta'-2N\lambda}{(\eta-\eta')^2}\,\left[\left|2N\lambda-\eta^2\right|\left|2N\lambda-\eta'^2\right|\right]^{-1/2} - N^{-\frac{1}{2\lambda}}\,\frac{2^{1-\frac{3}{2\lambda}}\pi^{-2+\frac{1}{\lambda}}}{\lambda^{2+\frac{3}{2\lambda}}} \\
& \mathcal{A}(\lambda)\,\frac{\left|2N\lambda-\eta'^2\right|^{1-\frac{3}{2\lambda}}}{(\eta-\eta')\left|2N\lambda-\eta^2\right|^{1/2}}\sin\left[\frac{\eta'}{\lambda}\sqrt{2N\lambda-\eta'^2}-2N\arccos\left(\frac{\eta'}{\sqrt{2N\lambda}}\right)\right] - N^{-\frac{1}{2\lambda}} \\
& \frac{2^{1-\frac{3}{2\lambda}}\pi^{-2+\frac{1}{\lambda}}}{\lambda^{2+\frac{3}{2\lambda}}}\mathcal{A}(\lambda)\,\frac{\left|2N\lambda-\eta^2\right|^{1-\frac{3}{2\lambda}}}{(\eta'-\eta)\left|2N\lambda-\eta'^2\right|^{1/2}}\sin\left[\frac{\eta}{\lambda}\sqrt{2N\lambda-\eta^2}-2N\arccos\left(\frac{\eta}{\sqrt{2N\lambda}}\right)\right] + \\
& + \left[\mathcal{A}(\lambda)\right]^2\,\frac{\left|2N\lambda-\eta^2\right|^{\frac{\lambda-3}{2\lambda}}\left|2N\lambda-\eta'^2\right|^{\frac{\lambda-3}{2\lambda}}}{|\eta-\eta'|^{\frac{2}{\lambda}}}\cdot \\
& \cdot\Bigg\{\left|\cos\left[\frac{1}{2}\left(\arcsin\left(\frac{\eta}{\sqrt{2N\lambda}}\right)+\arcsin\left(\frac{\eta'}{\sqrt{2N\lambda}}\right)\right)\right]\right|^{\frac{2}{\lambda}} + \\
& -\left|\sin\left[\frac{1}{2}\left(\arcsin\left(\frac{\eta}{\sqrt{2N\lambda}}\right)-\arcsin\left(\frac{\eta'}{\sqrt{2N\lambda}}\right)\right)\right]\right|^{\frac{2}{\lambda}}\Bigg\}\cdot \\
& \cdot\Bigg\{\left|\cos\left[\frac{1}{2}\left(\arcsin\left(\frac{\eta}{\sqrt{2N\lambda}}\right)+\arcsin\left(\frac{\eta'}{\sqrt{2N\lambda}}\right)\right)\right]\right|^{\frac{2}{\lambda}}\cos\Bigg[\frac{\eta}{\lambda}\sqrt{2N\lambda-\eta^2}+ \\
& -\frac{\eta'}{\lambda}\sqrt{2N\lambda-\eta'^2}+2N\left(\arccos\left(\frac{\eta'}{\sqrt{2N\lambda}}\right)-\arccos\left(\frac{\eta}{\sqrt{2N\lambda}}\right)\right)\Bigg] + \\
& -\left|\sin\left[\frac{1}{2}\left(\arcsin\left(\frac{\eta}{\sqrt{2N\lambda}}\right)-\arcsin\left(\frac{\eta'}{\sqrt{2N\lambda}}\right)\right)\right]\right|^{\frac{2}{\lambda}} \\
& \cos\left[\frac{\eta}{\lambda}\sqrt{2N\lambda-\eta^2}+\frac{\eta'}{\lambda}\sqrt{2N\lambda-\eta'^2}-2N\left(\arccos\left(\frac{\eta'}{\sqrt{2N\lambda}}\right)+\arccos\left(\frac{\eta}{\sqrt{2N\lambda}}\right)\right)\right]\Bigg\}\Bigg\}
\end{aligned}
\tag{2.132}
$$

and we remind that $\mathcal{A}(\lambda)=\frac{\Gamma\left(1+\frac{1}{\lambda}\right)}{(2\pi)^{1/\lambda}}$.

We report in Fig. 2.13 the behaviour of $\frac{g_2^{\mathrm{cft}}(\eta,0)}{[\rho(0)]^2}$ for different values of the interaction parameter λ. As can be seen from the plot the pair correlation function goes to zero both at short distances, since the inverse square interaction of the Calogero model prevents two particles from occupying the same position, and also at large distances, because of the presence of the trapping potential. Indeed for large separations between η and η' one expects a factorization of the correlation function, but then $\rho(\eta)\to 0$ for large η because of the external potential which confines the system.

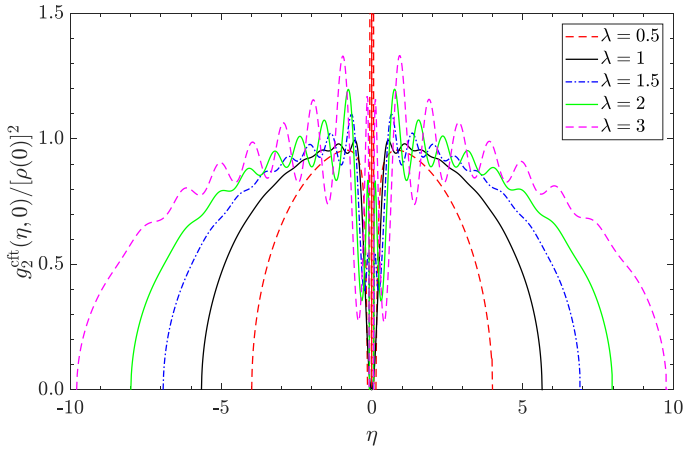

Figure 2.13: Normalized pair correlation function of the trapped Calogero with one coordinate fixed in the center of the trap for $\lambda = 0.5$, 1, 1.5, 2 and 3. The pair correlation function goes to zero both at small and large values of η, because of the nature of interactions and the trapping potential respectively.

APPENDIX

2.A GAUSS QUADRATURE METHOD

The Gauss quadrature rule is a method with which one can estimate in terms of a finite sum an integral of a function $f(x)$ of the form

$$\int_a^b f(x)\, w(x)\, dx\,, \tag{A2.1}$$

where $w(x)$ is some weight function. In the Gauss quadrature method the weights and nodes (points) where evaluating $f(x)$ are chosen in advance. This choice is based on the support of the integral in Eq. (A2.1). We have already seen the Gauss–Chebyshev quadrature method, but now we will extend to other cases. For example with the Gauss–Hermite quadrature one is able to compute integrals with $a \equiv -\infty$, $b \equiv \infty$ and weight function $w(x) = e^{-x^2}$, in the following way

$$\int f(x)\, e^{-x^2}\, dx \,\approx\, \sum_{i=1}^{Z} w_i\, f(\xi_i)\,, \tag{A2.2}$$

where the ξ_i's are the roots of the Hermite polynomial $H_Z(x)$, and (A2.2) is exact for all polynomials $f(x)$ of degree less or equal than $2Z-1$.

For the case of our interest $f(x) \equiv \rho(x,y)$. In order to recast (2.44) in the form of (A2.2), we have to multiply and divide by e^{-y^2}. By choosing $x = \xi_k$, with $k = 1, \ldots, Z$, we have Z equations of the form

$$\int \left[\rho(\xi_k, y)\, \varphi_j(y)\, e^{y^2}\right] e^{-y^2}\, dy \,=\, \lambda_j\, \varphi_j(\xi_k)\,. \tag{A2.3}$$

Using (A2.2) we then have

$$\sum_{i=1}^{Z} w_i\, \rho(\xi_k, \xi_i)\, \varphi_j(\xi_i)\, e^{\xi_i^2} \,=\, \lambda_j\, \varphi_j(\xi_k)\,, \tag{A2.4}$$

providing an eigenvalue equation for a $Z \times Z$ matrix S with entries

$$S_{k,i} \,=\, \rho(\xi_k, \xi_i)\, w_i\, e^{\xi_i^2}\,. \tag{A2.5}$$

Accordingly, one has to diagonalize this finite dimensional matrix to obtain the occupation numbers λ_j and the natural orbitals $\varphi_j(x)$. Of course, the larger is Z and the better are the approximation results for the integrals. One has anyway to check whether increasing Z the resulting value for the integral is converging. In the cases considered in the present Chapter, this condition was fulfilled and we used Z ranging from ≈ 80 to ≈ 170. Moreover, one has a condition to check, that is

$$\sum_{j=1}^{Z} \lambda_j \,=\, N\,, \tag{A2.6}$$

with N the number of particles in the system. If Eq. (A2.6) is not satisfied, then we have to increase Z.

If the support of the 1BDM is compact, as in the case of the CFT limit of Sec. (2.2.1.3), one can rely on other quadrature scheme. For instance, the Gauss–Legendre quadrature method can be applied to integrals having integration domain $[-1, 1]$ and gives

$$\int_{-1}^{1} f(x)\, dx \approx \sum_{i=1}^{Z} w_i\, f(\xi_i)\,. \tag{A2.7}$$

For the case of the half harmonic oscillator, one can use the same procedure but with different weights and nodes. The integration interval is $[0, \infty)$ and one has to apply the Gauss–Laguerre quadrature method

$$\int_{0}^{\infty} f(x)\, e^{-x}\, dx \approx \sum_{i=1}^{Z} w_i\, f(\xi_i)\,. \tag{A2.8}$$

The final form of the $Z \times Z$ matrix S to diagonalize is then

$$S_{k,i} = \rho(\xi_k, \xi_i)\, w_i\, e^{\xi_i}\,, \tag{A2.9}$$

for $k, i = 1, \ldots, Z$.

3

SCALING PROPERTIES OF INTERACTING BOSONS AT FINITE TEMPERATURE

Until now, we discussed off–diagonal long–range order and deviations from it, in the ground state ($T = 0$) of one–dimensional ($D = 1$) systems only. We remind that the Penrose–Onsager criterion applies with no conceptual problems in all dimensions and at any temperatures. Therefore we now desire to extend our studies to translational invariant bosonic systems living in a higher dimensional space $D \geq 2$. We as well remind that the dimensionality and temperatures play a central role on ordering properties of physical systems. This is mainly due to the Mermin-Wagner theorem [12, 13], which states that there is no long–range order phenomena that can happen at finite temperatures for translational invariant systems with continuous symmetry.

With the aim of extending our results in higher dimensional spaces, we redefine the one–body density matrix as:

$$\rho(\mathbf{x}, \mathbf{y}) = \left\langle \hat{\Psi}^{\dagger}(\mathbf{x}) \hat{\Psi}(\mathbf{y}) \right\rangle , \tag{3.1}$$

where the field operator $\hat{\Psi}(\mathbf{x})$ destroys a particle at the point identified by the D–dimensional vector $\mathbf{x}$. The 1BDM, as an Hermitian matrix, satisfies the eigenvalue equation:

$$\int \rho(\mathbf{x}, \mathbf{y})\, \phi_i(\mathbf{y})\, d\mathbf{y} = \lambda_i\, \phi_i(\mathbf{x}) , \tag{3.2}$$

with the eigenvalues λ_i being real and such that: $\sum_i \lambda_i = N$, with N being the number of particles. In this framework, since we are dealing with translational invariant systems, the indices i in Eq. (3.2) are wavevectors, which are conventionally denoted by the vector $\mathbf{k}$. Introducing the scaling formula:

$$\lambda_0 \sim N^{\mathcal{C}_0(T)} , \tag{3.3}$$

the Mermin-Wagner theorem implies that $\mathcal{C}_0(T) < 1$ for $T > 0$ and $D \leq 2$, so there is no ODLRO at finite temperature. We remind that the condition $0 < \mathcal{C}_0 < 1$ implies that, in translational invariant systems, the correlation function $\langle \hat{\Psi}^{\dagger}(\mathbf{x}) \hat{\Psi}(\mathbf{y}) \rangle$ have a power-law decay and we refer to this situation as *quasi-long–range order*.

Let us stress that, for a system of interacting bosons, the index $\mathcal{C}_0$ may also depend on the interaction strength and, moreover, one may expect that increasing the repulsion among the bosons, $\mathcal{C}_0$ gets dampened with respect to the weak interacting case, as we have seen explicitly in the $1D$ case at zero temperature for the Lieb–Liniger model.

In this Chapter, we are going to characterize ODLRO, and possible deviations from it, in translational invariant bosonic systems interacting via short-range potential in 1-, 2-

and 3-dimensions at finite temperatures. With "possible deviations" we also mean a study of the behaviour of the index $\mathcal{C}_k(T)$, defined as

$$\lambda_k \sim N^{\mathcal{C}_k(T)}\,, \tag{3.4}$$

where $k \neq 0$. The study of $\mathcal{C}_{k\neq 0}(T)$ gives an insight about the possible *quasi-fragmentation* of the system, *i.e.* how the particles occupy the other, $k \neq 0$, states. Notice that in literature usually one refers to fragmentation when more than one eigenvalue of the 1BDM scales with N. So, one can refer to the case in which at least two $\mathcal{C}_k$ are larger than zero (and at least one is smaller than 1) as a quasi-fragmentation.

We remind here that in translational invariant systems, there exist a direct relation between the eigenvalues of the density density matrix and the momentum distribution. For a D dimensional system, we define the momentum distribution $n(k)$ as:

$$\begin{aligned} n(\mathbf{k}) &= \left\langle \hat{\Psi}^\dagger(\mathbf{k})\hat{\Psi}(\mathbf{k})\right\rangle = \\ &= \frac{1}{(2\,\pi)^D}\int d\mathbf{x}\int d\mathbf{y}\, e^{i\,\mathbf{k}\cdot(\mathbf{x}-\mathbf{y})}\,\left\langle \hat{\Psi}^\dagger(\mathbf{x})\hat{\Psi}(\mathbf{y})\right\rangle\,, \end{aligned} \tag{3.5}$$

where we introduced the Fourier transform $\hat{\Psi}(\mathbf{k})$ of the field operator $\hat{\Psi}(\mathbf{x})$ written as:

$$\hat{\Psi}(\mathbf{k}) = \frac{1}{(2\,\pi)^{D/2}}\int d\mathbf{x}\, e^{i\,\mathbf{k}\cdot\mathbf{x}}\,\hat{\Psi}(\mathbf{x})\,. \tag{3.6}$$

For a homogeneous system, $\rho(x,y) = \left\langle \hat{\Psi}^\dagger(\mathbf{x})\hat{\Psi}(\mathbf{y})\right\rangle$ depends only on the distance among two points, therefore writing the relative distance vector as $\mathbf{r} = \mathbf{x} - \mathbf{y}$, we can rewrite $\rho(\mathbf{x},\mathbf{y}) = \rho(\mathbf{r})$ and assume $\rho(\mathbf{r}) = \rho(|\mathbf{r}|) \equiv \rho(r)$. Passing to center of mass and relative coordinates, since $\int d\mathbf{R} = L^D$ where L denotes the size of the system (*e.g.* L is the circumference of a ring in one–dimensional geometry), Eq. (3.5) can be rewritten in an universal form as:

$$n(\mathbf{k}) = \left(\frac{L}{2\,\pi}\right)^D \int e^{i\,\mathbf{k}\cdot\mathbf{r}}\,\rho(r)\,d\mathbf{r}\,. \tag{3.7}$$

The integral in the right-hand side depends of course on D. Notice that the momentum distribution peak is simply given by the integral of the 1BDM:

$$n(\mathbf{k}=0) = \left(\frac{L}{2\,\pi}\right)^D \int \rho(r)\,d\mathbf{r}\,, \tag{3.8}$$

and, as expected, the large distance asymptotic of the density matrix determines the small momenta behaviour of the momentum distribution.

For a homogeneous, isotropic system the quantum number labeling the occupation of natural orbitals is clearly the wavevector $\left|\mathbf{k}\right| \equiv k$. In particular, the Galilean invariance tells us that the effective single–particle states $\phi_k(\mathbf{x})$ may be written as plane waves, *i.e.* $\phi_k(\mathbf{x}) = \frac{1}{L^{D/2}}\,e^{i\,\mathbf{k}\cdot\mathbf{x}}$, therefore from Eqs. (3.2) and (3.7) we obtain that the dimensionless momentum distribution, $n(\mathbf{k})/L^D$, coincides with the eigenvalue equation of the one–body density matrix, apart from a $(1/2\,\pi)^D$ factor. Therefore, for a homogeneous system we have a one-to-one correspondence between the scaling of the eigenvalues of $\rho(r)$ and the scaling of the dimensionless momentum distribution:

$$\lambda_k \sim N^{\mathcal{C}_k(T)} \sim \frac{n(k)}{L^D}\,. \tag{3.9}$$

Since a complete closed form for the density matrix is not in general available for all interaction strengths and temperatures, we cannot directly compute the eigenvalues of $\rho(\mathbf{x},\mathbf{y})$ and then study their scaling with N. In order to obtain this information we will use the following procedure. From the large distance asymptotic behaviour of the 1BDM, whose expression for different configurations of the system is usually available in the literature, we first make it a periodic function of period L by adding terms which have the same scaling behaviour of the density matrix in the range $r \in \left[0, \frac{L}{2}\right)$, and which represent the reflected parts in the range $\left(\frac{L}{2}, L\right]$. In this way we construct a fully symmetric and circulant matrix, whose eigenvalues are known to be real, as required, since they represent the occupation numbers of the system. Finally we perform the Fourier transform of this symmetrized density matrix and obtain in this way the behaviour of the momentum distribution. Writing k as $k = \frac{2\pi}{L} l$ with $l \in \mathbb{N}$, the scaling of the largest eigenvalue of the 1BDM can be identified just imposing $l = 0$ and tracking its N dependence. In this way, we are able to explicitly compute the exponent $\mathcal{C}_0(T)$ of the system (and sometimes even the prefactor $\mathcal{B}_0$, as we are going to see). On the other hand, choosing $l \propto L$ the behaviour of the Fourier transform in the limit $N \to \infty$ at fixed density $n = N/L^D$ yields the expression for the exponents $\mathcal{C}_{k\neq 0}(T)$ via Eq. (3.9).

In the following, we aim to characterise the deviations from ODLRO at finite temperature for homogeneous interacting Bose gases in different dimensions. After discussing the explicit expression for $\mathcal{C}_0$, we will also discuss the finite non-zero momenta landscape, ruling out the possibility of having quasi-fragmentation in bosonic interacting systems with repulsive interactions. Our findings provide a counterpart to the corresponding results for fragmentation in macroscopically occupied states with eigenvalues scaling with N [179].

3.1 THREE DIMENSIONS

Let us begin with the case of a three–dimensional homogeneous Bose gas. It is well known that, below the critical temperature T_C, a BEC takes place and the lowest allowed state for the gas is then macroscopically occupied [18]. This amounts to saying that the momentum distribution of the system is constituted by two parts: a non-singular part, relative to the occupation of the single particle states according to the Bose-Einstein distribution, and a singular part $\propto N_0\delta(\mathbf{k})$ which refers to the macroscopic occupation $N_0 \propto N$ of the lowest energy state, also called the condensate state. Therefore, at $T < T_C$ ODLRO are found and the exponent will be $\mathcal{C}_0 = 1$ in the condensed phase. For temperatures above the critical T_C there is no more condensation and the singular part of the momentum distribution, *i.e.* the Dirac delta peak, disappears together with the system ordering. From all of these facts one can conclude that:

$$\mathcal{C}_0(T) = \begin{cases} 1, & \text{for } T < T_C \\ 0, & \text{for } T > T_C \end{cases} , \tag{3.10}$$

as shown in Fig. 3.1. For the case of a three–dimensional Bose gas one also has [18]:

$$N_0(T) = N\left[1 - \left(\frac{T}{T_C}\right)^{3/2}\right] , \tag{3.11}$$

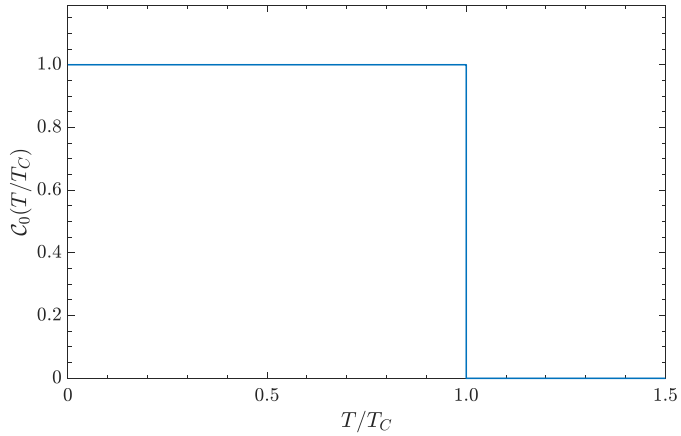

Figure 3.1: Power $\mathcal{C}_0(T/T_C)$ with which the momentum distribution peak of a homogeneous three–dimensional Bose gas scales with respect to the total number of particles N at different temperatures.

therefore, writing $\lambda_0 = \mathcal{B}_0(T) N^{\mathcal{C}_0(T)}$, we can also obtain the prefactor of the scaling for the largest eigenvalue of the 1BDM for an homogeneous three–dimensional Bose gas, and it reads:

$$\mathcal{B}_0(T) \,=\, 1 - \left(\frac{T}{T_C}\right)^{3/2} . \tag{3.12}$$

As can be noticed, it correctly goes to 1 for $T \to 0^+$, and it vanishes (*i.e.* no macroscopic occupation of the lowest natural orbital ground state) for $T = T_C$.

In the weakly interacting Bose gas, one may use the Bogoliubov approximation [18] to obtain the scaling of the momentum distribution at $\mathbf{k} \neq 0$. Indeed, at this approximation level, the non-singular part of the momentum distribution at $T < T_C$ reads:

$$\frac{n(\mathbf{k})}{L^D} \,=\, \frac{1}{(2\,\pi)^3} \frac{1}{e^{\varepsilon(k)/k_B T} - 1} , \tag{3.13}$$

where $\varepsilon(k) = \sqrt{\frac{g\,n}{m}\,\hbar^2 k^2 + \left(\frac{\hbar^2 k^2}{2m}\right)^2}$ is the Bogoliubov dispersion relation, and $g = \frac{4\pi\hbar^2 a}{m}$ weights the interaction among particles in terms of the s-wave scattering length a. Therefore for $\varepsilon(k)/k_B T \gg 1$ we obtain:

$$\frac{n(\mathbf{k})}{L^D} \,\simeq\, \frac{1}{(2\,\pi)^3} e^{-\frac{\hbar^2 k^2}{2 m k_B T}} \,\propto\, e^{-(l/L)^2} \,\propto\, N^0 , \tag{3.14}$$

where in the second equality we used $k \propto l/L$, and in the last one we acknowledged that $l \propto L$ in order to have a finite momentum k in the thermodynamic limit. A similar procedure may be used to prove the absence of fragmentation also for $T > T_C$, yielding:

$$\mathcal{C}_{k\neq 0}(T) \,=\, 0 , \tag{3.15}$$

at any temperature for the three–dimensional Bose gas. Notice that this result has been obtained using Bogoliubov theory and it may not be applicable to gases with non-weak interactions [180, 181]. However, since the exponents $\mathcal{C}$ are not expected to increase for larger interactions, one may reasonably conclude that this result is valid also for larger interactions.

3.2 ONE DIMENSION

We now turn to the study of a one–dimensional homogeneous Bose gas [63, 72], within the framework of the Lieb–Liniger model [53], where the interaction between particles is represented by a repulsive δ–potential. In Chapter 1 we already dealt with the study of the exponent $\mathcal{C}_0$ in the zero temperature case, but now we want to further analyse this model, in order to extract the scaling for λ_k both at zero and finite temperatures.

In order to study also the prefactor $\mathcal{B}$ of the scaling for the 1BDM eigenvalues with N, we need also to keep track of the coefficients of the scaling. Let us then start with the LL model at $T = 0$.

3.2.1 ZERO TEMPERATURE

The asymptotic leading behaviour of the reduced one–body density matrix for a Lieb–Liniger gas at $T = 0$ reads [cfr Eq. (1.69)]:

$$\rho(x-y) \equiv \rho(r) \simeq \frac{n\,B_0}{(n\,r)^{1/2K}}\,, \tag{3.16}$$

where $n = N/L$ is the density of the gas, B_0 is a prefactor which may be written as [182]

$$B_0 = \left(1+\frac{1}{2K}\right)\left(\frac{K}{4\pi}e^{1-\gamma}\right)^{1/2K}\,, \tag{3.17}$$

valid in the weakly interacting limit (but it gives good prediction also for large interactions, as can be seen in Table II in [182]), where K is the Luttinger parameter and $\gamma \simeq 0.57721566$ is the Euler-Mascheroni constant. The prefactor B_0 may be exactly computed using the numerical method sketched in [93].

In order to construct a fully symmetric and circulant density matrix, whose eigenvalues *i.e.* the occupation numbers of the system are real, we need to make Eq. (3.16) periodic with period equal to the circumference of the ring L in which the gas is enclosed. It can be done by simply requiring:

$$\rho^{\mathrm{hPBC}}(r) = \begin{cases} \frac{n\,B_0}{(n\,r)^{1/2K}} & \text{for } 0 \le r < L/2 \\ \frac{n\,B_0}{[n\,(L-r)]^{1/2K}} & \text{for } L/2 \le r < L \end{cases}\,, \tag{3.18}$$

or:

$$\rho^{\mathrm{sPBC}}(r) \simeq \frac{n\,B_0}{\left[n\,\frac{L}{\pi}\sin\left(\pi r/L\right)\right]^{1/2K}}\,, \tag{3.19}$$

where the superscripts hPBC and sPBC respectively stand for "*hard - Periodic Boundary Conditions*" and "*smooth - Periodic Boundary Conditions*", since in the first case $\frac{d\rho}{dr}$ is discontinuous in $L/2$ while in the second case is not.

For a homogeneous system the largest eigenvalue of the 1BDM λ_0 is simply given by:

$$\lambda_0 = \int_0^L \rho(r)\,dr\,. \tag{3.20}$$

Assuming $\lambda_0 = \mathcal{B}_0 N^{\mathcal{C}_0}$, then substituting the large distance behaviours for the symmetrized $\rho(r)$ one can obtain predictions both for the power scaling $\mathcal{C}_0$ and the numerical prefactor $\mathcal{B}_0$. Using (3.18), assuming that $L \propto N$ in order to maintain the density fixed in the thermodynamic limit, we get $\mathcal{C}_0 = 1 - \frac{1}{2K}$ and:

$$\mathcal{B}_0^{\mathrm{hPBC}}(K) \;=\; B_0\, 2^{1+\frac{1}{2K}}\, \frac{K}{2K-1}\,, \tag{3.21}$$

while with (3.19) we obtain $\mathcal{C}_0 = 1 - \frac{1}{2K}$ as well, but the equation for the prefactor changes as:

$$\mathcal{B}_0^{\mathrm{sPBC}}(K) \;=\; B_0\, \pi^{\frac{1+K}{2K}}\, \frac{\sec\left(\frac{\pi}{4K}\right)}{\Gamma\left(1-\frac{1}{4K}\right)\,\Gamma\left(\frac{1}{4}\left(2+\frac{1}{K}\right)\right)}\,. \tag{3.22}$$

Substituting $K = 1$ and B_0 from (3.17), *i.e.* considering the Tonks–Girardeau gas, in the above equations we obtain:

$$\mathcal{B}_0^{\mathrm{hPBC}}(1) \;=\; 1.47872$$

and:

$$\mathcal{B}_0^{\mathrm{sPBC}}(1) \;=\; 1.54681\,,$$

which has to be compared with the result from [100] where they predict $\mathcal{B}_0(1) = 1.54269$. Notice that using B_0 from the exact computation [93] in (3.22) one has $\mathcal{B}_0^{\mathrm{sPBC}} = 1.54265$, in very good agreement with Forrester's prediction, who used indeed smooth PBC. Using B_0 from [93] in (3.21), one has instead $\mathcal{B}_0^{\mathrm{hPBC}}(1) = 1.47474$, close to our result coming from the cut-off interpolation used in Chapter 1, which reads $\mathcal{B}_0^{\mathrm{interp}}(1) = 1.4741(1)$.

Our expressions allow also for predictions of the prefactor $\mathcal{B}_0$ for different values of the Luttinger parameter. In fig. 3.2 we checked the predictions coming from (3.21) with our other results obtained from the cut-off interpolation, where, because of the interpolation scheme, hard PBC has been used. The comparison shows good agreement.

By writing $k = \frac{2\pi}{L} j$, with $j \in \mathbb{N}$, in Eqs. (3.7) and (3.9), we can work out analytically also the parameters describing the scaling of the others λ_j eigenvalues, for $j \neq 0$, with respect to the number of particles. From Eqs. (3.18) and (3.19), using:

$$\lambda_j = \int_0^L \rho(r) e^{i2\pi r j/L}\, dr\,, \tag{3.23}$$

and by keeping only the leading term for growing N, we obtain:

$$\mathcal{B}_j^{\mathrm{hPBC}}(K) \;=\; B_0\, 2^{1+\frac{1}{2K}}\, \frac{K}{2K-1}\, {}_1F_2\left(\frac{1}{2}-\frac{1}{4K}; \frac{1}{2}, \frac{3}{2}-\frac{1}{4K}; -\frac{\pi^2}{4} j^2\right)\,, \tag{3.24}$$

for hPBC, where ${}_1F_2(a; b_1, b_2; c)$ is the generalized hypergeometric function, while for sPBC we get:

$$\mathcal{B}_j^{\mathrm{sPBC}}(K) \;=\; B_0\, \pi^{\frac{1}{2K}}\, \frac{\csc\left(\frac{\pi}{2K}\right)\Gamma\left(j+\frac{1}{4K}\right)\sin\left(\frac{\pi}{4K}\right)}{\Gamma\left(1+j-\frac{1}{4K}\right)\Gamma\left(\frac{1}{2K}\right)}\,, \tag{3.25}$$

while the power $\mathcal{C}_j(K)$ remains the same, *i.e.* Eq. (1.62), for every j. Notice that using Eq. (3.25) for $K = 1$, we retrieve the results of Eq. (48) in [100]. In Fig. 3.3 we plot the

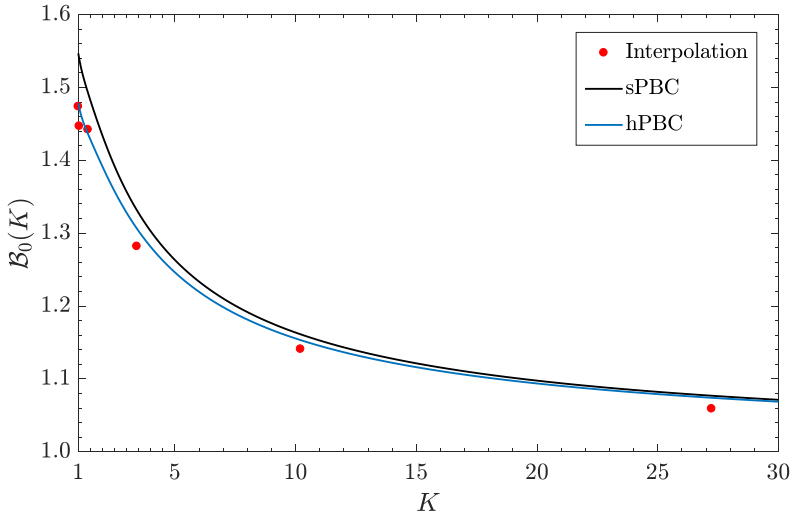

Figure 3.2: Numerical prefactor $\mathcal{B}_0(K)$ for the scaling $\lambda_0 \sim \mathcal{B}_0\, N^{\mathcal{C}_0}$ for the Lieb–Liniger gas. Numerical results (red dots) coming from the interpolation scheme, show good agreement with the analytical results of $\mathcal{B}_0^{\mathrm{hPBC}}$ of Eq. (3.21) reported in blue solid line. The analytical predictions for the prefactor $\mathcal{B}_0$ in the case of soft PBC, *i.e.* Eq. (3.22), are reported in black solid line.

behaviour of Eqs. (3.24) - (3.25) in dashed and solid lines, respectively. One can notice that for smaller and smaller interactions (*i.e.* growing K) the prefactors $\mathcal{B}_j(K)$ for $j \neq 0$ tend to vanish, while the prefactor for the scaling of the largest eigenvalue of the 1BDM for a Lieb–Liniger gas tends to unity, as it should do since: $\lambda_0 = N$, for $K = \infty$.

Let us now turn our attention to the study of the scaling of the momentum distribution for small momenta. For an homogeneous one–dimensional system we remind that:

$$\lambda_k \;=\; \int_0^L \rho(r) e^{ikr}\, dr \;=\; \frac{2\pi}{L}\, n(k)\,. \tag{3.26}$$

Interestingly enough, if we focus on the small momenta behaviour of the momentum distribution and perform the Fourier transform with ρ^{sPBC} or ρ^{hPBC}, we obtain the same results for both the periodic boundary conditions. In particular one gets:

$$\lambda_{k\to 0} \;=\; \left(\frac{n}{k}\right)^{1-\frac{1}{2K}}\; 2B_0\, \sin\left(\frac{\pi}{4K}\right) \Gamma\left(1-\frac{1}{2K}\right)\,. \tag{3.27}$$

Notice that by writing: $k = \frac{2\pi}{L} j$ with $j \in \mathbb{N}$, the scaling of λ_k in the thermodynamic limit is determined by choosing: $j \propto L$, in order to have a fixed and finite momentum in the $N \to \infty$ limit with fixed density $n = N/L$. From Eq. (3.27) we get the scaling for the natural orbital labeling the eigenstate with momentum k: $\lambda_{k\to 0} = \mathcal{B}_k(K)\, N^{\mathcal{C}_k(K)}$, where: $\mathcal{C}_k(K) = 0$, *i.e.* there is no fragmentation of the system to the other $k \neq 0$ momentum levels. While the scaling with k of the momentum distribution was known already in the literature [91], the prefactor which reads:

$$\mathcal{B}_k \;=\; 2\, k^{\frac{1}{2K}-1}\, B_0\, \sin\left(\frac{\pi}{4K}\right) \Gamma\left(1-\frac{1}{2K}\right)\,, \tag{3.28}$$

is quite interesting since we may check its correctness thanks to our expression for the complete form of the 1BDM in Eq. (1.71). Notice that since $\mathcal{C}_k = 0$ and $\mathcal{B}_k \neq 0$, we expect

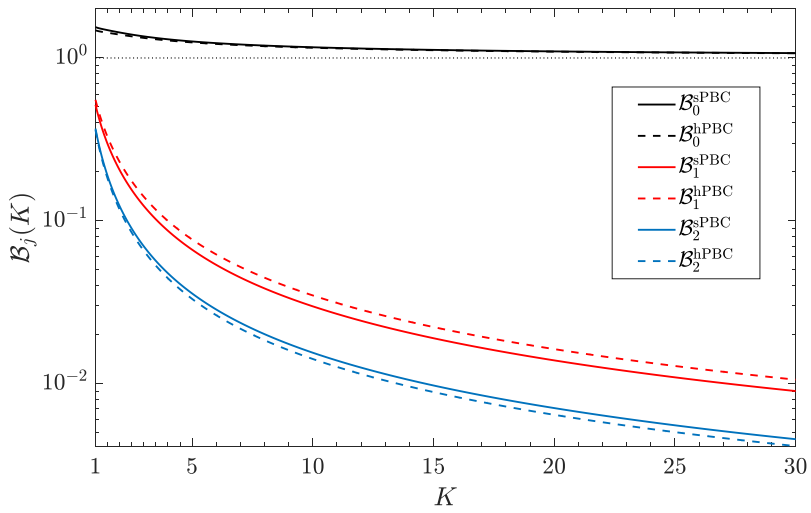

Figure 3.3: Log-scale plot of the numerical prefactor $\mathcal{B}_j(K)$ vs K for the scaling $\lambda_j \sim \mathcal{B}_j\, N^{\mathcal{C}_j}$ for the Lieb–Liniger gas with different periodic boundary conditions: In solid lines we show the results of Eq. (3.25), while in dashed we represent the analytical predictions of Eq. (3.24).

that the occupation numbers λ_k will tend to a constant equal to: $\frac{\mathcal{B}_k(K)}{2\pi}$ for small momenta and in the thermodynamic limit. For $k = 0$, the scaling is instead N-dependent and it coincides with the λ_0 results that we obtained before. From the numerics, by calculating λ_k from the Fourier transform of $\rho(r)$ of Eq. (1.71), we obtained indeed that for growing N there are small oscillations for λ_k due to the competition between the grow rate of j and N (in order to keep the momentum fixed), and these oscillations tend to vanish for very large particle numbers and the value reached by λ_k is indeed close to the predictions of Eq. (3.27). We report in Fig. 3.4–3.6 the behaviour of λ_k with $\gamma = 0.1$ for growing particle numbers and with: $k/n \simeq 0.00063$ (*i.e.* a ratio for j/N equals to 10^{-4}), $k/n \simeq 0.00628$ (for ratio: $j/N = 10^{-3}$) and $k/n \simeq 0.06283$ (for $j/N = 10^{-2}$) respectively. The analytical predictions for λ_k are reported in red dashed lines in all the plots and one can easily see that already from $j/N = 0.01$ the analytical predictions begin to depart from the numerics, and this is because our predictions hold in the small momenta regime. Finally notice that for the hard–core Bose gas, one retrieves the result for the prefactor of $n(k)$ of [100].

To complete our analysis, we may also wonder what happens for the momentum distribution at large momenta. In this case one has to evaluate the Fourier transform of the short–distance behaviour of the 1BDM which, for (smooth) periodic boundary conditions, reads [87]:

$$\rho(r) \;\simeq\; n\left\{1-\frac{1}{2}\left[e(\gamma)-\gamma\frac{de}{d\gamma}\right]\left[\frac{L}{\pi}\sin\left(\frac{\pi}{L}x\right)\right]^2+\frac{\gamma^2}{12}\frac{de}{d\gamma}\left[\frac{L}{\pi}\sin\left(\frac{\pi}{L}x\right)\right]^3\right\}, \qquad (3.29)$$

where $e(\gamma)$ is the ground state energy per particle for the Lieb–Liniger gas in the thermodynamic limit. From the Fourier transform one gets:

$$\left.\frac{n(k)}{L}\right|_{k\to\infty} = \left(\frac{n}{q}\right)^4 \frac{\gamma^2}{2\pi}\frac{de}{d\gamma}, \qquad (3.30)$$

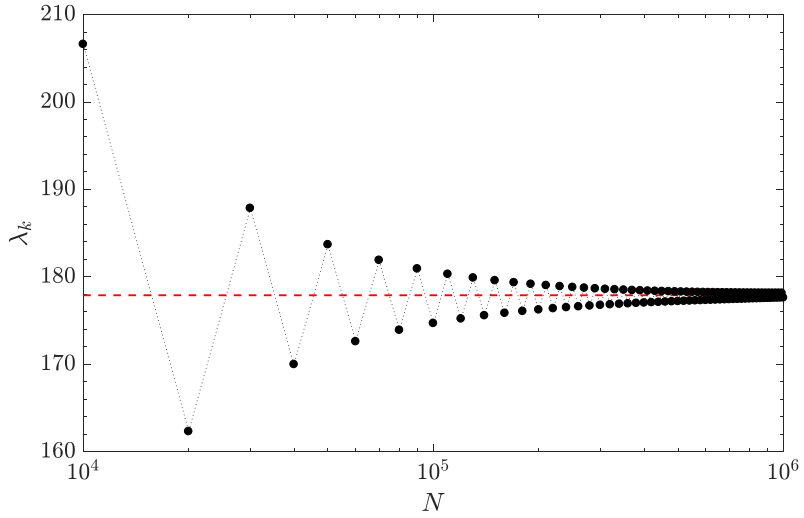

Figure 3.4: λ_k vs N in log-linear scale for the case with: $\gamma = 0.1$ and $k/n \simeq 0.00063$. We report with dotted points the numerical values of λ_k coming from using the interpolation formula of Eq. (1.71) for the 1BDM of the system. The black dotted line is a guide for the eye, while the red dashed line is the analytical estimate for λ_k coming from Eq. (3.27). One may observe that the analytical prediction well describes the value at which the occupation number with momentum k saturates in the thermodynamic limit.

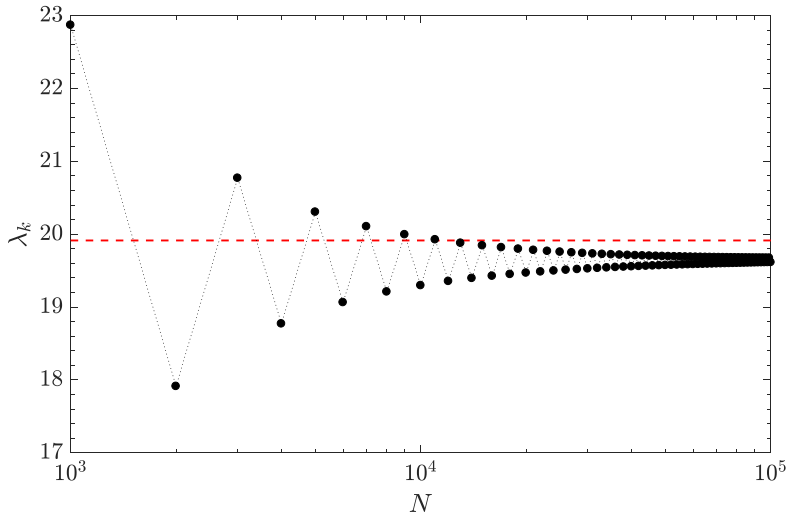

Figure 3.5: λ_k vs N in log-linear scale for the case with: $\gamma = 0.1$ and $k/n \simeq 0.00628$. We report with dotted points the numerical values of λ_k coming from using the interpolation formula of Eq. (1.71) for the 1BDM of the system. The black dotted line is a guide for the eye, while the red dashed line is the analytical estimate for λ_k coming from Eq. (3.27). In this case the analytical prediction deviates from the numerical result of λ_k for $N \to \infty$ of about 1.5%.

from which we can see that it does not scale with N in the thermodynamic limit for fixed k and density n, *i.e.* $\mathcal{C}_k = 0$ as we was expecting, and moreover in this case the prefactor of the scaling is the Tan's constant: $\frac{\gamma^2}{2\pi}\frac{de}{d\gamma}$, which was deeply studied in the literature [82, 87, 89, 100, 130, 183–186].

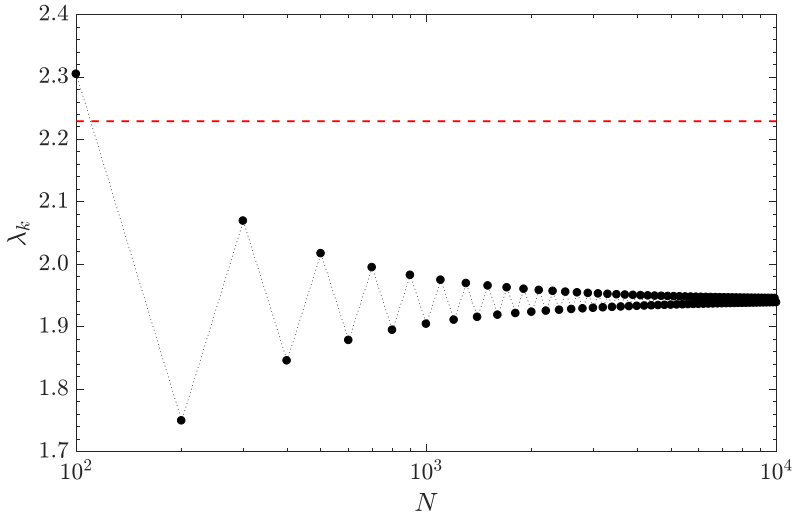

Figure 3.6: λ_k vs N in log-linear scale for the case with: $\gamma = 0.1$ and $k/n \simeq 0.06283$. Once again, we report with dotted points the numerical values of λ_k, while the black dotted line is a guide for the eye, and the red dashed line is the analytical estimate for λ_k coming from Eq. (3.27). In this case, even though the ratio k/n may seem rather small, the difference between the analytical estimate and the numerical result for λ_k in the thermodynamic limit is about 13%.

Finally, we can plot the complete behaviour of the momentum distribution: $\frac{n(k)}{L} = \frac{\lambda_k}{2\pi}$ and it is reported in Fig. 3.7, where we used the cut-off interpolation scheme to evaluate the 1BDM for $N = 300$ particles and with different interaction strengths. One may observe that by increasing the interaction the momentum distribution peak's intensity decreases, as we would expect.

3.2.2 FINITE TEMPERATURE

For the homogeneous Lieb–Liniger gas at finite temperature, the asymptotic leading behaviour for the 1BDM of the system is given by [187]:

$$\rho(r) \;=\; n B_0 \left[\frac{K^2\, m\, k_B T}{\pi\, n^2\, \hbar^2\, \sinh\left(\frac{K\, m\, k_B T}{n\, \hbar^2}\, r \right)} \right]^{1/2K} , \tag{3.31}$$

where k_B is the Boltzmann constant, B_0 is the numerical prefactor that we found also in the $T = 0$ case [cfr Eq. (3.17)], while the Luttinger parameter $K = \sqrt{v_J / v_N}$ may be found from the thermodynamic Bethe ansatz formalism [57]. One can see that for $T = 0$ the correlation function decays as a power law with exponent $1/2K$, as we already know, while for finite temperatures there is an intermediate power-law behaviour which turns into an exponential decay for $|r| \geq \frac{\pi\, n\, \hbar^2}{K\, m\, k_B T}$. Since we want to analyze the small momenta behaviour for the natural orbital occupation number labeled with momentum k, we are interested in the behaviour of Eq. (3.31) for large r, *i.e.*:

$$\rho(r) \;\simeq\; n B_0 \left(\frac{2\, K^2\, m\, k_B T}{\pi\, n^2\, \hbar^2} \right)^{1/2K} e^{-\frac{m\, k_B T}{2\, n\, \hbar^2}\, r} . \tag{3.32}$$

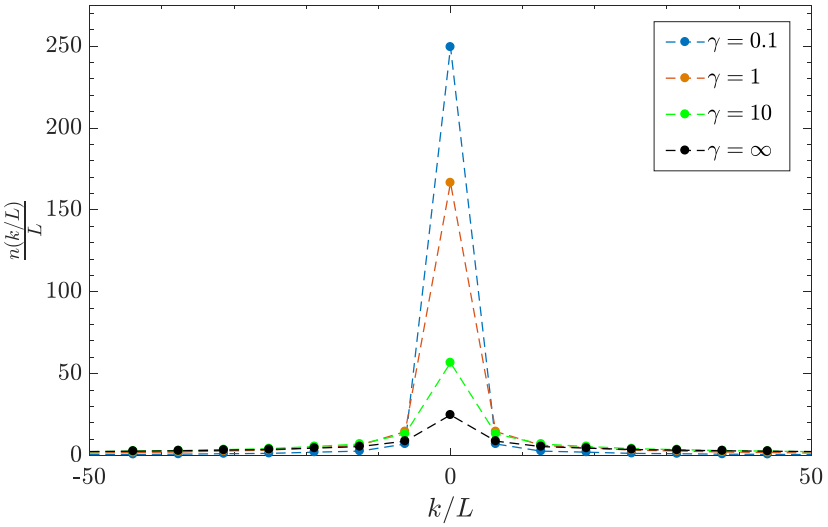

Figure 3.7: Dimensionless momentum distribution $\frac{n(k/L)}{L}$ for different interaction strengths evaluated from using the interpolation method for the 1BDM, with $N = 300$. The dashed lines are guides for the eyes, while the colored dots are the effective values of the momentum distribution.

The validity of this equation was proven using density-matrix renormalization group in [188], where it was also proved that even in trapped system at finite temperatures the decay of correlations follow the same scaling law.

If we now assume hard-periodic boundary conditions, we can write for the occupation number λ_k in Eq. (3.26):

$$\lambda_k = \int_0^{L/2} \rho(r)\, e^{ikr}\, dr + \int_{L/2}^{L} \rho(L-r)\, e^{ikr}\, dr\,, \tag{3.33}$$

and using Eq. (3.32) we find that in the thermodynamic limit the occupation number of the effective single particle states with small momenta can be written as:

$$\lambda_{k\to 0} = \frac{B_0}{4}\, K^{1/K}\, \frac{n^2}{(n\,\hbar)^{2+\frac{1}{K}}} \left(\frac{2}{\pi}\, m\, k_B T\right)^{1+\frac{1}{2K}} \frac{1}{\left(\frac{m\, k_B T}{2\,\hbar^2\, n}\right)^2 + k^2}\,. \tag{3.34}$$

Notice that both for $k = 0$ and $k \neq 0$ but small, the scaling of the λ_k in the thermodynamic limit is characterized by $\mathcal{C}_k(T \neq 0) = 0$. Let us appreciate the fact that this behaviour is very similar to the scaling of the momentum distribution [remember that, for homogeneous systems, there is only a factor 2π of difference between λ_k and $n(k)/L$] of a three–dimensional BEC for $T > T_C$ for small momenta, where one has [18]: $n(p) \propto \frac{1}{p_c^2+p^2}$, with $p_c^2 = 2\, m\, k_B T\,(1-z)$, and having indicated with z the fugacity. For the one–dimensional case: $T_C = 0$, therefore it is reasonable to compare the above two results and one finds that there is complete lack of ordering for both cases.

These results can be verified also from the exponential decay form of the 1BDM found in [189–191]. In particular, in [191] an expression for the 1BDM as a sum of exponential functions is given in the form:

$$\frac{\rho(r)}{n} = \sum_i \bar{B}_i\, e^{-\frac{r}{\xi[\bar{v}_i]}}\,, \tag{3.35}$$

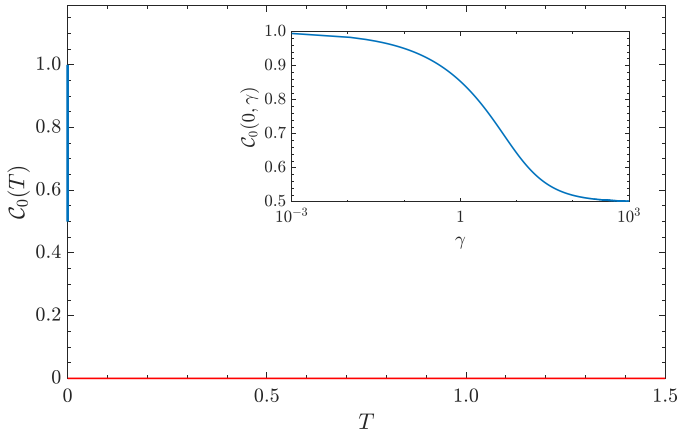

Figure 3.8: Exponent $\mathcal{C}_0(T)$ with which the largest eigenvalue of the 1BDM of a homogeneous one–dimensional Bose gas scales with respect to the total number of particles N at different temperatures. Only for $T = 0$ does one have that $\mathcal{C}_0$ is non-vanishing and depends on the dimensionless interaction parameter γ via (1.62), as shown in the inset.

where $\bar{B}_i$ are distance independent amplitudes and $\xi\left[\bar{v}_i\right]$ the correlation length (shown to be always positive), depending on the temperature-dependent functions $\bar{v}_i$ defined in [191], where it is also shown that the result in Eq. (3.35) reduces to Eq. (1.69) in the $T = 0$ case, as it should. We may now take the Fourier transform of the symmetrized version of Eq. (3.35), and obtain:

$$\frac{n(k)}{L} = \frac{1}{2\,\pi}\sum_i \bar{B}_i \left(\int_0^{L/2} e^{-\frac{r}{\xi[\bar{v}_i]}}\, dr + \int_{L/2}^{L} e^{-\frac{L-r}{\xi[\bar{v}_i]}}\, dr \right) \propto e^{-\frac{L}{\xi[\bar{v}_i]}}\,,$$

where the last proportionality is valid both at zero and non-zero momentum k. Since $L = N/n$, analyzing the N leading dependence only, we have that for $N \to \infty$ the dimensionless momentum distribution is just a constant for any k, leading to the finite temperature result:

$$\mathcal{C}_k(T \neq 0, \gamma) = 0\,, \tag{3.36}$$

which indicates complete absence of ordering.

In Fig. 3.8 we summarize the behaviour of the exponent $\mathcal{C}_0$ for a homogeneous one–dimensional Bose gas for different temperatures. An inset shows the relation between $\mathcal{C}_0$ and the interaction parameter γ in the zero temperature case, *i.e.* Eq. (1.62).

3.3 TWO DIMENSIONS

Properties of two–dimensional systems stand on their own and are between those of $1D$ – where $\mathcal{C}_0$ vanishes at finite temperature – and of $3D$ models – where $\mathcal{C}_0 = 1$ below the BEC critical temperature. As discussed in the beginning of the present Chapter, no ordinary phase transition takes place in $2D$, due to the lack of ODLRO. However, $2D$ systems often feature the BKT topological phase transition named after Berezinskii, Kosterlitz and Thouless who first discussed it in the two–dimensional XY model [192–194]. This transition is related to the presence of vortex and anti-vortex spin configurations at finite temperatures. At low T, below the BKT temperature T_{BKT}, vortex and anti-vortex pairs

with vanishing total winding numbers (neutrality condition) are present in the system and the correlation function between two distant spins decay as power-law, indicating a phase with quasi-long–range order, also called BKT phase.

A simple estimate of T_{BKT} in the XY model is the Peierls value $T_{BKT} = \frac{\pi J}{2k_B}$ [195], where J is the interaction strength among the spins. In the low-temperature BKT regime the only relevant configurations are the spin waves and the spin-wave approximation shall describe the system properly. As the temperature increases, the presence of free vortices with non-vanishing winding numbers becomes energetically favored, and, therefore, vortices and anti-vortices may unbind from each other. For temperatures above T_{BKT}, the presence of such topological excitations destroys the quasi-long–range order and the correlation functions become exponentially decaying [195–197]. An important statistical model used to approximatively describe the two–dimensional XY model is the one proposed by Villain [195, 198]. While in the XY model the spin waves interact with the vortices, in the Villain model the spin waves are decoupled from the vortices degrees of freedom, making its Hamiltonian simply quadratic. Both models have the same topological characteristics and they belong to the same universality class, as one can see from the critical behaviour of the anomalous dimension η of the two systems. The Villain model well describes the low temperature phase of the XY model, since the Hamiltonian is essentially constituted by two decoupled harmonic oscillators terms, one for the spin waves and one for the vortices. Notice that the Villain model can be used both as a model *per se* and also as a convenient way to approximate the XY model [199].

Let us pause here to comment on the qualitative similarity of the low dimensional ($D = 1$ and $D = 2$) systems studied in this Thesis. In the thermodynamic limit at low temperatures, both for the one– and the two–dimensional cases, the systems can be described by field theoretical models with Hamiltonians made up of two decoupled harmonic oscillator terms. These quadratic Hamiltonians are the Luttinger liquid and the Villain Hamiltonian for the one– and two–dimensional cases, respectively. Therefore bosonization in $D = 1$ systems plays to a certain extent a similar role as the spin wave approximation in $D = 2$ systems, both of them describing systems with quasi-long–range order in the low temperature phase and the absence of order above their critical temperatures (which is vanishing in $D = 1$). Nevertheless, the phase transitions that characterize the models are for short-range models intrinsically different in the one– and two–dimensional cases. In $D = 2$ this phase transition is related to the formation of single independent topological excitations, which cannot happen in $D = 1$ geometries. Moreover in one dimension there is no phase transition at all at finite T, since the quasi-long–range order is limited to the zero temperature limit.

Let us analyze the BKT phase transition in terms of the exponent $\mathcal{C}_0$. At the BKT critical point the two–points correlation function scales as [59]

$$\rho(r) \sim \frac{1}{r^{D-2+\eta}}\,, \tag{3.37}$$

where η is the anomalous dimension critical exponent, that depends on the system under consideration. What is universal is the value at $T = 0$, for which $\eta(T = 0) = 0$, and that at $T = T_{BKT}$, which is given by: $\eta(T = T_{BKT}) = 1/4$ [200]. The behaviour of η between 0 and T_{BKT} is not universal.

From the knowledge of the behaviour of the anomalous dimension – that will be discussed below – one can find an expression for the power $\mathcal{C}_0$ with which the dimensionless momentum distribution peak scales. One has:

$$\frac{n(k=0)}{L^2} = \frac{1}{2\,\pi}\lim_{L\to\infty}\left[\int_0^{L/2}\frac{dr}{r^{\eta-1}}+\int_{L/2}^{L}\frac{dr}{(L-r)^{\eta-1}}\right]\propto L^{2-\eta}\,, \tag{3.38}$$

where we symmetrized the density matrix in Eq. (3.37) in the radial coordinate variable r, passing to polar coordinates and performing the trivial integration over the azimuth angle. Since fixing the density $n = \frac{N}{L^2}$ in the large particle number limit implies that $L \propto \sqrt{N}$, then we can extract the power $\mathcal{C}_0(T/T_{BKT})$ with which the largest eigenvalue of the 1BDM scales, and it reads:

$$\mathcal{C}_0 = 1-\frac{\eta}{2}\,. \tag{3.39}$$

Notice that for the XY and Villain models the condensate fraction $\frac{\lambda_0}{N}$ is the magnetization density of the spin system and therefore Penrose-Onsager ODLRO manifests in a complete magnetization of the system, while having $\mathcal{C}_0 = 0$ is equivalent to saying that there exist no correlation and order between the spin variables.

Since the value of the anomalous dimension for such systems at the critical temperature is equal to $1/4$, one has:

$$\mathcal{C}_0\left(T=T_{BKT}\right) = \frac{7}{8}\,, \tag{3.40}$$

and $\mathcal{C}_0$ jumps to zero for $T > T_{BKT}$, reflecting the universal jump for the superfluid stiffness [200]. A study of small corrections (found to be $\approx 0.02\%$) to the Nelson-Kosterlitz jump of the superfluid stiffness is in Refs. [201, 202]. Using spin wave approximation, one finds that at $T = 0$ there is ODLRO and therefore $\mathcal{C}_0(0) = 1$. Notice that at $T = 0$ ODLRO is allowed because there is no entropy contribution to the free energy of the system and the Mermin-Wagner theorem does not apply.

3.3.1 VILLAIN MODEL

The Villain model is defined in terms of continuous classical fields φ_i defined at the sites i of a two–dimensional lattice. The Hamiltonian of the system reads [198]:

$$H_V = A\sum_{\langle i,j\rangle}\left(\varphi_i-\varphi_j\right)^2 + B\sum_i\left(\varphi_i - 2\pi\frac{v_i}{m}\right)^2\,, \tag{3.41}$$

where A and B are parameters tuning the amplitude of the two Hamiltonian terms, m is an integer number which describes a possible anisotropic field acting in the system, and finally v_i are proven to be vorticity variables. As can be easily seen, the Hamiltonian is made of two distinct part: Spin-wave and vortex contribution, both of which represented by harmonic oscillator terms. Notice moreover, that there is no interaction term among the two different types of variables.

In the case of the square lattice planar Villain model, one expects that the anomalous dimension should be of the form $\eta_V \simeq \frac{k_B T}{2\pi A}$ at low temperatures, since the theory is quadratic and the spin wave approximation shall apply everywhere, in particular very

close to the critical point, where vortex configurations become relevant. The value for A will be provided in the following. Villain [198] proposed a correction term to account for vortex contributions to the anomalous dimension close to the critical point. Assuming that the interaction between the vortices can be neglected, this correction yields [198]:

$$\eta_V = \frac{k_B T}{2\pi A} + \pi^2 k_B T \frac{e^{-\pi^2 A/k_B T}}{\pi A - 2k_B T}\,. \tag{3.42}$$

According to the renormalization group, the value for the critical temperature of the Villain models is found to be [203]

$$\frac{k_B T_{BKT}}{A} = \frac{1}{0.74} \simeq 1.351\,, \tag{3.43}$$

which coincides with the result obtained from the high precision Monte Carlo simulation performed in [203] up to $L = 512$ lattice sites. Substituting Eq. (3.43) into Eq. (3.42), we have an estimate for the behaviour of the anomalous dimension of the square lattice Villain model in terms of the dimensionless ratio T/T_{BKT}, which reads:

$$\eta_V(T/T_{BKT}) = \mathcal{A}\frac{T}{T_{BKT}} + \frac{\pi^2}{2}\frac{e^{-\mathcal{B}\frac{T_{BKT}}{T}}}{\left(-1+\mathcal{D}\frac{T_{BKT}}{T}\right)}\,, \tag{3.44}$$

where $\mathcal{A} \approx 0.215$, $\mathcal{B} \approx 7.304$ and $\mathcal{D} \approx 1.162$.

Introducing Eq. (3.44) into Eq. (3.39), one obtains the results plotted as the red intermediate solid line in Fig. 3.9. Notice that according to the approximation in Eq. (3.42), one has $\eta_V(T = T_{BKT}) \simeq 0.236$, *i.e.* $\mathcal{C}_0^V(1) = 0.882$, with "$V$" referring to the Villain model. This result differs from the one coming from Monte Carlo simulations [203], $\eta_V = 0.2495 \pm 0.0006$, for about 5%. Low temperature predictions for the exponent $\mathcal{C}_0^V(T)$ may be formulated in two ways:

1. Disregarding the second term in the right-hand side of Eq. (3.42), which may be safely neglected in the low temperature regime at $T \ll T_{BKT}$ [198], which yields, via Eq. (3.39),

$$\mathcal{C}_0^V(T/T_{BKT}) \simeq 1 - \frac{1}{2}\left(\frac{T}{2\,\pi\,T_{BKT}} \cdot \frac{1}{0.74}\right) \tag{3.45}$$

   with T_{BKT} obtained by Monte Carlo simulations [see Eq. (3.43)].

2. Using the Peierls argument $\frac{k_B T_{BKT}}{A} = \frac{\pi}{2}$, one has:

$$\mathcal{C}_0^V(T/T_{BKT}) \simeq 1 - \frac{1}{2}\left(\frac{T}{T_{BKT}} \cdot \frac{1}{4}\right)\,. \tag{3.46}$$

These two behaviours are reported as black solid and dashed lines, respectively, in Fig. 3.9. Notice from the plot that the low-T behaviour of Eq. (3.45) is good even in regions close to T_{BKT}, where the corrective term introduced by Villain starts to play a role. The predictions of (3.46), which at variance do not take into account the effect of vorticies, do not match with the same accuracy with the expected results already from $T \approx 0.5 T_{BKT}$.

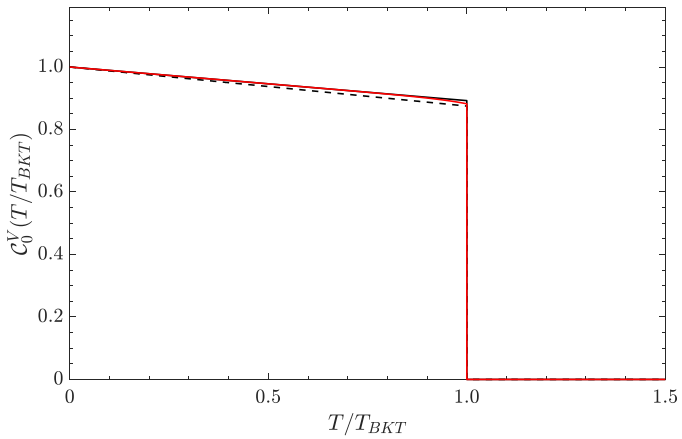

Figure 3.9: $\mathcal{C}_0^V(T/T_{BKT})$ vs T/T_{BKT} for the Villain square lattice model. The red intermediate solid line represents the predicted value for $\mathcal{C}_0$ using Eq. (3.44) in Eq. (3.39), while the black solid and dashed lines represent, respectively, the low temperature behaviours given respectively by Eqs. (3.45) and (3.46).

3.3.2 XY MODEL

For the two–dimensional classical XY model, the Hamiltonian of the system reads:

$$H_{XY} = -J \sum_{\langle i,j \rangle} \mathbf{s}_i \cdot \mathbf{s}_j \,, \tag{3.47}$$

where $\mathbf{s}_i$ is a unit spin vector centered in the i-th lattice site, with two real components, and the sum is over nearest neighbor sites of a square lattice. By normalizing the spin vector to unity, *i.e.* requiring that:

$$|\mathbf{s}_i|^2 = 1 \,, \qquad \forall i \,,$$

the Hamiltonian of the classical XY model can then be written in terms of the angle θ_i between the spin at site i and some reference direction, as:

$$H_{XY} = -J \sum_{\langle i,j \rangle} \cos\left(\theta_i - \theta_j\right) . \tag{3.48}$$

In the case of a square lattice, the critical temperature has been evaluated using Monte Carlo techniques obtaining [204–207]:

$$\frac{k_B T_{BKT}}{J} = 0.893 \pm 0.001 \,, \tag{3.49}$$

while recent approximate, semi-analytical functional renormalization group (FRG) results give $k_B T_{BKT} = (0.94 \pm 0.02)\, J$ [208]. The anomalous dimension is found to be equal to

$$\eta_{XY} = \frac{k_B T}{2\pi J_s(T)} \,, \tag{3.50}$$

where $J_s(T)$ is the superfluid (or spin) stiffness of the model, and has been recently calculated for the XY model in a square lattice in [209] using simulations up to 256 lattice sites.

Therefore we may now compute the $k = 0$ Fourier transform of the spin–spin correlation function as in Eq. (3.38). Similarly to Eq. (3.39), one has:

$$\mathcal{C}_0^{XY}(T) \;=\; 1 - \frac{\eta_{XY}}{2}\,. \tag{3.51}$$

Using the Villain approximation we can obtain an expression for the behaviour of the anomalous dimension for the XY model. The Villain approximation, indeed, is based on the fact that there exist a (non-exact) map between the interaction parameter A and the spin–spin interaction parameter J, which relates the Villain Hamiltonian to the XY model [198]. This mapping reads:

$$\frac{A}{k_B T} \;=\; -\frac{1}{2}\left\{\ln\left[\frac{I_1\left(\frac{J}{k_B T}\right)}{I_0\left(\frac{J}{k_B T}\right)}\right]\right\}^{-1}\,, \tag{3.52}$$

where $I_n(x)$ are the modified Bessel functions of the first kind of degree n. We may therefore substitute this expression into the approximation given in Eq. (3.42). We find:

$$\eta_{XY} = -\frac{1}{\pi}\ln\left[\frac{I_1\left(\frac{J}{k_B T}\right)}{I_0\left(\frac{J}{k_B T}\right)}\right] + \frac{\pi^2}{2} e^{\frac{\pi^2}{2}\left\{\ln\left[\frac{I_1\left(\frac{J}{k_B T}\right)}{I_0\left(\frac{J}{k_B T}\right)}\right]\right\}^{-1}} \cdot \left\{-1 + \frac{\pi}{\pi + 4\ln\left[I_1\left(\frac{J}{k_B T}\right)\right] - 4\ln\left[I_0\left(\frac{J}{k_B T}\right)\right]}\right\}\,. \tag{3.53}$$

Using the mapping of Eq. (3.52), the Monte Carlo results of [203] for the critical temperature of the Villain model, *i.e.* Eq. (3.43), translates into:

$$\frac{k_B T_{BKT}}{J} = 0.842\,, \tag{3.54}$$

which is pretty close to the Monte Carlo results of Refs. [204–207] reported in Eq. (3.49). The equation which relates A to J seems then to be reliable within a $\approx 6\%$ accuracy even very close to the critical point.

Similarly to what we have done for the Villain model, a low temperature prediction can be made by neglecting the second term in the right-hand side of Eq. (3.53). Using Eq. (3.51) we get:

$$\mathcal{C}_0^{XY}(T) \;\simeq\; 1 + \frac{1}{2\pi}\ln\left[\frac{I_1\left(\frac{J}{k_B T}\right)}{I_0\left(\frac{J}{k_B T}\right)}\right]\,. \tag{3.55}$$

On the other hand, one can also employ the low-temperature expansion results: $\frac{J_s(T)}{J} \simeq 1 - \frac{k_B T}{4J}$, which is known to be consistent with several approaches, such as self-consistent harmonic approximation [210], Monte Carlo simulations [211] and FRG [208]. This procedure leads to the expression:

$$C_0^{XY}(T/T_{BKT}) \;\simeq\; 1 - \frac{1}{\pi}\frac{T/T_{BKT}}{\frac{4J}{k_B T_{BKT}} - T/T_{BKT}}\,. \tag{3.56}$$

In Fig. 3.10 we report as blue points the behaviour of (3.51) for $\eta_{XY} = \frac{k_B T}{2\pi J_s(T)}$ with respect to the dimensionless quantity T/T_{BKT} obtained using the results of [209]. The

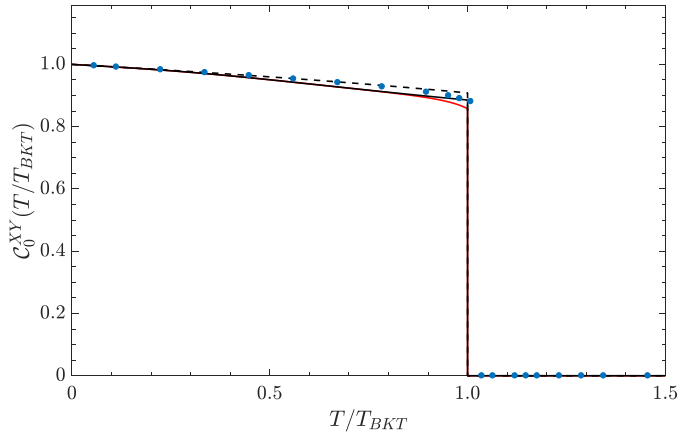

Figure 3.10: $\mathcal{C}_0^{XY}(T/T_{BKT})$ vs T/T_{BKT}. Blue points are the numerical values of $\mathcal{C}$ obtained from Eq. (3.51) with anomalous dimension $\eta_{XY} = \frac{T}{2\pi J_s(T)}$ and using the superfluid stiffness results of [209]. The universal jump from $\mathcal{C}_0(T_{BKT}) = \frac{7}{8}$ to $\mathcal{C}_0(T > T_{BKT}) = 0$ is evident. The bottom red solid line comes from the Villain prediction Eq. (3.53). Finally the black solid and dashed lines represent the low temperature predictions of Eqs. (3.55) and (3.56) respectively.

bottom red solid line represents the Villain prediction given in Eq. (3.53) with T_{BKT} given by Eq. (3.49), while the black solid and dashed lines represent the low temperature behaviours in Eqs. (3.55) and (3.56), respectively. Fig. 3.10 confirms the validity of the low temperature expansion in Eq. (3.56) in the range $T \in [0, 0.8T_{BKT}]$, while the Villain prediction in Eq. (3.56) remains reliable up to T_{BKT}.

3.3.3 BOSE GAS

Under certain conditions a two–dimensional Bose gas can be mapped onto the XY model and from this mapping one can derive the decay of correlation functions and the ordering type of the bosonic system [212–215]. Indeed, when density fluctuations are strongly suppressed the effective low–energy Hamiltonian of a two–dimensional Bose gas is equivalent to the continuous version of the Hamiltonian of the XY model on the lattice. The BKT phase of the XY model corresponds then to the superfluid state of the Bose gas and quasi-long–range order is present. Above the critical temperature the normal state appears and superfluidity breaks down. This abrupt change of phase is characterized by a universal jump of the superfluid density (stiffness), which switches between its low temperature value $\rho_s = \frac{2m^2 k_B T}{\pi \hbar^2}$ to $\rho_s = 0$ for $T > T_{BKT}$ [200, 201].

In Refs. [216, 217] it has been shown that the asymptotic behaviour of the 1BDM of a two–dimensional weakly interacting Bose gas at finite temperatures scales as:

$$\rho(r) \sim \frac{1}{r^{\frac{m^2 k_B T}{2\pi\hbar^2 \rho_s}}}, \tag{3.57}$$

where ρ_s is the superfluid density of the gas. The superfluid density of the system assumes the form [213]:

$$\rho_s = \frac{2m^2 k_B T}{\hbar^2 \pi} f(X), \tag{3.58}$$

where $X = \frac{\hbar^2(\mu-\mu_c)}{m\,k_B T U}$ measures the distance from the critical point, with μ the chemical potential and the critical value μ_c given by:

$$\mu_c = \frac{m\,k_B T U}{\hbar^2 \pi}\,\ln\left(\frac{\hbar^2 \xi_\mu}{m\,U}\right). \tag{3.59}$$

The function $f(X)$ in Eq. (3.58) is a dimensionless universal function, which has been numerically determined in [213]. The variable U appearing in X is the interparticle interaction strength, so that $\frac{mU}{\hbar^2} \ll 1$ and $X \gg 1$ correspond to the weakly interacting limit. While, the constant ξ_μ appearing in Eq. (3.59) is given by $\xi_\mu = 13.2 \pm 0.2$ [213].

Applying the same procedure used for the Villain and the XY models, we obtain the following exponent $\mathcal{C}_0$ for the scaling of the dimensionless momentum distribution peak with respect to the number of particles of the two–dimensional Bose gas:

$$\mathcal{C}_0^{\text{Bose}}(X) \;=\; 1 - \frac{1}{8 f(X)}\,. \tag{3.60}$$

The jump of the superfluid stiffness ρ_s at criticality implies that $f(X)$ will jump from 0 to 1 at $X = 0$, *i.e.* at the critical point. Therefore, the exponent $\mathcal{C}_0$ will jump from the universal value $\frac{7}{8}$ to 0 at the critical BKT temperature. The relation between the exponent $\mathcal{C}_0$ and the ratio T/T_{BKT} is constructed from the expression [213]:

$$\frac{T}{T_{BKT}}(X) \;=\; \frac{1}{1 + 2\,\pi\lambda(X)/\ln(\hbar^2\xi/mU)}\,, \tag{3.61}$$

where $\lambda(X) = [X + \theta(X) - \theta_0]\,/2$ with $\theta(X)$ found via numerical simulations for system sizes up to 512 in [213]. The (non-perturbative) constant ξ in Eq. (3.61) is given by [213]:

$$\xi = 380 \pm 3\,, \tag{3.62}$$

and $\theta_0 = \frac{1}{\pi}\ln\left(\frac{\xi}{\xi_\mu}\right)$ is then found to be $\theta = 1.07 \pm 0.01$.

Knowing the relation between T/T_{BKT} and X and the relation between $\mathcal{C}_0^{\text{Bose}}$ and X, we can then track down the dependence of the exponent $\mathcal{C}_0$ with which the dimensionless momentum distribution peak scales with the number of particles N for different temperatures. We report its behaviour in Fig. 3.11 for different values of the interaction U.

An important comment about Fig. 3.11 is that in the limit of the dimensionless interaction parameter $\frac{mU}{\hbar^2} \to 0$, the exponent $\mathcal{C}_0$ tends to be closer (with respect to higher values of U) to the unity up to temperatures closer to T_{BKT}. In other words, the smaller is U, the closer to 1 is $\mathcal{C}_0$ at fixed $T/T_{BKT} < 1$. Going even closer to T_{BKT} from below, the decrease to the value $\frac{7}{8}$ happens abruptly for $\frac{mU}{\hbar^2} \simeq 0$ at $T \simeq T_{BKT}$. Since $\mathcal{C}_0$ has to be $7/8$ at $T = T_{BKT}$, this is associated to a kind of *double jump* occurring for $T \to T_{BKT}^-$ for $U \to 0$, since in this limit $\mathcal{C}_0$ reaches a value different from (and larger than) $7/8$ coming from low temperature/large-X expansion that we are going to shortly introduce, then it abruptly jumps from this value to $7/8$ and then jumps from $7/8$ to 0. More comments on the double jump occurrence are below.

Finally, it is worth noting that the values for $\frac{mU}{\hbar^2} = 1$, reported in Fig. 3.11, are out of the validity range for the weak interacting gas. Then, the mean field arguments of [213] cannot be applied anymore, and one should take into account quantum fluctuations.

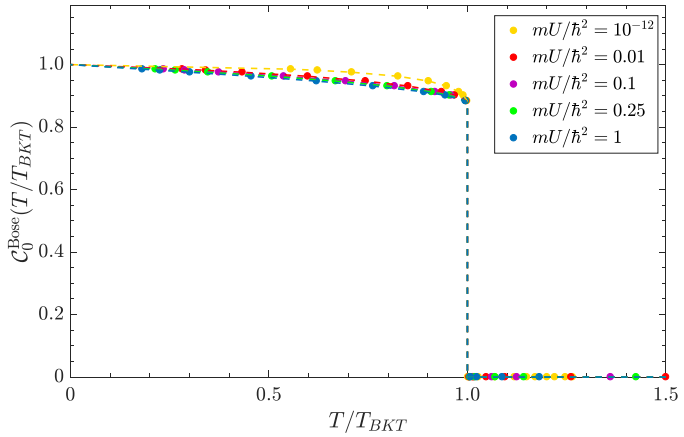

Figure 3.11: $\mathcal{C}_0^{\rm Bose}(T/T_{BKT})$ vs T/T_{BKT} for different interactions $\frac{mU}{\hbar^2}$. Points are the numerical value of $\mathcal{C}_0$ obtained from numerical simulations performed in [213], while dashed lines are drawn as a guide for the eyes. In each case the universal jump from $\mathcal{C}_0(T_{BKT}) = \frac{7}{8}$ to $\mathcal{C}_0(T > T_{BKT}) = 0$ is evident.

Low temperature predictions may also be formulated, similarly to what we did for the Villain and XY models, but with some subtleties to be worked out. In the low T regime (*i.e.* far from the critical point), it is $X \to \infty$ and the function $\theta(X)$ satisfies [213]:

$$\theta(X) - \frac{1}{\pi}\ln\theta(X) \;=\; X + \frac{1}{\pi}\ln(2\xi_\mu)\,, \tag{3.63}$$

which is a transcendental equation admitting two values for θ for a single value of X. These two solutions can be distinguished in terms of the behaviour of $\theta(X)$ for $X \to \infty$. The first set is the one having a vanishing vaue of $\theta(X \to \infty)$ and it is given by:

$$\theta(X \to \infty) \;=\; \frac{e^{-\pi X}}{2\xi_\mu}\,, \tag{3.64}$$

which is the solution of $-\frac{1}{\pi}\ln\theta(X) \;=\; X + \frac{1}{\pi}\ln(2\xi_\mu)$, and as well as a solution of Eq. (3.63) for $X \to \infty$. This first set is not interesting for us and we look for a function $\theta(X)$ which diverges for large X. This represents the second set of solutions and one has:

$$\theta^{(0)}(X \to \infty) \;=\; X + \frac{1}{\pi}\ln(2\xi_\mu)\,, \tag{3.65}$$

which is the zero-th order solution of Eq. (3.63) without the logarithmic term in the left hand side. In the low T regime one may also write [213]

$$f^{(0)}(X \to \infty) \;=\; \frac{\pi}{2}\theta^{(0)}(X) - \frac{1}{4} \;=\; \frac{2\pi X + 2\ln(2\xi_\mu) - 1}{4}\,, \tag{3.66}$$

where the last identity follows from Eq. (3.65). Reminding one that $\lambda(X) = [X + \theta(X) - \theta_0]/2$ and using Eq. (3.65), one has an expression also for the $\lambda(X)$ function in the low temperature regime at the zero-th order of approximation:

$$\lambda^{(0)}(X \to \infty) \;=\; X + \frac{1}{2\pi}\ln\left[\frac{2(\xi_\mu)^2}{\xi}\right]. \tag{3.67}$$

Therefore, substituting into Eq. (3.61), one can write an expression for X (at the zero-th order in terms of the variable T/T_{BKT}) reading:

$$X^{(0)} \;=\; -\frac{1}{2\pi}\ln\left[\frac{2(\xi_\mu)^2}{\xi}\right] + \frac{1}{2\pi}\ln\left(\frac{\hbar^2\xi}{mU}\right)\left(\frac{T_{BKT}}{T} - 1\right). \tag{3.68}$$

Finally, inserting Eq. (3.68) into Eq. (3.66), we may substitute the equation for $f^{(0)}(X \to \infty)$ into Eq. (3.60) to obtain an analytical expression for the exponent $\mathcal{C}_0^{\text{Bose}}$ at low temperatures:

$$\mathcal{C}_0^{\text{Bose}\,(0)}(T/T_{BKT}) \simeq 1 + \frac{1}{2}\left[1 - \ln(2\xi) - \ln\left(\frac{\hbar^2\xi}{mU}\right)\left(\frac{T_{BKT}}{T} - 1\right)\right]^{-1}, \tag{3.69}$$

where the superscript $^{(0)}$ denotes we are at the lowest order in the considered approximation. One can obtain higher order solutions by substituting the expression in Eq. (3.65) in the logarithmic term of the Eq. (3.63) and solve for $\theta(X)$, which will now be the solution at the first order of approximation, *i.e.* it reads:

$$\theta^{(1)}(X) = X + \frac{1}{\pi}\ln(2\xi_\mu) + \frac{1}{\pi}\ln\theta^{(0)}(X)\,. \tag{3.70}$$

Following the same procedure sketched above for the zero-th order case, we obtained the following analytical form for $\mathcal{C}_0^{\text{Bose}}$ at low temperatures at first order approximation:

$$\mathcal{C}_0^{\text{Bose}\,(1)}(T/T_{BKT}) \simeq 1 + \frac{1}{2}\left\{1 - 2\ln\left[\frac{2mU}{\hbar^2}\left(\frac{\hbar^2\xi}{2mU}\right)^{T_{BKT}/T}\right] + \right.$$
$$\left. + W\left(\frac{4\pi mU}{\hbar^2}\left(\frac{\hbar^2\xi}{2mU}\right)^{T_{BKT}/T}\right)\right\}^{-1}, \tag{3.71}$$

where $W(z)$ is the Lambert or product logarithm function. Higher order solutions may be obtained following the same recipe, but from the second order case is not possible to write an analytical expression for X in terms of T/T_{BKT}. Therefore, one can work out only the numerics in order to obtain the low temperature behaviour of the exponent $\mathcal{C}_0^{\text{Bose}\,(\text{j}\geq 2)}(T/T_{BKT})$. In the present work the third order approximation has been also investigated, but we envisage no particular difficulty in going beyond.

In Fig. 3.12 we report the comparison between the low temperature expansions with the values for $\mathcal{C}_0^{\text{Bose}}$ obtained from the numerical Monte Carlo results of [213] in the very small interaction limit $\frac{mU}{\hbar^2} = 10^{-12}$, and for the intermediate interaction case $\frac{mU}{\hbar^2} = 0.25$. The agreement is good up to 3% even for $T = T_{BKT}$, where

$$\mathcal{C}_0^{\text{Bose}\,(3)}(1) \simeq 0.912\,, \tag{3.72}$$

independently of the interaction parameter. It is important to notice that for smaller values of U the low temperature predictions for the exponent $\mathcal{C}_0^{\text{Bose}}$ are valid for a larger range of temperatures, since for very weak interactions the variable X is very large even at $T \approx T_{BKT}$. So, decreasing U the range of validity of the low temperature predictions increase up to a value which becomes increasingly close to T_{BKT}. Indeed, for $\frac{mU}{\hbar^2} = 10^{-12}$ the low T prediction remains reliable up to $T \approx 0.9T_{BKT}$.

This implies that for $U \to 0$, *and in practice* $\frac{mU}{\hbar^2}$ *extremely small*, there will be the above mentioned double jump phenomenon for the exponent $\mathcal{C}_0^{\text{Bose}}$ which will pass near below T_{BKT} from a value close to the quantity in Eq. (3.72), 0.912, to $\frac{7}{8} = 0.875$ for $T = T_{BKT}$. Then the second Nelson-Kosterlitz jump will lead $\mathcal{C}_0^{\text{Bose}}$ to pass from 7/8 to zero. It can be seen that there is not appreciable change in this result if one goes to higher orders of approximation. Despite being not too large in absolute value, the first jump should be

appreciable in experiments or simulations, one problem being that one has to go possibly to very small values of $\frac{mU}{\hbar^2}$. We observe that the prediction of the double jump is based on the validity of the low T expansion and its extension near T_{BKT} for U very small – and when T is scaled in units of T_{BKT}, which in turn depends on U. Therefore it could be that further corrections near T_{BKT} may soften the first jump, making it a very steep decrease. Notice, that due to Eq. (3.39), the value $\mathcal{C}_0 = 0.912$ corresponds to $\eta = 0.176$, which is pretty far from the universal value $\eta = 0.25$, so that going to very small U one should appreciate such relatively large variation of η near T_{BKT}. Further simulations would be extremely useful to better quantify such steep decrease of η close to T_{BKT}.

Interestingly enough, at low temperatures, the Bose gas can be described by the corresponding results for the XY model. Therefore, posing $\mathcal{C}_0^{XY} = \mathcal{C}_0^{\text{Bose}\,(0)}$ *i.e.* equating the low temperature result of the XY model in Eq. (3.56) to the low temperature result for the $2D$ Bose gas in Eq. (3.69) for *any* rescaled temperature T/T_{BKT}, one obtains the following value for the parameter ξ:

$$\xi = \frac{1}{2} e^{1+\frac{\pi}{2}(\mathcal{T}-1)}\,, \tag{3.73}$$

where $\mathcal{T} \equiv 4J/k_B T_{BKT}^{(XY)}$. When the dimensionless interaction strength satisfies the equation:

$$\frac{mU}{\hbar^2} = \frac{1}{2} e^{1-\frac{\pi}{2}} = 0.283\,, \tag{3.74}$$

the low T predictions in Eq. (3.69) equals Eq. (3.56), valid respectively for the $2D$ Bose gas and the XY model. Since for the XY model it is $k_B T_{BKT}^{(XY)}/J = 0.893 \pm 0.001$, one finds:

$$\xi = 321 \pm 3, \tag{3.75}$$

which should be compared with the Monte Carlo result $\xi = 380 \pm 3$. The comparison shows that this result (that depends only on the critical temperature of the $2D$ XY model) is not entirely unreasonable, given the non-perturbative nature of the parameter ξ and the well-known failure of mean-field calculations to determine it and in general the difficulty of obtaining analytical estimates for it.

Predictions can be made also for $T \simeq T_{BKT}$, *i.e.* $X \to 0^+$. We write the function $\theta(X)$ as:

$$\theta(X \to 0) \;=\; bX + \frac{1}{\pi} \ln\left(\frac{\xi}{\xi_\mu}\right)\,, \tag{3.76}$$

where b is a constant to be determined by fitting the values of $\theta(X)$ for small X coming from Monte Carlo simulations with the law in Eq. (3.76). It is found $b = 1.29 \pm 0.05$.

For the function $f(X)$ is found instead [193, 194, 213]:

$$f(X \to 0) \;=\; 1 + \sqrt{2\kappa' X}\,, \tag{3.77}$$

with $\kappa' = 0.61 \pm 0.01$. For $\lambda(X)$, from Eq. (3.76), is simply found that:

$$\lambda(X \to 0) \;=\; \frac{b-1}{2}\, X\,, \tag{3.78}$$

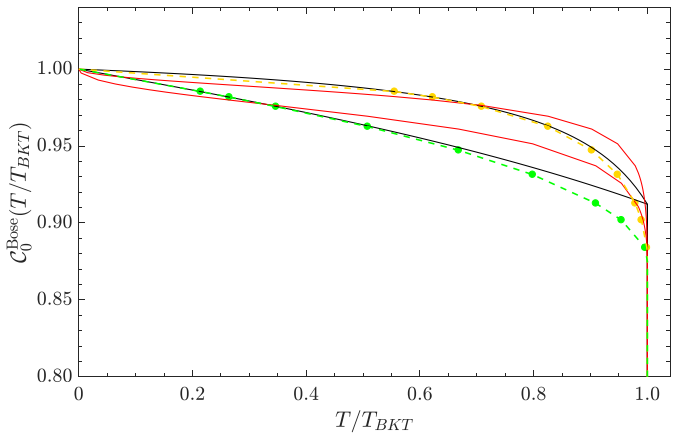

Figure 3.12: Comparison of low temperature predictions for $\mathcal{C}_0^{\rm Bose}(T/T_{BKT})$ vs T/T_{BKT} with numerical results for the two different interactions $\frac{mU}{\hbar^2} = 10^{-12}, 0.25$. Bottom green (top yellow) points are the numerical values from numerical simulations performed in [213], respectively for $\frac{mU}{\hbar^2} = 0.25$ ($\frac{mU}{\hbar^2} = 10^{-12}$), while dashed lines are drawn as a guide for the eye. Low temperatures predictions from third order approximation are reported in black solid lines for two different interaction strengths: the line below (above) is for $\frac{mU}{\hbar^2} = 0.25$ ($\frac{mU}{\hbar^2} = 10^{-12}$) . Red solid lines (standing above the black ones for both interaction strengths) represent the predictions for $T \simeq T_{BKT}$ from Eq. (3.80).

and therefore, following the same reasoning of the low T case, from Eq. (3.61) it follows that:

$$X = \frac{\ln\left(\frac{\hbar^2\xi}{mU}\right)}{\pi(b-1)}\left(\frac{T_{BKT}}{T} - 1\right) . \tag{3.79}$$

Finally we can substitute the above expression for X into Eq. (3.77) and then into Eq. (3.60) to obtain an expression for $\mathcal{C}_0^{\rm Bose}$ for $T \simeq T_{BKT}$ which reads:

$$\mathcal{C}_0^{\rm Bose}(T \to T_{BKT}) \simeq 1 - \frac{1}{8}\left[1 + \sqrt{\frac{2\kappa'}{\pi(b-1)}\ln\left(\frac{\hbar^2\xi}{mU}\right)\left(\frac{T_{BKT}}{T} - 1\right)}\right]^{-1} . \tag{3.80}$$

We report its behaviour in red solid lines in Fig. 3.12 along with numerical Monte Carlo results of $\mathcal{C}_0^{\rm Bose}$ obtained from [213] for different interactions. The agreement is good only for values $X \simeq 0$ and the analytical prediction of Eq. (3.80) gets rapidly worse for decreasing temperatures.

Equating the two behaviours in Eqs. (3.69) and (3.80) we can find how the temperature with which the two curves intersect depends on the dimensionless interaction parameter $\frac{mU}{\hbar^2}$. Substituting this expression back to either (3.69) or (3.80), it is found that the value for $\mathcal{C}_0^{\rm Bose}$ at which the two limiting behaviours intersect is independent on the interaction strength, and reads:

$$\begin{aligned}\mathcal{C}_0^{\rm Bose\,(0)} &= 1 - \frac{1}{8}\left[1 + \sqrt{\frac{2\kappa'}{\pi(b-1)}}\sqrt{5 - \ln(2\xi) + \frac{16\kappa'}{\pi(b-1)} - 4\sqrt{\frac{2\kappa'}{\pi(b-1)}}\sqrt{5 - \ln(2\xi) + \frac{8\kappa'}{\pi(b-1)}}}\right]^{-1} \\ &\simeq 0.914\,. \end{aligned} \tag{3.81}$$

This intersection value can also be obtained using the first order approximation formula $\mathcal{C}_0^{\mathrm{Bose}\,(1)}$, for which one gets 0.915.

Let us now study the scaling exponent $\mathcal{C}_{k\neq 0}$ for the eigenvalues of the 1BDM corresponding to non-vanishing momenta. As in the previous section, we have to compute the Fourier transform of the symmetrized asymptotic behaviour of the density matrix, hence:

$$\begin{aligned}\frac{n(k)}{L^2} &\propto \lim_{L\to\infty}\int_0^{2\pi} e^{ikr\cos(\theta)}d\theta\left[\int_0^{L/2}\frac{dr}{r^{\eta-1}}+\int_{L/2}^{L}\frac{dr}{(L-r)^{\eta-1}}\right]\\ &= \lim_{L\to\infty}\left[\int_0^{L/2}\frac{J_0(kr)}{r^{\eta-1}}\,dr+\int_{L/2}^{L}\frac{J_0(kr)}{(L-r)^{\eta-1}}\,dr\right],\end{aligned}$$

where we passed to polar coordinates symmetrizing on the radial component as was done for the XY model case, $J_0(x)$ is the Bessel function of the first kind, and $\eta=\frac{m^2\,k_BT}{2\pi\hbar^2\rho_s}$ for the weakly interacting Bose gas, while $\eta=\frac{T}{2\pi J_s(T)}$ for the XY model. Focusing only on the first half of the integration interval[1] we obtain:

$$\frac{n(k)}{L^2}\propto L^{2-\eta}\,{}_1F_2\left(1-\frac{\eta}{2};1,2-\frac{\eta}{2};-\frac{\pi^2l^2}{4}\right), \tag{3.82}$$

where we used $k\,L=2\,\pi\,l$ with $l\in\mathbb{N}$. Expanding the hypergeometric function for large l and focusing only the leading term, we obtain finally:

$$\frac{n(k)}{L^2}\propto L^{2-\eta}\,l^{\eta-2}\propto N^0, \tag{3.83}$$

where in the last proportion we wrote $l\propto L$ in order that k remains finite in the thermodynamic limit and $L\propto\sqrt{N}$, since the density $n=N/L^2$ is fixed. Therefore we simply read:

$$\mathcal{C}_{k\neq 0}(T)=0, \tag{3.84}$$

both for the XY and the two–dimensional Bose gas systems for zero and finite temperatures.

This ends our analysis on the ordering properties of different kind of systems both at zero and finite temperatures. Until now, we worked in the static regime and the stationary Schrödinger equation were considered all along. We will now deal with nonequilibrium situations, by first introducing a mean field approach to treat the problem.

1 We observe that symmetrizing the density matrix adding the mirrored term in the region $L/2$ to L serves to have a positive and real result for the momentum distribution and occupation numbers, but it does not affect the scaling of the λ_k eigenvalues in terms of L.

4

GENERALIZED GROSS–PITAEVSKII EQUATION

The study of the dynamics of bosonic quantum many–body systems is in general a challenging task. While in a later Chapter we will build an exact analytical solution for the case in which the quantum system is subjected to a linear time–varying potential, here we will introduce a mean field approach which generalizes the Gross–Pitaevskii equation and allows to deal with generic external potentials.

The Gross–Pitaevskii equation (GPE) is a notorious type of Schrödinger equation which describes both static and dynamic properties of Bose–Einstein condensates in different dimensions and, in general, in presence of a trapping potential [18]. The underlying idea is that the BEC state can be described by a unique wavefunction $\psi(\mathbf{r},t)$, since all the particles are found to be in the same quantum state. The time–dependent GPE reads [18, 218, 219]:

$$i\hbar\frac{\partial}{\partial t}\psi(\mathbf{r},t) = -\frac{\hbar^2}{2m}\nabla^2\psi(\mathbf{r},t) + V(\mathbf{r})\,\psi(\mathbf{r},t) + \frac{4\pi\hbar^2 a_s}{m}\left|\psi(\mathbf{r},t)\right|^2\psi(\mathbf{r},t)\,, \tag{4.1}$$

where a_s is the 3D scattering length, and the nonlinearity describes the contact interactions among atoms. The GPE is also referred to as the nonlinear Schrödinger equation and for generic different potentials its solution has to be found numerically. The GPE can be obtained by taking the functional derivative with respect to $\psi^\dagger(\mathbf{r},t)$ of the Hamiltonian of the BEC gas, which reads:

$$H_{\mathrm{GPE}} = \int d\mathbf{r}\,\left[-\frac{\hbar^2}{2m}\psi^\dagger(\mathbf{r},t)\nabla^2\psi(\mathbf{r},t) + V(\mathbf{r})\,\psi(\mathbf{r},t) + \frac{4\pi\hbar^2 a_s}{m}\psi^\dagger(\mathbf{r},t)\psi^\dagger(\mathbf{r},t)\psi(\mathbf{r},t)\psi(\mathbf{r},t)\right]. \tag{4.2}$$

Let us now focus on one–dimensional systems. At first, we will not specify the type of interactions occurring among particles, and only later we will focus on the case of contact interactions. We therefore write the Hamiltonian as:

$$H = \int dz\,\left[-\psi^\dagger(z,t)\frac{\hbar^2}{2m}\frac{\partial^2}{\partial z^2}\psi(z,t) + V(z)\,\psi(z,t) + G[\rho(z,t)]\right], \tag{4.3}$$

where $\psi(z,t)$ is the wavefunction, $\rho(z,t)$ is the density:

$$\rho(z,t) = \psi^\dagger(z,t)\psi(z,t)\,, \tag{4.4}$$

and $G[\rho]$ is a generic nonlinear term which describes the interactions. From this Hamiltonian, proceeding in the same way as one does for the GPE, we derive the following equation of motion for the wavefunction of the system:

$$i\hbar\frac{\partial}{\partial t}\psi(z,t) = -\frac{\hbar^2}{2m}\frac{\partial^2}{\partial z^2}\psi(z,t) + V(z)\,\psi(z,t) + f[\rho(z,t)]\psi(z,t)\,. \tag{4.5}$$

The functional $f[\rho]$ is related to $G[\rho]$ by the following equation:

$$f[\rho] = \frac{\delta}{\delta\rho} G[\rho] \,. \tag{4.6}$$

We name Eq. (4.5) the generalized (time-dependent) Gross–Pitaevskii equation (GGPE). Depending on the form of the nonlinearity which describes the interactions among different particles of the system, one will obtain different forms for the time–dependent Schrödinger equation of the wavefunction $\psi(z,t)$. Notice that, in the same line of the Gross–Pitaevskii formalism, these results, and in particular the wavefunction, will describe systems made up of many particles at $T = 0$, and therefore this will allow us to make use of equations valid in the thermodynamic limit of the ground state of the system considered.

Let us now discuss more on the functional form of $f[\rho]$: First of all it is a functional since, for a generic trapping potential, the density ρ is actually position-dependent, because of the inhomogeneity. Then one can prove that the functional $f[\rho]$ is related to the energy per particle as (see Appendix 4.4.A):

$$f[\rho] = \mathcal{E}[\rho] + \rho \frac{\delta}{\delta\rho} \mathcal{E}[\rho] \,, \tag{4.7}$$

where:

$$\mathcal{E}[\rho] = \frac{E(\psi = \text{const})}{N} \,. \tag{4.8}$$

This make it possible to identify the functional $f[\rho]$ as the Gibbs free energy per particle of the homogeneous system [220], since only in the homogeneous case the ground state wavefunction is uniform, and hence constant.

Coming back to the GGPE in Eq. (4.5), we can get informations on the static properties of the system by assuming that the wavefunction can be simply factorized as:

$$\psi(z,t) = \psi(z) e^{-i\frac{\mu}{\hbar}t} \,, \tag{4.9}$$

where μ is the chemical potential, and $\psi(z)$ is now a real function. Eq. (4.5) becomes:

$$\mu\psi(z) = -\frac{\hbar^2}{2m}\frac{\partial^2}{\partial z^2}\psi(z) + V(z)\,\psi(z) + f[\rho(z)]\,\psi(z) \,, \tag{4.10}$$

where $\rho(z) = \psi(z)^2$.

Let us focus on the case of a one–dimensional Bose gas with contact interactions, *i.e.* the Lieb–Liniger model. For the LL model at $T = 0$ we know that the energy per particle can be written as (we will drop the subscript B, which was instead present in Chapter 1):

$$\mathcal{E}[\rho] = \frac{\hbar^2}{2m}\rho^2 e(\gamma) \,, \tag{4.11}$$

where $e(\gamma)$ is the dimensionless ground state energy density that we deeply studied in Chapter 1. Therefore the nonlinearity which characterize the GGPE for the LL model reads:

$$f[\rho] = \frac{\delta}{\delta\rho} G[\rho] = \frac{\hbar^2}{2m}\left[3e(\gamma) + \frac{\delta}{\delta\rho} e(\gamma)\right]\rho^2 \,, \tag{4.12}$$

which can also be rewritten as:

$$f[\rho] = \frac{\hbar^2}{2m}\left[3e(\gamma) - \gamma\frac{\partial e}{\partial \gamma}\right]\rho^2\,. \tag{4.13}$$

An acute reader may notice that this exactly coincides with the definition of the chemical potential of the LL model [53], *i.e.* the energy necessary to add one particle to the system. We can finally write the time–dependent GGPE for the LL model as [221]:

$$i\hbar\frac{\partial}{\partial t}\psi(z,t) = -\frac{\hbar^2}{2m}\frac{\partial^2}{\partial z^2}\psi(z,t) + V(z)\,\psi(z,t) + \frac{\hbar^2}{2m}\left[3e\left(\gamma(z,t)\right) - \gamma(z,t)\frac{\partial e}{\partial \gamma}\right]\rho(z,t)^2\,\psi(z,t)\,. \tag{4.14}$$

Since the gas is subjected to an external trapping potential, $V(z)$, then also the density will have a z-dependence because of the inhomogeneity. Moreover, since the dimensionless coupling strength depends inversely on the density of the gas [cfr Eq. (1.6)], it follows that it depends as well on the position variable. Notice that the nonlinearity is highly nontrivial for the LL model, since the dependence on the density it is also encoded in the ground state energy density $e(\gamma)$ in a form which is not known analytically (this basically follows from the fact that the Lieb equations cannot be exactly solved in all the regimes of interactions). Therefore if one wants to numerically solve Eq. (4.14), the evaluation of the nonlinear term would be computational demanding. Our compact analytical expression for the function $e(\gamma)$ in all the regimes of interactions, *i.e.* Eq. (1.55), come in huge help here. Indeed, for a fixed t, once $\psi(z)$ is known, then also $\rho(z,t)$ and $\gamma(z,t)$ are known and can be substituted to the $e^{3r}(\gamma)$ function which gives immediately a reliable result which is in turn used to get the behaviour of $\psi(z, t+\Delta t)$. More on this will be discussed later in this Chapter.

We want to remark here that the above GGPE for the Lieb–Liniger Bose gas may be obtained also using an hydrodynamic approach (CHD). The nonlinear Schrödinger equation is indeed connected to the hydrodynamic formulation via the Madelung transformations [222], which consist in writing the wavefunction as: $\psi(z,t) = \sqrt{\rho(z,t)}\exp[iS(z,t)/\hbar]$, where $S(z,t)$ is the quantum action related to the velocity field as: $v(z,t) = \partial_z S(z,t)/m$. With these notations, substituting into the time–dependent nonlinear Schrödinger equation, one arrives at the classical hydrodynamic equations for the density of the gas and the fluid velocity:

$$\frac{\partial}{\partial t}\rho(z,t) + \frac{\partial}{\partial z}[\rho(z,t)\,v(z,t)] = 0\,, \tag{4.15}$$

$$\frac{\partial}{\partial t}v(z,t) + v(z,t)\frac{\partial}{\partial z}v(z,t) = -\frac{1}{m}\frac{\partial}{\partial z}\left\{f[\rho] + V(z)\right\}\,. \tag{4.16}$$

By adding an additional quantum pressure term [221], the hydrodynamic formulation leads to the GGPE (4.14). These equations actually suppose that the trapped gas is in local thermal equilibrium at each position z, with local energy per particle given by Eq. (4.8). Therefore the hydrodynamic equations involve the local density approximation of the system, which corresponds to the case of zero temperature thermodynamic limit. But from the point of view of the interaction strengths, it is remarkable to notice that they hold for any values of interactions, ranging from the Thomas–Fermi (*i.e.* high density and hence weak interactions) to the Tonks–Girardeau (*i.e.* low density, hence strong repulsive interactions) regimes [220,223]. More on these two limits will be discussed in the following,

as well as comments on the regimes of validity of CHD, which we resume here by saying that it is safe to use CHD (and hence the GGPE) at $T = 0$ and for finite evolution times.

In this Chapter we will study some interesting properties that can be extracted from the analysis of both the time–dependent and independent GGPE for a generic system. First we will focus on the case when there is no external trapping potential and the ground state of the system is homogeneous. We will show that, in this scenario, the study of solitonic solutions for repulsive gases is possible. Since we will treat as an example the case of the LL repulsive gas, the study will focus on black and grey solitons solution, which represent excited states of the system where there is a "negative" modulation of the density profile [18, 70]. Solitons are characterized by a profile density which moves in the medium at a constant velocity and whose shape is preserved during the evolution. In the case of repulsive interactions, it is possible to construct excited solutions where the density is completely (black soliton) or partially (grey soliton) suppressed. The existence of these peculiar solutions, also called as solitary waves, is strictly related to the nonlinearity present in the differential equation [224], which in this case is the time–dependent GGPE. After this we will study the effect of a trapping potential on the density of a LL gas described by Eq. (4.14). We will deal with a numerical approach which will allow us to find a solution of the static equation, letting us finding the ground state density profile for different potentials and interaction strengths. As a final remark, we will also sketch how one should deal with the study of the dynamics of the trapped system.

4.1 BLACK SOLITONS IN THE GGPE

Let us start by rewriting Eq. (4.10) as:

$$\mu\psi(z) = -\frac{\hbar^2}{2m}\frac{\partial^2}{\partial z^2}\psi(z) + f[\psi^2(z)]\psi(z)\,. \tag{4.17}$$

Since in this Section we will consider black solitons, which are characterized by a localized complete drop in the particle density, we will assume that the wavefunction is monotonic increasing and that the derivatives of $\psi(z)$ are zero at infinite distances. Furthermore, we will assume that $\psi(z = 0) = 0$, that is the density vanishes at the origin, as a complete drop would require. Let us call the density at infinity ρ_∞.

From Eq. (4.10), with the aforementioned conditions, we see that the chemical potential is given by:

$$\mu = f[\rho_\infty]\,, \tag{4.18}$$

where the functional is given by Eq. (4.7). At $z = 0$, the wavefunction vanishes while sufficiently far from that point, the density approaches ρ_∞, which is the bulk value. The distance over which the wavefunction rises from zero at the origin to close to its bulk value, may be estimated from the Gross–Pitaevskii equation. When we are sufficiently far from $z = 0$, the total energy of the system is of order of $f[\rho_\infty]$, while if we denote by ξ_H the spatial scale of variations, then from Eq. (4.10) we get:

$$\frac{\hbar^2}{2m\xi_H^2} = f[\rho_\infty]\,,$$

that is:

$$\xi_H = \frac{1}{\sqrt{\frac{2m}{\hbar^2}\mu}}\,, \tag{4.19}$$

where Eq. (4.18) has been used. ξ_H is known as the healing length of the system [18, 70], and it provides a natural length scale with respect to which we can express dimensionful quantities. Indeed we can define a dimensionless position variable as: $x = z/\xi_H$, and a dimensionless wavefunction: $\varphi(x) = \psi(\xi_H x)/\rho_\infty^{1/2}$, thanks to which Eq. (4.17) becomes:

$$\varphi''(x) = -\varphi(x) + h[\varphi^2]\varphi\,, \tag{4.20}$$

where the primes indicate the derivatives with respect to x, and we defined:

$$h[\varphi^2] = \frac{2m\xi_H^2}{\hbar^2} f[\rho_\infty \varphi^2]\,. \tag{4.21}$$

Notice that, since $\varphi(x \to \infty) = 1$, then $h[1] = 1$, according to Eq. (4.19). We will refer to Eq. (4.20) as the dimensionless time-independent generalized Gross–Pitaevskii equation. In analogy with the functional $G[\rho]$, we can define a functional $H[\varphi^2]$ as:

$$h[\varphi^2] = \frac{\delta}{\delta\varphi^2} H[\varphi^2]\,. \tag{4.22}$$

We now notice a similarity between Eq. (4.20) and the Newton's second law of motion:

$$\frac{d^2q}{dt^2} = -\frac{\partial}{\partial q} V(q)\,,$$

where we have indicated with q the position and V a generic time-independent potential. In classical dynamics, this allows to define the energy E as a constant of motion:

$$E = \frac{1}{2}\frac{dq}{dt}^2 + V(q)\,.$$

Similarly, we can rewrite Eq. (4.20) as:

$$\varphi''(x) = -\frac{\delta}{\delta\varphi}\tilde{V}[\varphi^2]\,, \tag{4.23}$$

where the "potential" is given by:

$$\tilde{V}[\varphi^2] = \frac{1}{2}\varphi^2 - \frac{1}{2}H[\varphi^2]\,, \tag{4.24}$$

while the "constant of motion", $\tilde{E}$, reads:

$$\tilde{E} = \frac{1}{2}(\varphi')^2 + \tilde{V}[\varphi^2]\,. \tag{4.25}$$

In order to verify that $\tilde{E}$ is indeed a constant of motion, we derive the "energy" with respect to x, obtaining:

$$\tilde{E}' = \varphi'\left[\varphi'' + \frac{\delta}{\delta\varphi}\tilde{V}[\varphi^2]\right] = 0\,,$$

where Eq. (4.23) has been used. Since it is a constant, it is convenient to fix $\tilde{E}$ by what happens at infinite distance. There, since we want to study a black soliton solution, the derivatives of the wavefunction vanish, and therefore we have:

$$\tilde{E} = \tilde{V}[1] = \frac{1}{2} - \frac{1}{2}H[1]\,. \tag{4.26}$$

Now, finally, we are able to find a black soliton solution for the problem: Eq. (4.25) allows us to write:

$$\varphi' = \sqrt{2(\tilde{E} - \tilde{V}[\varphi^2])}\,, \tag{4.27}$$

which gives:

$$x = \int_0^{\varphi(x)} \frac{d\tilde{\varphi}}{\sqrt{2(\tilde{E} - \tilde{V}(\tilde{\varphi}^2)]}}\,,$$

and can also be rewritten as:

$$x = \int_0^{\varphi(x)} \frac{d\tilde{\varphi}}{\sqrt{1 - \tilde{\varphi}^2 - H[1] + H[\tilde{\varphi}^2]}}\,, \tag{4.28}$$

from using the definition of the "potential" $\tilde{V}$. The problem now consists in finding a solution for Eq. (4.28). We note that this procedure, until now, is completely general and does not depend on a particular nonlinear function. Once the nonlinearity is fixed, a solution can be found by fixing $\varphi \in [0, 1]$ and by numerically evaluating the integral in Eq. (4.28), in such a way that one finds the corresponding value x where the black soliton solution acquires the value φ. This procedure makes sense since the wavefunction is a monotonic increasing function and therefore is invertible.

As an explanatory example, we will now study black soliton solutions for the homogeneous Lieb–Liniger Bose gas. There the nonlinearity is highly nontrivial but we have in our hand a method that allows to easily compute the functional $f[\rho]$.

4.1.1 BLACK SOLITONS IN THE LIEB–LINIGER MODEL

For the Lieb–Liniger gas, a fundamental physical variable is the dimensionless coupling γ:

$$\gamma(z) = \frac{c}{\rho(z)} = \frac{c}{\rho_\infty \varphi(x\xi_H)^2}\,, \tag{4.29}$$

where we remind that ρ_∞ is the density at infinity, and c is the coupling strength having dimensions of the inverse of a length, and we used: $\varphi = \psi/\rho_\infty^{1/2}$. The chemical potential of the gas is given by:

$$\mu = f[\rho_\infty] = \frac{\hbar^2}{2m}\left[3e\left(\frac{c}{\rho_\infty}\right) - \frac{c}{\rho_\infty}\frac{\delta e}{\delta \gamma}\bigg|_{\gamma=\frac{c}{\rho_\infty}}\right]\rho_\infty^2\,, \tag{4.30}$$

therefore we may rewrite the healing length as:

$$\xi_H = \frac{1}{\sqrt{\frac{2m}{\hbar^2}\mu}} = \frac{1}{\rho_\infty \sqrt{3e\left(\frac{c}{\rho_\infty}\right) - \frac{c}{\rho_\infty}\frac{\delta e}{\delta \gamma}\Big|_{\gamma=\frac{c}{\rho_\infty}}}}\,. \tag{4.31}$$

For the LL model the nonlinearity is given by Eq. (4.13), and hence the dimensionless nonlinearity functional $h[\varphi^2]$ is given by:

$$h[\varphi^2] = \xi_H^2 \, \rho_\infty^2 \left[3e\left(\frac{c}{\rho_\infty \varphi^2}\right) - \frac{c}{\rho_\infty \varphi^2} \frac{\delta e}{\delta \gamma}\Big|_{\gamma=\frac{c}{\rho_\infty \varphi^2}} \right] \varphi^4 \,, \tag{4.32}$$

where we used its definition in Eq. (4.21). From (4.22), it then follows that:

$$H[\varphi^2] = \xi_H^2 \, \rho_\infty^2 \, e\left(\frac{c}{\rho_\infty \varphi^2}\right) \varphi^6 \,. \tag{4.33}$$

From these functional forms, and using (4.31) for the healing length, we can rewrite Eq. (4.28) explicitly as:

$$\begin{aligned} x = & \sqrt{3e\left(\frac{c}{\rho_\infty}\right) - \frac{c}{\rho_\infty} \frac{\delta e}{\delta \gamma}\Big|_{\gamma=\frac{c}{\rho_\infty}}} \cdot \\ & \cdot \int_0^{\varphi(x)} \left\{ \left[3e\left(\frac{c}{\rho_\infty}\right) - \frac{c}{\rho_\infty} \frac{\delta e}{\delta \gamma}\Big|_{\gamma=\frac{c}{\rho_\infty}} \right] (1-\tilde{\varphi}^2) - e\left(\frac{c}{\rho_\infty}\right) + e\left(\frac{c}{\rho_\infty \tilde{\varphi}^2}\right) \tilde{\varphi}^6 \right\}^{-1/2} d\tilde{\varphi} \,. \end{aligned} \tag{4.34}$$

It is now convenient to perform the following change in the integration variable:

$$t = 2\frac{\tilde{\varphi}}{\varphi(x)} - 1 \,, \tag{4.35}$$

which gives:

$$\begin{aligned} x = & \frac{1}{2}\varphi(x) \sqrt{3e\left(\frac{c}{\rho_\infty}\right) - \frac{c}{\rho_\infty} \frac{\delta e}{\delta \gamma}\Big|_{\gamma=\frac{c}{\rho_\infty}}} \cdot \\ & \cdot \int_{-1}^{1} \left\{ \left[3e\left(\frac{c}{\rho_\infty}\right) - \frac{c}{\rho_\infty} \frac{\delta e}{\delta \gamma}\Big|_{\gamma=\frac{c}{\rho_\infty}} \right] [1-\tilde{\varphi}^2(t)] - e\left(\frac{c}{\rho_\infty}\right) + e\left(\frac{c}{\rho_\infty \tilde{\varphi}^2(t)}\right) \tilde{\varphi}^6(t) \right\}^{-1/2} dt \,, \end{aligned} \tag{4.36}$$

where we wrote for simplicity:

$$\tilde{\varphi}(t) = \frac{1}{2}\varphi(x)(t+1) \,. \tag{4.37}$$

As we already explained, the fact that $\varphi(x)$ is monotonically increasing, implies that it is invertible and it allows to find a solution of the above equation. Indeed the values of x can be found once we fix a value for $\varphi(x) \in [0,1]$. The only problem is that the evaluation of the integral is computationally demanding, since the integrand function depends on the dimensionless ground state energy density function, whose value, in turn, is determined once the Lieb–Liniger integral equations are solved (see Chapter 1 for details). It comes in huge help our closed rather simple compact form for the $e(\gamma)$ function given by Eq. (1.55), where once the argument of the function is fixed, the resulting value is immediately

obtained. Therefore by computing the integral of Eq. (4.36) using the Chebyshev quadrature method with 100 points, we find the black soliton solutions for the Lieb–Liniger gas. In Fig. 4.1, we report the results for the dimensionless wavefunctions of black solitons, for several values of the ratio c/ρ_∞ which tunes the interaction among the particles. In Fig. 4.2 we plotted the dimensionless density $\rho(x)/\rho_\infty = \varphi^2(x)$, for the same interaction strengths.

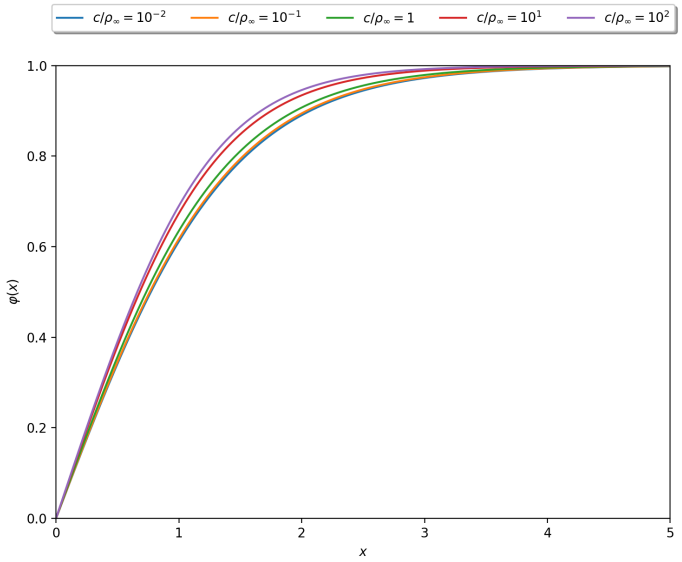

Figure 4.1: Black soliton dimensionless wavefunctions for the Lieb–Liniger model. They are found by numerically solving Eq. (4.36), for different values of the dimensionless ratio c/ρ_∞ which controls the interaction among the particles of the gas.

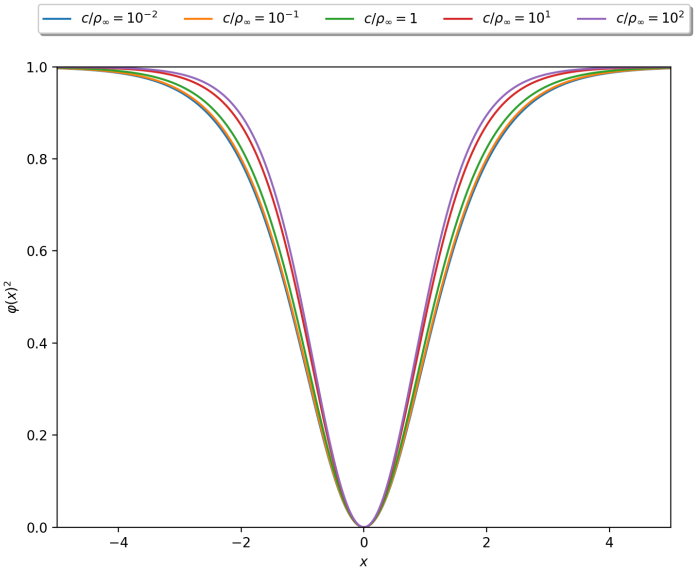

Figure 4.2: Black soliton dimensionless density for the Lieb–Liniger model, simply obtained by squaring the results of Fig. 4.1. We report with different colors the densities at different interaction strengths c/ρ_∞.

We note that the growth of the density is steeper for higher values of c/ρ_∞. This should be intuitively understood by considering that higher values of c/ρ_∞ mean a stronger repulsive interaction far from the minimum of the soliton. Such stronger interaction competes with the tendency of the particles to move away from $x = 0$, where the interaction parameter $\gamma = c/(\rho_\infty \varphi^2)$ diverges [as can be verified from Fig. 4.3].

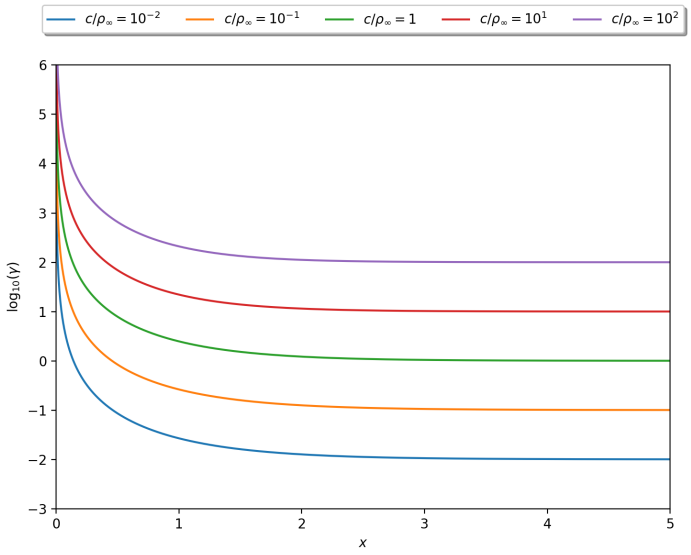

Figure 4.3: Dimensionless Lieb–Liniger interaction parameter γ vs the dimensionless position variable $x = z/\xi_H$, for different values of the ratio c/ρ_∞. Around $x = 0$ the interaction parameter diverges, as it should since in $x = 0$ the black soliton has its minimum, *i.e.* it is the point where the density vanishes.

Let us see what happens in the Tonks–Girardeau limit: For $c/\rho_\infty \to \infty$, we have that Eq. (4.36) can be written as:

$$\frac{x}{\sqrt{3}} = \int_0^{\varphi(x)} \frac{d\tilde{\varphi}}{(1-\tilde{\varphi})(1+\tilde{\varphi})\sqrt{2+\tilde{\varphi}^2}}\,, \tag{4.38}$$

and it can be exactly solved, giving the dimensionless density for a black soliton solution in a Tonks–Girardeau gas:

$$\varphi^2(x) = \frac{2\tanh(x)^2}{3-\tanh(x)^2}\,. \tag{4.39}$$

From the numerical results, we note that already for $c/\rho_\infty = 100$, the solution well approximates this limit.

4.2 GREY SOLITONS IN THE GGPE

In this Section, we will study grey soliton solutions. These solitary waves are characterized, analogously to the black solitons, by a localized drop in the particle density, but in these solutions the density minimum is not zero anymore. Collectively, grey and black solitons are called dark solitons, in contrast to bright solitons which are characterized by a localized peak in the particle density [18,70]. As we did previously, we start by studying grey soliton

solutions for the GGPE without specifying the form of the nonlinearity. Only later, in a Subsection, we will consider as an example the Lieb–Liniger gas.

This time, we will search for solutions of Eq. (4.5) of the form:

$$\psi(z,t) = \rho_\infty^{1/2}\left[g\left(\frac{z-vt}{\xi_H}\right) + ik\right] e^{-i\frac{\mu}{\hbar}t}\,, \tag{4.40}$$

where we remind that the chemical potential and the healing length are related via Eq. (4.19). In (4.40) we are assuming that the solitary waves will move with a constant velocity v (while for the black solitons we were assuming a complete static situation) and the peculiar form of the soliton will be encoded in the dimensionless real function g, while the real, dimensionless, positive constant k is related to the depth of the grey soliton. In particular k^2 will coincide with the value of the dimensionless density of the soliton at the minimum, therefore for $k = 1$ the soliton structure is lost, while for $k = 0$ the grey soliton coincides with the black soliton solution. Notice that in this case we write:

$$\rho(z) = |\psi(z,t)|^2 \to \rho_\infty\,, \quad \text{for } (z - vt) \to \infty\,,$$

and we define a dimensionless variable x, as: $x = \frac{z-vt}{\xi_H}$. With these notations, from (4.40), we have that:

$$g^2(x) + k^2 \to 1\,, \quad \text{for } x \to \infty\,, \tag{4.41}$$

which implies that $k \leq 1$. Since we are considering the case of a grey soliton, we will also require that $g(x)$ is a monotonic increasing function with vanishing derivatives at infinity, and that $g(0) = 0$. This has been chosen in order that when $v = 0$, and $k = 0$, one recovers the black soliton solution studied in the previous Section.

Substituting Eq. (4.40) into Eq. (4.5) in terms of g and k, we get:

$$-i\hbar\frac{v}{\xi_H}g'(x) + \mu(g(x) + ik) = -\frac{\hbar^2}{2m\xi_H^2}g''(x) + f[\rho_\infty(g^2 + k^2)](g(x) + ik)\,, \tag{4.42}$$

from which we note that, for $x \to \infty$, we have: $\mu = f[\rho_\infty]$, that is the chemical potential acquires the same value of the case in which one considers the time–independent Gross–Pitaevskii equation [see Eqs. (4.17) and (4.18)]. We can recast Eq. (4.42) in the form:

$$2iUg'(x) - g''(x) = ik(1 - h[g^2(x) + k^2]) + g(x)(1 - h[g^2 + k^2])\,, \tag{4.43}$$

where we defined the dimensionless velocity variable:

$$U = \frac{m\xi_H v}{\hbar}\,, \tag{4.44}$$

and the functional:

$$h[g^2 + k^2] = \frac{2m\xi_H^2}{\hbar^2}f[\rho_\infty(g^2(x) + k^2)]\,. \tag{4.45}$$

By taking separately the imaginary and real part of Eq. (4.43), we find respectively:

$$g'(x) = \frac{k}{2U}(1 - h[g^2 + k^2])\,, \tag{4.46}$$

and:

$$g''(x) = -g(x) + h[g^2 + k^2]g(x)\,. \tag{4.47}$$

In a similar way of the case of black solitons, we can now recast Eq. (4.47) in a form that recalls the Newton's second law, by writing:

$$g''(x) = -\frac{\delta}{\delta g(x)}\tilde{V}[g^2 + k^2]\,, \tag{4.48}$$

where:

$$\tilde{V}[g^2 + k^2] = \frac{1}{2}\left[g^2(x) + k^2\right] - \frac{1}{2}H[g^2 + k^2]\,, \tag{4.49}$$

with, in turn, the functional H related to h by:

$$h[g^2 + k^2] = \frac{\delta}{\delta\left(g(x)^2 + k^2\right)}H[g^2 + k^2]\,. \tag{4.50}$$

We can therefore define a costant of motion, $\tilde{E}$, given by:

$$\tilde{E} = \frac{1}{2}\left(g'\right)^2 + \tilde{V}[g^2 + k^2]\,. \tag{4.51}$$

It is straightforward to check that it is indeed a constant of motion, indeed if we take the derivative with respect to the position variable, we have that:

$$\tilde{E}' = g'(x)\left[g''(x) + \frac{\delta}{\delta g(x)}\tilde{V}[g^2 + k^2]\right] = 0\,,$$

thanks to Eq. (4.48). It is convenient to fix the constant value $\tilde{E}$ by considering the effects of boundary conditions on the soliton wavefunction, which permits to write the value of the "energy" as:

$$\tilde{E} = \frac{1}{2} - \frac{1}{2}H[1]\,. \tag{4.52}$$

Coming back to Eq. (4.46), we can rewrite it as:

$$\frac{1}{2}(1-k^2) - \frac{1}{2}H[1] = \frac{k^2}{8U^2}(1 - h[g^2(x) + k^2])^2 + \frac{1}{2}g^2(x) - \frac{1}{2}H[g^2 + k^2]\,,$$

which, for $x = 0$, gives:

$$\frac{1}{2}(1-k^2) - \frac{1}{2}H[1] = \frac{k^2}{8U^2}(1 - h[k^2])^2 - \frac{1}{2}H[k^2]\,.$$

Let us work more on this: Solving for k, we get:

$$k = \frac{\sqrt{1 + H[k^2] - H[1]}}{\sqrt{1 + \frac{1}{4U^2}(1 - h[k^2])^2}}\,. \tag{4.53}$$

We know that when the velocity of the grey soliton approaches the sound velocity of the (Luttinger) liquid in which it moves, the solitary wave cannot propagate anymore. It is

therefore convenient to introduce the sound velocity of the system. The sound velocity is related to the density at the bulk via the relation (see Appendix) [1]:

$$s = \frac{\sqrt{\frac{\delta f}{\delta \rho}\Big|_{\rho=\rho_\infty} \rho_\infty}}{\sqrt{m}}\,,$$

which is equivalent to:

$$s = \frac{\hbar}{\sqrt{2} m \xi_H} h^{'}[1]\,, \tag{4.54}$$

where: $h'[1] = \frac{\delta h}{\delta(g^2+k^2)}\Big|_{g^2+k^2=1}$. By defining the dimensionless sound velocity U_s as:

$$U_s = \frac{m\xi_H}{\hbar} s\,,$$

then:

$$U_s = \sqrt{\frac{h'[1]}{2}}\,. \tag{4.55}$$

Therefore we can finally rewrite Eq. (4.53) in terms of the soliton velocity U, and the fluid sound velocity U_s where it propagates:

$$k = \frac{U_s \sqrt{1 + H[k^2] - H[1]}}{\sqrt{U_s^2 + \frac{1}{4}\frac{U_s^2}{U^2}(1 - h[k^2])^2}}\,. \tag{4.56}$$

In the next Section, we will see that in the case of the LL model, when $v = s$, i.e. $U/U_s = 1$, we have that $k = 1$, which implies that the soliton lose its structure and there is no density drop in the gas.

It is only left to find an equation for the soliton function $g(x)$. Up to now, we did not use the real part of Eq. (4.43), so we can obtain the soliton function from there. Indeed, by rewriting Eq. (4.51), which was obtained from the real part analysis, as:

$$g'(x) = \sqrt{2(\tilde{E} - \tilde{V}[g^2 + k^2])}\,,$$

we can invert the equation and get:

$$x = \int_0^{g(x)} \frac{d\tilde{g}}{\sqrt{2(\tilde{E} - \tilde{V}[\tilde{g}^2 + k^2])}} = \int_0^{g(x)} \frac{d\tilde{g}}{\sqrt{1 - (\tilde{g}^2 + k^2) - H[1] + H[\tilde{g}^2 + k^2]}}\,, \tag{4.57}$$

where Eqs. (4.49) and (4.52) have been used. Notice that if the soliton velocity is null, $U = 0$, then from Eq. (4.56) also k is vanishing, and therefore Eq. (4.57) reduces to the black soliton equation in (4.28), as it should. Once the model subjected to study is determined, and hence the nonlinearity fixed, one should first solve the trascendental equation (4.56), for a fixed chosen soliton velocity, and then substitute the value found for k in Eq. (4.57), which can be solved by fixing a certain $g \in [0, 1]$ and finding the corresponding position x, as we did for the black soliton case.

In the following Section we will focus on the case of the Lieb–Liniger model, and we will numerically obtain the grey solitons solutions for different values of the solitary wave velocities and interaction strengths.

1 We substituted ϕ_0^2 with ρ_∞ since we recall that ρ_∞ here is the bulk density.

4.2.1 GREY SOLITONS IN THE LIEB–LINIGER MODEL

Within the grey soliton notations of the previous Section, we define the dimensionless coupling strength γ as:

$$\gamma(z) = \frac{c}{\rho(z)} = \frac{c}{\rho_\infty}\frac{1}{g^2(z)+k^2}\,. \tag{4.58}$$

For the LL model, the nonlinear term is given by Eq. (4.13), and therefore the dimensionless nonlinearty functional can be written as:

$$h[g^2+k^2] = \frac{\left[3e\left(\frac{c}{\rho_\infty}\frac{1}{g^2+k^2}\right) - \frac{c}{\rho_\infty}\frac{1}{g^2+k^2}\frac{\delta e}{\delta\gamma}\Big|_{\gamma=\frac{c}{\rho_\infty}\frac{1}{g^2+k^2}}\right](g^2+k^2)^2}{\left[3e\left(\frac{c}{\rho_\infty}\right) - \frac{c}{\rho_\infty}\frac{\delta e}{\delta\gamma}\Big|_{\gamma=\frac{c}{\rho_\infty}}\right]}\,, \tag{4.59}$$

where we used Eq. (4.31). On the other hand, the functional $H[g^2+k^2]$ assumes the form:

$$H[g^2+k^2] = \frac{e\left(\frac{c}{\rho_\infty}\frac{1}{g^2+k^2}\right)(g^2+k^2)^3}{\left[3e\left(\frac{c}{\rho_\infty}\right) - \frac{c}{\rho_\infty}\frac{\delta e}{\delta\gamma}\Big|_{\gamma=\frac{c}{\rho_\infty}}\right]}\,. \tag{4.60}$$

Hence, the completely explicit form of Eq. (4.53) for the LL model is given by:

$$k = \frac{\sqrt{1 + \frac{e\left(\frac{c}{\rho_\infty}\frac{1}{k^2}\right)k^6}{3e\left(\frac{c}{\rho_\infty}\right) - \frac{c}{\rho_\infty}\frac{\delta e}{\delta\gamma}\Big|_{\gamma=\frac{c}{\rho_\infty}}} - \frac{e\left(\frac{c}{\rho_\infty}\right)}{3e\left(\frac{c}{\rho_\infty}\right) - \frac{c}{\rho_\infty}\frac{\delta e}{\delta\gamma}\Big|_{\gamma=\frac{c}{\rho_\infty}}}}}{\sqrt{1+\frac{1}{4U^2}\left\{1 - \frac{\left[3e\left(\frac{c}{\rho_\infty k^2}\right) - \frac{c}{\rho_\infty k^2}\frac{\delta e}{\delta\gamma}\Big|_{\gamma=\frac{c}{\rho_\infty k^2}}\right]k^4}{3e\left(\frac{c}{\rho_\infty}\right) - \frac{c}{\rho_\infty}\frac{\delta e}{\delta\gamma}\Big|_{\gamma=\frac{c}{\rho_\infty}}}\right\}^2}}\,, \tag{4.61}$$

which has to be solved in order to find the minimum depth of the grey soliton solution. While for the shape of the soliton, one needs to solve Eq. (4.57), which for the LL model reads:

$$\begin{aligned} x = &\sqrt{3e\left(\frac{c}{\rho_\infty}\right) - \frac{c}{\rho_\infty}\frac{\delta e}{\delta\gamma}\Big|_{\gamma=\frac{c}{\rho_\infty}}}\cdot \\ &\cdot\int_0^{g(x)}\left\{\left[3e\left(\frac{c}{\rho_\infty}\right) - \frac{c}{\rho_\infty}\frac{\delta e}{\delta\gamma}\Big|_{\gamma=\frac{c}{\rho_\infty}}\right]\left[1-(\tilde g^2+k^2)\right] - e\left(\frac{c}{\rho_\infty}\right) + \right. \\ &\left. + e\left(\frac{c}{\rho_\infty}\frac{1}{\tilde g^2+k^2}\right)\left(\tilde g^2+k^2\right)^3\right\}^{-1/2} d\tilde g\,. \end{aligned} \tag{4.62}$$

Therefore, once U is fixed, we numerically solve Eq. (4.61), and the solution of Eq. (4.62) can be found with the same procedure as in the black soliton case described in the previous

Section, *i.e.* changing the integration variable and then fixing a value for $g \in [0,1]$ in order to find the corresponding position for that particular value of the soliton function intensity.

Before doing so, it is useful to study the relation with the sound velocity of the Lieb–Liniger gas. The velocity of sound for the Lieb–Liniger model (see Appendix), is given by:

$$s = \frac{\hbar}{m}\rho_\infty \sqrt{3e\left(\frac{c}{\rho_\infty}\right) - 2\frac{c}{\rho_\infty}\frac{\delta e}{\delta\gamma}\bigg|_{\gamma=\frac{c}{\rho_\infty}} + \frac{1}{2}\left(\frac{c}{\rho_\infty}\right)^2 \frac{\delta^2 e}{\delta\gamma^2}\bigg|_{\gamma=\frac{c}{\rho_\infty}}}\,, \tag{4.63}$$

and hence the dimensionless sound velocity reads:

$$U_s = \frac{\sqrt{3e\left(\frac{c}{\rho_\infty}\right) - 2\frac{c}{\rho_\infty}\frac{\delta e}{\delta\gamma}\Big|_{\gamma=\frac{c}{\rho_\infty}} + \frac{1}{2}\left(\frac{c}{\rho_\infty}\right)^2 \frac{\delta^2 e}{\delta\gamma^2}\Big|_{\gamma=\frac{c}{\rho_\infty}}}}{\sqrt{3e\left(\frac{c}{\rho_\infty}\right) - \frac{c}{\rho_\infty}\frac{\delta e}{\delta\gamma}\Big|_{\gamma=\frac{c}{\rho_\infty}}}}\,. \tag{4.64}$$

In Fig. 4.4 we plotted U_s with respect to the dimensionless coupling strength c/ρ_∞. For low and high values of the coupling we have that:

$$\lim_{c/\rho_\infty \to 0} e(c/\rho_\infty) = c/\rho_\infty\,, \quad \text{therefore}: \; U_s \to \frac{1}{\sqrt{2}}\,, \tag{4.65}$$

$$\lim_{c/\rho_\infty \to \infty} e(c/\rho_\infty) = \frac{\pi^2}{3}\,, \quad \text{therefore}: \; U_s \to 1\,. \tag{4.66}$$

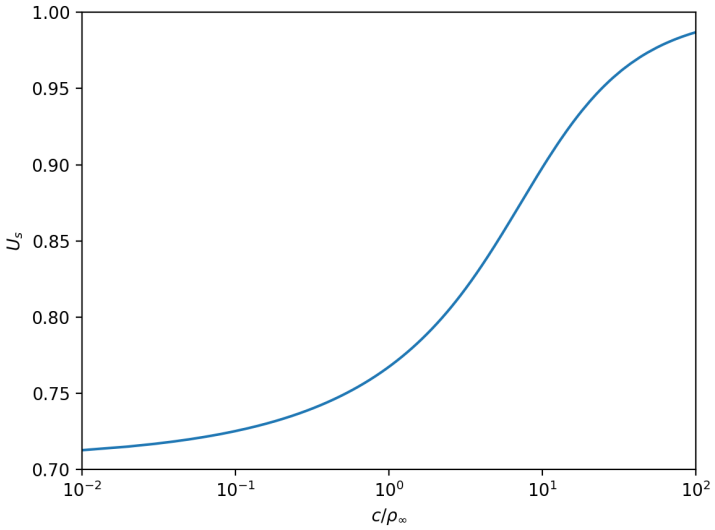

Figure 4.4: Dimensionless sound velocity $U_s = (m\xi_H s)/\hbar$, with respect to the dimensionless coupling c/ρ_∞. The values in the strong and weak coupling regimes can be obtained analytically and read as in Eqs. (4.65) and (4.66).

In Fig. 4.5 instead, we report the numerical solution of the trascendental equation (4.61), which allows to obtain the value for the dimensionless density of the grey soliton at the minimum, *i.e.* k. We note that when $U = U_s$, i.e. $v = s$, we have that $k = 1$. As it is expected, the soliton does not exist if $v = s$, since $k = 1$ implies that there is no density depression.

In order to check the consistency of our results, notice that in the low coupling regime:

$$k \to \sqrt{2}U = \frac{U}{U_s} = \frac{v}{s}\,, \tag{4.67}$$

which is the same relation that one finds in the Gross–Pitaveskii equation. By taking the same limit in Eq. (4.62), we recover the following result for the density of the grey soliton:

$$\frac{\rho(x)}{\rho_\infty} = \frac{v^2}{s^2} + \left(1 - \frac{v^2}{s^2}\right) \tanh^2\left[\frac{x}{\sqrt{2}}\left(1 - \frac{v^2}{s^2}\right)\right]\,, \tag{4.68}$$

which is indeed the same expression found for a grey solitary wave in the GPE [18]. This is due to the fact that for low values of γ, the interaction term in the Hamiltonian becomes quadratic in the wavefunction, or in other words: $f[\rho] = \frac{\hbar c}{m}\rho$, as in the case of the Gross–Pitaevskii equation. This can be seen also from Fig. 4.5, where for low values of the ratio c/ρ_∞, k is almost linear with respect to v/s. We note, however, that this comparison holds when U is much greater than c/ρ_∞.

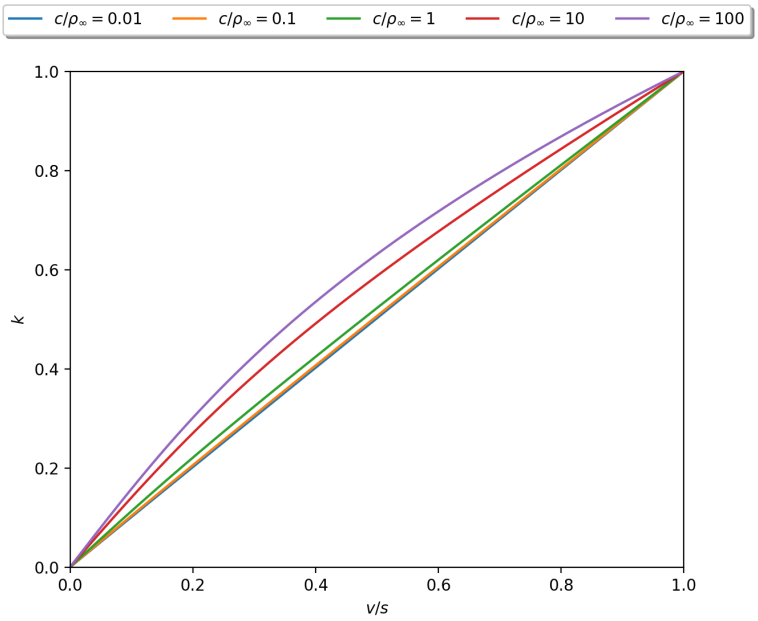

Figure 4.5: k vs v/s, where v and s are the soliton and sound velocities respectively. Different solid lines correspond to different values of the coupling c/ρ_∞. Notice that for low values of the coupling strength, k is approximately linear with respect to v/s.

On the other hand, for the Tonks-Girardeau limit, $c/\rho_\infty = \infty$, we have that the solution, for non-vanishing U, of Eq. (4.61) is given by:

$$k = \frac{1}{\sqrt{3}}\sqrt{\frac{4U^2 + \left[2U(12U + \sqrt{9 + 132U^2 - 16U^4})^{1/3} - 1\right]^2}{\left[1 + 2U(2U + \sqrt{9 + 132U^2 - 16U^4}\right]^{1/3}}}\,, \tag{4.69}$$

while the grey soliton shape is found from Eq. (4.62), and reads:

$$g(x) = \frac{\sqrt{2 + k^2}\,\tanh(x\sqrt{1 - k^2})}{\sqrt{\frac{3}{1-k^2} - \tanh^2(x\sqrt{1 - k^2})}}\,. \tag{4.70}$$

The dimensionless density is then given by:

$$\frac{\rho(x)}{\rho_\infty} = k^2 + \frac{(2+k^2)\tanh^2(x\sqrt{1-k^2})}{\frac{3}{1-k^2} - \tanh^2(x\sqrt{1-k^2})}\,. \tag{4.71}$$

Notice that for $U = 0$, one finds: $k = 0$ from Eq. (4.69), and from (4.71) one gets exactly the result obtained in the case of a black soliton solution, *i.e.* Eq. (4.39). We stress that for $c/\rho_\infty = 100$ the numerical solution are in good agreement with the analytical results just seen for the Tonks-Girardeau limit.

For a generic coupling strength c/ρ_∞, one needs to rely on numerical approaches in order to find the soliton minimum and the solitary wave's shape from Eqs. (4.61) and (4.62). These equations could not be solved numerically if we did not have a closed rather simple expression for the dimensionless ground state energy density $e(\gamma)$, which we instead provided thanks to the Chebyshev Hermite interpolation three-range scheme [cfr Eq. (1.55)]. In Figs. 4.6 – 4.10 we report the behaviour of the dimensionless grey soliton densities $\rho(x)/\rho_\infty = g^2(x) + k^2$, for fixed values of the coupling c/ρ_∞, and each plots presents results at several different values of the soliton velocity U. As it is expected, by decreasing U we approach the shape of the black soliton, which is obtained using the results of the previous Section, while for growing U (up to the sound velocity of the Luttinger liquid) the grey soliton minimum increases and the soliton structure starts to be lost.

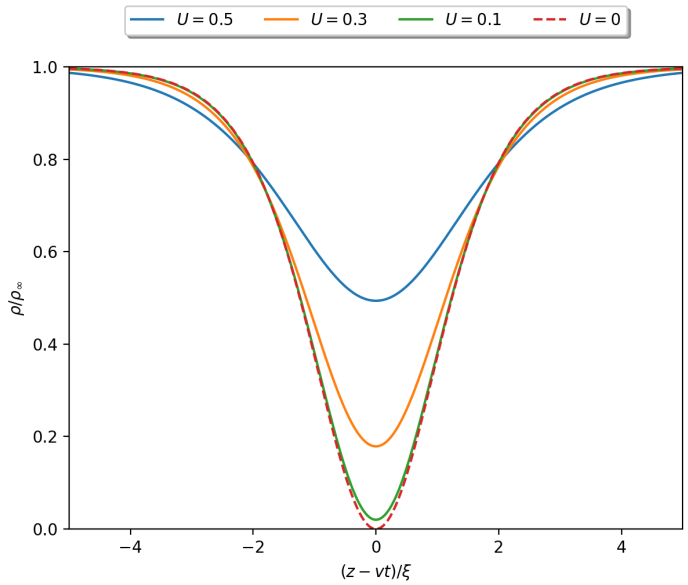

Figure 4.6: Grey soliton dimensionless density for several values of the soliton velocity U, and at fixed coupling strength: $c/\rho_\infty = 0.01$. The black soliton solution ($U = 0$ and hence $k = 0$) is reported in dashed line.

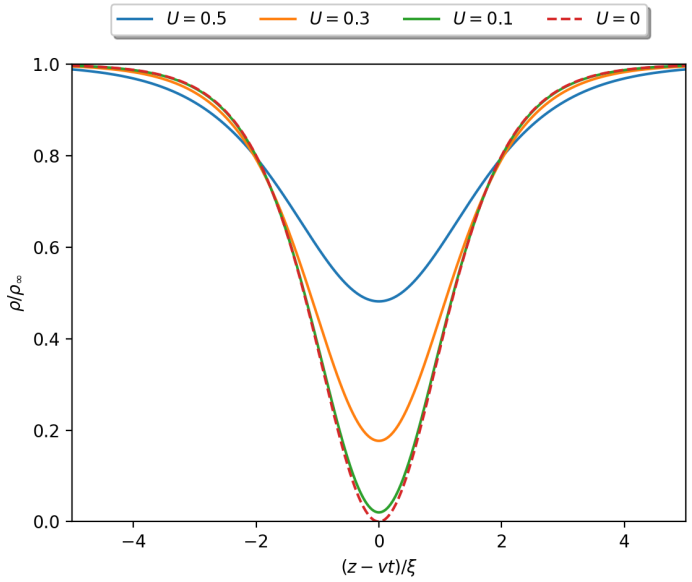

Figure 4.7: Grey soliton dimensionless density for several values of the soliton velocity U, and at fixed coupling strength: $c/\rho_\infty = 0.1$. The black soliton solution ($U = 0$ and hence $k = 0$) is reported in dashed line.

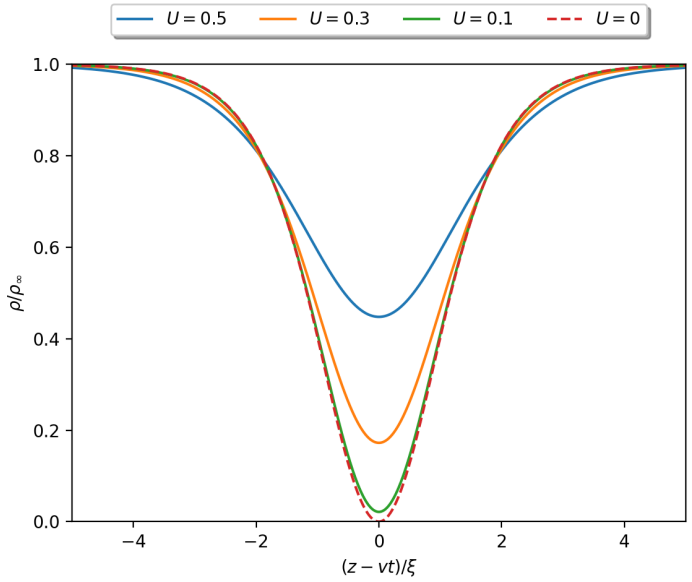

Figure 4.8: Grey soliton dimensionless density for several values of the soliton velocity U, and at fixed coupling strength: $c/\rho_\infty = 1$. The black soliton solution ($U = 0$ and hence $k = 0$) is reported in dashed line.

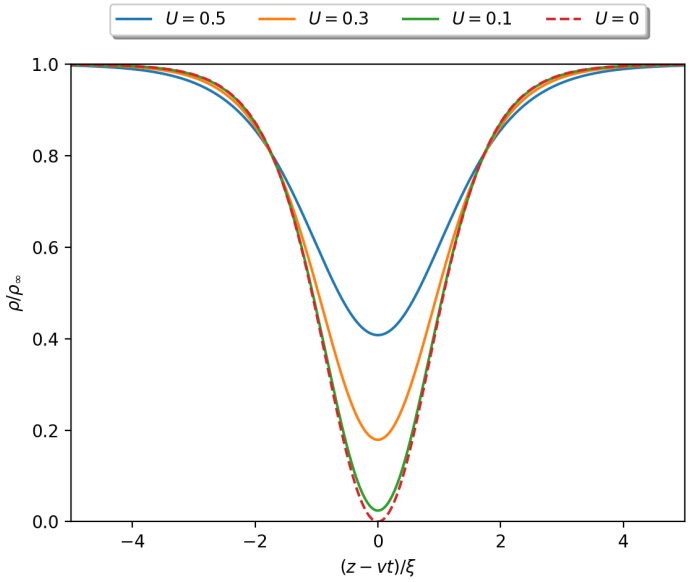

Figure 4.9: Grey soliton dimensionless density for several values of the soliton velocity U, and at fixed coupling strength: $c/\rho_\infty = 10$. The black soliton solution ($U = 0$ and hence $k = 0$) is reported in dashed line.

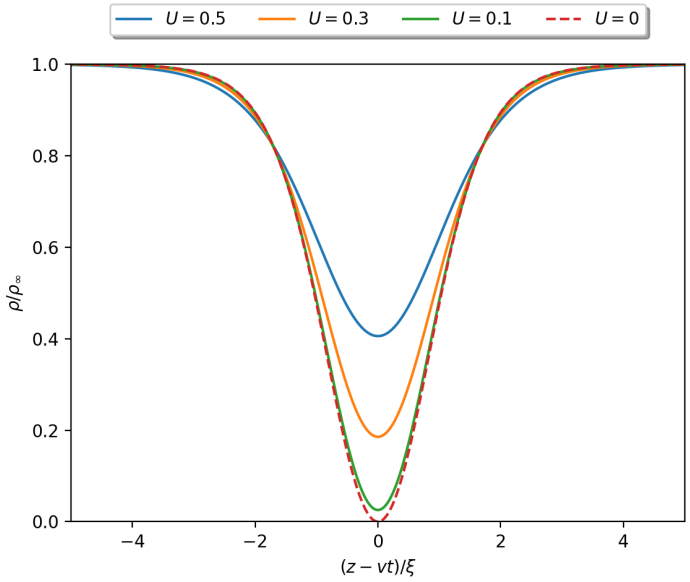

Figure 4.10: Grey soliton dimensionless density for several values of the soliton velocity U, and at fixed coupling strength: $c/\rho_\infty = 100$. The black soliton solution ($U = 0$ and hence $k = 0$) is reported in dashed line.

Finally, in Fig. 4.11, we plot the dimensionless grey soliton densities $\rho(x)/\rho_\infty$, but this time we vary, in the same plot, both the coupling c/ρ_∞ (represented with different colored lines) and the soliton velocity U (represented with different line's styles). We can notice that, analogously to the case of the black solitary wave solution, the growth of the density is steeper for higher values of the ratio c/ρ_∞. Also in this case, the reason is that a stronger repulsive interaction at the bulk competes with the tendency of the particles to move away from the minimum. Moreover notice that the higher is the soliton velocity,

and the stronger are the effects of the interaction strength among particles, as can be seen from the colored solid lines of Fig. 4.11.

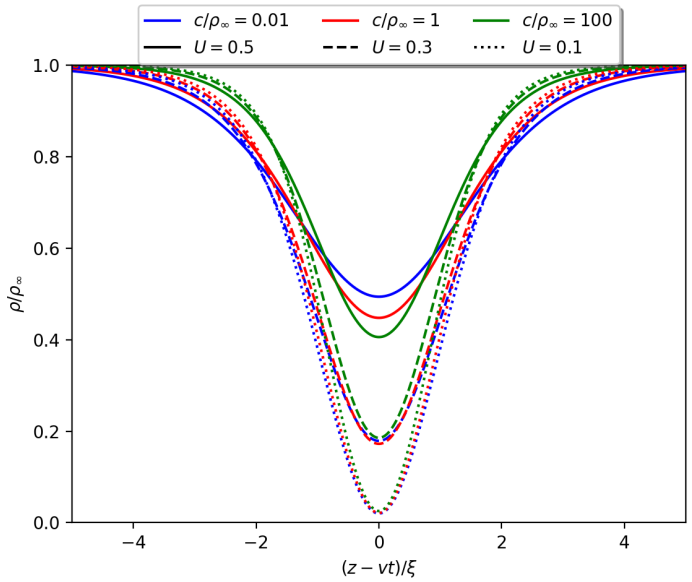

Figure 4.11: Grey soliton dimensionless density for several values of the soliton velocity U (represented with different line's styles), and coupling strength c/ρ_∞ (represented with different colored lines).

4.3 INHOMOGENEOUS GGPE: THE TRAPPED LIEB–LINIGER BOSE GAS

Let us go back to the more general case of the GGPE in presence of a trapping potential, *i.e.* Eq. (4.5). When an external potential is present, even the ground state density of the system will be characterized by a spatial dependence because of the inhomogeneity itself. It is the most interesting case, both theoretically and experimentally, since in real world experiments the gases (or in general the systems subject of studies) are confined in some geometry. In one–dimensional systems, the Lieb–Liniger model in presence of a trapping potential is a very interesting apparatus to work on, since it can describe real quantum gases confined to move only in one direction and subjected to a confinement, which usually comes from the application of laser beams [63]. From the theoretical point of view the model is interesting as well, since the breaking of translational invariance spoils the integrability properties of the system (see [59,68], for example). In that case we know that the nonlinear functional reads as in Eq. (4.13), where both the dimensionless coupling and the density will depend on the spatial variable z. For such systems, the Schrödinger equation that needs to be solved in order to determine the evolution dynamics of a certain initial state $\psi(z, t = 0)$, will then be Eq. (4.14), while static properties, like the determination of the ground state density and the corresponding energy, can be found from Eq. (4.10).

The interest on a solution of this problem, even though approximation and numerical approaches are mandatory, reflects on the number of papers in the literature. While many efforts are done in the direction of a generalized hydrodynamic approach (GHD) [225,226],

where local averages of physical quantities are to be evaluated in the so called generalized Gibbs ensables (GGE), and interesting results were obtained for spin chains and repulsive Bose gases [227–234] (just to cite some, but the literature on this topic during these last years is outstandingly huge), we will drive the discussion by treating the GGPE (sometimes also called as modified nonlinear Schrödinger equation) of the LL model. This way is maybe less popular, but still there were efforts in this direction [188, 221, 223].

The reason for its "unpopularity" can be resumed in two reasons: 1) CHD fails in the description of physical systems at finite temperature and it also leads to shocks propagation, which are instead not present in the system as, instead, GHD predicts [235]. Only at $T = 0$ and at finite evolution times (which are the case considered in this Thesis), the GHD reduces to the CHD and we can safely use its results. 2) The unpopularity of CHD is also due to the fact that in order to solve numerically the time–dependent or independent GGPE one has to sharpen the wits, since the computation of the nonlinear function at each time step and for each position is computational demanding, since in principle one needs to solve the Lieb's integral equations everytime. For example, in [221] they were proposing to study the dynamics of the GGPE for only 25 particles by adiabatically change the number of atoms in the system, in order to reach a converging stable result. It would be very interesting to easily extend this method in order to deal with much more particles. Thanks to our smart three-range expression for the ground state energy density function $e^{3r}(\gamma)$, we are actually able to make such extension, and we will provide explanatory examples of calculation, where we will find the ground state density for different trapping potentials and number of particles.

Let us start the analysis, by studying two different limiting behaviour of the gas: The Tonks–Girardeau and the Thomas–Fermi limits. In the limit of very low densities, the dimensionless coupling γ approaches an infinite value, and the Tonks–Girardeau limit is hence characterized by [223]:

$$\rho\,|a_{1\mathrm{D}}| \to 0\,, \quad \mathcal{E}[\rho] \simeq \frac{\pi^2\hbar^2}{6m}\,\rho^2\,, \tag{4.72}$$

where we remind that $|a_{1\mathrm{D}}| = 2/\rho\gamma$, is the one–dimensional scattering length [66]. The Thomas–Fermi limit, instead, describes the case of high gas densities, and therefore describes weak interaction regimes. Within this limit:

$$\rho\,|a_{1\mathrm{D}}| \to \infty\,, \quad \mathcal{E}[\rho] \simeq \frac{\hbar^2 c}{2m}\,\rho\,, \tag{4.73}$$

where c is the coupling strength having dimension of the inverse of a length.

For these two limiting behaviours, one can easily obtain expressions for the steady state solutions of the system in the weak and strong interacting regimes. This can be done by solving the hydrodynamic equations (4.15) and (4.16), imposing: $\partial\rho/\partial t = 0$ and $\partial v/\partial t = 0$. By doing so, one finds that:

$$f[\rho] + V(z) = \mu\,, \quad \text{for}: \ |z| \le R\,, \tag{4.74}$$

$$\rho(z) = 0\,, \quad \text{for}: \ |z| \ge R\,, \tag{4.75}$$

where μ is the chemical potential fixed by the normalization condition:

$$\int_{-R}^{R} \rho(z)\,dz = N\,, \tag{4.76}$$

and R is the atomic cloud radius given by the condition: $V(R) = \mu$. Let us consider, as an explanatory example, the case of a harmonic trap, *i.e.* $V(z) = m\omega^2 z^2/2$. For this trapping potential, the atomic cloud radius reads:

$$R = \sqrt{\frac{2\mu}{m\omega^2}}\,.$$

Therefore, in the low density (Tonks–Girardeau) limit, from Eq. (4.74) we get:

$$\rho^{\mathrm{TG}}(z) = \sqrt{\frac{2m\mu}{\pi^2\hbar^2} - \left(\frac{m\omega z}{\pi\hbar}\right)^2}\,,$$

and substituting to Eq. (4.76), we get the following expression for the chemical potential:

$$\mu^{\mathrm{TG}} = \hbar\omega N\,. \tag{4.77}$$

Therefore one can finally write the ground state density profile for a trapped Tonks–Girardeau gas as [154]:

$$\rho^{\mathrm{TG}}(z) = \rho_0^{\mathrm{TG}}\sqrt{1 - \frac{z^2}{(R^{\mathrm{TG}})^2}}\,, \tag{4.78}$$

for $|z| \leq R$, while $\rho^{\mathrm{TG}}(|z| \geq R) = 0$, and where:

$$\rho_0^{\mathrm{TG}} = \sqrt{\frac{2m\omega}{\pi^2\hbar}\,N}\,,$$
$$R^{\mathrm{TG}} = \sqrt{2N\,\frac{\hbar}{m\omega}}\,.$$

In the opposite limit, *i.e.* high densities and weak interactions (Thomas–Fermi), the functional $f[\rho]$ is actually linear in the density and proceeding as we did above for the hard–core interactions, one will obtain the so called Thomas–Fermi parabola [236]:

$$\rho^{\mathrm{TF}}(z) = \rho_0^{\mathrm{TF}}\left(1 - \frac{z^2}{(R^{\mathrm{TF}})^2}\right)\,, \tag{4.79}$$

for $|z| \leq R$, while $\rho^{\mathrm{TG}}(|z| \geq R) = 0$, and where:

$$\rho_0^{\mathrm{TF}} = \left[\left(\frac{3m\omega}{8\hbar}\right)^2 N^2\,|a_{1\mathrm{D}}|\right]^{1/3}\,,$$
$$R^{\mathrm{TF}} = \left[\frac{3N}{|a_{1\mathrm{D}}|}\left(\frac{\hbar}{m\omega}\right)^2\right]^{1/3}\,.$$

The chemical potential in the Thomas–Fermi regime reads:

$$\mu^{\mathrm{TF}} = \left(\frac{2\hbar^2}{m\,|a_{1\mathrm{D}}|}\right)\rho_0^{\mathrm{TF}}\,. \tag{4.80}$$

We will compare with these analytical results in the weak and strong interacting regimes for the Lieb–Liniger model.

If we want to find the density profile for a trapped Lieb–Liniger Bose gas with generic (maybe intermediate) interactions, then we should deal with the stationary GGPE, which will read:

$$\mu\psi(z) = -\frac{\hbar^2}{2m}\frac{\partial^2}{\partial z^2}\psi(z) + V(z)\,\psi(z) + \frac{\hbar^2}{2m}\left[3e(\gamma) - \gamma\frac{\partial e}{\partial\gamma}\right]|\psi(z)|^4\,\psi(z)\,, \tag{4.81}$$

where γ is actually $\gamma(z) = c/\,|\psi(z)|^2$, and $V(z)$ is a generic external potential. We find convenient to introduce the effective dimensionless coupling γ_{eff}, defined in [221], in order to have a coupling parameter which does not have a spatial dependence. It is related to the maximum steady state density in the center of the atomic cloud in the Tonks–Girardeau limit, and reads:

$$\gamma_{\text{eff}} = \frac{2}{\rho_0^{\text{TG}}\,|a_{\text{1D}}|}\,. \tag{4.82}$$

The interaction term, which follows from Eq. (4.13), encodes a highly nontrivial nonlinearity in the system, therefore sometimes it renders difficult to reach a fast and reliable convergence of the method used to solve such differential equation. A convenient numerical method for obtaining the ground state density profile solution of the stationary GGPE, is through the imaginary time propagation [237, 238]. The idea is to write the wavefunciton $\psi(z,t)$ as a superposition of eigenstates $\phi_k(x)$, with time–dependent amplitudes $a_k(t)$, and energies E_k, as: $\psi(z,t) = \sum_k a_k(t)\phi_k(z)$, and after passing to imaginary time, one writes the time evolved state as:

$$\psi(z,t+\Delta t) = e^{-\frac{\Delta t}{\hbar}\hat{H}}\,\psi(z,t) = \sum_k a_k(t)\,\phi_k(z)\,e^{-\frac{\Delta t}{\hbar}E_k}\,,$$

where $\hat{H}$ is the quantum Hamiltonian in Eq. (4.81). Since the amplitudes of each eigenstate contribution decays over time, and the ground state characterized by the lowest E_k decaying as the slowest, then the wavefunction will evolve towards the ground state. Notice that one should renormalize ψ at each temporal step, to ensure the conservation of atoms number. In order to check the convergence of this method, one should monitor the "energy potential" behaviour, conveniently defined as:

$$\epsilon(z,t) = \frac{\hbar}{\Delta t}\ln\left|\frac{\psi(z,t)}{\psi(z,t+\Delta t)}\right|\,.$$

Indeed when ϵ is vanishingly small at a certain postion z, it means that:
$\ln|\psi(z,t)/\psi(z,t+\Delta t)| \simeq 0$, therefore: $\psi(z,t) \simeq \psi(z,t+\Delta t)$, and we have reached convergence for this method.

As a final remark for the numerical procedure, once the external potential, number of particles and interaction strength are fixed, in order to compute the time evolution of a certain initial state (which we will take simply to be a gaussian state) $\psi(z,0)$, we rely on the split-step Fourier method [237, 239]. It is based on the fact that the kinetik energy operator and the external potential (and nonlinear interaction) terms are simply multiplication factors in momentum and position space, respectively. Then by conveniently Fourier transforming the wavefunction, one is able to easily compute the action of the Hamiltonian on a generic state (making the approximation that: $[\hat{T},\hat{V}] = 0$) as:

$$\psi(z,t+\Delta t) \simeq e^{-i\frac{\Delta t}{2\hbar}\{V(z)+f[\rho]\}}\cdot\mathcal{F}\left\{e^{-i\frac{\hbar k^2}{2m}\Delta t}\cdot\mathcal{F}\left[e^{-i\frac{\Delta t}{2\hbar}\{V(z)+f[\rho]\}}\cdot\psi(z,t)\right]\right\}\,,$$

where errors of order of $O(\Delta t^3)$ are present, and $\mathcal{F}$ denotes the Fourier transform operation.

With the methods above mentioned, and by using the analytical interpolated expression for the dimensionless ground state energy density in Eq. (1.55), we are able to find the steady state densities for trapped Lieb–Liniger gases with generic interaction strengths and atom numbers. For the case of an harmonic trapping potential, $V(z) = m\omega^2 z^2/2$, using $N = 100$ particles and a time step of: $\omega\Delta t = 10^{-3}$, we find the results reported in Figs. 4.12 – 4.15 for the density profiles at different interactions γ_{eff} (we defined the dimensionless position variable: $z = x\sqrt{\hbar m\omega}$).

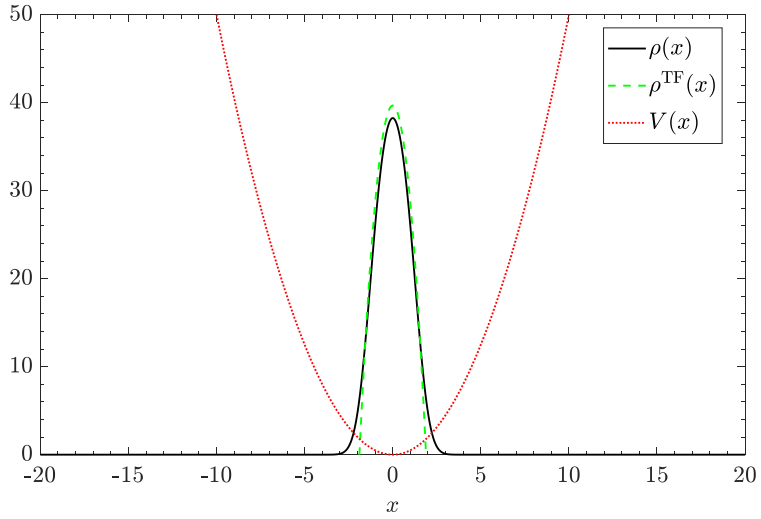

Figure 4.12: Density profile obtained from solving the static GGPE for the LL gas made of $N = 100$ particles with interaction strength $\gamma_{\text{eff}} = 0.01$. In black solid line there is the numerical result, while the green dashed line represents the analytical prediction coming from Thomas–Fermi approximation, *i.e.* Eq. (4.79), and finally in red dotted line there is reported the trapping potential.

Finally in Fig. 4.16 we report the behaviour for the energy per particle functions. They can be written in terms of the steady state wavefunction obtained numerically and read:

$$
\begin{aligned}
E_{\text{ho}} &= \frac{1}{N}\int_{-\infty}^{\infty} \psi(z)^* \left[-\frac{1}{2}\frac{d}{dx} + \frac{x^2}{2}\right]\psi(z)\,, \\
E_{\text{int}} &= \frac{1}{N}\int_{-\infty}^{\infty} \psi(z)^* f[\rho]\psi(z)\,, \\
E_{\text{tot}} &= E_{\text{ho}} + E_{\text{int}}\,,
\end{aligned}
$$

respectively for the kinetik + potential, interaction and total energy. As one would expect, the interaction energy term increases for high values of the effective dimensionless interaction parameter, and it reaches a maximum which can be estimated from using $\rho^{\text{TG}}(z)$ of Eq. (4.78) in the definition of the interaction energy. Notice moreover that the interaction energy term is greater than the kinetik + potential energy term also for very small values of interactions, in particular up to $\gamma_{\text{eff}} = 0.01$.

In principle there is no difficulty in treating the time–dependent problem and solving therefore the GGPE in (4.14) with the split-step Fourier method sketched above. This can range from studying the breathing modes for systems made of many particles and with

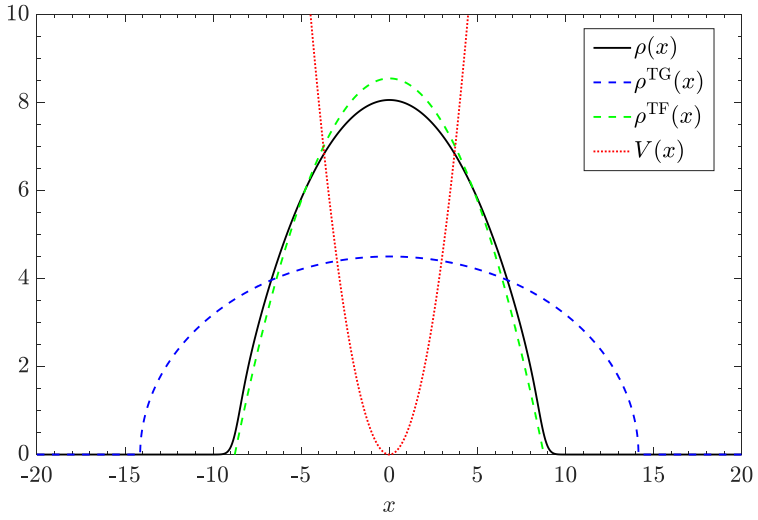

Figure 4.13: Density profile obtained from solving the static GGPE for the LL gas made of $N = 100$ particles with interaction strength $\gamma_{\mathrm{eff}} = 1$. In black solid line there is the numerical result, while the green and blue dashed lines represent the analytical prediction coming from Tonks–Girardeau and Thomas–Fermi approximations, *i.e.* Eqs. (4.78) and (4.79) respectively, and finally in red dotted line there is reported the trapping potential. In the regime of intermediate interactions, the Thomas–Fermi approximation describes more accurately the numerical results.

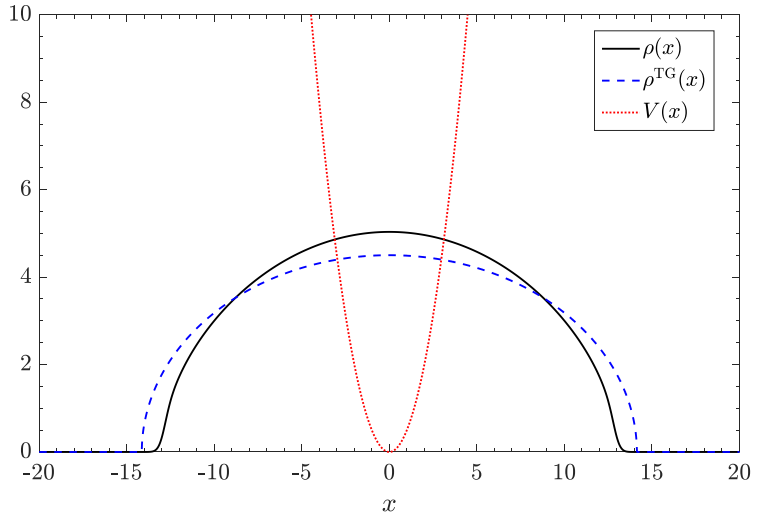

Figure 4.14: Density profile obtained from solving the static GGPE for the LL gas made of $N = 100$ particles with interaction strength $\gamma_{\mathrm{eff}} = 10$. In black solid line there is the numerical result, while the green dashed line represent the analytical prediction coming from Tonks–Girardeau approximation, *i.e.* Eq. (4.78), and finally in red dotted line there is reported the trapping potential. The Tonks–Girardeau approximation is not so bad with respect to the numerical results, even though γ_{eff} is not very high.

different interaction strengths, to characterize the effects that a time varying gravitational potential has on the system. In this Thesis we will not deal with this case, but future works on these directions are certainly of our interest.

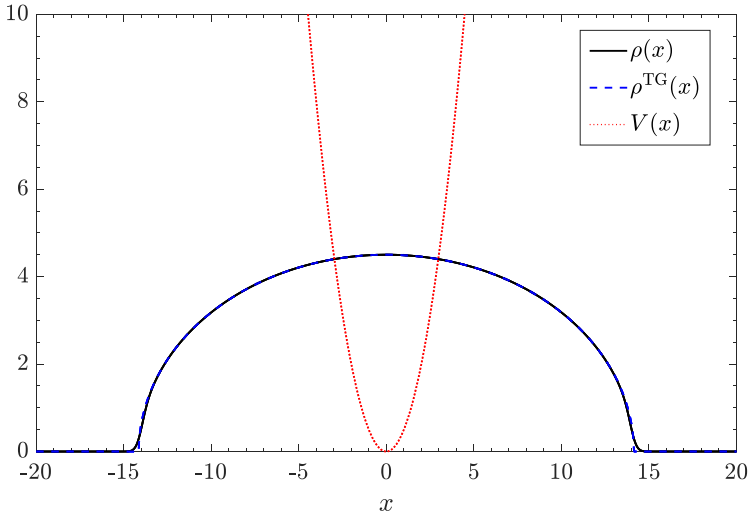

Figure 4.15: Density profile obtained from solving the static GGPE for the LL gas made of $N = 100$ particles with interaction strength $\gamma_{\mathrm{eff}} = 10^5$. In black solid line there is the numerical result, while the green dashed line represent the analytical prediction coming from Tonks–Girardeau approximation, *i.e.* Eq. (4.78), and finally in red dotted line there is reported the trapping potential. In this case the Tonks–Girardeau approximation excellently describes the numerical results.

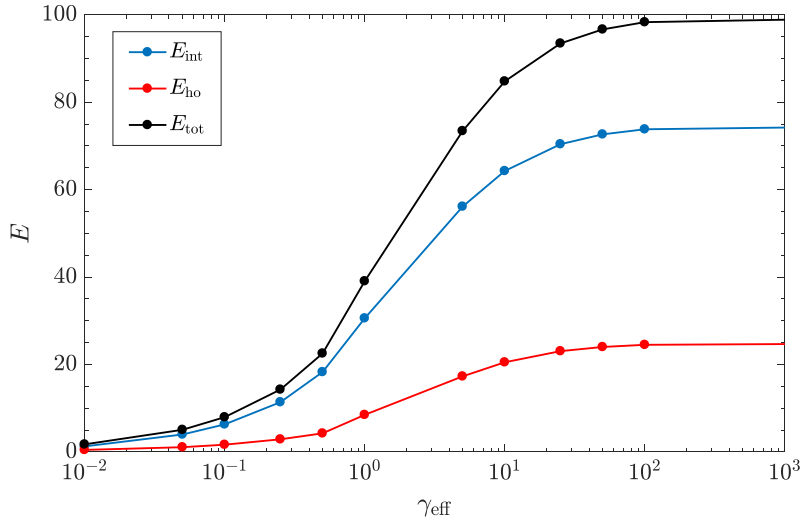

Figure 4.16: Linear-log scale of the values of the kinetik + potential, interaction and total energy per particle of a system of harmonically trapped $N = 100$ Lieb–Liniger bosons. For growing values of the interaction parameter γ_{eff}, the interaction energy increases, as we would expect, reaching a maximum finite value in the Tonk–Girardeau limit.

Nevertheless there exist exactly solvable time–dependent problems with many–body quantum systems subjected to an external potential. The case where the one–dimensional system is under the action of a time varying electric or gravitational field, is one important example. Next we will deal with this problem, extending the study also to the three–dimensional free fall of a quantum system.

APPENDIX

4.A PROOF OF EQ. (4.7).

Hereafter the one–dimensional system is assumed to have length L while the temperature is kept at $T = 0$, so that no thermal fluctuations are considered. We will generally refer to the "ground state" instead of the "condensate state", since for a $D = 1$ homogeneous system there is no condensation even at $T = 0$ as we saw from the behaviour of $\mathcal{C}_0(T = 0)$.

Let us assume that our physical system obeys the following time-dependent GGPE:

$$i\hbar\dot{\psi} = \Big(\hat{T} + V + f[\rho]\Big)\,\psi\,, \tag{A4.1}$$

where $\psi = \psi(x,t) = \sqrt{\rho(x,t)}e^{iS(x,t)}$, is the macroscopic wavefunction describing the ground state, while ρ and S being the density and phase distribution of the ground state, $\hat{T} = -(\hbar^2/2m)\,\mathrm{d}^2/\mathrm{d}x^2$ is the kinetik energy term, $V = V(x,t)$ is the potential acting on the wavefunction (which, in general, may depend on position and time) and finally $f[\rho]$ is a generic nonlinear function of the density which encodes the interaction energy term. This term could represent in a mean-field sense *any* complicated interaction potential between the particles. It is important to note that we are not assuming any restriction on the type and the strength of the interaction. At any fixed time t the wavefunction is normalized to N atoms, i.e.,

$$\int_0^L |\psi(x,t)|^2\,dx = N\,. \tag{A4.2}$$

The energy functional is assumed to be

$$\begin{aligned} E[\psi] &= \int_0^L \psi^*(x,t)\Big(T + V + \mathcal{E}[\rho]\Big)\psi(x,t)\,dx = \\ &= E_{\mathrm{kin}} + E_{\mathrm{pot}} + E_{\mathrm{int}}\,, \end{aligned} \tag{A4.3}$$

where $\mathcal{E}[\rho]$ is a function of the density whose physical meaning will be shown in the following to be that of the *free* interacting ground state energy *per particle*. Providing that the potential V is independent of time, then the energy $E = E_{\mathrm{kin}} + E_{\mathrm{pot}} + E_{\mathrm{int}}$, is conserved during the time evolution of the ground state.

We now want to prove:

$$f[\rho] = \mathcal{E}[\rho] + \rho\frac{\delta\mathcal{E}}{\delta\rho}[\rho]\,. \tag{A4.4}$$

To prove Eq. (A4.4), we just need to get the dynamics equation of motion by using: $i\hbar\dot{\psi}(x) = \frac{\delta E[\psi]}{\delta\psi^*(x)}$, and it reads:

$$\begin{aligned}\frac{\delta E[\psi]}{\delta\psi^*(x)} &= \int_0^L \mathrm{d}y\, \frac{\delta\psi^*(y)}{\delta\psi^*(x)}\Big[\hat{T}_y + V(y) + \mathcal{E}[\rho(y)]\Big]\psi(y) + \int_0^L \mathrm{d}y\, \psi^*(y)\frac{\delta\mathcal{E}[\rho(y)]}{\delta\rho(y)}\frac{\delta\rho(y)}{\delta\psi^*(x)}\psi(y) \\ &= \int_0^L \mathrm{d}y\, \delta(y-x)\Big[\hat{T}_y + V(y) + \mathcal{E}[\rho(y)]\Big]\psi(y) + \int_0^L \mathrm{d}y\, \delta(y-x)\,\frac{\delta\mathcal{E}[\rho(y)]}{\delta\rho(y)}\rho(y)\psi(y) = \\ &= \Big[\hat{T}_x + V(x) + \mathcal{E}[\rho(x)]\Big]\psi(x) + \frac{\delta\mathcal{E}[\rho(x)]}{\delta\rho(x)}\rho(x)\psi(x) \\ &= \hat{T}\psi(x) + V(x)\psi(x) + \left[\mathcal{E}[\rho] + \rho\frac{\delta\mathcal{E}[\rho]}{\delta\rho}\right]\psi(x).\end{aligned}$$

Thus, we see that the generic nonlinearity of the GGPE assumes indeed the form in Eq. (A4.4).

Now let us discuss more about the meaning of the function $\mathcal{E}(\rho)$: Suppose that the system is homogeneous, $V(x) = 0$ in Eq. (A4.1), so that the stationary solution (i.e. the ground state) is uniform and the wavefunction is a real constant, $\psi = \psi_0 = \sqrt{\rho_0}$, where $\rho_0 = N/L$. Since in this case ρ_0 is constant everywhere, it follows from Eq. (A4.3), that $E_{\mathrm{kin}} = 0$, and the energy integral is easily calculated as:

$$\begin{aligned}E[\psi_0] &= \int_0^L \rho_0\,\mathcal{E}[\rho_0]\,\mathrm{d}x = \\ &= L\,\rho_0\,\mathcal{E}[\rho_0] = \\ &= N\,\mathcal{E}[\rho_0]\,,\end{aligned} \tag{A4.5}$$

from which follows:

$$\frac{E[\psi_0]}{N} \equiv \mathcal{E}[\rho_0]. \tag{A4.6}$$

Therefore have shown that the energy of the homogeneous ground state per particle is given by the function $\mathcal{E}$.

4.B SOUND VELOCITY

In this Appendix, we will study the velocity of sound for a system described by the time-dependent generalized Gross–Pitakeskii equation:

$$i\hbar\frac{\partial}{\partial t}\psi(z,t) = -\frac{\hbar^2}{2m}\frac{\partial^2}{\partial z^2}\psi(z,t) + f[\rho(z,t)]\,\psi(z,t)\,. \tag{B4.1}$$

Writing ψ as: $\psi(z,t) = \phi(z,t)e^{-\frac{i}{\hbar}\mu t}$ we have that Eq. (B4.1) can be rewritten as:

$$i\hbar\frac{\partial}{\partial t}\phi(z,t) + \mu\phi(z,t) = -\frac{\hbar^2}{2m}\frac{\partial^2}{\partial z^2}\phi(z,t) + f[|\phi(z,t)|^2]\,\phi(z,t)\,. \tag{B4.2}$$

In order to compute the sound velocity, s, we will need the expression of the spectrum of the fluctuations around the mean-field (MF). At the MF, we have that:

$$\phi(z,t) = \phi_0\,,$$

with ϕ_0 homogenous, constant in time and assumed to be real, without losing generality. At the MF, we have that Eq. (B4.2) gives an expression for the chemical potential of the system:

$$\mu\phi_0 = f[\phi_0^2]\,\phi^0 \;\rightarrow\; \mu = f[\phi_0^2]\,. \tag{B4.3}$$

Let us now include the fluctuations namely by writing:

$$\phi(z,t) = \phi_0 + \chi(z,t)\,,$$

where $\chi(z,t)$ is the fluctuation field. Up to the linear order in χ, Eq. (B4.2) reads:

$$i\hbar\frac{\partial}{\partial t}\chi(z,t) = -\frac{\hbar^2}{2m}\frac{\partial^2}{\partial z^2}\chi(z,t) + \left.\frac{\delta f}{\delta\phi^2}\right|_{\phi^2=\phi_0^2}\phi_0^2\,\left[\chi(z,t)+\chi^*(z,t)\right]\,, \tag{B4.4}$$

where we used Eq. (B4.3). From now on we will write, for simplicity:

$$\bar{f}_0 = \left.\frac{\delta f}{\delta\phi^2}\right|_{\phi^2=\phi_0^2}\,.$$

Then Eq. (B4.4), along with its complex conjugate, reads:

$$\begin{aligned} i\hbar\frac{\partial}{\partial t}\chi(z,t) &= -\frac{\hbar^2}{2m}\frac{\partial^2}{\partial z^2}\chi(z,t) + \bar{f}_0\phi_0^2\,\left[\chi(z,t)+\chi^*(z,t)\right]\,,\\ i\hbar\frac{\partial}{\partial t}\chi(z,t)^* &= -\frac{\hbar^2}{2m}\frac{\partial^2}{\partial z^2}\chi^*(z,t) + \bar{f}_0\phi_0^2\,\left[\chi(z,t)^*+\chi(z,t)\right]\,. \end{aligned}$$

Let us now define the Fourier transform of the fluctuation field as:

$$\chi(z,t) = \sum_q e^{-i\omega t}\tilde{\chi}_q e^{iqz}\,,$$

where q is the wave-number and ω is the angular velocity. We therefore have that:

$$\left(\hbar\omega - \frac{\hbar^2q^2}{2m} - \bar{f}_0\phi_0^2\right)e^{-i\omega t}\tilde{\chi}_q - \bar{f}_0 e^{i\omega t}\tilde{\chi}^*_{-q} = 0\,, \tag{B4.5}$$

$$\left(-\hbar\omega - \frac{\hbar^2q^2}{2m} - \bar{f}_0\phi_0^2\right)e^{-i\omega t}\tilde{\chi}^*_{-q} - \bar{f}_0 e^{i\omega t}\tilde{\chi}_q = 0\,. \tag{B4.6}$$

These equations admit a solution when the determinant of the associated matrix is zero, i.e.:

$$\hbar^2\omega^2 = \frac{\hbar^4q^4}{4m^2} + 2\bar{f}_0\phi_0^2\,\frac{\hbar^2q^2}{2m}\,,$$

which gives the expression of the spectrum:

$$\epsilon_q = \hbar\omega = \sqrt{\frac{\hbar^2q^2}{2m}\left(\frac{\hbar^2q^2}{2m} + 2\bar{f}_0\phi_0^2\right)}\,. \tag{B4.7}$$

The sound velocity can now be obtained by using its usual definition:

$$\hbar s = \lim_{q\to 0}\frac{\partial\epsilon_q}{\partial q}\,,$$

which gives:

$$s = \frac{\sqrt{\bar{f}_0}\phi_0}{\sqrt{m}}\,. \tag{B4.8}$$

In the case of the Lieb–Liniger model (see Sections 2.1 and 2.2), we have that:

$$f[\rho] = \frac{\hbar^2}{2m}\left[3e(\gamma) - \gamma\frac{\partial e}{\partial \gamma}\right]\rho^2\,, \tag{B4.9}$$

where the dimensionless coupling reads $\gamma = \frac{c}{\rho}$. At the MF, we have that:

$$f[\phi_0^2] = \frac{\hbar^2}{2m}\left[3e(\gamma_0) - \gamma_0 e'(\gamma_0)\right]\phi_0^4\,, \tag{B4.10}$$

with:

$$\gamma_0 = \frac{c}{\phi_0^2}\,.$$

This implies that $\bar{f}_0$ is equal to:

$$\bar{f}_0 = \frac{\hbar^2}{m}\left[3e(\gamma_0) - 2\gamma_0 e^{'}(\gamma_0) + \frac{1}{2}\gamma_0^2 e^{''}(\gamma_0)\right]\phi_0^4\,.$$

Therefore, from Eq. (B4.8), we can finally write the sound velocity for the Lieb–Liniger gas as:

$$s = \frac{\hbar}{m}\sqrt{3e(\gamma_0) - 2\gamma_0 e'(\gamma_0) + \frac{1}{2}\gamma_0^2 e''(\gamma_0)}\phi_0^2\,, \tag{B4.11}$$

which indeed agrees with the result in [53].

5

QUANTUM MANY–BODY SYSTEMS SUBJECTED TO A LINEAR POTENTIAL

Floquet theory is a powerful tool to study differential equations whose coefficients are time–periodic functions [50] and, for this reason, it is widely used in Quantum Mechanics in presence of a time–periodic Hamiltonian [51, 52]. If the system is initially in state $\chi(t=0)$ and subjected to a periodic driving, then the Floquet Hamiltonian H_F is the operator that formally gives the state of the system at multiples of the period T:

$$\chi(t=nT) = e^{-i\frac{nT}{\hbar}H_F}\,\chi(t=0)\,. \tag{5.1}$$

H_F depends on the parameters of the original driven Hamiltonian, H, and of course on the time–dependent perturbation. The eigenvalues of the Floquet Hamiltonian are the *quasi-energies* $\mathcal{E}_F$. Often referred as Floquet engineering [33, 49], time–periodic driving allows to construct interesting effective H_F with novel physical properties as, for instance, dynamic localization effects [25], suppression of inter–well tunneling in a Bose condensate subjected to a strongly driven optical lattice [26–32] (see [33] for more references), topological Floquet phases [34, 35], time crystals [36–43], dynamics in driven systems [44–46] and Floquet prethermalization [47, 48].

Within this framework, a natural question is whether one can have an integrable nontrivial Floquet Hamiltonian perturbing an interacting model with a time–periodic perturbation. Despite exactly solvable time–dependent Hamiltonians can be constructed [54, 55], the problem of finding an integrable Floquet Hamiltonian H_F from undriven interacting (possibly integrable) Hamiltonian H is in general a challenging one. A discussion of integrable Floquet systems not exhibiting chaotic behaviour even under a time-dependent perturbation is presented in [240]. Here our scope is to present explicitly an interacting many-body bosonic system whose Floquet Hamiltonian is integrable and therefore exactly solvable by means of integrability techniques [58, 59]. This implies, in particular, that we can have access to the exact spectrum of the quasi-energies and also to the wavefunctions of the system at stroboscopic times (multiples of the period of the driving). It is useful to stress that one of the difficulties in identifying integrable Floquet Hamiltonians is that the integrability of these Hamiltonians is not at all guaranteed by the integrability of the original time-independent undriven model (see, for instance, [56] where starting from the original BCS model the corresponding BCS gap equation in presence of a periodic driving is derived and solved numerically).

The external perturbation that we are going to apply to the system is the one with a potential of the form:

$$V(x,t) = f(t)\,x\ , \tag{5.2}$$

with a driving function $f(t)$ that can have a generic dependence on time, but in order to apply the Floquet approach, it has to be such that: $f(t) = f(t+T)$, with T the period.

The original time–independent system that we consider in the following is the Lieb–Liniger (LL) model, but our methods can be applied to any quantum systems. Interestingly enough, if the original undriven quantum model is integrable, then it remains exactly solvable also when it is perturbed by an external time–periodic potential *linear* in the coordinates x_i of the particles, as it happens for the classical counterpart of the LL model given by the non–linear Schrödinger equation which remains solvable also in presence of an external linear time–dependent potential [241–243]. Moreover we will see that the Floquet Hamiltonian of an integrable model driven with a periodic linear potential such that the condition:

$$\int_0^T f(\tau)\, d\tau = 0 \ , \tag{5.3}$$

holds, is itself an integrable Hamiltonian. Our system is then the quantum analog of a classical mechanics problem consisting of a body (subjected to the gravitational force) put on a slide which changes periodically its slope by rotating around a pin posed at the origin.

We remark that we are referring to the integrability of the Floquet Hamiltonian of the system, which is a time–independent Hamiltonian and therefore by *integrable* we mean that there exist an infinite number of conserved charges and hence one can find an exact solution for the stroboscopic time–independent problem. In particular the integrability of the Floquet Hamiltonian allows to find the eigenfunctions of $\hat{H}_F$ and to write the behaviour of a generic wavepacket at stroboscopic times.

The evolution of the state at intermediate times instead is determined by the *micro-motion operator* $\hat{U}_F(t,0)$, defined as:

$$\hat{U}(t,0) = \hat{U}_F(t,0)\, e^{-i\frac{t}{\hbar}\hat{H}_F} \ , \tag{5.4}$$

in terms of the time evolution operator of the system $\hat{U}(t,0)$. *Floquet states* $|\psi_F(t)\rangle$, can then be obtained from the action of the micro-motion operator on the eigenstates of the Floquet Hamiltonian. Floquet states form a complete and orthonormal set of functions and therefore any solution of the original time–dependent Schrödinger equation can be written in terms of those as:

$$\chi(t) = \int dk\, A(k)\ |\psi_F(t)\rangle \ ,$$

where k is a momentum variable, related to the energy of the system ($k \propto \sqrt{E}$), and the $A(k)$'s are time–independent coefficients. It is therefore desirable to obtain $\hat{H}_F$ and $\hat{U}_F(t,0)$, in order to have access to the full quantum dynamics of the system.

In the following we present a detailed analysis of all these aspects of the problem and, in particular, we show how to extract the time evolution of generic wavefunctions at all times by first computing the micro-motion operators and then the Floquet states, with which we can expand the wavefunction. After discussing a general two-body interaction term, we focus on the paradigmatic and experimentally relevant case of the Lieb–Liniger model.

5.1 ONE-BODY PROBLEM

5.1.1 GENERIC DRIVING FUNCTION

Let us consider the one–dimensional Schrödinger equation for a particle of mass m in a linear potential with a time varying strength:

$$i\hbar\frac{\partial\chi}{\partial t} = -\frac{\hbar^2}{2m}\frac{\partial^2\chi}{\partial x^2} + x\, f(t)\,\chi(x,t)\,. \tag{5.5}$$

In what follows, $f(t)$ is a generic driving function that will be taken to be periodic at the end of this Section. In the literature, Eq. (5.5) has been studied and solved in different ways [244–247]. Here we solve it with a method that will be particularly useful to study the Floquet dynamics.

The key point of the solution of Eq. (5.5) is to perform a gauge transformation on the wavefunction

$$\chi(x,t) = e^{i\theta(x,t)}\,\eta(y(t),t)\,, \tag{5.6}$$

where $y(t) = x - \xi(t)$, while $\xi(t)$ and $\theta(x,t)$ are two functions that are determined below. Substituting Eq. (5.6) into (5.5), and imposing:

$$\frac{d\xi}{dt} = \frac{\hbar}{m}\frac{\partial\theta}{\partial x}\,, \tag{5.7}$$

and

$$-\hbar\frac{\partial\theta}{\partial t} = \frac{\hbar^2}{2m}\left(\frac{\partial\theta}{\partial x}\right)^2 + xf(t)\,, \tag{5.8}$$

we find that $\eta(y,t)$ satisfies the Schrödinger equation with no external potential in the spatial variable y:

$$i\hbar\frac{\partial\eta}{\partial t} = -\frac{\hbar^2}{2m}\frac{\partial^2\eta}{\partial y^2}\,. \tag{5.9}$$

Hence, once $\theta(x,t)$ is known, $\eta(y,t)$ will be readily determined from the free dynamics. To find the gauge phase $\theta(x,t)$ we make the ansatz:

$$\theta(x,t) = \frac{m}{\hbar}\frac{d\xi}{dt}\,x + \Gamma(t)\,, \tag{5.10}$$

that leads to the conditions:

$$m\frac{d^2\xi}{dt^2} = -f(t)\,, \qquad \hbar\frac{d\Gamma}{dt} = -\frac{m}{2}\left(\frac{d\xi}{dt}\right)^2\,, \tag{5.11}$$

which give the translational parameter $\xi(t)$ and the function $\Gamma(t)$ in terms of $f(t)$. Notice that the equation for $\xi(t)$ is the Newton's second law equation of motion, where $d^2\xi/dt^2$ represents the acceleration of the center of mass of the system, and $-f(t)$ the driving force.

Solving the equations (5.11), with the initial conditions $\xi(0) = d\xi(0)/dt = 0$ and $\Gamma(0) = 0$, we get:

$$\theta(x,t) = -\frac{x}{\hbar}\int_0^t f(\tau)\,d\tau - \frac{1}{2\,m\,\hbar}\int_0^t d\tau\left[\int_0^\tau f(\tau')\,d\tau'\right]^2\,, \tag{5.12}$$

which, together with Eq. (5.6) and Eq. (5.9), completely solves Eq. (5.5).

Since: $\theta(x,0)=0$ and $y(0)=x$, we have from Eq. (5.6) that:

$$\chi(x,0)=\eta(x,0)\,, \tag{5.13}$$

for which the solution of the Schrödinger equation (5.5) reads:

$$\chi(x,t)\;=\;e^{i\theta(x,t)}e^{-i\frac{t}{\hbar}\frac{\hat{p}^2}{2m}}\,\eta(y,0)\;=\;e^{i\theta(x,t)}e^{-i\frac{t}{\hbar}\frac{\hat{p}^2}{2m}}e^{-i\frac{\xi(t)}{\hbar}\hat{p}}\,\chi(x,0)\,, \tag{5.14}$$

where we have used the definition of the translation operator and the free time evolution operator. Notice that no boundary conditions in the wavefunction have been considered in the above calculations *i.e.* $x\in\mathbb{R}$.

In terms of the solution (5.14), one can easily compute the expectation values of various physical quantities, such as momentum, position as well as their variances. Assuming as initial values $\langle\hat{x}\rangle\,(t=0)=x_0$, and $\langle\hat{p}\rangle\,(t=0)=p_0$, and using the canonical commutation relations among different powers of position and momentum operators, we have:

$$\langle\hat{x}\rangle\,(t)\equiv\langle\chi(x,t)\,|\hat{x}|\,\chi(x,t)\rangle=x_0+\frac{t}{m}p_0+\xi(t)\,. \tag{5.15}$$

This means that the mean position of a generic wavepacket, under the action of a linear time–dependent potential, is governed by the parameter $\xi(t)$ which is readily determined by Eq. (5.11). Moreover, concerning the expectation value of the momentum we have:

$$\langle\hat{p}\rangle\,(t)\equiv\langle\chi(x,t)\,|\hat{p}|\,\chi(x,t)\rangle\;=\;p_0-\int_0^t f(\tau)\,d\tau\,, \tag{5.16}$$

meaning that the value of the momentum is shifted away from its initial value by a term that depends on the driving function $f(t)$. As expected, the motion of the center of the wavepacket in Eq. (5.15) is the same of a classical particle moving in one dimension under the action of a time–dependent gravitational force. Concerning the variance of the position, we have:

$$\Delta x(t)\equiv\sqrt{\langle\hat{x}^2\rangle\,(t)-\langle\hat{x}\rangle^2\,(t)}=\Delta x_{\text{undriven}}(t)\,, \tag{5.17}$$

where the subscript "undriven" stands for the undriven evolution of the variance, which is calculated using the wavefunction $\eta(x,t)$ instead of $\chi(x,t)$, *i.e.*

$$\Delta x_{\text{undriven}}(t)\equiv\sqrt{\langle\eta(x,t)\,|\hat{x}^2|\,\eta(x,t)\rangle-\langle\eta(x,t)\,|\hat{x}|\,\eta(x,t)\rangle^2}\,. \tag{5.18}$$

For the variance of the momentum we have:

$$\Delta p(t)\equiv\sqrt{\langle\hat{p}^2\rangle\,(t)-\langle\hat{p}\rangle^2\,(t)}=\Delta p_{\text{undriven}}(t)\,. \tag{5.19}$$

This means that it remains constant and equal to its initial value at $t=0$.

The solution presented so far, and its consequences, are valid for any driving function. In the sequel, as a preparation for later Sections, we shall focus our attention on periodic drivings.

5.1.2 FLOQUET APPROACH

When $f(t)$ is periodic with period T, the Schrödinger equation (5.5) becomes a differential equation with periodic coefficients where we can apply the Floquet theory. This leads us to define the Floquet Hamiltonian $\hat{H}_F$, which, according to Eq. (5.1), controls the time evolution of the wavefunction at stroboscopic times $t = nT$, with $n \in \mathbb{N}$. Switching for simplicity to the bra-ket notation, Eq. (5.1) reads:

$$|\chi(nT)\rangle = e^{-i\frac{nT}{\hbar}\hat{H}_F}\ |\chi(t=0)\rangle\ . \tag{5.20}$$

The eigenvalues of the Floquet Hamiltonian will be denoted by $\mathcal{E}_F$ and are known as the quasi-energies. Since $\hat{H}_F$ is hermitian, they are real numbers. The quasi-energies are the time–like analogues of the quasi-momenta in the study of crystalline solids. Let $\hat{U}(t,0) = e^{-i\frac{t}{\hbar}\hat{H}}$ be the time evolution operator, i.e. the quantum operator that, when applied to a wavefunction describes its evolution from time 0 to time t. According to the Floquet theory and the notation of [33], we can decompose $\hat{U}(t,0)$ as in Eq. (5.4): $\hat{U}(t,0) = \hat{U}_F(t,0)\, e^{-i\frac{t}{\hbar}\hat{H}_F}$. This relation defines the micro-motion operator $\hat{U}_F(t,0)$ in terms of the Floquet Hamiltonian $\hat{H}_F$ and $\hat{U}(t,0)$. $\hat{U}_F$ is periodic in time and equals to the unity at every stroboscopic times, implying that $\hat{U}(nT,0) = e^{-i\frac{nT}{\hbar}\hat{H}_F}$. Therefore $\hat{U}(t+T,0) = \hat{U}(t,0)\hat{U}(T,0)$. This means that it is enough to know the evolution operator for times $t \in [0,T]$ in order to obtain the evolution of the system at all times $t \geq 0$.

The importance of these concepts becomes clear once one realises that any solution of the time–dependent periodic Schrödinger equation (5.5) can be expressed in terms of the Floquet operator and their eigenfunctions. Indeed, writing the eigenvalue equation for the Floquet Hamiltonian:

$$\hat{H}_F\,|\tilde{u}\rangle = \mathcal{E}_F\,|\tilde{u}\rangle\ , \tag{5.21}$$

one can apply the micro-motion operator on the wavefunctions $|\tilde{u}\rangle$ to write the Floquet modes (or Floquet functions according to the notation of [45]) as:

$$|u(t)\rangle = \hat{U}_F(t,0)\,|\tilde{u}\rangle\ , \tag{5.22}$$

which are time–periodic states, as follows from the properties of the micro-motion operator stated above. It is now straightforward to construct the Floquet states, which are solutions of the time–dependent Schrödinger equation (5.5) with periodic $f(t)$:

$$|\psi_F(t)\rangle = |u(t)\rangle\, e^{-i\frac{t}{\hbar}\mathcal{E}_F}\ . \tag{5.23}$$

These states form a complete and orthonormal set of eigenfunctions of the time evolution operator over a driving period:

$$|\psi_F(t+T)\rangle = \hat{U}(t+T,t)\,|\psi_F(t)\rangle = e^{-i\frac{T}{\hbar}\mathcal{E}_F}\,|\psi_F(t)\rangle\ .$$

Hence, any solution of the Schrödinger equation (5.5) can be written as a superposition of Floquet states as:

$$|\chi(t)\rangle\ =\ \int A(k)\,|u(t)\rangle\, e^{-i\frac{t}{\hbar}\mathcal{E}_F}\,dk\ =\ \int A(k)\,|\psi_F(t)\rangle\ dk\,, \tag{5.24}$$

weighted with time–independent coefficients A, which depend on the momenta of the particle k. Looking at the last expression, notice that the Floquet states have an occupation probabilities $|A|^2$ (preserved in time) and a phase factor $e^{-i\frac{t}{\hbar}\mathcal{E}_F}$, resembling the

usual factor $e^{-i\frac{t}{\hbar}E}$ present in any time–evolution of energy eigenstates with eigenvalues E when their Hamiltonian does not depend on time. Therefore the quasi-energies look as if they were effective energies and these are the quantities which determine the linear phase evolution of the system. Finally, notice that if the system is prepared in a Floquet state, its time evolution is periodic in time and in this case it is called a "quasi-stationary evolution".

Before obtaining an expression for the micro-motion operator $\hat{U}_F$ from Eq. (5.4), it is convenient first to derive an expression for the Floquet Hamiltonian $\hat{H}_F$ of the system which will be useful in the many-body case. To get an equation for $\hat{H}_F$ we need to rewrite Eq. (5.14) for $t = nT$ in a single exponential operator as in Eq. (5.20). To do this, we can use the Baker-Campbell-Hausdorff formula between momentum and position exponential operators, arriving at:

$$\begin{aligned}\hat{H}_F &= \frac{\hat{p}^2}{2m} + \left[\frac{\xi(nT)}{nT} + \frac{1}{2m}\int_0^{nT} f(\tau)\,d\tau\right]\hat{p} - \hbar\frac{\theta(x,nT)}{nT} + \\ &\quad -\frac{1}{2mnT}\left[\int_0^{nT} f(\tau)\,d\tau\right]\cdot\int_0^{nT} d\tau\left[\int_0^{\tau} f(\tau')\,d\tau'\right] + \frac{1}{12m}\left[\int_0^{nT} f(\tau)\,d\tau\right]^2 .\end{aligned} \tag{5.25}$$

From this expression one is tempted to say that the translation of the center of mass of the wavepacket at different stroboscopic times, would be $\frac{\xi(nT)}{nT} + \frac{1}{2m}\int_0^{nT} f(\tau)\,d\tau$, since this is the factor that multiplies the operator $\hat{p}$. However, this is not true since to evaluate $\langle\chi(x,nT)|\hat{x}|\chi(x,nT)\rangle$, one has to split the operators in the exponential recovering the state Eq. (5.14), where the translation factor is simply $\frac{\xi(nT)}{nT}$. Notice that one could consider periodic boundary conditions requiring that the periodic driving function satisfies the two conditions $f(nT) = 0$, for $n \in \mathbb{N}$, and $\int_0^T f(t)\,dt = 0$, as discussed in Appendix 5.5.B.

Moreover, it is not manifest from Eq. (5.25) that the Floquet Hamiltonian is independent of n, as it should be the case [33]. To clarify this issue we study in more detail the translational parameter and the gauge phase. From the first equation in (5.11), we derive:

$$\xi(t) = -\frac{1}{m}\int_0^t d\tau\left[\int_0^{\tau} f(\tau')\,d\tau'\right], \tag{5.26}$$

from which follows that:

$$\xi(t+T) = \xi(T) + \xi(t) - \frac{t}{m}\int_0^T f(\tau)\,d\tau\,. \tag{5.27}$$

In a similar way, one gets for the gauge phase:

$$\begin{aligned}\theta(x,t+T) = \theta(x,T) + \theta(x,t) - \frac{t}{2m\hbar}\left[\int_0^T f(\tau)\,d\tau\right]^2 + \\ -\frac{1}{m\hbar}\left[\int_0^T f(\tau)\,d\tau\right]\cdot\int_0^t d\tau\left[\int_0^{\tau} f(\tau')\,d\tau'\right].\end{aligned} \tag{5.28}$$

Setting $t = nT$, with $n \in \mathbb{N}$, in the above equations yields:

$$\xi(nT) = n\xi(T) - \frac{T}{m}\frac{n(n-1)}{2}\int_0^T f(\tau)\,d\tau\,, \tag{5.29}$$

and:

$$\theta(x,nT) = n\theta(x,T) - \frac{T}{2m\hbar}\frac{n(n-1)}{2}\left[\int_0^T f(\tau)\,d\tau\right]^2 + \\ -\frac{1}{m\hbar}\frac{n(n-1)(2n-1)}{6}\left[\int_0^T f(\tau)\,d\tau\right]\cdot\int_0^T d\tau\left[\int_0^\tau f(\tau')\,d\tau'\right]. \tag{5.30}$$

To continue with the proof of the n-independence of the Floquet Hamiltonian, we split the analysis in two cases: (1) when the integral of the driving function over one period vanishes, and (2) when it does not.

$\int_0^t f(t)\,dt = 0$

When the integral on a time–period is vanishing, from Eq. (5.29) we have $\xi(nT) = n\xi(T)$ and therefore the term linear in momentum of the Floquet Hamiltonian in (5.25) is n-independent. Moreover, since $\xi(nT)$ is linear in terms of the stroboscopic factor n, the stroboscopic motion of the wavepacket has a constant velocity, as can be inferred from Eq. (5.15). The constant term in the Floquet Hamiltonian is also trivially n-independent since $\theta(x,nT) = n\theta(x,T)$, as follows from Eq. (5.30). Hence, in this case the Floquet Hamiltonian can be simply written as:

$$\hat{H}_F = \frac{\hat{p}^2}{2m} + \frac{\xi(T)}{T}\hat{p} - \hbar\,\frac{\theta(T)}{T}\,, \tag{5.31}$$

where $\theta(x,T) \equiv \theta(T)$, since the gauge phase is x-independent (in the considered case of: $\int_0^T f(t)\,dt = 0$), as one can see from Eq. (5.12). Moreover, the Floquet Hamiltonian can be rewritten as:

$$\hat{H}_F = \frac{\hat{p}^2}{2m} - \frac{\hat{p}}{m}\frac{1}{T}\int_0^T d\tau\int_0^\tau f(\tau')\,d\tau' + \frac{1}{2m}\frac{1}{T}\int_0^T d\tau\left[\int_0^\tau f(\tau')\,d\tau'\right]^2.$$

Notice that we can also express the Hamiltonian in Eq. (5.31) as:

$$\hat{H}_F = \frac{[\hat{p} + m\xi(T)/T]^2}{2m} + C\,, \tag{5.32}$$

where $C = -\hbar\theta(T)/T - (m/2)[\xi(T)/T]^2$. Now, applying the unitary transformation

$$\hat{\tilde{H}}_F \equiv e^{ia\hat{x}/\hbar}\hat{H}_F e^{-ia\hat{x}/\hbar}\,, \tag{5.33}$$

with $a = m\xi(T)/T$, we get finally:

$$\hat{\tilde{H}}_F = \frac{\hat{p}^2}{2m} + C\,. \tag{5.34}$$

Using these results we can derive the micro-motion operator $\hat{U}_F$. First of all, from Eq. (5.14), the time evolution operator is:

$$\hat{U}(t,0) = e^{i\theta(x,t)}e^{-i\frac{t}{\hbar}\frac{\hat{p}^2}{2m}}e^{-i\frac{\xi(t)}{\hbar}\hat{p}}\,. \tag{5.35}$$

Hence, inverting Eq. (5.4) and knowing the Floquet Hamiltonian from Eq. (5.31), we get:

$$\hat{U}_F(t,0) = e^{\frac{i}{\hbar}t\left\{\left[\frac{\xi(T)}{T}-\frac{\xi(t)}{t}\right]\hat{p} - \hbar\left[\frac{\theta(T)}{T}-\frac{\theta(x,t)}{t}\right] + \frac{1}{2}\left[\int_0^t f(\tau)\,d\tau\right]\cdot\left[\frac{\xi(T)}{T}-\frac{\xi(t)}{t}\right]\right\}}\,, \tag{5.36}$$

where we used the Baker-Campbell-Hausdorff formula. An alternative expression of the micro-motion operator is:

$$\hat{U}_F(t,0) = e^{it\left[\frac{\theta(x,t)}{t} - \frac{\theta(T)}{T}\right]} e^{\frac{i}{\hbar}t\left[\frac{\xi(T)}{T} - \frac{\xi(t)}{t}\right]\hat{p}}, \tag{5.37}$$

which has been derived using the Zassenhaus formula.

Let discuss a simple, yet instructive, application of these results. Imagine we are interested in describing the time evolution of a Gaussian wavepacket with initial variance σ in the infinite homogeneous space, *i.e.* $\chi(x,0) = \frac{1}{\sqrt[4]{2\pi\sigma^2}} e^{-x^2/(2\sigma)^2}$. As we saw in the previous Section, in order to determine its time evolution, we have first to find the eigenvalues and eigenfunctions of the Floquet Hamiltonian in (5.31). In this case the complete set of eigenfunctions is simply the plane wave set, and the associated quasi-energies are then easy to determine:

$$\tilde{u}(x) = \frac{1}{\sqrt{2\pi}} e^{ikx}, \qquad \mathcal{E}_F = \frac{\hbar^2 k^2}{2m} + \frac{\xi(T)}{T}\hbar k - \hbar\frac{\theta(T)}{T}, \tag{5.38}$$

where k is the plane wave's momentum. The Floquet modes can be easily obtained from the action of $\hat{U}_F$ from Eq. (5.37) on the eigenstates: $|\tilde{u}\rangle$:

$$u(x,t) = \frac{1}{\sqrt{2\pi}} e^{ix\left[k - \frac{1}{\hbar}\int_0^t f(\tau)\,d\tau\right]} e^{-it\left\{\frac{1}{2m\hbar t}\left[\int_0^t d\tau\left(\int_0^\tau f(\tau')\,d\tau'\right)^2 - \frac{t}{T}\int_0^T d\tau\left(\int_0^\tau f(\tau')\,d\tau'\right)^2\right] + k\left[\frac{\xi(t)}{t} - \frac{\xi(T)}{T}\right]\right\}}, \tag{5.39}$$

where we used Eq. (5.12). The Floquet modes are plane waves with a momentum that varies in time,

$$\left\langle u(t)\left|\hat{k}\right|u(t)\right\rangle = k - \frac{1}{\hbar}\int_0^t f(\tau)\,d\tau,$$

and which return to their initial value k at stroboscopic times. As required, the Floquet modes are time–periodic with period T. The Floquet states are obtained from Eqs. (5.23) and (5.38),

$$\psi_F(x,t) = \frac{1}{\sqrt{2\pi}} e^{i[kx + \theta(x,t)] - it\frac{\hbar k^2}{2m} - ik\xi(t)}. \tag{5.40}$$

They are plane waves, periodic in time with period T and their momentum expectation value varies in the same way as does for the Floquet modes. One can now evaluate the time evolution of the Gaussian wavepacket from Eq. (5.24). In order to do so, we compute the amplitude $A(k)$

$$A(k) = \int_{-\infty}^{\infty} \chi(x,0)\psi_F^*(x,0) = \sqrt[4]{\frac{2\sigma^2}{\pi}} e^{-(k\sigma)^2},$$

and perform the Gaussian integration in Eq. (5.24), arriving at:

$$\chi(x,t) = \frac{1}{\sqrt[4]{2\,\pi\,\sigma^2}} \frac{e^{i\,\theta(x,t)}}{\sqrt{1 + i\,\frac{\hbar\,t}{2\,m\,\sigma^2}}} e^{-\frac{[x-\xi(t)]^2}{4\left(\sigma^2 + i\,\frac{\hbar\,t}{2\,m}\right)}}. \tag{5.41}$$

The wavepacket has a Gaussian shape centered at $\xi(t)$ and spreads in time as:

$$\Delta x(t) = \sqrt{\sigma^2 + \frac{\hbar^2\,t^2}{4\,m^2\,\sigma^2}}, \tag{5.42}$$

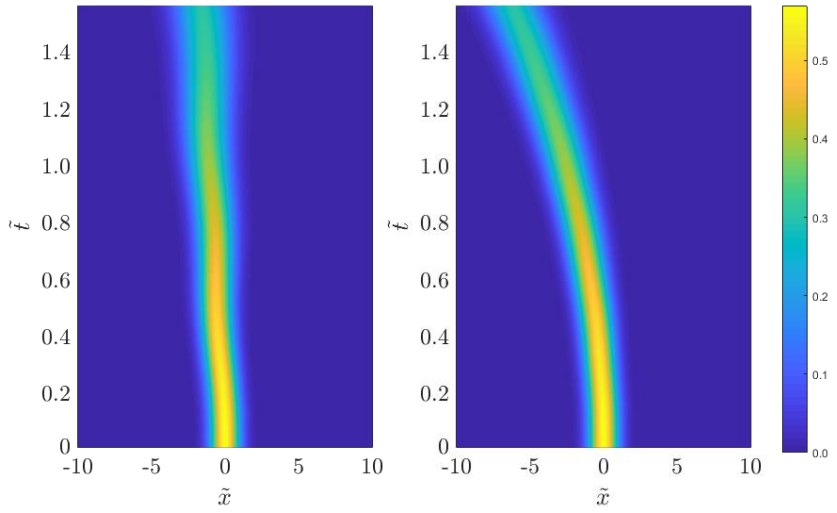

Figure 5.1: Time evolution of density profiles of Gaussian wavepackets $|\chi(x,t)|^2$ for a single particle in a potential: $xf(t)$. The left plot shows an evolution with a driving force $f(t) = \ell \sin(\omega t)$: the motion proceeds with a constant stroboscopic velocity towards the left. The right plot shows the evolution under a driving force $f(t) = \ell \sin^2(\omega t)$: the motion is uniformly accelerated to negative values of x. The figures are calculated via the split-step Fourier method and in both $\tilde{\sigma} = 2^{-1/2}$, $\tilde{\ell} = 10$, and $\tilde{\omega} = 10$.

in agreement with Eq. (5.17). The left side of Fig. 5.1 shows an example, where

$$f(t) = \ell \sin(\omega t) \tag{5.43}$$

(see Appendix 5.5.A for a discussion about cosinusoidal and sinusoidal forces). The center of mass of the wavepacket is located at $\xi(t) = \frac{\ell}{m\omega^2}[\sin(\omega t) - \omega t]$, and it spreads according to Eq. (5.42). We use the parametrization $\ell = l \cdot \tilde{\ell}$ and $\omega = u \cdot \tilde{\omega}$, where $\tilde{\ell}$ and $\tilde{\omega}$ are dimensionless, and define $\tilde{t} = t/u$ and $\tilde{x} = x\sqrt[3]{\frac{ml}{\hbar^2}}$. In the left side of Fig. 5.1 we set: $\tilde{\sigma} = \sigma\sqrt[3]{\frac{ml}{\hbar^2}} = 2^{-1/2}$, $\tilde{\ell} = 10$, and $\tilde{\omega} = 10$.

$\int_0^t f(t)\,dt \neq 0$

In this case, the independence of the Floquet Hamiltonian (5.25) on n is more difficult to demonstrate. Let us define a function $F(t)$, such that $\frac{dF}{dt} = f(t)$. We have $\int_0^T f(t)\,dt = F(T) = c$, where c depends on the driving parameters and, by definition, $F(0) = 0$. It follows that $F(nT) = nF(T) = nc$. It is easy to prove that $F(t+T) = F(T) + F(t) = c + F(t)$. Therefore $F(nT+t) = nc + F(t)$ and $\xi(nT)$ can be written as:

$$\xi(nT) = -\frac{1}{m}\int_0^{nT} F(t)\,dt = -\frac{n^2}{m} I\,, \tag{5.44}$$

where $I = \int_0^T F(t)\,dt$. Thus $\xi(nT)$ depends quadratically on the stroboscopic factor n, and the stroboscopic motion experiences a uniform acceleration $-\frac{1}{m}I$. Next, since $\xi(nT) \propto n^2$, one has $\xi(-T) = \xi(T)$ and, choosing $n = -1$ in Eq. (5.29), yields: $\xi(T) = -\frac{T}{2m}\int_0^T f(t)\,dt$. This can be substituted back into Eq. (5.29) to obtain:

$$\xi(nT) = -\frac{n^2 T}{2m}\int_0^T f(t)\,dt\,. \tag{5.45}$$

If we now take $t = nT$ in (5.26) and use (5.45), we derive the relevant equation:

$$\int_0^{nT} d\tau \int_0^{\tau} f(\tau')\, d\tau' \;=\; \frac{n^2 T}{2} \int_0^{T} f(t)\, dt\,,$$

that holds when the integral of the driving function over a driving period does not vanish. Using these results into (5.25), we can write:

$$\hat{H}_F = \frac{\hat{p}^2}{2m} - \hbar \frac{\theta(x,T)}{T} - \frac{1}{6m}\left[\int_0^T f(\tau)\, d\tau\right]^2 , \tag{5.46}$$

or, equivalently,

$$\hat{H}_F = \frac{\hat{p}^2}{2m} + x\,\frac{1}{T}\int_0^T f(\tau)\, d\tau + \frac{1}{2m}\frac{1}{T}\int_0^T d\tau \left[\int_0^{\tau} f(\tau')\, d\tau'\right]^2 - \frac{1}{6m}\left[\int_0^T f(\tau)\, d\tau\right]^2 .$$

This expression is independent on n, a fact which completes the proof. Unlike the case where $\int_0^T f(t)\, dt = 0$, the Floquet Hamiltonian does not contain a term proportional to $\hat{p}$, but a static linear potential. This term forces the particle to move to the left/right for positive/negative values of $\int_0^T f(t)\, dt$. An example is given in Fig. 5.1-right where $\frac{1}{T}\int_0^T f(\tau)\, d\tau = \frac{\ell T}{2} > 0$, so that the wavepacket moves with an acceleration of $-\frac{\ell T^2}{4m}$. However, its spread does not depends on the external driving force as predicted in Eq. (5.17).

The eigenfunctions of the Floquet Hamiltonian are the Airy function Ai [248] of the form:

$$\tilde{u}(x) = C Ai\left\{\left(\frac{2mT^2}{\hbar^2\left[\int_0^T f(\tau)\, d\tau\right]^2}\right)^{1/3}\left(\frac{x}{T}\int_0^T f(\tau)\, d\tau - \mathcal{E}_F + \Omega\right)\right\}, \tag{5.47}$$

where C is a normalization constant and:

$$\Omega = \frac{1}{2m}\frac{1}{T}\int_0^T d\tau \left[\int_0^{\tau} f(\tau')\, d\tau'\right]^2 - \frac{1}{6m}\left[\int_0^T f(\tau)\, d\tau\right]^2 .$$

The Floquet Hamiltonian has a continuous spectrum spanning the whole range of energy values $\mathcal{E}_F$ from $-\infty$ to $+\infty$.

The micro-motion operator is obtained inverting Eq. (5.4), and it leads to:

$$\begin{aligned}\hat{U}_F(t,0) \;=\; & e^{\frac{i}{\hbar}\left\{t\hbar\left[\frac{\theta(x,t)}{t} - \frac{\theta(x,T)}{T}\right] - \frac{t}{2m}\int_0^T f(\tau)\, d\tau \cdot \left[\frac{1}{3}\left(1+2\frac{t^2}{T^2}\right)\int_0^T f(\tau)\, d\tau\right] - \xi(t)\frac{t}{T}\int_0^T f(\tau)\, d\tau\right\}} \\ & \cdot e^{-\frac{i}{\hbar}\left[\xi(t) + \frac{t^2}{2mT}\int_0^T f(\tau)\, d\tau\right]\hat{p}} .\end{aligned} \tag{5.48}$$

This expression makes it complicated to determine the time evolution, even for a Gaussian wavepacket, using Eq.(5.24). To circumvent this problem we perform the unitary transformation

$$\chi(x,t) = \hat{U}_F(t,0)\tilde{\chi}(x,t)\,,$$

where the transformed wavefunction satisfies [45]:

$$i\hbar\frac{\partial\tilde{\chi}}{\partial t} = \hat{H}_F\tilde{\chi}(x,t)\,.$$

Since $\hat{H}_F$ has a linear potential term, we can apply the same reasoning used to solve the original equation (5.5) for a constant driving function $\tilde{f} = \frac{1}{T}\int_0^T f(\tau)\,d\tau$, therefore we translate and gauge transform the wavefunction $\tilde{\chi}(x,t)$ in order to wash out the x-linear term in the Floquet Hamiltonian. By doing so, we finally get Eq. (5.14), which is thus the convenient way to obtain the time–evolved wavepacket. In summary, we need first to calculate the free expansion of $\chi(x,0)$, then to translate the solution and finally to multiply it by the gauge phase.

The detailed analysis performed so far is valid for a single particle subjected to a linear potential which varies periodically in time. We shall show below that it can be extended straightforwardly to two- or many-particles interacting with a generic interacting potential $V_{2b}(x_j - x_i)$.

5.2 INTRODUCING INTERACTIONS: THE TWO-BODY PROBLEM

Let us now consider a one–dimensional system of two interacting particles subjected to a linear time–periodic potential. The Schrödinger equation reads:

$$i\,\hbar\,\frac{\partial\chi}{\partial t} = \sum_{j=1}^{2}\left[-\frac{\hbar^2}{2\,m}\frac{\partial^2}{\partial x_j^2} + x_j\,f(t)\right]\chi + V_{2b}(x_2 - x_1)\chi\,, \tag{5.49}$$

where $V_{2b}(x_2 - x_1)$ is a generic potential between the two particles. To solve the Schrödinger equation (5.49), we can employ the same method discussed in the previous Section: First we perform the gauge transformation

$$\chi(x_1, x_2, t) = e^{i[\theta(x_1,t)+\theta(x_2,t)]}\eta(y_1(t), y_2(t), t)\,, \tag{5.50}$$

where $y_j(t) = x_j - \xi(t)$, for $j = 1, 2$. The wavefunction $\eta(y_1, y_2, t)$ satisfies the Schrödinger equation for two interacting particles with no external potential:

$$i\,\hbar\frac{\partial\eta}{\partial t} = -\frac{\hbar^2}{2\,m}\left[\frac{\partial^2}{\partial y_1^2} + \frac{\partial^2}{\partial y_2^2}\right]\eta + V_{2b}(y_2 - y_1)\,\eta\,, \tag{5.51}$$

while $\xi(t)$ and $\theta(x_j, t)$ obey Eqs. (5.26) and (5.12), once we use the same initial conditions of the previous case.

Notice that $V_{2b}(y_1 - y_2) = V_{2b}(x_1 - x_2)$, because $y_j(t) = x_j - \xi(t)$. Moreover, since $\xi(0) = 0$, the two wavefunctions coincide at initial time: $\chi(x_1, x_2, 0) = \eta(x_1, x_2, 0)$, hence the solution of (5.49) can be written as:

$$\chi(x_1, x_2, t) = e^{i\theta(x_1,t)+i\theta(x_2,t)}e^{-i\frac{\xi(t)}{\hbar}(\hat{p}_1+\hat{p}_2)}e^{-i\frac{t}{\hbar}\left[\frac{\hat{p}_1^2+\hat{p}_2^2}{2m}+V_{2b}(x_2-x_1)\right]}\chi(x_1, x_2, 0)\,. \tag{5.52}$$

With this expression, using the procedure discussed in the previous Section, we can compute the expectation values of physical observables and their variances. More precisely, the expectation value of a single particle operator $\hat{O}_j$ is defined as:

$$\left\langle\hat{O}_j\right\rangle(t) \equiv \left\langle\chi(x_1, x_2, t)\left|\hat{O}_j\right|\chi(x_1, x_2, t)\right\rangle = \int_{-\infty}^{\infty}dx_1\int_{-\infty}^{\infty}dx_2\,\chi^*(x_1, x_2, t)\,\hat{O}_j\,\chi(x_1, x_2, t)\,, \tag{5.53}$$

and expectation values of position and momentum can be computed using the Baker-Campbell-Hausdorff formula.

We will show below that there is a decoupling between the linear potential term and the interacting one. This decoupling arises from the separation of the center of mass motion (which is determined by the external potential), and the relative motion (determined by the interacting potential). The diffusion of the wavepacket evolves as it would be free from the linear time dependent potential, but of course depends on the interaction.

The undriven Hamiltonian is given by:

$$\hat{H}_0 = \frac{\hat{p}_1^2 + \hat{p}_2^2}{2m} + V_{2b}(x_2 - x_1)\,. \tag{5.54}$$

This implies that the total momentum of the system $\hat{P} = \hat{p}_1 + \hat{p}_2$ is conserved, i.e. $\left[\hat{H}_0, \hat{P}\right] = 0$. An example is the contact interaction $V_{2b}(x_2 - x_1) = \lambda\,\delta(x_2 - x_1)$, with λ the coupling strength. This property allows us to calculate the total energy of the state:

$$E(t) = \left\langle \hat{H} \right\rangle (t) = \left\langle \chi(x_1, x_2, t) \left| \left[\frac{\hat{p}_1^2 + \hat{p}_2^2}{2m} + f(t)\,(x_1 + x_2) + V_{2b}\,(x_2 - x_1) \right] \right| \chi(x_1, x_2, t) \right\rangle . \tag{5.55}$$

After a lengthy calculation (see Appendix 5.5.C), using the canonical commutation relations and Eq. (5.52), we obtain for a generic driving function $f(t)$, including as well the non-periodic cases:

$$\begin{aligned} E(t) \;=\; & E(0) + \frac{1}{m}\left[\int_0^t f(\tau)d\tau\right]^2 + \sum_{j=1}^{2} p_{0,j}\left[\frac{t}{m}f(t) - \frac{1}{m}\int_0^t f(\tau)d\tau\right] + \\ & -\frac{2f(t)}{m}\int_0^t d\tau \int_0^\tau f(\tau')d\tau' + \sum_{j=1}^{2} x_{0,j}\left[f(t) - f(0)\right] , \end{aligned} \tag{5.56}$$

where $E(0)$ is the initial energy of the state, containing all the interaction effects. The remaining terms arise from the linear driving potential and depend on the position $x_{0,j}$ and momenta $p_{0,j}$, of the j-th particle at time $t = 0$. If $f(t)$ is constant, as for a constant (gravitational or electric) force, then the energy is conserved. On the other hand, if $f(t)$ is periodic, its integral over a time–period vanishes, and $f(t = 0) = 0$, then the energy is conserved at stroboscopic times.

Next we shall study the models where $f(t)$ is periodic. As done in the previous Section, we shall consider two cases: $\int_0^T f(t)\,dt = 0$, and $\int_0^T f(t)\,dt \neq 0$. The evolution operator can be read from (5.52):

$$\hat{U}(t,0) \;=\; e^{i[\theta(x_1,t)+\theta(x_2,t)]} e^{-i\frac{\xi(t)}{\hbar}(\hat{p}_1+\hat{p}_2)} e^{-i\frac{t}{\hbar}\left[\frac{\hat{p}_1^2+\hat{p}_2^2}{2m} + V_{2b}(x_2-x_1)\right]} . \tag{5.57}$$

It is convenient to use the center of mass and relative coordinates: $x = x_2 - x_1$ and $X = \frac{x_1+x_2}{2}$. In these variables the effects of the linear time dependent potential and the interactions are completely decoupled. The time evolution in these coordinates reads:

$$\begin{aligned} \hat{U}(t,0) \;&=\; \hat{U}^{\rm com}(t,0)\hat{U}^{\rm rel}(t,0) = \\ &=\; e^{-\frac{i}{\hbar}\left\{2X\int_0^t f(\tau)\,d\tau + \frac{1}{m}\int_0^t d\tau\left[\int_0^\tau f(\tau')\,d\tau'\right]^2\right\}} e^{-i\frac{\xi(t)}{\hbar}\hat{P}} e^{-i\frac{t}{\hbar}\frac{\hat{p}^2}{4m}} e^{-i\frac{t}{\hbar}\left[\frac{\hat{p}^2}{m} + V_{2b}(x)\right]} , \end{aligned} \tag{5.58}$$

where $\hat{P}$ is the total momentum, that commutes with the undriven Hamiltonian, and $\hat{p} = \hat{p}_2 - \hat{p}_1$, is the relative momentum of the particles.

$\int_0^t f(t)\,dt = 0$

In this case one finds:

$$\hat{H}_F = \sum_{j=1}^{2}\left[\frac{\hat{p}_j^2}{2\,m} + \frac{\xi(T)}{T}\hat{p}_j - \hbar\frac{\theta(T)}{T}\right] + V_{2b}(x_2 - x_1)\,, \tag{5.59}$$

where $\theta(x_j, T) = \theta(T)$, as follows from Eq. (5.12).

From the analysis performed so far, and for the similarities with the one-body case, we know that the stroboscopic motion described by the Floquet Hamiltonian occurs with a constant velocity, since the translational parameter is: $\xi(nT) \propto n$. Notice that if the Schrödinger equation with the original undriven Hamiltonian is solvable, then also the Floquet Hamiltonian associated to the motion under the action of a linear time dependent potential is solvable, since it is described by the same two-body potential of the original problem with no driving, apart from a momentum shift. We observe that it is not convenient to solve the dynamics via Eq. (5.24) with respect to the eigenfunctions of the Floquet Hamiltonian in Eq. (5.59), while it is instead more advantageous to pass to relative and center of mass coordinates. Using the center of mass and relative coordinates the Floquet Floquet Hamiltonian decouples in two parts:

$$\hat{H}_F^{\rm com} = \frac{\hat{P}^2}{4m} + \frac{\xi(T)}{T}\hat{P} - 2\hbar\frac{\theta(T)}{T}\,, \tag{5.60}$$

and

$$\hat{H}_F^{\rm rel} = \frac{\hat{p}^2}{m} + V_{2b}(x)\,. \tag{5.61}$$

The same factorization occurs for the micro-motion operators, by defining:

$$\hat{U}(t,0) = \hat{U}_F^{\rm com}(t,0)e^{-i\frac{t}{\hbar}\hat{H}_F^{\rm com}}\,\hat{U}_F^{\rm rel}(t,0)e^{-i\frac{t}{\hbar}\hat{H}_F^{\rm rel}}\,. \tag{5.62}$$

Using Eq. (5.58), the micro-motion operator for the center of mass evolution has a form:

$$\hat{U}_F^{\rm com}(t,0) = e^{-it\left\{\frac{2X}{\hbar t}\int_0^t f(\tau)\,d\tau + \frac{1}{m\hbar t}\int_0^t d\tau\left[\int_0^\tau f(\tau')\,d\tau'\right]^2 + 2\frac{\theta(T)}{T}\right\}}\; e^{i\frac{t}{\hbar}\left[\frac{\xi(T)}{T} - \frac{\xi(t)}{t}\right]\hat{P}}\,, \tag{5.63}$$

while the micro-motion operator for the relative coordinate is instead trivial, and reads:

$$\hat{U}_F^{\rm rel}(t,0) = \hat{1}\,. \tag{5.64}$$

The time evolution for the relative motion depends of course on the interacting potential $V_{2b}(x)$. Concerning the center of mass motion, we notice the similarity of Eq. (5.60) with the Floquet Hamiltonian (5.31) for a single particle, that allow us to use the results of the previous Section. The eigenfunctions of the Floquet Hamiltonian (5.60) are plane waves with a continuous spectrum of quasi-energies:

$$\tilde{u}^{\rm com}(X) = \frac{1}{\sqrt{2\pi}}e^{iKX}\,, \qquad \mathcal{E}_F^{\rm com} = \frac{\hbar^2K^2}{4m} + \frac{\xi(T)}{T}\,\hbar K - 2\hbar\frac{\theta(T)}{T}\,, \tag{5.65}$$

where K is the center of mass momentum. Next, we can get the Floquet modes by applying $\hat{U}_F^{\rm com}(t,0)$ onto $\tilde{u}^{\rm com}(X)$, obtaining:

$$\begin{aligned} u^{\rm com}(X,t) \;=\; & \frac{1}{\sqrt{2\pi}}e^{iX\left[K - \frac{2}{\hbar}\int_0^t f(\tau)\,d\tau\right]} \\ & e^{-it\left\{\frac{1}{m\hbar t}\left[\int_0^t d\tau\left(\int_0^\tau f(\tau')\,d\tau'\right)^2 - \frac{2t}{T}\int_0^T d\tau\left(\int_0^\tau f(\tau')\,d\tau'\right)^2\right] + K\left[\frac{\xi(t)}{t} - \frac{\xi(T)}{T}\right]\right\}}\,, \end{aligned} \tag{5.66}$$

where we used Eq. (5.12). As in the one-body problem, the Floquet modes are plane waves with a momentum varying in time as:

$$\left\langle u(t)\left|\hat{K}\right|u(t)\right\rangle = K - \frac{2}{\hbar}\int_0^t f(\tau)\,d\tau\,,$$

which implies that $\langle K\rangle(nT) = K$. We finally get the Floquet states from Eq. (5.23) and (5.65),

$$\psi_F^{\rm com}(X,t) = \frac{1}{\sqrt{2\pi}} e^{i\left\{KX - \frac{2X}{\hbar t}\int_0^t f(\tau)\,d\tau - \frac{1}{m\hbar t}\int_0^t d\tau\left[\int_0^\tau f(\tau')\,d\tau'\right]^2\right\} - it\frac{\hbar K^2}{4m} - iK\xi(t)}\,, \tag{5.67}$$

that are plane waves, periodic in time with period T, and whose average center of mass momentum behaves like that of the Floquet modes. Therefore the center of mass component of the wavefunction, solution of (5.49), reads as:

$$\phi(X,t) = \int A(K)\psi_F^{\rm com}(X,t)\,dK\,, \tag{5.68}$$

where we have written: $\chi(x_1,x_2,t) = \phi(X,t)\varphi(x,t)$.

$\int_0^t f(t)\,dt \neq 0$

Using the methods presented in previous Sections, we find:

$$\hat{H}_F = \sum_{j=1}^{2}\left[\frac{\hat{p}_j^2}{2m} - \hbar\frac{\theta(x_j,T)}{T}\right] - \frac{1}{3m}\left[\int_0^T f(\tau)\,d\tau\right]^2 + V_{2b}(x_2-x_1)\,. \tag{5.69}$$

This expression contains a linear potential, hidden in the gauge phases $\theta(x_j,T)$. Analogously to the one-body example, the stroboscopic motion of the particles is uniformly accelerated,

$$\frac{d^2\langle x_j\rangle}{dt^2}(nT) = -\frac{1}{m}\int_0^T d\tau\int_0^\tau f(\tau')\,d\tau'\,.$$

Using the center of mass and relative coordinates, the Floquet Hamiltonian (5.69) splits in two parts:

$$\hat{H}_F^{\rm com} = \frac{\hat{P}^2}{4m} + \hat{X}\frac{1}{T}\int_0^T f(\tau)\,d\tau + \frac{1}{m}\frac{1}{T}\int_0^T d\tau\left[\int_0^\tau f(\tau')\,d\tau'\right]^2 - \frac{1}{3m}\left[\int_0^T f(\tau)\,d\tau\right]^2, \tag{5.70}$$

while the Floquet Hamiltonian of the relative motion is given by Eq. (5.61). The difference between the cases (1) and (2) stems only from the center of mass motion which has an additional linear dependence on $\hat{P}$ in the first case, and $\hat{X}$ in the second. The micro-motion operator can be split as well, obtaining Eq. (5.64) for the relative part, and:

$$\hat{U}_F^{\rm com}(t,0) = e^{\frac{i}{\hbar}\left\{t\left[X\left(\frac{1}{T}\int_0^T f(\tau)\,d\tau - \frac{1}{t}\int_0^t f(\tau)\,d\tau\right) + \frac{1}{mT}\int_0^T d\tau\left[\int_0^\tau f(\tau')\,d\tau'\right]^2 + \frac{1}{mt}\int_0^t d\tau\left[\int_0^\tau f(\tau')\,d\tau'\right]^2\right] + \right.}$$
$$\left. - \frac{t}{m}\int_0^T f(\tau)\,d\tau\cdot\left[\frac{1}{3}\left(1+2\frac{t^2}{T^2}\right)\int_0^T f(\tau)\,d\tau\right] + -2\xi(t)\frac{t}{T}\int_0^T f(\tau)\,d\tau\right\} e^{-\frac{i}{\hbar}\hat{P}\left[\xi(t)+\frac{t^2}{2mT}\int_0^T f(\tau)\,d\tau\right]}\,, \tag{5.71}$$

for the center of mass.

The dynamics of the relative part can be analysed once the two-body potential is given, while the analysis performed on the center of mass part follows the same line of the one-body case. By this we mean that one has to perform a unitary transformation on the center of mass wavefunction: $\Phi(X,t) = \hat{U}_F \tilde{\Phi}(X,t)$, and therefore the new wavefunction $\tilde{\Phi}(X,t)$ satisfies a time dependent Schrödinger equation with the Floquet Hamiltonian (5.70). Washing away the X-linear dependence of the Floquet Hamiltonian by means of a translation and a gauge transformation, for the center of mass part of Eq. (5.52) we have:

$$\Phi(X,t) = e^{-\frac{i}{\hbar}\left\{2X\int_0^t f(\tau)\,d\tau + \frac{1}{m}\int_0^t d\tau\left[\int_0^\tau f(\tau')\,d\tau'\right]^2\right\}} e^{-i\frac{\xi(t)}{\hbar}\hat{P}} e^{-i\frac{t}{\hbar}\frac{\hat{P}^2}{4m}}\,\Phi(X,0)\,, \tag{5.72}$$

where Eq. (5.58) has been used.

As an example, we use the above results to study the time evolution of two particles with contact interactions initially prepared in a Gaussian wavepacket.

5.2.1 CONTACT INTERACTIONS

Let consider a contact potential: $V_{2b}(x_2 - x_1) = \lambda\delta(x_2 - x_1)$, where $\lambda > 0$ is the repulsive interaction parameter. At the initial time we prepare a Gaussian wavepacket with variance σ:

$$\chi(x_1, x_2, 0) = \frac{1}{\sqrt{\pi\sigma^2}} e^{-\left(x_1^2 + x_2^2\right)/2\sigma^2}\,, \tag{5.73}$$

that factorizes into the center of mass and relative parts:

$$\Phi(X,0) = \sqrt[4]{\frac{2}{\pi\sigma^2}}\, e^{-X^2/\sigma^2} \quad , \qquad \varphi(x,0) = \frac{1}{\sqrt[4]{2\pi\sigma^2}} e^{-x^2/4\sigma^2}\,. \tag{5.74}$$

Let us start with the case: $\int_0^T f(\tau)\,d\tau = 0$. Finding the time–independent coefficient $A(K)$ appearing in Eq. (5.68) at $t = 0$, and using (5.74), yields:

$$\Phi(X,t) = \sqrt[4]{\frac{2}{\pi\sigma^2}}\, \frac{e^{i\theta(X,t)}}{\sqrt{1 + i\frac{\hbar\, t}{m\sigma^2}}}\; e^{-\frac{[X-\xi(t)]^2}{\sigma^2\left(1 + i\frac{\hbar\, t}{m\sigma^2}\right)}}\,. \tag{5.75}$$

Concerning the relative motion, we use the propagator $G(x, x'; t, 0)$ in the presence of a Dirac δ-potential [249, 250]

$$\varphi(x,t) = \int_{-\infty}^{\infty} G(x, x'; t, 0)\, \varphi(x', 0)\, dx'\,, \tag{5.76}$$

with:

$$G(x, x'; t, 0) = \frac{1}{\sqrt{4\,\pi\, i\,\hbar\, t/m}}\, e^{i\,\frac{m\,(x-x')^2}{4\,\hbar\, t}} - \frac{m\,\lambda}{4\,\hbar^2}\, e^{\frac{m\,\lambda}{2\,\hbar^2}(|x| + |x'|) + i\,\frac{m\,\lambda^2\, t}{4\,\hbar}}\, \mathrm{erfc}\left(\frac{|x| + |x'| + i\frac{\lambda\, t}{\hbar}}{\sqrt{4\, i\,\hbar\, t/m}}\right)\,, \tag{5.77}$$

with erfc being the complementary error function:

$$\mathrm{erfc}(z) = \frac{2}{\sqrt{\pi}} \int_z^\infty e^{-t^2}\, dt\,.$$

The numerical integration of (5.76), provides the wavefunction $\chi(x_1, x_2, t)$ for any value of $\lambda > 0$. In the limit of hard–core interactions, $\lambda \to \infty$, the integral (5.76) can be computed analytically:

$$\varphi(x,t) = \frac{1}{(2\pi)^{1/4}} \sqrt{\frac{im\sigma/\hbar t}{-1+im\sigma^2/\hbar t}}\ \mathrm{erf}\left(\frac{m\,\sigma\,x}{2\hbar t\sqrt{-1+im\sigma^2/\hbar t}}\right)\ e^{-\frac{m}{4\hbar t}\frac{x^2}{i+m\sigma^2/\hbar t}}\,, \quad (5.78)$$

where $\mathrm{erf}(z) = 1 - \mathrm{erfc}(z)$. We have studied the time evolution of the density matrix:

$$\rho(x_1,t) = 2\int_{-\infty}^{\infty} |\chi(x_1,x_2,t)|^2\ dx_2\,, \quad (5.79)$$

in order to visualize the evolution of the wavepacket. The density matrix (5.79) reads in the center of mass and relative wavefunctions, as:

$$\rho(x,t) = 2\int_{-\infty}^{\infty} \left|\Phi\left(\frac{x_1}{2}+x,t\right)\right|^2 |\varphi(x_1,t)|^2\ dx_1\,, \quad (5.80)$$

The results are reported in Fig. 5.2 for different times and coupling strengths λ, using the driving function:

$$f(t) = \ell\left[\cos^2(\omega t) - 1 + \frac{4}{3}\sin^4(\omega t)\right]\,.$$

We choose the same dimensionless variables as in the one-body case: dimensionless coupling strength $\tilde{\lambda} = l\frac{m\lambda}{\hbar^2}$, $\tilde{\ell} = 200$, $\tilde{\omega} = 2$ and $\tilde{\sigma} = 1$. The values $\tilde{\lambda} = 0$, 1 and ∞, correspond to the left, center and right sides of Fig. 5.2. Here:

$$\xi(t) = \frac{\ell}{12m\omega^2}\sin^4(\omega t)\,,$$

vanishes at stroboscopic times, as checked in the numerical simulations. We have also verified that the wavepacket expands as it was not subjected to the linear oscillating potential, in agreement with the theoretical prediction.

Fig. 5.2 shows that increasing the parameter λ, the variance of the wavepacket increases in time more rapidly. We have been able to fit this behaviour with the approximation:

$$\Delta x_j(t) \approx \frac{\sigma}{\sqrt{2}}\sqrt{1+\left(\frac{\hbar\,t}{m\,\sigma^2}\right)^2\left(1+\mathcal{B}\,\frac{m\,\lambda\,\sigma}{2\,\hbar^2}\right)}\,, \quad (5.81)$$

where $\mathcal{B} \approx 1.23$. For $\lambda = 0$ one retrieves an expression similar to Eq. (5.42), while in the limit $\lambda \to \infty$, Eq. (5.81) diverges for all t because the tail of the density matrix decays as $\propto x^2$, even starting from a Gaussian. In particular, from Eq. (5.78), we may employ the fact that for large x:

$$\mathrm{erf}(x) \simeq 1 - \frac{e^{-x^2}}{\sqrt{\pi}x} + \frac{e^{-x^2}}{2\sqrt{\pi}x^3}\,,$$

and therefore, after straightforward calculations, one gets that:

$$x^2\,|\varphi(x,t)|^2 \xrightarrow{x\to\infty} \sqrt{\frac{32}{\pi^3}}\frac{\hbar t}{m\sigma^2}\,,$$

hence we can see that for a Tonks–Girardeau wavepacket the variance will diverge at any times, since it has constant non-vanishing contributes at large distances.

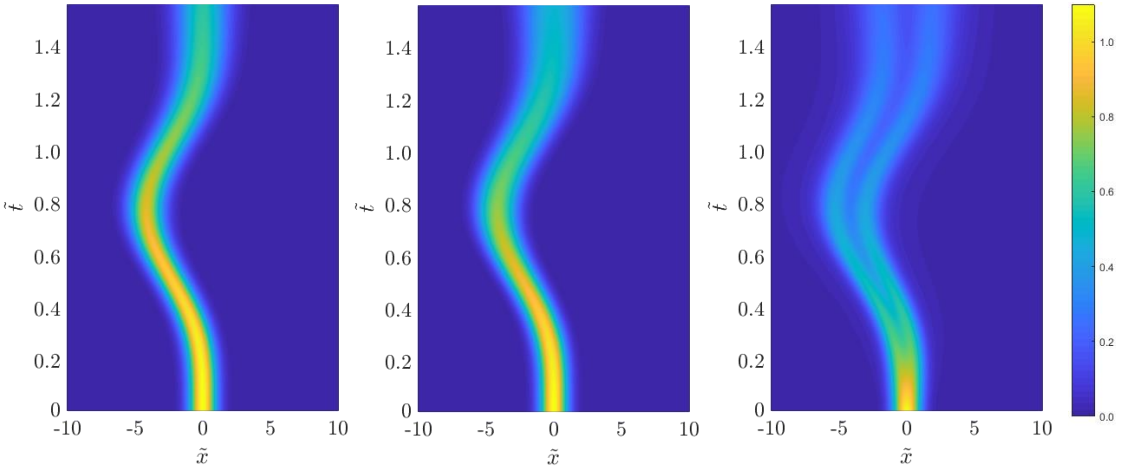

Figure 5.2: Time evolution of density matrix profiles (5.79) for a Gaussian wavepacket (5.73), under the action of a linear external potential: $xf(t)$, with driving function $f(t) = \ell\left[\cos^2(\omega t) - 1 + \frac{4}{3}\sin^4(\omega t)\right]$. The left side plot is the free case, $\tilde{\lambda} = 0$, the central plot has $\tilde{\lambda} = 1$, while the right side plot has $\tilde{\lambda} = \infty$. The center of mass moves with constant stroboscopic velocity, as predicted analytically, and the wavepacket spreads over time as it would do for the undriven case $\ell = 0$. As one can see from the right side plot, for very large interactions, the wavepacket rapidly tends to split in two specular parts. In all the figures the values $\tilde{\ell} = 200$, $\tilde{\omega} = 2$ and $\tilde{\sigma} = 1$ have been chosen.

As an additional check, we have calculated numerically the total energy of a two-particle system driven with $f(t) = \ell \sin^3(\omega t)$, separating its center of mass and relative components. The analytical value can be obtained from Eq. (5.56), and is represented by the solid, dashed and dotted lines in Fig. 5.3. The circular dots represent the values calculated numerically. We have used $\tilde{\ell} = 200$, $\tilde{\omega} = 60$, $\tilde{\sigma} = 2^{-1/2}$ and $p_{0,j} = x_{0,j} = 0$ for $j = 1, 2$. The interaction strengths, $\tilde{\lambda} = 0.1$, 1 and 10, only displace the curves since their effects are encoded in the initial energy factor $E(0)$ of Eq. (5.56), as can be seen from the inset of the plot. For this driving function we have $f(nT) = \int_0^T f(\tau)\, d\tau = 0$, therefore from Eq. (5.56) the energies at the stroboscopic times are equal to the initial energy, *i.e.* $E(nT) = E(0)$ for every n, and there is no heating of the system, in agreement with theoretical results [31, 32] and experimental findings [251].

In the case where $\int_0^T f(\tau)\, d\tau \neq 0$, we used Eq. (5.72) for the center of mass initial wavefunction of Eq. (5.74), obtaining the same result as when $\int_0^T f(\tau)\, d\tau = 0$, *i.e.* we retrieved Eq. (5.75). For the relative motion we have applied the same reasoning as before, by which we know that the relative part of the wavepacket evolves according to Eq. (5.76). We have performed a numerical simulation of a system made of two δ-interacting particles under the action of a linear potential with driving function: $f(t) = \ell\left[\cos(\omega t) - 1\right]$. The results for different interaction strengths λ are reported in Fig. 5.4, where the density matrices calculation (5.80) is plotted, in correspondence of $\tilde{\ell} = 10$, $\tilde{\omega} = 5$ and $\tilde{\sigma} = 1$. In this case the motion is uniformly accelerated to the right side of the x-axis, indeed the translational parameter reads $\xi(t) = \frac{\ell}{2m\omega^2}\left[\omega^2 t^2 - 2 + 2\cos(\omega t)\right]$. This has to be compared with the case $\int_0^T f(t)\, dt = 0$, where the center of mass does not accelerate.

Concerning the spreading of the wavepacket, it is the same as in the case without a driving potential and it also satisfies Eq. (5.81) with $\mathcal{B} \approx 1.23$. In conclusion, there is no

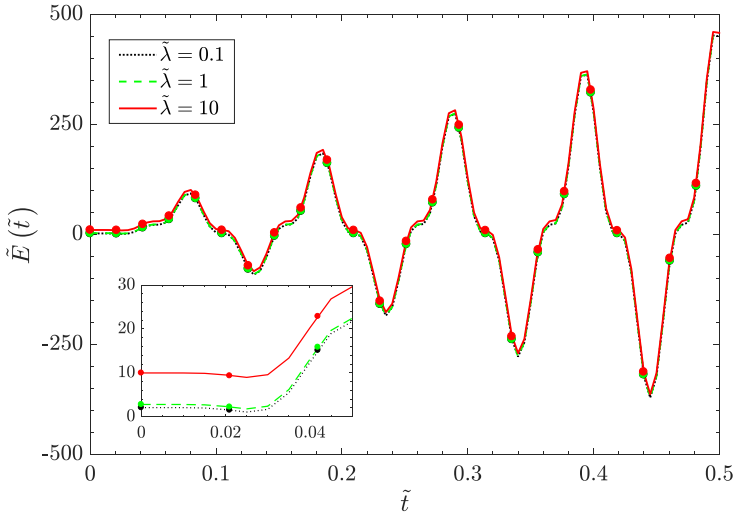

Figure 5.3: Time evolution of the energy $\tilde{E} = \sqrt[3]{\frac{m}{\hbar^2 l}}\, E$ for two interacting particles subjected to a linear external potential: $x f(t)$, with driving function $f(t) = \ell \sin^3(\omega t)$. The system is prepared in the Gaussian wavepacket state (5.73). The curves represent different values of the parameter $\tilde{\lambda}$, which only shifts the total energy, as shown in the inset for short times $\tilde{t}$ and different coupling strengths. The circular dots represent the energy values calculated from the numerical computation.

difference for the wavepacket spreading between the results of a driving function whose integral over a period vanishes or not.

5.3 MANY-BODY PROBLEM

The analysis done so far can be generalized to many-body systems with N interacting particles, a generic interacting potential $V_{2b}(x_j - x_i)$ and under the action of an external linear time–dependent potential. The Schrödinger equation reads:

$$i\,\hbar\,\frac{\partial \chi}{\partial t} = \sum_{j=1}^{N}\left[-\frac{\hbar^2}{2\,m}\frac{\partial^2}{\partial x_j^2} + x_j\, f(t)\right]\chi + \sum_{j>i} V_{2b}(x_j - x_i)\chi\,. \tag{5.82}$$

Performing the translation and a gauge transformation

$$\chi(x_1, \ldots, x_N, t) \equiv \prod_{j=1}^{N} e^{i\theta(x_j,t)}\eta(y_1, \ldots, y_N, t)\,, \tag{5.83}$$

the wavefunction $\eta(y_1, \ldots, y_N, t)$ satisfies the Schrödinger equation without the external driving, *i.e.*

$$i\,\hbar\,\frac{\partial \eta}{\partial t} = -\frac{\hbar^2}{2\,m}\sum_{j=1}^{N}\frac{\partial^2 \eta}{\partial y_j^2} + \sum_{j>i} V_{2b}(y_j - y_i)\eta\,, \tag{5.84}$$

where $y_j(t) = x_j - \xi(t)$, $\forall j$, therefore the interacting potential is invariant under these transformations: $V_{2b}(y_j - y_i) = V_{2b}(x_j - x_i)$.

Using the initial conditions $\xi(0) = 0$ and $\theta(x_j, 0) = 0$, $\forall j$, the parameter $\xi(t)$ and the gauge phase $\theta(x_j, t)$ satisfy Eqs. (5.26) and (5.12). Hence, the two wavefunctions coincide at initial time $t = 0$.

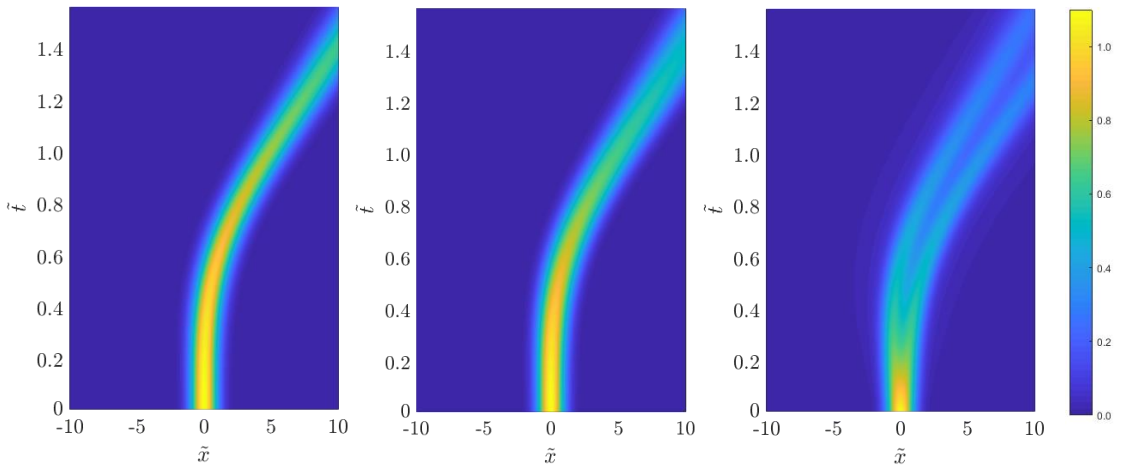

Figure 5.4: Evolution of density matrix (5.79) for a Gaussian wavepacket (5.73) under the action of a linear external potential: $xf(t)$, where the driving function is $f(t) = \ell\,[\cos(\omega t) - 1]$. Notice that the center of mass motion is uniformly accelerated to the right, as predicted analytically, and the wavepacket spreads over time as it would do for the undriven case. From left to right panels one has $\tilde{\lambda} = 0, 1, \infty$; moreover, $\tilde{\ell} = 10$, $\tilde{\omega} = 5$ and $\tilde{\sigma} = 1$.

The complete solution of the Schrödinger equation (5.82) can be formally written as:

$$\chi(x_1, \ldots, x_N, t) \;=\; \prod_{j=1}^{N} \left[e^{i\theta(x_j,t)} e^{-i\frac{\xi(t)}{\hbar}\hat{p}_j} \right] e^{-i\frac{t}{\hbar}\hat{H}_0} \eta(x_1, \ldots, x_N, 0)\,, \tag{5.85}$$

where the undriven Hamiltonian of one–dimensional many-particles systems has the general form:

$$\hat{H}_0 = \sum_{j=1}^{N} \frac{\hat{p}_j^2}{2m} + \sum_{j>i} V_{2b}(x_j - x_i)\,. \tag{5.86}$$

In (5.85) the momentum operator $\hat{p}_j$ is the generator of the translation for the j-th particle, and η is the solution of the Schrödinger equation with no linear driving.

The generalization of the two-body results for the expectation values of physical observables is straightforward. First, we can compute the total energy of the system evaluating the expectation value of the driven Hamiltonian. In the calculation we use the conservation of the total momentum $\hat{P} = \sum_{j=1}^{N} \hat{p}_j$ for the undriven Hamiltonian $\hat{H}_0$, *i.e.* $\left[\hat{H}_0, \hat{P}\right] = 0$, valid in the considered case in which the interaction V_{2b} depends on the relative distance between the particles (see more comments in Section 5.5.3.1). Using the commutation relations we find for a general (also non-periodic) driving function $f(t)$:

$$\begin{aligned} E(t) \;=\; & E(0) + \frac{N}{2m}\left[\int_0^t f(\tau)d\tau\right]^2 + \sum_{j=1}^{N} p_{0,j}\left[\frac{t}{m}f(t) - \frac{1}{m}\int_0^t f(\tau)d\tau\right] + \\ & -\frac{Nf(t)}{m}\int_0^t d\tau \int_0^\tau f(\tau')d\tau' + \sum_{j=1}^{N} x_{0,j}\left[f(t) - f(0)\right]\,, \end{aligned} \tag{5.87}$$

which generalizes Eq. (5.56). See Appendix 5.5.C for the demonstration of this equation. As for the two-body case, if $f(t)$ is periodic in time and its integral over a time–period vanishes, then the energy is conserved at stroboscopic times if $f(t = 0) = 0$. Once again,

there is a decoupling between the interactions and the external linear driving potential, since the effect of the interactions among particles is encoded in the initial value of the energy $E(0)$, while the remaining terms collect the effect of the external potential.

Thanks to the simple rewriting of the many–body wavefunction in Eq. (5.85), we are also able to write the one–body density matrix of the driven system in terms of the undriven one. We recall that the one–body density matrix is defined as [18]

$$\rho(x,x',t) \;=\; N \int dx_2 \dots dx_N \, \chi^*(x,x_2,\dots,x_N,t)\, \chi(x',x_2,\dots,x_N,t)\,, \tag{5.88}$$

Therefore using Eq. (5.85) we can rewrite the density matrix as:

$$\rho(x,x',t) \;=\; N\, e^{i[\theta(x',t)-\theta(x,t)]} \int dy_2 \dots dy_N \, \eta^*(y,y_2,\dots,y_N,t)\, \eta(y',y_2,\dots,y_N,t)\,, \tag{5.89}$$

since $dx_j = dy_j$ for every j, while $y(t) = x - \xi(t)$, $y'(t) = x' - \xi(t)$. So finally:

$$\rho(x,x',t) \;=\; e^{i[\theta(x',t)-\theta(x,t)]}\, \rho_{\text{undriven}}(y,y',t)\,, \tag{5.90}$$

where $\rho_{\text{undriven}}(y,y',t)$ is defined in terms of the wavefunction η solution of the Schrödinger equation without the driving term.

For a translational invariant system, the above equation may be further simplified by writing everything in terms of the relative coordinate $r \equiv x - x'$. In this case, since it is also true that: $r = y - y'$, then Eq. (5.164) may be rewritten as:

$$\rho(r,t) \;=\; e^{i\frac{r}{\hbar}\int_0^t f(\tau)\,d\tau}\, \rho_{\text{undriven}}(r,t)\,. \tag{5.91}$$

We may further analyse the eigenvalues of the one–body density matrix for a translational invariant system. In the equilibrium, the one–body density matrix satisfies the eigenvalue equation [18]

$$\int \rho(x,x',t)\, \varphi_i(x,t)\, dx \;=\; \lambda_i(t)\, \varphi_i(x',t)\,, \tag{5.92}$$

where $\lambda_i(t)$ is the occupation number of the i–th natural orbital eigenvector $\varphi_i(x,t)$. The λ_i are such that at every time: $\sum_i \lambda_i(t) = N$. For the dynamics, when the Galilean invariance is not broken (correspondingly requiring appropriate initial conditions), the quantum number labeling the occupation of the natural orbitals is the wavenumber k, and the natural orbitals at time t are simply plane waves. Therefore we may write Eq. (5.166) for a driven translational invariant many–body system as:

$$\lambda_k(t) \;=\; \int \rho(r,t)\, e^{i\,k\,r}\, dr\,. \tag{5.93}$$

Now, thanks to Eq. (5.165), we can write the following relation between the natural orbitals occupation numbers of the driven system with those of the undriven one:

$$\lambda_k(t) \;=\; \lambda_{\tilde{k}}^{\text{undriven}}(t)\,, \tag{5.94}$$

where $\tilde{k}(t) = k + \frac{1}{\hbar}\int_0^t f(\tau)\,d\tau$, and we have defined the occupation numbers of the system without driving as:

$$\lambda_k^{\text{undriven}}(t) \;=\; \int \rho_{\text{undriven}}(r,t)\, e^{ikr}\, dr\,. \tag{5.95}$$

From the above relations, one may observe that there is only a time–dependent translation over the momentum wavenumber which identifies the occupation numbers of the driven system with respect to the undriven case.

Let us now focus on periodic driving functions. As before, we discuss separately the cases when $\int_0^T f(\tau)\,d\tau = 0$ and $\neq 0$. In the first case, the gauge phase at stroboscopic times is independent on the position variables, while the parameter ξ is linear in the stroboscopic factor n, indicating a stroboscopic motion with constant velocity. Using the fact that $\left[\hat{H}_0, \hat{P}\right] = 0$ and the Baker-Campbell-Hausdorff formula on Eq. (5.85) evaluated at $t = nT$, we find the Floquet Hamiltonian:

$$\hat{H}_F = \sum_{j=1}^{N}\left[\frac{\hat{p}_j^2}{2\,m} + \frac{\xi(T)}{T}\hat{p}_j - \hbar\frac{\theta(T)}{T}\right] + \sum_{j<i} V_{2b}(x_j - x_i)\,. \tag{5.96}$$

Hence, if the undriven Hamiltonian describes an integrable model, also the Floquet Hamiltonian is exactly solvable since it has the same two-body interaction potential among particles and presents only a shift in the momenta. For the micro-motion operator one finds:

$$\hat{U}_F(t,0) = e^{it\sum_{j=1}^{N}\left[\frac{\theta(x_j,t)}{t} - \frac{\theta(T)}{T}\right]}\, e^{i\frac{t}{\hbar}\left[\frac{\xi(T)}{T} - \frac{\xi(t)}{t}\right]\sum_{j=1}^{N}\hat{p}_j}\,. \tag{5.97}$$

If $f(t)$ has a non-vanishing integral over a driving period, then the Floquet Hamiltonian reads:

$$\hat{H}_F = \sum_{j=1}^{N}\left[\frac{\hat{p}_j^2}{2m} - \hbar\frac{\theta(x_j,T)}{T}\right] - \frac{N}{6m}\left[\int_0^T f(\tau)\,d\tau\right]^2 + \sum_{j<i} V_{2b}(x_j - x_i)\,, \tag{5.98}$$

which presents a time–independent x-linear potential term acting on all the particles. In this case, as we saw for the one-body problem, the system is governed by a stroboscopic dynamics with a uniform acceleration, since the translational parameter depends quadratically on the stroboscopic factor: $\xi(nT) \propto n^2$. The micro-motion operator reads:

$$\begin{aligned}\hat{U}_F(t,0) \;=\; & e^{\frac{i}{\hbar}\left\{t\hbar\sum_{j=1}^{N}\left[\frac{\theta(x_j,t)}{t} - \frac{\theta(x_j,T)}{T}\right] - N\frac{t}{2m}\int_0^T f(\tau)\,d\tau\cdot\left[\frac{1}{3}\left(1+2\frac{t^2}{T^2}\right)\int_0^T f(\tau)\,d\tau\right] - N\xi(t)\frac{t}{T}\int_0^T f(\tau)\,d\tau\right\}}\,. \\ & \cdot\, e^{-\frac{i}{\hbar}\left[\xi(t) + \frac{t^2}{2mT}\int_0^T f(\tau)\,d\tau\right]\sum_{j=1}^{N}\hat{p}_j}\,.\end{aligned} \tag{5.99}$$

5.3.1 APPLICABILITY OF OUR RESULTS

We pause here to comment on the generality of our findings. The main results in the case $\int_0^T f(\tau)\,d\tau = 0$ are Eqs. (5.96) and (5.97). They are valid for any form of the two-body potential V_{2b} and therefore for any interacting Hamiltonian (5.86), integrable or not. The crucial assumption we have made is that the two-body potential V_{2b} depends only on the relative distance $x_i - x_j$, otherwise $V_{2b}(x_i, x_j)$ would be in general different from $V_{2b}(y_i, y_j)$ when the transformation $y_j = x_j - \xi(t)$ is done. Since $V_{2b}(x_j - x_i) = V_{2b}(y_j - y_i)$ then the equations of motions for the wavefunction $\eta(y_1, \ldots, y_N, t)$ are exactly the same of those for the wavefunction $\chi(x_1, \ldots, x_N, t)$, except for the fact that the time–periodic linear potential has been removed. Notice, that in presence of one-body potentials $V_{1b}(x_i)$, breaking translational invariance, this fact would be no longer valid. When the interacting many-body Hamiltonian has only the kinetic term plus a time–independent two-body

potential V_{2b} depending only on the relative distance between the particles, then the conservation of the total momentum of the undriven Hamiltonian $\hat{H}_0$ is guaranteed:

$$\left[\hat{H}_0, \hat{P}\right] = 0\,,$$

a relation we subsequently used to determine the Floquet Hamiltonian, the micro-motion operator and the expression of the energy at time t.

We conclude that if, in addition, $\hat{H}_0$ turns out to be integrable, then the associated Floquet Hamiltonian is integrable too. We have presented the analysis for a many-body systems made of bosons, but it could equally be applied to a many-body systems made of fermions or Bose–Fermi mixtures. In few words, our results are valid for any one–dimensional integrable Hamiltonian in the *continuum*. This also includes the Gaudin–Yang model for one–dimensional Fermi gases, integrable Bose-Fermi mixtures, integrable multi-component Lieb–Liniger Bose gases and Calogero–Sutherland models (in the absence of external one-body harmonic potential) [58, 59, 69, 115].

Hence, having in mind the broad generality of our results, we shall present below a study of the paradigmatic Lieb–Liniger model driven by an external linear time–dependent potential whose driving function has a vanishing integral over a driving period.

It is therefore clear that since the Gaudin–Yang model for a one–dimensional Fermi gas is described by the same Hamiltonian of the Lieb–Liniger model (cfr Chatper 1), but with the only difference of having attractive interactions (*i.e.* the sign of the interaction parameter will change), the method presented will apply also in that case. Finally when one considers Bose-Fermi mixtures or multi-component Lieb–Liniger Bose gases, the Hamiltonian has more terms, for intra and interspecies interactions, but each of them separately satisfies the required conditions of having two-body potentials which depend only on the relative distances among particles and our method can be applied as well. Let us take as an example the case of a mixture of two distinguishable bosonic species labeled with A and B. The Hamiltonian of the system reads [252]

$$H = \sum_{\sigma=A,B} H_\sigma + H_{AB}\,,$$

where the single-species Hamiltonian is:

$$H_\sigma = \sum_{j=1}^{N_\sigma}\left[-\frac{\hbar^2}{2\,m_\sigma}\frac{\partial^2}{\partial x_{\sigma,j}^2} + x_{\sigma,j}\,f(t)\right] + \lambda_\sigma \sum_{j>i}\delta(x_{\sigma,j} - x_{\sigma,i})\,,$$

while the interspecies Hamiltonian reads:

$$H_{AB} = \lambda_{AB}\sum_{a=1}^{N_A}\sum_{b=1}^{N_B}\delta(x_{A,a} - x_{B,b})\,,$$

where N_A and N_B are the number of particles of species A and B respectively. Therefore, when the driving function $f(t)$ is the same for both the species, the method which consists of making a gauge transformation of the wavefunction and a translation will allow one to eliminate the external linear potential separately in H_A and H_B, while the interspecies Hamiltonian will not be affected at all if the masses of the two species are equal (more on this case will be discussed later, when we will deal with the quantum fall of an atom). In the more specific case when the undriven mixture is integrable, which happens when the

masses of bosons and fermions are the same and when they have equal repulsive interactions between Bose-Fermi and Bose-Bose particles [76], then also the Floquet Hamiltonian will be integrable for the same reasons that we have seen for a generic interacting potential $V_{2\mathrm{b}}(x_i, x_j)$.

5.3.2 DRIVEN LIEB–LINIGER GAS

The Lieb–Liniger model describes a gas of N bosons with δ-contact repulsive interactions in $D = 1$ [53], that is $V_{2b}(x_j - x_i) = \lambda\delta(x_j - x_i)$, with $\lambda > 0$ the interaction parameter. The dynamics of the Lieb–Liniger model in a linear potential was studied in [253], while we refer to [241,242,254] for a study of the classical counterpart of the Lieb–Liniger model, the nonlinear Schrödinger equation, in the presence of a time–dependent linear potential.

The undriven Hamiltonian of this system, *i.e.*

$$\hat{H}_0 = \sum_{j=1}^{N} \frac{\hat{p}_j^2}{2m} + \lambda \sum_{j<i} \delta(x_j - x_i) \tag{5.100}$$

is an integrable Hamiltonian and an exact expression of its eigenfunction can be obtained using the Bethe ansatz technique [57, 58]. Therefore we can write the eigenfunctions for the Floquet Hamiltonian (5.96) as Bethe ansatz states:

$$\tilde{u}(x_1, \ldots, x_N) = \sum_P A_P(Q)\, e^{\frac{i}{\hbar}\sum_{j=1}^{N} k_{P_j} x_j}\,, \tag{5.101}$$

where Q is the permutation index which specifies the order of the particles, while P is the permutation index of the pseudo-rapidities k_j, which are undetermined until boundary conditions are chosen [58, 59] (in a subsequent Section we will discuss about the relation between the boundary conditions and the external linear potential). The amplitudes $A_P(Q)$ can be written as:

$$A_P = \mathcal{N}\,(-1)^P \prod_{j<l} \left(k_{P_j} - k_{P_l} + i\frac{m\lambda}{\hbar^2} \right)\,,$$

where $\mathcal{N}$ represents the normalization factor. The respective quasi-energies are given by:

$$\mathcal{E}_F = \frac{\hbar^2}{2m} \sum_{j=1}^{N} k_j^2 + \hbar\frac{\xi(T)}{T} \sum_{j=1}^{N} k_j - N\hbar\frac{\theta(T)}{T}\,. \tag{5.102}$$

For convenience, we will indicate the state $\tilde{u}$ as $\mathrm{BAS}(k_1, \ldots, k_N)$, where BAS stands for *Bethe Ansatz State*. In order to understand what happens for the N–body case, it is convenient to start from the two-body problem. In this case we can write [68]

$$\mathrm{BAS}(k_1, k_2) = g(x_1, x_2)\theta_H(x_2 - x_1) + g(x_2, x_1)\theta_H(x_1 - x_2)\,, \tag{5.103}$$

where $\theta_H(x)$ is the Heaviside step function, while:

$$g(x_1, x_2) = \left[i(k_1 - k_2) - \frac{m\lambda}{\hbar^2} \right] e^{i(k_1 x_1 + k_2 x_2)} + \left[i(k_1 - k_2) + \frac{m\lambda}{\hbar^2} \right] e^{i(k_2 x_1 + k_1 x_2)}\,.$$

Hence, $g(x_1+a,x_2+a)=g(x_1,x_2)\,e^{ia(k_1+k_2)}$ for generic a, and the action of the micromotion operator (5.97) on the BAS will give the following Floquet modes:

$$u(t)=\mathrm{BAS}\left(k_1-\frac{1}{\hbar}\int_0^t f(\tau)\,d\tau,k_2-\frac{1}{\hbar}\int_0^t f(\tau)\,d\tau)\right)\,e^{i(k_1+k_2)t\left[\frac{\xi(T)}{T}-\frac{\xi(t)}{t}\right]}\,e^{-i\left\{\frac{1}{m\hbar}\int_0^t d\tau\left[\int_0^\tau f(\tau')\,d\tau'\right]^2+2\frac{t}{T}\theta(T)\right\}}. \quad (5.104)$$

Apart from a phase, the Floquet modes are then Bethe ansatz states with shifted pseudomomenta. The Floquet states from Eqs. (5.23) and (5.102), read:

$$\psi_F(t)=\mathrm{BAS}\left(k_1-\frac{1}{\hbar}\int_0^t f(\tau)\,d\tau,k_2-\frac{1}{\hbar}\int_0^t f(\tau)\,d\tau)\right)\,e^{-i(k_1+k_2)\xi(t)}\,e^{-\frac{i}{m\hbar}\int_0^t d\tau\left[\int_0^\tau f(\tau')\,d\tau'\right]^2}, \quad (5.105)$$

and the total momentum expectation value of the Floquet states is therefore $\left\langle\hat{P}\right\rangle_F(t)=\hbar\,(k_1+k_2)-\frac{2}{\hbar}\int_0^t f(\tau)\,d\tau$. These results may be easily extended to the many-body case. The Floquet modes can be written as:

$$\begin{aligned}u(t)\;&=\;\mathrm{BAS}\left(k_1-\frac{1}{\hbar}\int_0^t f(\tau)\,d\tau,\ldots,k_N-\frac{1}{\hbar}\int_0^t f(\tau)\,d\tau)\right)\,e^{it\left[\frac{\xi(T)}{T}-\frac{\xi(t)}{t}\right]\sum_{j=1}^N k_j}\,\cdot\\ &\cdot\,e^{-i\left\{\frac{N}{2m\hbar}\int_0^t d\tau\left[\int_0^\tau f(\tau')\,d\tau'\right]^2+N\frac{t}{T}\theta(T)\right\}},\end{aligned} \quad (5.106)$$

while the Floquet states read:

$$\begin{aligned}\psi_F(t)\;&=\;\mathrm{BAS}\left(k_1-\frac{1}{\hbar}\int_0^t f(\tau)\,d\tau,\ldots,k_N-\frac{1}{\hbar}\int_0^t f(\tau)\,d\tau)\right)\,e^{-i\xi(t)\sum_{j=1}^N k_j}\,\cdot\\ &\cdot e^{-i\frac{N}{m\hbar}\int_0^t d\tau\left[\int_0^\tau f(\tau')\,d\tau'\right]^2}.\end{aligned} \quad (5.107)$$

The total momentum of the Floquet states is then:

$$\left\langle\hat{P}\right\rangle_F(t)=\hbar\sum_{j=1}^N k_j-\frac{N}{\hbar}\int_0^t f(\tau)\,d\tau\,. \quad (5.108)$$

In particular one can calculate the time evolution of a generic wavepacket for this system as:

$$\chi(x_1,\ldots,x_N,t)=\int A(k_1,\ldots,k_N)\,\psi_F(t)\,d^Nk\,, \quad (5.109)$$

which is an extension of the one-body equation (5.24).

It is worth stressing that this is a non-trivial expansion to evaluate: Indeed, once the initial wavepacket has been chosen at $t=0$, one needs to evaluate the time–independent amplitudes $A(k_1,\ldots,k_N)$ inverting the integral by multiplying by $\psi_F^*(t)$, and then evaluate the N-dimensional integral on the right hand side.

5.3.3 BOUNDARY CONDITIONS AND A POSSIBLE EXPERIMENTAL REALIZATION

The Floquet eigenfunctions in Eq. (5.101) are defined in terms of the pseudorapidities k_j obtained from the coordinate Bethe ansatz approach, ones proper boundary conditions

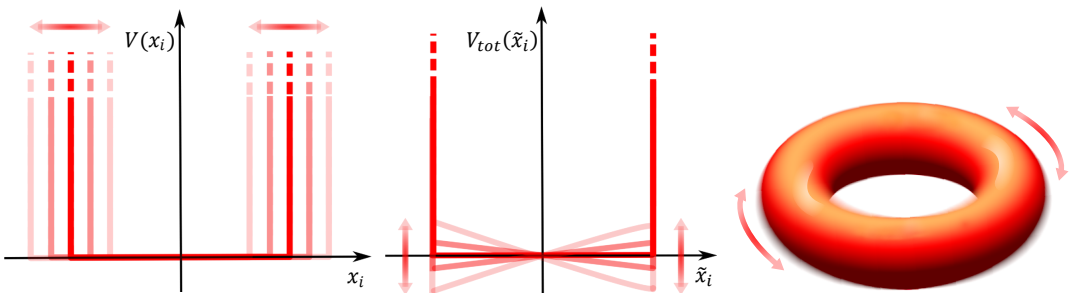

Figure 5.5: Left: pictorial visualization of the motion of a hard wall box. Center: the respective potential seen in the comoving frame of reference. Right: periodic rotation of a ring potential.

are defined, for example one may think to use periodic boundary conditions (PBC). An acute reader may object to the use of PBC in presence of an oscillating linear potential and, of course, he/she would have a good reason for that. Notice that confining the $1D$ Bose gas in a hard-wall potential and periodically moving the hard-wall potential back and forth (see Fig. 5.5-left, center), the proper boundary conditions to impose on such a system are instead the open boundary conditions (OBC) (see the discussion in Appendix 5.5.B). However, confining the gas in a $1D$ ring and periodically rotating the ring potential (see Fig. 5.5-right), with the condition that at stroboscopic times $f(t)$ vanishes, the proper boundary conditions of the system are the PBC. It is crucial that $f(t)$ vanishes at stroboscopic times: Indeed, if this condition holds and if the initial state is homogeneous in space, nothing at stroboscopic times changes, consistently with the fact that the potential is in turn translationally invariant. This discussion suggests that a suitable way to experimentally realise a periodically tilted $1D$ LL model is to shake the confining waveguide (possibly ring-shaped to implement PBC for the LL models) in which the atoms are trapped.

Anyway, we remark here that in the case of a linear external potential acting on systems enclosed in a hard wall box, we cannot apply the above reasoning already from the one-particle case, and the problem needs to be treated numerically [45, 255]. This is due to the fact that the momentum operator of a particle constrained to move in a box is not an hermitian well-definite operator [256, 257], and it does not share the same eigenfunctions of $\hat{H}(t)$ and they do not commute, which is instead not the case when the particle moves on the real axis.

5.4 LATTICE SYSTEMS

In the case of a gradient magnetic field (eventually time dependent) acting on a lattice system [258–261] one may think to act in a similar way, by gauge transforming the Hamiltonian of the system using an operator $\mathcal{U}(t)$ analogues to: $e^{i\theta(x,t)}$. This method has been applied to the case of Bose–Hubbard model in [33], where the linear external driving has been washed out thanks to the gauge transformation. In the case of a high frequency perturbation, the Floquet Hamiltonian is proven to be the one of the undriven Bose–Hubbard model with a renormalized coefficient for the tunneling matrix element J_{eff}, which vanishes for certain frequencies giving rise to the notorious phenomenon of coher-

ent destruction of tunneling. In a very similar way, in [262] they were studying the XXZ spin chain under the action of a periodic driving of the form:

$$H_1(t) \;=\; \sum_{j=1}^{N} f_j(t)\,\sigma_z^j\,,$$

from which one can notice that the linearity of the external potential is translated into a linearity of the σ_z^j variables and not of the j-th dependence of the driving force $f_j(t)$, which can be of any form. They showed that performing a gauge transformation on the total Hamiltonian of the form: $\mathcal{U}(t) = \mathcal{T}\exp\left[-i\int_0^t H_1(\tau)\,d\tau\right]$, where $\mathcal{T}$ is the time ordering operator, this gives rise to a transformed Hamiltonian which, in the high frequency limit, is described by a Floquet Hamiltonian of an XXZ spin chain with no driving and with renormalized coefficients for the $\sigma_x^j\,\sigma_x^{j+1}$ and $\sigma_y^j\,\sigma_y^{j+1}$ variables.

Following this reasoning, we are able to tackle the problem of the transverse field Ising model with an additional longitudinal field, described by the Hamiltonian:

$$H(t) \;=\; J\sum_{j=1}^{N}\sigma_z^j\sigma_z^{j+1} + h\sum_{j=1}^{N}\sigma_x^j + \sum_{j=1}^{N} f_j(t)\sigma_z^j\,. \tag{5.110}$$

Passing from $H(t)$ of the driven transverse Ising model to: $\tilde{H}(t) = \mathcal{U}^\dagger(t)H(t)\mathcal{U}(t) - \mathcal{U}^\dagger(t)\partial_t\mathcal{U}(t)$, with $\mathcal{U}(t) = \mathcal{T}\exp\left[-i\sum_j\sigma_z^j\int_0^t f_j(\tau)\,d\tau\right]$, one gets:

$$\tilde{H}(t) \;=\; J\sum_{j=1}^{N}\sigma_z^j\sigma_z^{j+1} + h\sum_{j=1}^{N}\mathcal{U}^\dagger(t)\,\sigma_x^j\,\mathcal{U}(t)\,.$$

Now, from the Baker-Campbell-Hausdorff formula, we have that:

$$\begin{aligned}\mathcal{U}^\dagger(t)\,\sigma_x^{\tilde{j}}\,\mathcal{U}(t) \;\;=\;\; & \sigma_x^{\tilde{j}} + i\sum_j\int_0^t f_j(\tau)\,d\tau\left[\sigma_x^{\tilde{j}}\,,\,\sigma_z^j\right] - \frac{1}{2}\Bigg[\sum_j\sigma_z^j\int_0^t f_j(\tau)\,d\tau\,,\\ & \left[\sigma_x^{\tilde{j}}\,,\,\sum_j\sigma_z^j\int_0^t f_j(\tau)\,d\tau\right]\Bigg] + \dots\,,\end{aligned}$$

and by simply evaluating the commutators we finally get:

$$\tilde{H}(t) \;=\; J\sum_{j=1}^{N}\sigma_z^j\sigma_z^{j+1} + h\sum_{j=1}^{N}\cos\left[2\int_0^t f_j(t)\,dt\right]\sigma_x^j - h\sum_{j=1}^{N}\sin\left[2\int_0^t f_j(t)\,dt\right]\sigma_y^j\,,$$

i.e. a transverse Ising model with longitudinal and transverse external fields both depending on time. In the high frequency limit, $\hbar\omega \gg J$, we can average over the rapid oscillations and the time evolution operator at stroboscopic times may be written in terms of the cycle average of the Hamiltonian $\tilde{H}(t)$, *i.e.*

$$U(T) \;=\; \mathcal{T}\exp\left[-\frac{i}{\hbar}\int_0^T\tilde{H}(t)\,dt\right] \;\simeq\; e^{-i\,T\,H_{\text{eff}}}\,, \tag{5.111}$$

with:

$$H_{\text{eff}} \;=\; \frac{1}{T}\int_0^T\tilde{H}(t)\,dt\,. \tag{5.112}$$

This is also called rotating-wave approximation [33], and allows to obtain an approximation valid in the high frequency limit for the Floquet Hamiltonian of the system, which can be read from Eq. (5.111) and it is:

$$H_F \;=\; J\sum_{j=1}^{N}\sigma_z^j\sigma_z^{j+1}+\sum_{j=1}^{N}J^j_{\rm eff}\,\sigma_x^j-\sum_{j=1}^{N}J^j_{\rm eff'}\,\sigma_y^j\,. \tag{5.113}$$

The two coefficients for σ_x and σ_y read respectively:

$$J^j_{\rm eff} \;=\; \frac{h}{T}\int_0^T\cos\left[2\int_0^t f_j(\tau)\,d\tau\right]dt\,, \tag{5.114}$$

and

$$J^j_{\rm eff'} \;=\; \frac{h}{T}\int_0^T\sin\left[2\int_0^t f_j(\tau)\,d\tau\right]dt\,. \tag{5.115}$$

This is very interesting, indeed if we assume that: $f_j(t) \;=\; A_j\cos(\omega t)$, with A_j some coefficients in general different for each lattice site, then we have:

$$J^j_{\rm eff} \;=\; h\,J_0\left(\frac{2A_j}{\omega}\right)\,,\qquad\qquad J^j_{\rm eff'} \;=\; 0\,, \tag{5.116}$$

where $J_0(x)$ is the zeroth order Bessel function of the first kind, and therefore the Floquet Hamiltonian in the high frequency limit is an Hamiltonian of a transverse field Ising model with a renormalized external field $J^j_{\rm eff}$. Notice that if the coefficients A_j are independent on the lattice site, *i.e.* $A_j = A$, then the Floquet Hamiltonian is an integrable Hamiltonian since it resembles the one of the transverse field Ising model. More interesting is the case in which: $\frac{2A_j}{\omega}$ is a zero of the Bessel function $J_0(x)$: In this case the dynamic of the system at stroboscopic times is frozen, or, in other words, the spin flips originated by the Pauli matrix σ_x are suppressed. This is the analogous of the phenomena of coherent destruction of tunneling [33], but for spin systems such as the transverse field Ising model.

Finally notice that if we used the rotating-wave approximation on the original Hamiltonian Eq.(5.110), we would obtain

$$H_{\rm eff} \;=\; J\sum_{j=1}^{N}\sigma_z^j\sigma_z^{j+1}+h\sum_{j=1}^{N}\sigma_x^j+\frac{1}{T}\sum_{j=1}^{N}\left[\int_0^T f_j(t)\,dt\right]\sigma_z^j\,, \tag{5.117}$$

and if the integral over one stroboscopic period of the driving function $f_j(t)$ vanishes [*e.g.* for $f_j(t) = A_j\sin(\omega t)$], then the Floquet (effective) Hamiltonian is simply the one of the transverse field Ising model, without a renormalized coefficient for the transverse field.

Notice that in the XXZ and Ising spin chains, one may also think to pass to the field operators c_j via the Jordan-Wigner transformation and the problem will maps to the Wannier-Stark problem of electrons in a lattice subjected to a time–varying force. Then one may proceed by washing away the external linear term of the form: $\sum_j f_j(t)c_j^\dagger c_j$, in a similar way as was done by Eckardt [33].

Let us finally appreciate the difference in the case of a continuous space: For a one-body problem described with the Schrödinger equation in (5.5), we may gauge transform the Hamiltonian with $\mathcal{U}(t) = e^{i\theta(x,t)}$, and the Schrödinger equation will be rewritten as:

$$i\hbar\frac{\partial\eta}{\partial t} \;=\; \left[\frac{\hat p^2}{2m}-\frac{\hat p}{m}\int_0^t f(\tau)\,d\tau\right]\eta(t)\,, \tag{5.118}$$

therefore in order to eliminate the p-linear term from the above equation, one should pass from the x variable to $y(t) = x - \xi(t)$ as it was done in previous sections. This last passage is the one which differ from the lattice case problems.

In a complete similar way as what we did up to now, we can generalize our studies to the case of a three–dimensional quantum system subjected to a gravitational force. We will first show the relation with the Einstein's equivalence principle, and then we will deal with the single–, two– and many–body quantum problem, presenting as examples the case in which an atom falls under the action of gravity.

5.5 FREE FALL OF A QUANTUM SYSTEM

In Classical Mechanics one of the first paradigmatic problems that students encounter in their study is the dynamics of a falling body, *i.e.* an object pulled down to the ground (*e.g.* from the Pisa's tower) by the constant force of Earth's gravity. However, amazingly enough, the same problem is rarely discussed in a course of Quantum Mechanics and the reason is due to the sharp contrast of the physical simplicity of the problem and the difficulty of its mathematical description due to how basic Quantum Mechanics courses are structured, largely based on the solution of the time-dependent Schrödinger equation $i\hbar\frac{\partial\psi}{\partial t} = H\psi$ for the wavefunction ψ in terms of the eigenfunctions and eigenvalues of the time-independent equation $H\psi = E\psi$. Indeed, in the traditional quantum mechanics approach to the problem of determining the wavefunction at time t, it is necessary to involve the Airy functions and the projection of the wavefunction of the falling body into this set of eigenfunctions. Here we show that an alternative and easier way to deal with the quantum treatment of the problem of the falling body is both pedagogically very simple to introduce and at the same time general enough to be applicable to the single particle case and to general quantum many–body systems. It is based on the exact same idea that we saw in the one–dimensional regime, *i.e.* we will perform a gauge transformation of the wavefunction in correspondence to a change of references frames, from the inertial frame of the laboratory to the accelerated frame of the falling body. In the new frame there is of course no longer any gravitational effect and therefore the system appears to be *"free"*, *i.e.* non subject to the gravity.

5.5.1 THE QUANTUM EINSTEIN'S ROCKET

Let us begin by considering the notorious Einstein's *gedankenexperiment* of a rocket of length L in an empty space (*i.e.* very far from any other celestial body), and subject to an acceleration equal to $g \simeq 9.81\frac{m}{s^2}$. Suppose that inside the rocket there is a single quantum object, *e.g.* an Einsteinium atom, for which the relevant Schrödinger equation is simply:

$$i\hbar\frac{\partial}{\partial t}\chi(x,t) = \left[-\frac{\hbar^2}{2m}\frac{\partial^2}{\partial x^2} + V_r(x,t)\right]\chi(x,t)\,, \tag{5.119}$$

where we've chosen x as the vertical direction along which the rocket is moving, while $V_r(x,t)$ is a potential representing the confining action of the rocket walls during the

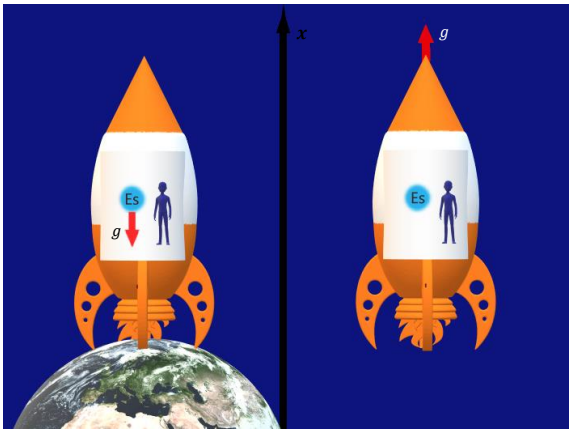

Figure 5.6: Pictorial visualization of the Einstein's *gedankenexperiment*. The effect of an inertial force $F = -m\,g$ in the Einsteinium atom due to the acceleration of the rocket (right side picture) is the same as if the rocket would be at rest on Earth (left side picture).

motion. If we now pass to the reference frame comoving with the rocket, by changing the spatial variable from x to $\tilde{x} = x - g\,\frac{t^2}{2}$, the Schrödinger equation reads:

$$i\hbar\frac{\partial}{\partial t}\chi(\tilde{x},t) = \left[-\frac{\hbar^2}{2m}\frac{\partial^2}{\partial\tilde{x}^2} + V_r(\tilde{x}) + i\,\hbar\,g\,t\,\frac{\partial}{\partial\tilde{x}}\right]\chi(\tilde{x},t)\,, \tag{5.120}$$

where the rocket potential in the new reference is denoted by $V_r(\tilde{x})$.

If we now transform the wavefunction as:

$$\chi(\tilde{x},t) \equiv \exp\left[\frac{i\,m\,gt}{\hbar}\left(\tilde{x} + \frac{g\,t^2}{2}\right)\right]\bar{\chi}(\tilde{x},t)\,, \tag{5.121}$$

we can get rid of the term linear in $\hat{p}$, *i.e.* in $\frac{\partial}{\partial\tilde{x}}$, in Eq. (5.120) and the Schrödinger equation becomes:

$$i\hbar\frac{\partial}{\partial t}\bar{\chi}(\tilde{x},t) = \left[-\frac{\hbar^2}{2m}\frac{\partial^2}{\partial\tilde{x}^2} + V_r(\tilde{x}) + m\,g\,\tilde{x}\right]\bar{\chi}(\tilde{x},t)\,. \tag{5.122}$$

Therefore in the comoving frame of reference, the Einsteinium atom feels the presence of a gravitational force

$$F = -\frac{\partial V}{\partial x} = -m\,g \tag{5.123}$$

pulling it to the ground of the rocket, as sketched in Fig. 5.6. This is essentially the Einstein's equivalence principle, which states that there is no difference between the gravitational and a fictitious force experienced by an observer in a non-inertial frame of reference. For a more detailed discussion on the Einstein's equivalence principle in a Quantum Mechanics context see [263].

In the following we are going to discuss how to deal with a Schrödinger equation of the form of (5.122), performing a gauge transformation on the wavefunction to wash away the gravitational potential. Notice that the above derivation can and will be repeated as well for a many–body quantum system made of interacting particles.

5.5.2 FREE FALL OF A QUANTUM PARTICLE

It is simple to extend the analysis which we presented above to the case of a single particle falling along the x–direction (once the axis are opportunely chosen) in a three–dimensional space. In this case the Schrödinger equation reads:

$$i\hbar\frac{\partial}{\partial t}\chi(\mathbf{r},t) \;=\; i\hbar\frac{\partial}{\partial t}\chi(x,y,z,t) \;=\; \left(-\frac{\hbar^2}{2m}\nabla_x^2 + m\,g\,x\right)\chi(\mathbf{r},t)\,, \tag{5.124}$$

where the vector position $\mathbf{r}$ is expressed in Cartesian coordinates in the second equality, and we have denoted with:

$$\nabla_x^2 \;\equiv\; \frac{\partial^2}{\partial x^2} + \frac{\partial^2}{\partial y^2} + \frac{\partial^2}{\partial z^2}$$

the Laplacian. Proceeding in the same way as for the $1D$ case, we perform a gauge transformation on the wavefunction

$$\chi(\mathbf{r},t) \;=\; e^{i\,\theta(x,t)}\,\eta(\rho(t),y,z,t)\,, \tag{5.125}$$

where $\rho(t) = x - \xi(t)$, and the gauge phase $\theta(x,t)$ and the translational parameter $\xi(t)$ satisfy Eqs. (5.7) and (5.8). Once we solve the differential equations (5.11) with the trivial initial conditions $\xi(0) = d\xi(0)/dt = 0$ and $\Gamma(0) = 0$, we get the following expression for the gauge phase:

$$\theta(x,t) \;=\; -\frac{m\,g\,t}{\hbar}\,x - \frac{m\,g^2\,t^3}{6\,\hbar}\,, \tag{5.126}$$

while the "translational" parameter ξ reads:

$$\xi(t) \;=\; -\frac{g\,t^2}{2}\;. \tag{5.127}$$

Within these conditions, the Schrödinger equation (5.124) is reduced to the free Schrödinger equation for $\eta(\rho,y,z,t)$:

$$i\hbar\frac{\partial}{\partial t}\eta(\rho,y,z,t) \;=\; -\frac{\hbar^2}{2m}\nabla_\rho^2\,\eta(\rho,y,z,t)\,, \tag{5.128}$$

where we define:

$$\nabla_\rho^2 \;\equiv\; \frac{\partial^2}{\partial \rho^2} + \frac{\partial^2}{\partial y^2} + \frac{\partial^2}{\partial z^2}\,.$$

Therefore choosing $\theta(x,t)$ to be (5.126) and $\xi(t)$ given by Eq. (5.127), we can rewrite (5.125) with respect to the evolution and translation operators as:

$$\chi(\mathbf{r},t) \;=\; \exp\left\{i\theta(x,t) - i\frac{t}{\hbar}\frac{\hat{\mathbf{p}}^{\,2}}{2m} - i\frac{\xi(t)}{\hbar}\hat{p}_x\right\}\;\chi(\mathbf{r},0)\,, \tag{5.129}$$

where we have defined:

$$\hat{\mathbf{p}}^{\,2} \;=\; \hat{p}_x^2 + \hat{p}_y^2 + \hat{p}_z^2\,,$$

with the momentum operators acting on different Cartesian coordinates as $\hat{p}_\alpha \to -i\,\hbar\,\frac{\partial}{\partial\alpha}$. We are now able to study how expectation values of different physical quantities evolve. First we redefine expectation values of position operator and its powers as:

$$\left\langle \alpha^{\mathcal{N}} \right\rangle (t) \equiv \left\langle \chi(\mathbf{r},t)|\,\hat{\alpha}^{\mathcal{N}}\,|\chi(\mathbf{r},t)\right\rangle = \int_{-\infty}^{\infty} dx \int_{-\infty}^{\infty} dy \int_{-\infty}^{\infty} dz\, |\chi(\mathbf{r},t)|^2\, \alpha^{\mathcal{N}}\,, \quad (5.130)$$

where α can be the x, y or z coordinate, while for the powers of the momentum:

$$\left\langle p_\alpha^{\mathcal{N}} \right\rangle (t) \equiv \left\langle \chi(\mathbf{r},t)|\,\hat{p}_\alpha^{\mathcal{N}}\,|\chi(\mathbf{r},t)\right\rangle = (-i\hbar)^{\mathcal{N}} \int_{-\infty}^{\infty} dx \int_{-\infty}^{\infty} dy \int_{-\infty}^{\infty} dz\, \chi^*(\mathbf{r},t)\, \frac{\partial^{\mathcal{N}}}{\partial\alpha^{\mathcal{N}}}\chi(\mathbf{r},t)\,, \quad (5.131)$$

where α labels the x, y or z component. From Eq. (5.129) it is straightforward to perform the calculation of expectation values of different coordinates, and since operators acting on different spaces commutes (like $\hat{x}$ and $\hat{p}_y$ or $\hat{p}_y$ and $\hat{p}_z$ and so on) then the motion on y and z directions is trivially evaluated to be the free one ($g = 0$), while for the x component one relies on the results presented previously for the one–dimensional case.

Notice that by writing the vector position in three dimensions as:

$$\mathbf{r} = x\cdot\mathbf{e}_x + y\cdot\mathbf{e}_y + z\cdot\mathbf{e}_z\,, \quad (5.132)$$

where $\mathbf{e}_x$, $\mathbf{e}_y$ and $\mathbf{e}_z$ are the usual unit vectors in Cartesian coordinate system, *i.e.*

$$\mathbf{e}_x = \begin{pmatrix}1\\0\\0\end{pmatrix}, \quad \mathbf{e}_y = \begin{pmatrix}0\\1\\0\end{pmatrix}, \quad \mathbf{e}_z = \begin{pmatrix}0\\0\\1\end{pmatrix}, \quad (5.133)$$

then the expectation value of the vector position $\mathbf{r}$ can be written in terms of its single components expectation values:

$$\langle \mathbf{r}\rangle (t) = \mathbf{e}_x\cdot\langle x\rangle (t) + \mathbf{e}_y\cdot\langle y\rangle (t) + \mathbf{e}_z\cdot\langle z\rangle (t)\,, \quad (5.134)$$

and similarly can be done for the squared vector position $\mathbf{r}^2 = \mathbf{r}\cdot\mathbf{r}$, which will read:

$$\left\langle \mathbf{r}^{\,2}\right\rangle (t) = \left\langle x^2\right\rangle (t) + \left\langle y^2\right\rangle (t) + \left\langle z^2\right\rangle (t)\,. \quad (5.135)$$

The same decomposition in terms of the single components expectation values obviously holds also for the momentum operators.

So, in summary, the motion of a wavepacket in three–dimensions under the action of gravity is described by a spreading which is completely analogous to the spreading of a free (no gravity) expansion in all directions, while its center of mass moves along the direction of the gravitational force as a classical particle would do.

5.5.3 FREE FALL OF TWO INTERACTING PARTICLES

We now study a three–dimensional system made of 2 interacting particles subject to gravity. The Schrödinger equation reads:

$$i\,\hbar\frac{\partial}{\partial t}\chi(\mathbf{r}_1,\mathbf{r}_2,t) = \left[-\frac{\hbar^2}{2m}\left(\nabla_{r_1}^2 + \nabla_{r_2}^2\right) + V(|r_2 - r_1|) + mg\,(x_1 + x_2)\right]\chi(\mathbf{r}_1,\mathbf{r}_2,t)\,,$$

(5.136)

where

$$\nabla^2_{r_j} \equiv \frac{\partial^2}{\partial x_j^2} + \frac{\partial^2}{\partial y_j^2} + \frac{\partial^2}{\partial z_j^2}\,, \tag{5.137}$$

for $j = 1, 2$, and $V(|\mathbf{r}_2 - \mathbf{r}_1|)$ describes the interaction among particles and depends only on the distance between them:

$$|\mathbf{r}_2 - \mathbf{r}_1| = \sqrt{(x_2 - x_1)^2 + (y_2 - y_1)^2 + (z_2 - z_1)^2}\,. \tag{5.138}$$

In order to solve the Schrödinger equation, we employ the same method outlined in the previous Section: We perform a gauge transformation on the wavefunction

$$\chi(\mathbf{r}_1, \mathbf{r}_2, t) = e^{i[\theta(x_1,t)+\theta(x_2,t)]}\, \eta(\boldsymbol{\varrho}_1(t), \boldsymbol{\varrho}_2(t), t)\,, \tag{5.139}$$

where $\boldsymbol{\varrho}_j(t) = (\rho_j\,,\, y_j\,,\, z_j)$, with $\rho_j(t) = x_j - \xi(t)$, while $\theta(x_j, t)$ and $\xi(t)$ obey Eqs. (5.8) - (5.7) for $x = x_j$ and with $j = 1, 2$. Notice that because the interacting potential depends on distance among the particles, it will remain of the same form after the definition of the new spatial variables $\rho_j(t)$ and $\boldsymbol{\varrho}_j(t)$. Using the ansatz (5.10) and by choosing $\xi(0) = d\xi(0)/dt = 0$ and $\Gamma(0) = 0$ we have that $\theta(x_j, t)$ is given by (5.126), while $\xi(t)$ is given by (5.127). Under these conditions, $\eta(\varrho_1, \varrho_2, t)$ will satisfy the free Schrödinger equation for two interacting particles

$$i\hbar\frac{\partial}{\partial t}\eta(\boldsymbol{\varrho}_1, \boldsymbol{\varrho}_2, t) = \left[-\frac{\hbar^2}{2m}\left(\nabla^2_{\varrho_1} + \nabla^2_{\varrho_2}\right) + V(|\varrho_2 - \varrho_1|)\right]\eta(\boldsymbol{\varrho}_1, \boldsymbol{\varrho}_2, t)\,, \tag{5.140}$$

with:

$$\nabla^2_{\varrho_j} \equiv \frac{\partial^2}{\partial \rho_j^2} + \frac{\partial^2}{\partial y_j^2} + \frac{\partial^2}{\partial z_j^2}\,, \tag{5.141}$$

for $j = 1, 2$. Therefore if one knows how to solve Eq. (5.140), then the complete solution of (5.136) reads:

$$\chi(\mathbf{r}_1, \mathbf{r}_2, t) = \exp\left[-i\frac{m\,g\,t}{\hbar}\left(\frac{g\,t^2}{3} + x_1 + x_2\right)\right]\,\eta\left(x_1 + \frac{g\,t^2}{2}, y_1, z_1; x_2 + \frac{g\,t^2}{2}, y_2, z_2; t\right)\,, \tag{5.142}$$

where we have used the solution of the original Schrödinger equation with a gravitational force term, with respect to the free ($g = 0$) solution of (5.140).

We can now ask the same questions as before: If we start from a generic wavepacket $\chi(\mathbf{r}_1, \mathbf{r}_2, 0)$ and we let it evolve under the action of gravity, how do its variances and expectation values of powers of position behave? Let us define as usual:

$$\left\langle \alpha_j^{\mathcal{N}} \right\rangle(t) \equiv \left\langle \chi(\mathbf{r}_1, \mathbf{r}_2, t)|\, \hat{\alpha}_j^{\mathcal{N}}\, |\chi(\mathbf{r}_1, \mathbf{r}_2, t)\right\rangle = \int dr_1 \int dr_2\, |\chi(\mathbf{r}_1, \mathbf{r}_2, t)|^2\, \alpha_j^{\mathcal{N}} \tag{5.143}$$

with α which can be either x, y or z, while $j = 1, 2$ labels the particles. For the expectation value of powers of the momenta $\hat{p}_{\alpha_j}$ for $j = 1, 2$ we have:

$$\left\langle p_{\alpha_j}^{\mathcal{N}} \right\rangle(t) \equiv \left\langle \chi(\mathbf{r}_1, \mathbf{r}_2, t)|\, \hat{p}_{\alpha_j}^{\mathcal{N}}\, |\chi(\mathbf{r}_1, \mathbf{r}_2, t)\right\rangle = (-i\hbar)^{\mathcal{N}} \int dr_1 \int dr_2\, \chi^*(\mathbf{r}_1, \mathbf{r}_2, t)\, \frac{\partial^{\mathcal{N}}}{\partial \alpha_j^{\mathcal{N}}}\chi(\mathbf{r}_1, \mathbf{r}_2, t)$$

(5.144)

with $\int dr_j = \int_{-\infty}^{\infty} dx_j \int_{-\infty}^{\infty} dy_j \int_{-\infty}^{\infty} dz_j$. For the initial conditions we take ($j = 1, 2$):

$$\langle \alpha_j \rangle (0) = \alpha_0^{(j)} , \qquad \left\langle p_{\alpha_j} \right\rangle (0) = p_{\alpha 0}^{(j)} , \tag{5.145}$$

It is actually very simple to prove that the same results for the position variables of the one particle case will hold, that is to say the variances of positions of the particles will behave as the free expanding case, while the expectation values of powers of the x component for positions have the same expressions of the one body case, see Eqs. (5.15) and (5.17), with an additional index $j = 1, 2$ to label the particles. For y and z components instead one has as result the formulas referring to $g = 0$, since the gravitational potential acts only along the x direction. The simplicity of this result comes from the fact that the commutators among operators acting on different particles vanish, therefore[1]:

$$\begin{aligned}
\left[\hat{x}_j, e^{-i\,a\,\hat{p}_{x_k}}\right] &= \hbar\, a\, e^{-i\,a\,\hat{p}_{x_k}}\, \delta_{j,k} , \\
\left[\hat{x}_j^2, e^{-i\,a\,\hat{p}_{x_k}}\right] &= e^{-i\,a\,\hat{p}_{x_k}} \left(a^2 - 2a\,\hat{x}_j\right) \delta_{j,k} , \\
\left[\hat{x}_j, e^{-i\,b\,\hat{p}_{x_k}^2}\right] &= 2\,\hbar\, b\, e^{-i\,b\,\hat{p}_{x_k}^2}\, \hat{p}_{x_k}\, \delta_{j,k} , \\
\left[\hat{x}_j^2, e^{-i\,b\,\hat{p}_{x_k}^2}\right] &= \left[4\,\hbar\, b\, e^{-i\,b\,\hat{p}_{x_k}^2} \hat{p}_{x_k}\, \hat{x}_j + (2\,\hbar\, b)^2\, e^{-i\,b\,\hat{p}_{x_k}^2} \hat{p}_{x_k}^2 + 2\,i\,\hbar^2\, b\, e^{-i\,b\,\hat{p}_{x_k}^2}\right] \delta_{j,k} ,
\end{aligned}$$

where $\delta_{j,k}$ is the Kronecker delta and we have rewritten $\theta(\hat{x}_j, t) = \hat{x}_j A + B$. We can rewrite (5.139) as:

$$\begin{aligned}
\chi(\mathbf{r}_1, \mathbf{r}_2, t) &= \exp\left\{ i[\theta(\hat{x}_1, t) + \theta(\hat{x}_2, t)] - i\frac{t}{\hbar}\left[\frac{\hat{p}_1^2 + \hat{p}_2^2}{2m} + V\left(|\hat{\varrho}_2 - \hat{\varrho}_1|\right)\right]\right\} \eta(\varrho_1, \varrho_2, 0) = \\
&= \exp\left\{ i[\theta(\hat{x}_1, t) + \theta(\hat{x}_2, t)] - i\frac{t}{\hbar}\hat{H}_0 - i\frac{\xi(t)}{\hbar}(\hat{p}_{x_1} + \hat{p}_{x_2})\right\} \chi(\mathbf{r}_1, \mathbf{r}_2, 0) ,
\end{aligned}$$

where we have defined:

$$\hat{H}_0 \equiv \frac{\hat{p}_1^2 + \hat{p}_2^2}{2m} + V\left(|\hat{\varrho}_2 - \hat{\varrho}_1|\right) . \tag{5.146}$$

One can repeat the exact same steps performed in the previous Section to obtain the expressions for the expectation values of different physical quantities. We summarize the results below:

$$\langle x_j \rangle (t) = \frac{t}{m}\, p_{x0}^{(j)} + \xi(t) + x_0^{(j)} , \tag{5.147}$$

$$\left\langle x_j^2 \right\rangle (t) = \xi^2(t) - 2\,\xi(t)\,\frac{t}{m}\, p_{x0}^{(j)} - 2\,\xi(t)\, x_0^{(j)} + \left\langle x_j^2 \right\rangle_{\text{free}} (t) , \tag{5.148}$$

$$\Delta x_j(t) = \sqrt{\left\langle x_j^2 \right\rangle (t) - \langle x_j \rangle^2 (t)} = (\Delta x_j)_{\text{free}} (t) , \tag{5.149}$$

where as usual we label with the subscript "free" the expectation values evaluated on the wavefunction $\eta(r_1, r_2, t)$ of the free expanding problem[2]. The same expressions, but with $g = 0$, are valid for the expectation values on the y and z components.

1 We report for convenience only the commutators on the x components, but the same commutator rules will be valid also for y and z.

2 Notice however that in order to evaluate them, one needs to know how to solve the Schrödinger equation (5.140) for that specific interacting potential.

We therefore conclude that our gauge transformation can be also used to reduce the initial Schrödinger equation describing the dynamic of two falling interacting particles to the simpler Schrödinger equation where no gravitational potential is present, and with the same interacting potential among the particles. The fundamental requirement is that the two–body potential depends only on the relative distance between the particles, after all a typical feature for a many–body system. When this condition holds, it is straightforward to generalize the results presented so far for a quantum many–body system subject to a gravitational force.

THE FREE FALL OF PROTIUM

Let us now extend our study to the case of the quantum fall of the *protium*, ^1H, *i.e.* the most common hydrogen isotope and also the simplest isotope, consisted only by one proton and one electron. The Hamiltonian of a protium falling in a three–dimensional space reads

$$i\hbar\frac{\partial}{\partial t}\chi(\mathbf{r}_p,\mathbf{r}_e,t) \;=\; \left[-\frac{\hbar^2}{2m_p}\nabla^2_{r_p}-\frac{\hbar^2}{2m_e}\nabla^2_{r_e}-\frac{e^2}{4\pi\varepsilon_0}\frac{1}{|r_p-r_e|}+m_p\,g\,x_p+m_e\,g\,x_e\right]\chi(\mathbf{r}_p,\mathbf{r}_e,t)\,, \tag{5.150}$$

where we have indicated with $\mathbf{r}_p$ ($\mathbf{r}_e$) the vector position of the proton (electron), while with m_p (m_e) the mass of the proton (electron). Notice that we have explicitly written the two–body interaction potential as the electric field potential, $V\left(|r_p-r_e|\right)=-\frac{e^2}{4\pi\varepsilon_0}\frac{1}{|r_p-r_e|}$, where e indicates the electric charge, and ε_0 the vacuum permittivity. In order to eliminate the external gravitational potential term, we should perform two distinct gauge transformations, one for the proton identified by:

$$\theta_p(x_p,t)=-\frac{m_p\,g\,t}{\hbar}\,x_p-\frac{m_p\,g^2\,t^3}{6\,\hbar}\,, \tag{5.151}$$

and one for the electron, identified instead by the gauge phase

$$\theta_e(x_e,t)=-\frac{m_e\,g\,t}{\hbar}\,x_e-\frac{m_e\,g^2\,t^3}{6\,\hbar}\,, \tag{5.152}$$

while the translational parameter reads as in Eq. (5.127), which therefore remains the same for the two particles. With these notations, the Eq. (5.139) becomes in this case

$$\chi(\mathbf{r}_p,\mathbf{r}_e,t) \;=\; e^{i[\theta_p(x_p,t)+\theta_e(x_e,t)]}\,\eta(\boldsymbol{\varrho}_p(t),\boldsymbol{\varrho}_e(t),t)\,, \tag{5.153}$$

where $\boldsymbol{\varrho}_j(t)=(\rho_j\,,\,y_j\,,\,z_j)$, with $\rho_j(t)=x_j-\xi_j(t)$, where $j=p$ or e, respectively for the proton and electron. Notice that since the translational parameter does not depend on the mass of the particle, after the translational transformation the electric field potential remain the same, *i.e.* $V\left(|r_p-r_e|\right)=V\left(|\varrho_p-\varrho_e|\right)$.

Using Eqs. (5.151), (5.152) and (5.127), we can write the Schrödinger equation for the wavefunction η as

$$i\hbar\frac{\partial}{\partial t}\eta(\boldsymbol{\varrho}_p,\boldsymbol{\varrho}_e,t) \;=\; \left[-\frac{\hbar^2}{2m_p}\nabla^2_{\varrho_p}-\frac{\hbar^2}{2m_e}\nabla^2_{\varrho_e}-\frac{e^2}{4\pi\varepsilon_0}\frac{1}{|\varrho_p-\varrho_e|}\right]\eta(\boldsymbol{\varrho}_p,\boldsymbol{\varrho}_e,t)\,, \tag{5.154}$$

which, once it has been solved, together with Eq. (5.153), completely solve the problem of the free fall of a protium isotope. The behaviour of interesting physical observables like the expectation values of positions operators are the same as the one reported in Eqs. (5.147) – (5.149), where m corresponds to the particle considered, *i.e.* $m=m_p$ for $j=p$, and $m=m_e$ for $j=e$.

5.5.4 FREE FALL OF A QUANTUM MANY–BODY SYSTEM

In the literature the problem of describing the motion of a "structured", many–body quantum system under the action of a gravitational potential has been addressed for various situations ranging from Bose–Einstein condensates [241, 242, 264, 265] to one–dimensional integrable systems [253, 266]. Nevertheless the case of a general three–dimensional many–body system subject to gravity can be explicitly addressed using the method described in the previous Sections, even though it should be now clear how to approach it.

Let us then focus our attention on the Schrödinger equation of N (for simplicity spinless) interacting particles subject to gravity along the x direction:

$$i\hbar\frac{\partial}{\partial t}\chi(\mathbf{r}_1,\ldots,\mathbf{r}_N,t) = \left[-\frac{\hbar^2}{2m}\sum_{j=1}^{N}\nabla^2_{r_j}+\sum_{j<k}V(|r_k-r_j|)+m\,g\sum_{j=1}^{N}x_j\right]\chi(\mathbf{r}_1,\ldots,\mathbf{r}_N,t)\,, \tag{5.155}$$

where the interacting potential depends on the relative distances among particles (5.138), and the kinetic part is written in terms of (5.137). To solve the Schrödinger equation we perform, as usual, a gauge transformation on the wavefunction

$$\chi(\mathbf{r}_1,\ldots,\mathbf{r}_N,t) = \prod_{j=1}^{N}e^{i\theta(x_j,t)}\,\eta(\boldsymbol{\varrho}_1(t),\ldots,\boldsymbol{\varrho}_N(t),t)\,, \tag{5.156}$$

which is a trivial generalization to the N particle case of Eq. (5.139). If the gauge phase $\theta(x_j,t)$ and the translational parameter $\xi(t)$ satisfy (5.8) and (5.7), respectively, with $x=x_j$, then $\eta(\varrho_1(t),\ldots,\varrho_N(t),t)$ is the solution of the free Schrödinger equation:

$$i\hbar\frac{\partial}{\partial t}\eta(\boldsymbol{\varrho}_1,\ldots,\boldsymbol{\varrho}_N,t) = \left[-\frac{\hbar^2}{2m}\sum_{j=1}^{N}\nabla^2_{\varrho_j}+\sum_{j<k}V(|\varrho_k-\varrho_j|)\right]\eta(\boldsymbol{\varrho}_1,\ldots,\boldsymbol{\varrho}_N,t)\,, \tag{5.157}$$

where the kinetic part is expressed in terms of (5.141) for every j. Using Eq. (5.156) one can easily prove that all results presented in the previous Sections, in particular those reported in Eqs. (5.147) – (5.149) and the same expressions for y and z coordinates but with $g=0$, also hold for the many–body system. Finally, using Eqs. (5.134) and (5.135) one can derive the laws describing the time evolution of expectation values of the position of the wavepacket. In particular, given that the system conserves the x, y and z-components of the total momentum, *i.e.* $\left[\hat{H}_0,\sum_{j=1}^{N}\hat{p}_{\alpha_j}\right]=0$ for $\alpha=x,y$ and z, one can explicitly work out the total momentum and the energy expectation values of the system in terms of the free case ($g=0$). Using the commutation relations founded previously, one gets that:

$$\langle P\rangle(t) = \left\langle\chi(\mathbf{r}_1,\ldots,\mathbf{r}_N,t)\middle|\hat{\mathbf{P}}\middle|\chi(\mathbf{r}_1,\ldots,\mathbf{r}_N,t)\right\rangle = P_0-\mathbf{e}_x\,N\,m\,g\,t\,, \tag{5.158}$$

where

$$\hat{\mathbf{P}} = \sum_{\alpha=x,y,z}\sum_{j=1}^{N}\mathbf{e}_\alpha\,\hat{p}_{\alpha_j} \tag{5.159}$$

represents the total momentum of the system, written in terms of the unit vectors defined in Eq. (5.133), while P_0 is the initial $t=0$ total momentum:

$$P_0 = \sum_{\alpha=x,y,z}\sum_{j=1}^{N}\mathbf{e}_\alpha\,p^{(j)}_{\alpha 0}\,. \tag{5.160}$$

For the total energy of the system instead, one can compute:

$$E(t) \,=\, \left\langle \hat{H} \right\rangle (t) \,=\, \left\langle \chi(\mathbf{r}_1,\ldots,\mathbf{r}_N,t) \middle| \frac{1}{2m}\hat{\mathbf{P}}^2 + \sum_{j<k} \hat{V}(|r_k - r_j|) + m\,g \sum_{j=1}^{N} \hat{x}_j \middle| \chi(\mathbf{r}_1,\ldots,\mathbf{r}_N,t) \right\rangle , \tag{5.161}$$

and using the above results, after an elementary but lengthy calculation (see Appendix 5.5.C), one obtains that the energy is conserved during the motion: $E(t) = E(0)$, $\forall t > 0$, as one would expect.

Thanks to the simple rewriting of the many–body wavefunction in Eq. (5.156), we are also able to write the one–body density matrix of the falling system in terms of the free, *free* non-falling system. In this case, the one–body density matrix is defined as [18]:

$$\rho(\mathbf{r},\mathbf{r}',t) \,=\, N \int d\mathbf{r}_2 \ldots d\mathbf{r}_N\, \chi^*(\mathbf{r},\mathbf{r}_2,\ldots,\mathbf{r}_N,t)\, \chi(\mathbf{r}',\mathbf{r}_2,\ldots,\mathbf{r}_N,t)\,. \tag{5.162}$$

Therefore using Eq. (5.156) we can rewrite the density matrix as:

$$\rho(\mathbf{r},\mathbf{r}',t) \,=\, N\, e^{i[\theta(x',t)-\theta(x,t)]} \int d\boldsymbol{\varrho}_2 \ldots d\boldsymbol{\varrho}_N\, \eta^*(\boldsymbol{\varrho},\boldsymbol{\varrho}_2,\ldots,\boldsymbol{\varrho}_N,t)\, \eta(\boldsymbol{\varrho}',\boldsymbol{\varrho}_2,\ldots,\boldsymbol{\varrho}_N,t)\,, \tag{5.163}$$

since $d\mathbf{r}_j = d\boldsymbol{\varrho}_j$ for every j, while: $\boldsymbol{\varrho}(t) = \mathbf{r} - \xi(t)$, $\boldsymbol{\varrho}'(t) = \mathbf{r}' - \xi(t)$, and with x and x' being the x-components of $\mathbf{r}$ and $\mathbf{r}'$ respectively. So finally:

$$\rho(\mathbf{r},\mathbf{r}',t) \,=\, e^{i[\theta(x',t)-\theta(x,t)]}\, \rho_{\text{free}}(\boldsymbol{\varrho},\boldsymbol{\varrho}',t)\,, \tag{5.164}$$

where $\rho_{\text{free}}(\boldsymbol{\varrho},\boldsymbol{\varrho}',t)$ is defined in terms of the wavefunction η solution of the Schrödinger equation without gravitational field.

For a translational invariant system, the above equation may be further simplified by writing everything in terms of the relative coordinate $\mathbf{R} \equiv \mathbf{r} - \mathbf{r}'$. In this case, since it is also true that $\mathbf{R} = \boldsymbol{\varrho} - \boldsymbol{\varrho}'$, then Eq. (5.164) may be rewritten as:

$$\rho(\mathbf{R},t) \,=\, e^{i\,m\,g\,t\,X/\hbar}\, \rho_{\text{free}}(\mathbf{R},t)\,, \tag{5.165}$$

where Eq. (5.126) has been used and X is the x-component of the $\mathbf{R}$ vector position.

We may further analyse the eigenvalues of the one–body density matrix for a translational invariant system. In the static case, the one–body density matrix satisfies the eigenvalue equation [18]:

$$\int \rho(\mathbf{r},\mathbf{r}',t)\, \varphi_i(\mathbf{r}',t)\, d\mathbf{r}' \,=\, \lambda_i(t)\, \phi_i(\mathbf{r},t)\,, \tag{5.166}$$

where $\lambda_i(t)$ is the occupation number of the i–th natural orbital eigenvector $\phi_i(\mathbf{r}(t))$. Once again, we recall that the $\lambda_i(t)$ are such that $\sum_i \lambda_i(t) = N$ at every time t. When the Galilean invariance is not broken, the quantum number labeling the occupation of the natural orbitals is the wavevector $\mathbf{k}$, and for an homogeneous system the effective single particle states are simply plane waves. Therefore we may write Eq. (5.166) for a falling translational invariant many–body system as:

$$\lambda_{\mathbf{k}}(t) \,=\, \int \rho(\mathbf{R},t)\, e^{i\mathbf{k}\cdot\mathbf{R}}\, d\mathbf{R}\,. \tag{5.167}$$

Now, thanks to Eq. (5.165), we can write the following relation between the natural orbitals occupation numbers of the falling system with those of the free non-falling one:

$$\lambda_{\mathbf{k}}(t) \,=\, \lambda^{\mathrm{free}}_{\tilde{\mathbf{k}}}(t)\,, \tag{5.168}$$

where $\tilde{\mathbf{k}} \,=\, (k_x + m\,g\,t/\,\hbar)\cdot\mathbf{e}_x + k_y\cdot\mathbf{e}_y + k_z\cdot\mathbf{e}_z$, and we have defined the occupation numbers of the system without gravity ($g = 0$) as:

$$\lambda^{\mathrm{free}}_{\mathbf{k}}(t) \,=\, \int \rho_{\mathrm{free}}(\mathbf{R},t)\, e^{i\mathbf{k}\cdot\mathbf{R}}\, d\mathbf{R}\,. \tag{5.169}$$

From the above relations, one may observe that there is only a time–dependent translation over the x-component of the momentum wavevector which identifies the occupation numbers of the falling system with respect to the "free" case with no gravitational potential. This is an extension of Eq. (5.94) to the three–dimensional regime.

FREE FALL OF AN ATOM

Let us now discuss the case where an atom of atomic number Z and (rounded) mass number M, falls under the action of a gravitational potential. The Schrödinger equation describing the system reads

$$\begin{aligned} & i\,\hbar\frac{\partial}{\partial t}\chi(\mathbf{r}_p^{(1)},\ldots,\mathbf{r}_p^{(Z)},\mathbf{r}_e^{(1)},\ldots,\mathbf{r}_e^{(Z)},\mathbf{r}_n^{(1)},\ldots,\mathbf{r}_n^{(M-Z)},t) \,= \\ & = \Bigg\{ -\frac{\hbar^2}{2m_p}\sum_{j=1}^{Z}\nabla^2_{r_p^{(j)}} - \frac{\hbar^2}{2m_e}\sum_{j=1}^{Z}\nabla^2_{r_e^{(j)}} - \frac{\hbar^2}{2m_n}\sum_{j=1}^{M-Z}\nabla^2_{r_n^{(j)}} + \frac{1}{2}\frac{e^2}{4\pi\varepsilon_0}\sum_{j\neq k}^{Z}\Bigg[\frac{1}{\left|r_e^{(k)}-r_e^{(j)}\right|}+ \\ & + \frac{1}{\left|r_p^{(k)}-r_p^{(j)}\right|}\Bigg] - \frac{e^2}{4\pi\varepsilon_0}\sum_{j,k=1}^{Z}\frac{1}{\left|r_p^{(k)}-r_e^{(j)}\right|} + m_p\,g\sum_{j=1}^{Z}x_p + m_e\,g\sum_{j=1}^{Z}x_e + m_n\,g\sum_{j=1}^{M-Z}x_p\Bigg\}\cdot \\ & \cdot\,\chi(\mathbf{r}_p^{(1)},\ldots,\mathbf{r}_p^{(Z)},\mathbf{r}_e^{(1)},\ldots,\mathbf{r}_e^{(Z)},\mathbf{r}_n^{(1)},\ldots,\mathbf{r}_n^{(M-Z)},t)\,, \end{aligned} \tag{5.170}$$

where we used the fact that the atom has Z protons (labeled with p), Z electrons (labeled with e) and $(M-Z)$ neutrons (labeled with n). In this equation we have considered the kinetik and gravitational potential energy of protons, electrons and neutrons separately, and then we wrote the repulsive electric field potential between electrons and protons in the nucleus (where the factor $1/2$ in front corrects for the fact that the summation counts each pair of particles twice) and finally the attractive electric field between the nucleus and the electrons.

In order to eliminate the gravitational potential acting on each particles, we need to perform the following gauge transformation and translation on the wavefunction

$$\begin{aligned} & \chi(\mathbf{r}_p^{(1)},\ldots,\mathbf{r}_p^{(Z)},\mathbf{r}_e^{(1)},\ldots,\mathbf{r}_e^{(Z)},\mathbf{r}_n^{(1)},\ldots,\mathbf{r}_n^{(M-Z)},t) \,= \\ & = \prod_{j=1}^{N} e^{\,i\left[\theta_p(x_p^{(j)},t)+\theta_e(x_e^{(j)},t)+\theta_n(x_n^{(j)},t)\right]}\,\eta(\boldsymbol{\varrho}_p^{(1)}(t),\ldots,\boldsymbol{\varrho}_p^{(Z)}(t),\boldsymbol{\varrho}_e^{(1)}(t),\ldots,\boldsymbol{\varrho}_e^{(Z)}(t), \\ & \qquad\qquad ,\boldsymbol{\varrho}_n^{(1)}(t),\ldots,\boldsymbol{\varrho}_n^{(M-Z)}(t),t)\,, \end{aligned} \tag{5.171}$$

where the gauge phases for protons and electrons are written as in Eqs. (5.151) and (5.152), respectively, while the gauge phase for the protons reads

$$\theta_n(x_n,t) = -\frac{m_n\,g\,t}{\hbar}\,x_n - \frac{m_n\,g^2\,t^3}{6\,\hbar}\,, \tag{5.172}$$

and we used the usual definition of translated coordinates, *i.e.* $\boldsymbol{\varrho}_j^{(k)}(t) = \mathbf{r}_j^{(k)} - \xi(t)$, for each particle. With these transformations, the wavefunction η satisfies a Schrödinger equation similar to Eq. (5.170) but without the gravitational potential, and where the coordinates $\mathbf{r}_j^{(k)}$ are substituted with $\boldsymbol{\varrho}_j^{(k)}$. Notice that also in this case the electric interacting potential remains untouched by the translation transformation.

One can easily prove that the energy is conserved during the motion, and the total momentum expectation value transforms in time as:

$$\langle P \rangle (t) = \left\langle \chi(\mathbf{r}_1, \ldots, \mathbf{r}_N, t) \middle| \hat{\mathbf{P}} \middle| \chi(\mathbf{r}_1, \ldots, \mathbf{r}_N, t) \right\rangle = P_0 - \mathbf{e}_x \, g \, t \, [Z m_p + Z m_e + (M - Z) m_n] \, , \tag{5.173}$$

where we used the same notation of the previous section for the initial total momentum P_0.

The procedure just presented can be straightforwardly extended to a generic isotope or chemical species with different numbers of protons, electrons and/or neutrons.

We conclude here our study of the linear external (either time varying or constant) potential. We have seen that the method of gauge transformation appears to be highly versatile and easily applicable, since the expectation values of relevant physical quantities can be computed in terms of the free expanding results. In particular we have shown that the variances of the initial wavepacket are exactly the same as if the system doesn't feel any gravitational force at all.

APPENDIX

5.A SINUSOIDAL AND COSINUSOIDAL FORCES

We will show that the case of a sinusoidal force is drastically different from the case of a cosinusoidal force from the point of view of the center of mass motion, even though the two driving functions act similarly (the sine function is simply a cosine function with argument shifted by $\pi/2$). This is due to the fact that one assumes the same initial condition for both cases, while physically it would not be the case. In order to clarify what we mean by this, let us take the case of a classical particle, a ball, which may be subjected to a linear external potential with driving function $f^{(1)}(t) = \ell \sin(\omega t)$, or $f^{(2)}(t) = \ell \cos(\omega t)$. The position of the ball will be described by:

$$x^{(j)}(t) = x_0^{(j)} + v_0^{(j)} t - \frac{1}{m} \int_0^t dt' \int_0^{t'} dt'' \, f^{(j)}(t'') \,,$$

with $j = 1$ or 2. Let us assume that: $x_0^{(j)} = x^{(j)}(t = 0) = 0$, for simplicity. If we impose: $v_0^{(j)} = v^{(j)}(t = 0) = \dot{x}^{(j)}(t = 0) = 0$, both for $j = 1$ and 2, we will have: $x^{(1)}(T) = -\frac{\ell T}{m\omega}$, while the position at stroboscopic times for a cosine driving function will simply be: $x^{(2)}(T) = 0$. This difference finds a reason in the different initial setup for the two systems: In the case $j = 1$ the particle is found to be in a flat slide for $t = 0$ and with vanishing velocity, while for the case $j = 2$ the particle is already subjected to an inclined plane with $V(x, 0) = \ell x$, but again with a vanishing velocity. The external potential at $t = 0$ for $j = 2$, is equal to the external potential for $j = 1$ at $t = T/4$, and there the velocity for the system with $j = 1$ is not null. One should therefore impose that: $v^{(2)}(t = 0) = v^{(1)}(T/4) = -\frac{\ell}{m\omega}$. By doing so, one finally gets that: $x^{(2)}(T) = -\frac{\ell T}{m\omega}$, as it happens for the case with a sinusoidal driving force.

5.B BOUNDARY CONDITIONS

We discuss how one could obtain periodic boundary conditions (PBC) in a system subjected to a time–dependent linear external potential. Before doing that, is better to start the discussion with open boundary conditions (OBC).

Let us first consider the case of a Schrödinger equation describing a moving hard wall box with one-particle inside

$$i\hbar \frac{\partial}{\partial t} \chi(x,t) = \left[-\frac{\hbar^2}{2m} \frac{\partial^2}{\partial x^2} + V(x,t) \right] \chi(x,t) \,, \tag{B5.1}$$

where

$$V(x,t) = \begin{cases} 0 & \text{for } -\frac{L}{2} + h(t) < x < \frac{L}{2} + h(t) \\ \infty & \text{elsewhere} \end{cases} . \tag{B5.2}$$

The function $h(t)$ describes the motion of the box. For example in the case in which the box translates with constant acceleration a, then $h(t) \propto a\frac{t^2}{2}$, while if the box oscillates around the origin with a maximum amplitude of oscillation x_0 and frequency ω, then $h(t) = x_0 \sin(\omega t)$. Because of the potential (B5.2), the wavefunction will satisfy the following moving OBC

$$\chi(x = -L/2 + h(t), t) = \chi(x = L/2 + h(t), t) = 0\,. \tag{B5.3}$$

Let us describe the system in the comoving frame of reference. This can be done by changing the spatial variable from x to

$$\tilde{x} = x - h(t)\,, \tag{B5.4}$$

thanks to which we pass from (B5.1) to

$$i\hbar\frac{\partial}{\partial t}\chi(\tilde{x}, t) = \left[-\frac{\hbar^2}{2m}\frac{\partial^2}{\partial \tilde{x}^2} + V(\tilde{x}) + i\hbar\,\frac{dh}{dt}\,\frac{\partial}{\partial \tilde{x}}\right]\chi(\tilde{x}, t)\,, \tag{B5.5}$$

and now the wavefunction satisfies the fixed boundary conditions

$$\chi(\tilde{x} = -L/2, t) = \chi(\tilde{x} = L/2, t) = 0\,. \tag{B5.6}$$

To get rid of the term $\propto \hat{p}$ in (B5.5), we transform the wavefunction as

$$\chi(\tilde{x}, t) \equiv e^{i\beta(t)\tilde{x}}\,\tilde{\chi}(\tilde{x}, t)\,, \tag{B5.7}$$

where $\beta(t)$ is a function to be determined in order to eliminate the term linear in the momentum. Substituting (B5.7) in the Schrödinger equation (B5.5) and choosing $\beta(t) = \frac{m}{\hbar}\frac{dh}{dt}$, we get

$$i\hbar\frac{\partial}{\partial t}\tilde{\chi}(\tilde{x}, t) = \left[-\frac{\hbar^2}{2m}\frac{\partial^2}{\partial \tilde{x}^2} + V(\tilde{x}) + m\frac{d^2h}{dt^2}\,\tilde{x} - \frac{3}{2}m\left(\frac{dh}{dt}\right)^2\right]\tilde{\chi}(\tilde{x}, t)\,. \tag{B5.8}$$

If we now perform the following transformation of the wavefunction

$$\tilde{\chi}(\tilde{x}, t) = e^{\frac{i}{\hbar}\frac{3m}{2}\int_0^t\left(\frac{dh}{d\tau}\right)^2 d\tau}\,\bar{\chi}(\tilde{x}, t)\,, \tag{B5.9}$$

we arrive at the Schrödinger equation describing a particle enclosed in a fixed hard wall box and subjected to the action of a linear external potential, which reads

$$i\hbar\frac{\partial}{\partial t}\bar{\chi}(\tilde{x}, t) = \left[-\frac{\hbar^2}{2m}\frac{\partial^2}{\partial \tilde{x}^2} + V(\tilde{x}) + m\frac{d^2h}{dt^2}\,\tilde{x}\right]\bar{\chi}(\tilde{x}, t)\,, \tag{B5.10}$$

and the wavefunction fulfills

$$\bar{\chi}(\tilde{x} = -L/2, t) = \bar{\chi}(\tilde{x} = L/2, t) = 0\,. \tag{B5.11}$$

The presence of the external potential linear in $\tilde{x}$ is coming from the fact that passing to the comoving frame of reference [via the spatial transformation (B5.4)], the particle feels the presence of an inertial force related to the second time derivative of $h(t)$.

The procedure described above can be extended for the $1D$ LL model of N atoms in a moving box of length L, where the many–body Schrödinger equation reads

$$i\hbar\frac{\partial}{\partial t}\chi(x_1, \ldots, x_N, t) = H\chi(x_1, \ldots, x_N, t)\,, \tag{B5.12}$$

with Hamiltonian

$$H = -\frac{\hbar^2}{2m}\sum_{j=1}^{N}\frac{\partial^2}{\partial x_j^2} + \lambda\sum_{j<l}\delta(x_j - x_l) + \sum_{j=1}^{N}V(x_j,t)\,. \tag{B5.13}$$

where the external potential is the same as in (B5.2) for $x = x_j$, and the wavefunction satisfies moving OBC

$$\chi(x_1 = \pm L/2 + h(t), x_2, \ldots, x_N, t) = \cdots = 0\,. \tag{B5.14}$$

Passing to the comoving frame by changing the spatial variables as in (B5.4), we get

$$i\hbar\frac{\partial}{\partial t}\chi = \left\{ -\frac{\hbar^2}{2m}\sum_{j=1}^{N}\frac{\partial^2}{\partial\tilde{x}_j^2} + \lambda\sum_{j<l}\delta(\tilde{x}_j - \tilde{x}_l) + \sum_{j=1}^{N}\left[V(\tilde{x}_j) + i\hbar\frac{dh}{dt}\frac{\partial}{\partial\tilde{x}_j}\right]\right\}\chi\,, \tag{B5.15}$$

and the OBC gets modified into

$$\chi(\tilde{x}_1 = \pm L/2, \tilde{x}_2, \ldots, \tilde{x}_N, t) = \cdots = 0\,. \tag{B5.16}$$

We then transform the wavefunction as

$$\chi(\tilde{x}_1, \ldots, \tilde{x}_N, t) \equiv e^{i\frac{m}{\hbar}\frac{dh}{dt}\sum_{j=1}^{N}\tilde{x}_j}\,\tilde{\chi}(\tilde{x}_1, \ldots, \tilde{x}_N, t)\,, \tag{B5.17}$$

under which the Schrödinger equation (B5.15) becomes

$$i\hbar\frac{\partial}{\partial t}\tilde{\chi} = \left\{ -\frac{\hbar^2}{2m}\sum_{j=1}^{N}\frac{\partial^2}{\partial\tilde{x}_j^2} + \lambda\sum_{j<l}\delta(\tilde{x}_j - \tilde{x}_l) + +\sum_{j=1}^{N}\left[V(\tilde{x}_j) + m\frac{d^2h}{dt^2}\,\tilde{x}_j\right] - \frac{3}{2}\,m\,N\left(\frac{dh}{dt}\right)^2\right\}\tilde{\chi}\,. \tag{B5.18}$$

Finally, by performing the transformation

$$\tilde{\chi}(\tilde{x}_1, \ldots, \tilde{x}_N, t) = e^{\frac{i}{\hbar}\frac{3Nm}{2}\int_0^t\left(\frac{dh}{d\tau}\right)^2 d\tau}\,\bar{\chi}(\tilde{x}_1, \ldots, \tilde{x}_N, t)\,, \tag{B5.19}$$

we have the Schrödinger equation

$$i\,\hbar\,\frac{\partial}{\partial t}\bar{\chi} = \left\{ -\frac{\hbar^2}{2\,m}\sum_{j=1}^{N}\frac{\partial^2}{\partial\tilde{x}_j^2} + \lambda\sum_{j<l}\delta(\tilde{x}_j - \tilde{x}_l) + \sum_{j=1}^{N}\left[V(\tilde{x}_j) + V_{fict}(\tilde{x}_j)\right]\right\}\bar{\chi}\,, \tag{B5.20}$$

with the external linear "fictitious" potential

$$V_{fict}(\tilde{x}_j) = m\,\frac{d^2h}{dt^2}\,\tilde{x}_j\,, \tag{B5.21}$$

and the boundary conditions

$$\bar{\chi}(\tilde{x}_1 = \pm L/2, \tilde{x}_2, \ldots, \tilde{x}_N, t) = \cdots = 0\,, \tag{B5.22}$$

i.e. fixed OBC. Therefore we can describe the LL model in a shaken hard wall box as a fixed one subjected to the action of a linear potential in the comoving frame. See Fig. 2 left and center for a visualization of the case in which $h(t) = x_0\,\sin(\omega\,t)$. In this case, (B5.21) is a linear time–periodic potential

$$V_{fict}(\tilde{x}_j) = -m\,\omega^2\,x_0\,\tilde{x}_j\,\sin(\omega\,t)\,. \tag{B5.23}$$

We now discuss the case of PBC starting from a single particle enclosed in a rotating ring of circumference L

$$i\hbar\frac{\partial}{\partial t}\chi(\varphi,t) = -\frac{\hbar^2}{2mL^2}\frac{\partial^2}{\partial\varphi^2}\chi(\varphi,t)\,, \tag{B5.24}$$

where φ is the angle variable such that in x–y coordinates one would have

$$\begin{cases} x_i = \frac{L}{2\pi}\,\cos(\varphi_i) \\ y_i = \frac{L}{2\pi}\,\sin(\varphi_i) \end{cases} \tag{B5.25}$$

and the wavefunction satisfies moving PBC

$$\chi\left(\varphi = 0 + \int_0^t \bar{\mathcal{F}}(\tau)\,d\tau, t\right) = \chi\left(\varphi = 2\pi + \int_0^t \bar{\mathcal{F}}(\tau)\,d\tau, t\right)\,, \tag{B5.26}$$

in which $\bar{\mathcal{F}}(t)$ represents the angular velocity under which the ring is rotating, see Fig. 2 right, and will coincide with the primitive of the driving $f(t)$. Analogously to what we've done for the hard wall problem, we pass to the comoving frame of reference by changing the angle variables

$$\tilde{\varphi} = \varphi - \int_0^t \bar{\mathcal{F}}(\tau)\,d\tau\,, \tag{B5.27}$$

under which the Schrödinger equation (B5.24) becomes

$$i\hbar\frac{\partial}{\partial t}\chi(\tilde{\varphi},t) = \left[-\frac{\hbar^2}{2mL^2}\frac{\partial^2}{\partial\tilde{\varphi}^2} + i\,\hbar\,\bar{\mathcal{F}}(t)\frac{\partial}{\partial\tilde{\varphi}}\right]\chi(\tilde{\varphi},t)\,, \tag{B5.28}$$

and now we have fixed PBC

$$\chi(\tilde{\varphi}=0,t) = \chi(\tilde{\varphi}=2\pi,t)\,. \tag{B5.29}$$

Next we transform the wavefunction

$$\chi(\tilde{\varphi},t) \equiv e^{i\frac{mL^2}{\hbar}\bar{\mathcal{F}}(t)\tilde{\varphi}}\,\tilde{\chi}(\tilde{\varphi},t)\,, \tag{B5.30}$$

in such a way that the Schrödinger equation has a $\tilde{\varphi}$–linear dependent term

$$i\hbar\frac{\partial}{\partial t}\tilde{\chi}(\tilde{\varphi},t) = \left[-\frac{\hbar^2}{2mL^2}\frac{\partial^2}{\partial\tilde{\varphi}^2} + mL^2\frac{d\bar{\mathcal{F}}}{dt}\tilde{\varphi} - \frac{3}{2}mL^2\bar{\mathcal{F}}^2(t)\right]\tilde{\chi}(\tilde{\varphi},t)\,. \tag{B5.31}$$

Notice that using transformation (B5.30) in the fixed PBC (B5.29), implies that the wavefunction $\tilde{\chi}$ satisfies twisted boundary conditions

$$\tilde{\chi}(\tilde{\varphi}=0,t) = e^{i\frac{2\pi mL}{\hbar}\bar{\mathcal{F}}(t)}\,\tilde{\chi}(\tilde{\varphi}=2\pi,t)\,. \tag{B5.32}$$

Finally we perform the transformation on the wavefunction

$$\tilde{\chi}(\tilde{\varphi},t) \equiv e^{\frac{i}{\hbar}\frac{3mL^2}{2}\int_0^t\bar{\mathcal{F}}^2(\tau)\,d\tau}\,\bar{\chi}(\tilde{\varphi},t)\,, \tag{B5.33}$$

thanks to which the Schrödinger equation reads

$$i\hbar\frac{\partial}{\partial t}\bar{\chi}(\tilde{\varphi},t) = \left[-\frac{\hbar^2}{2mL^2}\frac{\partial^2}{\partial\tilde{\varphi}^2} + mL^2\frac{d\bar{\mathcal{F}}}{dt}\tilde{\varphi}\right]\bar{\chi}(\tilde{\varphi},t)\,, \tag{B5.34}$$

while the boundary conditions remain the same for the new wavefunction

$$\bar{\chi}(\tilde{\varphi}=0,t)=e^{i\frac{2\pi mL}{\hbar}\bar{\mathcal{F}}(t)}\,\bar{\chi}(\tilde{\varphi}=2\pi,t)\,. \tag{B5.35}$$

Let us now compare with the equations of the main text (19): There we studied the case of periodic driving, *i.e.* periodic angular velocity $\bar{\mathcal{F}}(t)$, imposing PBC and we have the identification $f(t)=m\frac{d\bar{\mathcal{F}}}{dt}$. Notice from (B5.35) that in order to have PBC in the wavefunction $\bar{\chi}$ at stroboscopic times, we need to impose $\bar{\mathcal{F}}(nT)=\frac{\hbar}{mL}\bar{n}$, where $\bar{n}$ is an integer number. Moreover at $t=0$, because $\tilde{\varphi}=\varphi$ and $\chi(\varphi,0)=\tilde{\chi}(\varphi,0)=\bar{\chi}(\varphi,0)$, then the Schrödinger equations (B5.34) and (B5.31) should both reduce to (B5.24), and this happens if $\bar{\mathcal{F}}(0)=0$ and $\frac{d\bar{\mathcal{F}}}{dt}(0)=0$, which amounts to say that at stroboscopic times the driving function $f(t)$ should vanishes, *i.e.* $f(nT)=0$, as well as $\int_0^{nT}f(\tau)\,d\tau=0$, since $\bar{\mathcal{F}}(t)$ and its derivatives are periodic functions.

Let us now generalize to the case of LL model of N atoms enclosed in a ring of circumference L which is rotating with an angular velocity $\bar{\mathcal{F}}(t)$. The following Schrödinger equation holds for the system

$$i\hbar\frac{\partial}{\partial t}\chi=\left\{-\frac{\hbar^2}{2mL^2}\sum_{j=1}^{N}\frac{\partial^2}{\partial\varphi_j^2}+\frac{\lambda}{L}\sum_{j<i}\delta(\varphi_j-\varphi_i)\right\}\chi\,, \tag{B5.36}$$

where φ_i is the angle variable related to x–y coordinates via (B5.25). We have then moving PBC, written as

$$\chi\left(\varphi_1=0+\int_0^t\bar{\mathcal{F}}(\tau)\,d\tau,\varphi_2,\ldots,\varphi_N,t\right)=\chi\left(\varphi_1=2\pi+\int_0^t\bar{\mathcal{F}}(\tau)\,d\tau,\varphi_2,\ldots,\varphi_N,t\right)\,. \tag{B5.37}$$

As usual, we should pass to the comoving frame by changing the variables as (B5.27), under which the Schrödinger equation becomes:

$$i\hbar\frac{\partial}{\partial t}\chi=\left\{-\frac{\hbar^2}{2mL^2}\sum_{j=1}^{N}\frac{\partial^2}{\partial\tilde{\varphi}_j^2}+\frac{\lambda}{L}\sum_{j<i}\delta(\tilde{\varphi}_j-\tilde{\varphi}_i)+i\,\hbar\,\bar{\mathcal{F}}(t)\sum_{j=1}^{N}\frac{\partial}{\partial\tilde{\varphi}_j}\right\}\chi\,, \tag{B5.38}$$

and the PBC reads

$$\chi(\tilde{\varphi}_1=0,\tilde{\varphi}_2,\ldots,\tilde{\varphi}_N,t)=\chi(\tilde{\varphi}_1=2\pi,\tilde{\varphi}_2,\ldots,\tilde{\varphi}_N,t)\,. \tag{B5.39}$$

If we now transform the wavefunction

$$\chi(\tilde{\varphi}_1,\ldots,\tilde{\varphi}_N,t)\equiv e^{i\frac{mL^2}{\hbar}\left[\frac{3N}{2}\int_0^t\bar{\mathcal{F}}^2(\tau)\,d\tau+\bar{\mathcal{F}}(t)\sum_{j=1}^{N}\tilde{\varphi}_j\right]}\,\bar{\chi}(\tilde{\varphi}_1,\ldots,\tilde{\varphi}_N,t)\,, \tag{B5.40}$$

then we arrive to a Schrödinger equation describing N bosons with contact interaction

$$i\hbar\frac{\partial}{\partial t}\bar{\chi}=\left\{-\frac{\hbar^2}{2mL^2}\sum_{j=1}^{N}\frac{\partial^2}{\partial\tilde{\varphi}_j^2}+\frac{\lambda}{L}\sum_{j<i}\delta(\tilde{\varphi}_j-\tilde{\varphi}_i)+L^2\sum_{j=1}^{N}V_{fict}(\tilde{\varphi}_j)\right\}\bar{\chi}\,, \tag{B5.41}$$

which are subjected to a linear external time–dependent fictitious potential

$$V_{fict}(\tilde{\varphi}_j)=m\frac{d\bar{\mathcal{F}}}{dt}\,\tilde{\varphi}_j\,, \tag{B5.42}$$

and the wavefunction satisfies twisted boundary conditions

$$\bar{\chi}(\tilde{\varphi}_1 = 0, \tilde{\varphi}_2, \ldots, \tilde{\varphi}_N, t) = e^{i\frac{2\pi m L}{\hbar}\bar{\mathcal{F}}(t)}\bar{\chi}(\tilde{\varphi}_1 = 2\pi, \tilde{\varphi}_2, \ldots, \tilde{\varphi}_N, t)\,. \tag{B5.43}$$

Using the same reasoning of the single particle problem, we see that in order to restore PBC at stroboscopic times we have to require that $\bar{\mathcal{F}}(nT) = 0$ as well as $\frac{d\bar{\mathcal{F}}}{dt} = 0$, from the comparison of the Schrödinger equations (B5.38) and (B5.41), with (B5.36).

If we specify to the case $L\bar{\mathcal{F}}(t) = \frac{\ell}{m\omega}\left[1 - \cos(\omega\, t)\right]$, we then describe a LL model enclosed in a periodically rotating ring as a LL model in a fixed (not moving) ring with PBC and a linear potential along the ring itself. This last model is the same one, once some subtleties are clarified as we are going to discuss now, as that studied in the main text.

Indeed, one may wonder if the method to solve the LL model in an external potential presented previously, would still be valid after we introduced a spatial variable (B5.27) which now depends on time. We find that for the potential in (5.2), the function $\theta(x,t)$ does get modified, but actually only in the x–linear term, which do disappear anyway when $\int_0^T f(\tau)d\tau = 0$.

To show this, we can repeat the same steps used previously in the solution of the Schrödigner equation with a x–linear term, taking into account the fact that now also the spatial variable has a time dependence. First of all it is convenient to pass from the angle variables to spatial one via

$$L\,\tilde{\varphi}(t) \to \tilde{x}(t) = x - \int_0^t \bar{\mathcal{F}}(\tau)d\tau\,, \tag{B5.44}$$

where

$$\bar{\mathcal{F}}(t) = \frac{\ell}{m\omega}\left[1 - \cos(\omega\, t)\right]\,. \tag{B5.45}$$

according to the prescription (B5.27). At stroboscopic times the potential (B5.42) reduces to the one in (5.2) for (5.43), which is the case of interest. Notice that the potential (5.43) is zero at stroboscopic times, so that there are no problems for the PBC at these times.

We introduce the new spatial variable $\tilde{y}(t) = \tilde{x}(t) - \xi(t)$ accordingly:

$$\begin{aligned}
&\frac{\partial}{\partial\tilde{x}} = \frac{\partial}{\partial\tilde{y}}\,,\\
&\frac{\partial}{\partial t} = \frac{\partial\tilde{y}}{\partial t}\frac{\partial}{\partial\tilde{y}} + \frac{\partial}{\partial t} = -\left[\bar{\mathcal{F}}(t) + \frac{d\xi}{dt}\right]\frac{\partial}{\partial\tilde{y}} + \frac{\partial}{\partial t}\,.
\end{aligned}$$

Therefore we now need to change the conditions of Eqs. (5.7) and (5.8), into

$$\begin{aligned}
&\bar{\mathcal{F}}(t) + \frac{d\xi}{dt} = \frac{\hbar}{m}\frac{\partial\theta}{\partial\tilde{x}}\,,\\
&-\hbar\frac{\partial\theta}{\partial t} = \frac{\hbar^2}{2m}\left(\frac{\partial\theta}{\partial\tilde{x}}\right)^2 + \tilde{x}\,\ell\,\sin(\omega\, t)\,.
\end{aligned} \tag{B5.46}$$

One could then make the following ansatz for the gauge phase

$$\theta(\tilde{x}, t) = \frac{m}{\hbar}\left[\bar{\mathcal{F}}(t) + \frac{d\xi(t)}{dt}\right]\tilde{x} + \Gamma(t)\,, \tag{B5.47}$$

under which, by replacing into (B5.46), we find the following equations for $\xi(t)$ and $\Gamma(t)$

$$m\left[\frac{d\bar{\mathcal{F}}}{dt}+\frac{d^2\xi(t)}{dt^2}\right]=-\ell\sin(\omega t)\,,$$
$$\hbar\frac{d\Gamma(t)}{dt}=-\frac{m}{2}\left[\bar{\mathcal{F}}(t)+\frac{d\xi(t)}{dt}\right]^2\,. \tag{B5.48}$$

From the first of the above equations one has $\xi(t)=0$ by imposing $\xi(0)=d\xi/dt(0)=0$ as initial conditions, while from the second equation, using (B5.46), one has

$$\Gamma(t)=-\frac{\ell^2}{2m\hbar}\int_0^t\left[\int_0^\tau\sin(\omega\tau')\,d\tau'\right]^2 d\tau\,, \tag{B5.49}$$

having imposed $\Gamma(0)=0$. Notice that $\Gamma(t)$ is not changed, while the term linear in $\tilde{x}$ of the gauge phase is changed and the whole phase reads

$$\theta(\tilde{x},t)=\frac{m}{\hbar}\bar{\mathcal{F}}(t)\tilde{x}-\frac{\ell^2}{2m\hbar}\int_0^t\left[\int_0^\tau\sin(\omega\tau')d\tau'\right]^2 d\tau\,. \tag{B5.50}$$

Therefore notice that still $\theta(\tilde{x},nT)$ doesn't depend on $\tilde{x}$ but only on time, if we require that PBC holds at stroboscopic times. Summarizing, when the condition in Eq. (5.3) is satisfied and $f(t)$ is vanishing at the stroboscopic times [as it happens for $f(t)\propto\sin(\omega t)$], then the gauge phase term is not changed and the final results coming from the stroboscopic analysis are unchanged as well. One should then stress out the fact that in obtaining our results for the stroboscopic dynamics we can use PBC, simply because we work at times multiple of the period of oscillation.

5.C PROOF OF EQ. (5.87)

Let us now prove Eq. (5.87) with a generic two–body interaction potential and a generic driving function $f(t)$. From Eq. (5.83) we can write the expectation value of the Hamiltonian in Eq. (5.82) as:

$$E(t)\;=\;\left[\prod_{j=1}^N e^{-i\theta(x_j,t)}\right]\left\langle\eta(y_1,\ldots,y_N,t)\right|\left\{\sum_{j=1}^N\left[\frac{\hat{p}_j^2}{2m}+x_jf(t)\right]+\sum_{j>i}V_{2b}(x_j-x_i)\right\}\cdot$$
$$\cdot\left[\prod_{j=1}^N e^{i\theta(x_j,t)}\right]\left|\eta(y_1,\ldots,y_N,t)\right\rangle. \tag{C5.1}$$

From the commutation relation among different operators, we have:

$$\left[\sum_{l=1}^N\hat{p}_l^2\,,\prod_{j=1}^N e^{i\theta(x_j,t)}\right]\;=\;\sum_{l=1}^N\left[\prod_{j\neq l}^N e^{i\theta(x_j,t)}\right]\left\{\left[\int_0^t f(\tau)\,d\tau\right]^2 e^{i\theta(x_l,t)}-2e^{i\theta(x_l,t)}\hat{p}_l\int_0^t f(\tau)\,d\tau\right\}=$$
$$=\;\left[\prod_{j=1}^N e^{i\theta(x_j,t)}\right]\sum_{l=1}^N\left\{\left[\int_0^t f(\tau)\,d\tau\right]^2-2\hat{p}_l\int_0^t f(\tau)\,d\tau\right\}\,, \tag{C5.2}$$

and obviously:

$$\left[\sum_{j>i}V_{2b}(x_j-x_i)\,,\prod_{j=1}^N e^{i\theta(x_j,t)}\right]=0\,, \tag{C5.3}$$

therefore Eq. (C5.1) may be rewritten as:

$$E(t) = \frac{N}{2m}\left[\int_0^t f(\tau)\,d\tau\right]^2 - \frac{1}{m}\left[\int_0^t f(\tau)\,d\tau\right]\sum_{j=1}^N p_{0,j} + \\ + \left\langle \eta(y_1,\ldots,y_N,t)\right| \left\{\sum_{j=1}^N\left[\frac{\hat{p}_j^2}{2m} + x_j f(t)\right] + \sum_{j>i} V_{2b}(x_j - x_i)\right\} \left|\eta(y_1,\ldots,y_N,t)\right\rangle , \tag{C5.4}$$

where we also used the fact that:

$$\left\langle \eta(y_1,\ldots,y_N,t)\right| \sum_{j=1}^N \hat{p}_j \left|\eta(y_1,\ldots,y_N,t)\right\rangle = \left[\prod_{j=1}^N e^{i\frac{\xi(t)}{\hbar}\hat{p}_j}\right] e^{i\frac{t}{\hbar}\hat{H}_0}\cdot \\ \cdot \left\langle \eta(x_1,\ldots,x_N,0)\right| \left[\sum_{j=1}^N \hat{p}_j\right] \left[\prod_{j=1}^N e^{-i\frac{\xi(t)}{\hbar}\hat{p}_j}\right] e^{-i\frac{t}{\hbar}\hat{H}_0} \left|\eta(x_1,\ldots,x_N,0)\right\rangle = \\ = \sum_{j=1}^N p_{0,j}\,, \tag{C5.5}$$

since $\hat{p}_j$ commutes with functions of the operator itself and moreover: $\left[\hat{H}_0, \sum_{j=1}^N \hat{p}_j\right] = 0$. Let us focus now on the expectation value in Eq. (C5.4): The kinetik and two–body interaction terms over the wavefunction $\eta(y_1,\ldots,y_N,t)$ can be simply written as

$$\left\langle \eta(y_1,\ldots,y_N,t)\right| \left[\sum_{j=1}^N \frac{\hat{p}_j^2}{2m} + \sum_{j>i} V_{2b}(x_j - x_i)\right] \left|\eta(y_1,\ldots,y_N,t)\right\rangle = \\ = \left\langle \eta(x_1,\ldots,x_N,t)\right| \left[\sum_{j=1}^N \frac{\hat{p}_j^2}{2m} + \sum_{j>i} V_{2b}(x_j - x_i)\right] \left|\eta(x_1,\ldots,x_N,t)\right\rangle = \\ = E(0) - f(0)\sum_{j=1}^N x_{0,j}\,, \tag{C5.6}$$

where in the second equality we used the operator: $e^{-i\frac{\xi(t)}{\hbar}\sum_j \hat{p}_j}$ as the generator of the translations over all the coordinates and the fact that it commutes with $\hat{H}_0$ (since $\hat{P}$ does), while in the last equality we first wrote the exponential operator in terms of $\hat{H}_0$ which describes the time evolution of $\eta(x_1,\ldots,x_N,t)$, and then we used the definition of $E(0)$ coming from the expectation value of the Hamiltonian $\hat{H}$, *i.e.*:

$$E(0) = \left\langle \eta(x_1,\ldots,x_N,0)\right| \left\{\sum_{j=1}^N\left[\frac{\hat{p}_j^2}{2m} + x_j f(0)\right] + \sum_{j>i} V_{2b}(x_j - x_i)\right\} \left|\eta(x_1,\ldots,x_N,0)\right\rangle \\ = \left\langle \eta(x_1,\ldots,x_N,0)\right|\hat{H}_0\left|\eta(x_1,\ldots,x_N,0)\right\rangle + f(0)\sum_{j=1}^N x_{0,j}\,. \tag{C5.7}$$

Finally for what concerns the x linear term, since:

$$\left[\sum_{j=1}^N x_j\,,\, e^{-i\frac{\xi(t)}{\hbar}\sum_l \hat{p}_l}\right] = \sum_{j=1}^N \xi(t)\, e^{-i\frac{\xi(t)}{\hbar}\sum_l \hat{p}_l}\,, \tag{C5.8}$$

then we can write:

$$\left\langle \eta(y_1,\dots,y_N,t)\right| \left[\sum_{j=1}^{N} x_j f(t)\right] \left|\eta(y_1,\dots,y_N,t)\right\rangle = \\ = N\, f(t)\, \xi(t) + f(t) \left\langle \eta(x_1,\dots,x_N,t)\right| \left[\sum_{j=1}^{N} x_j\right] \left|\eta(x_1,\dots,x_N,t)\right\rangle , \quad \text{(C5.9)}$$

and since $\left[\sum_{j=1}^{N} x_j\,,\, \sum_{l>i} V_{2b}(x_l - x_i)\right] = 0$ then the last term of the above equation is:

$$f(t) \left\langle \eta(x_1,\dots,x_N,t)\right| \left[\sum_{j=1}^{N} x_j\right] \left|\eta(x_1,\dots,x_N,t)\right\rangle = \\ = f(t)\, e^{i\frac{t}{\hbar}\sum_j \frac{\hat{p}_j^2}{2m}} \left\langle \eta(x_1,\dots,x_N,0)\right| \left[\sum_{j=1}^{N} x_j\right] e^{-i\frac{t}{\hbar}\sum_j \frac{\hat{p}_j^2}{2m}} \left|\eta(x_1,\dots,x_N,0)\right\rangle . \quad \text{(C5.10)}$$

From the commutation relation:

$$\left[\sum_{j=1}^{N} x_j\,,\, e^{i\frac{t}{\hbar}\sum_l \frac{\hat{p}_l^2}{2m}}\right] = e^{i\frac{t}{\hbar}\sum_l \frac{\hat{p}_l^2}{2m}} \sum_{j=1}^{N} \frac{t}{m}\hat{p}_j\,, \quad \text{(C5.11)}$$

we have finally that:

$$f(t) \left\langle \eta(x_1,\dots,x_N,t)\right| \left[\sum_{j=1}^{N} x_j\right] \left|\eta(x_1,\dots,x_N,t)\right\rangle = \frac{t}{m} f(t) \sum_{j=1}^{N} p_{0,j} + f(t) \sum_{j=1}^{N} x_{0,j}\,. \quad \text{(C5.12)}$$

Collecting all the above results, we find that the energy of the driven system at time t can be written as in Eq. (5.87).

SUMMARY AND CONCLUSIONS

This Thesis may be subdivided in two main parts: Scaling properties of correlation functions were studied in Chapters 1, 2 and 3, while in Chapters 4 and 5 we discussed Floquet engineering and dynamical properties of many–body quantum systems.

Namely, the goal of the first three Chapters, have been to characterize the off–diagonal long–range order (ODLRO) properties of interacting homogeneous or inhomogeneous systems at zero and/or finite temperatures through the study of the eigenvalues' scaling of the one–body density matrix (1BDM) vs the number of particles N. After introducing some basic definitions and properties of the 1BDM, we discussed how to obtain the exponents $\mathcal{C}_k$ directly from the large distance behaviour of the 1BDM. The ODLRO in the three–dimensional case for temperatures below the Bose-Einstein critical temperature has been described, as well as quasi-long–range order in the one– and two–dimensional Bose gases for different interactions and temperatures, discussing the connection of the Mermin-Wagner theorem with the occurrence of mesoscopic condensation.

We showed that in $1D$ it is $\mathcal{C}_0 = 0$ for non-vanishing temperature, while at $T = 0$ we built a cut-off interpolation method with which it was possible to obtain the exponent scaling and the prefactors of the eigenvalues of the 1BDM. We then extended the study to systems having anyonic statistics, showing that in this case the exponent $\mathcal{C}_0$ has a non-monotonic behaviour with respect to the coupling γ. We tested our predictions on the hard–core anyon gas, obtaining very good agreement.

In presence of an inhomogeneity, *i.e.* an external trapping potential, in Chapter 2 we were able to characterize ODLRO only for one–dimensional gases, where the conformal field theory arguments were used in order to extract the exponent $\mathcal{C}_0$ and prefactor $\mathcal{B}_0$ of the scaling for λ_0, as well as the scaling for the momentum distribution peak. In this context we extended our interest to the case of long–range interacting particles, focusing on the Calogero and Calogero–Sutherland models, which reduce to the Tonks–Girardeau gas when the dimensionless interacting parameter, λ, equals unity. We showed that for these systems, independently on the quantum statistics, when two particles cannot be found in the same position (hard–core interactions) then the ordering of the system is the same as in the homogeneous case. Further studies will be done in the direction of trapped gases with finite interactions.

In Chapter 3 we came back to the case of homogeneous systems, analyzing the effect of dimensionality and temperatures on the gases. We checked that in $3D$ it is $\mathcal{C}_0 = 1$ ($\mathcal{C}_0 = 0$) for temperatures smaller (larger) than the Bose-Einstein critical temperature. After some digressions on the $1D$ case, we then focused on the two–dimensional case. We presented the application of our methods to the XY and Villain models, where ODLRO is translated as a fully magnetization of the system, and to the $2D$ Bose gases. A universal jump of the power $\mathcal{C}_0$ from $\frac{7}{8}$ to 0 is found at the Berezinskii–Kosterlitz–Thouless temperature T_{BKT}, reflecting the universal jump for the superfluid stiffness. The dependence of $\mathcal{C}_0$ between $T = 0$ (at which $\mathcal{C}_0 = 1$) and T_{BKT} is studied in the different models. We found a weak dependence of it when the reduced temperature T/T_{BKT} is used. An estimate

for the (non-perturbative) parameter ξ entering the equation of state of the $2D$ Bose gases was obtained using low temperature expansions and compared with the Monte Carlo result. We also unveiled a "double jump"-like behaviour for $\mathcal{C}_0$, and correspondingly of the anomalous dimension η, right below T_{BKT} in the limit of vanishing interactions. When the dimensionless parameter $mU/\hbar^2$ is very small, the validity region of the low-temperature expansions enlarges towards T_{BKT} as soon as that $mU/\hbar^2$ decreases. When such regime is reached, then $\mathcal{C}_0$ tends to the value ≈ 0.912, and again moving towards T_{BKT} from below it abruptly (or, at least, in a very steep way) decreases to the universal value $7/8$, then jumping again to 0. We presented a detailed discussion of the weakly interacting regime and we commented how the double jump behaviour could be appreciable for very low values of the parameter $mU/\hbar^2$. Then we analyzed the behaviour of $\mathcal{C}_{k\neq 0}$, finding that in none of the cases presented there is quasi-fragmentation, *i.e.* $\mathcal{C}_{k\neq 0} = 0$.

The investigation of Chapter 3 was based both on the homogeneity of space and the thermodynamic limit, and therefore it will be interesting to study in a future work whether adding a confining external potential could change our predictions and how a finite number of particles affects the results. Moreover, it would be of interest to consider long–range interactions in more dimensions [267] and the presence of disorder, where rigorous results are available in literature [268, 269]. We also mention that for $2D$ anyonic gases, despite the presence of a considerable literature, see *e.g.* [270–273] and references therein, to the best of our knowledge no results for the scaling exponents $\mathcal{C}_k(T)$ are available at date.

Finally, we observe that for interacting fermions ODLRO are, of course, not present for the 1BDM, but they may exist for the 2BDM in the presence of attractions, so that it would be interesting to perform a parallel study to the one presented here for fermionc systems. In particular, in two-dimensional attractive Fermi gases at the BEC-BCS crossover, the scaling behaviour of the 2BDM has been recently connected to the presence of quantum anomaly and the ODLRO analysis may clarify its relation to the finite temperature superfluid transition [274, 275]. Moreover, the recently achieved direct measurements of momentum correlations in one–dimensional Fermi systems [276] would provide an excellent experimental counterpart to the study of ODLRO in these systems, where several theoretical evidences of dynamical critical scaling have been found [277–281].

In the last two Chapters, instead, we focused on the dynamics of quantum many–body systems. In Chapter 4 we came back to the problem of a one–dimensional Bose gas and showed how one can generalize the Gross–Pitaevskii equation in order to describe (within a mean field approach) generic interactions among atoms. From the definition of the GGPE we then obtained dark soliton solutions for the Lieb–Liniger gas, where, thanks to the Chebyshev interpolation formula for $e_B(\gamma)$ that we built in Chapter 1, we were able to study the shape and evolution of solitary waves in the $T = 0$ regime. Within this interpolation scheme, we also studied the ground state density profile for a Lieb–Liniger gas subjected to an harmonic confinement, but there is no conceptual problem in considering different trapping potentials. Even though the main idea was sketched in the last sentences of this Chapter, the determination of nonequilibrium properties from the time-dependent GGPE, is of great interest and will be then subject of future studies.

In Chapter 5 we have studied the effect of a time–dependent linear external potential on one–dimensional quantum systems made of one-, two- and many-particles. The potential could physically represent a time varying gravitational linear force, or a time varying electric field acting on the system, therefore its analysis is interesting in many different

contexts. The key point of our approach has been to solve the problem for a generic driving function by applying a gauge transformation on the wavefunction and a translation over the position variables. Doing so, we have been able to compute expectation values for different observables such as the center of mass position of a wavepacket and its variance, and the way these observables depend on time. We have observed that the external driving does not affect the spread of a wavepacket, which depends instead only on the interaction effects. This is the result of the decoupling of the external potential which takes place already from the two-particles case, due to the linearity of the potential. This decoupling acts at the level of the center of mass and relative coordinates and can be observed also in the behaviour of the total energy of the system, which oscillates in time depending on the form of the driving function $f(t)$. We derived expressions for the energy of the state at any time also for non-periodic driving function. The system in general does not conserve the energy, apart from some specific cases, *e.g.* if $f(t)$ is constant in time. However, when f is periodic in time and its integral on a time–period vanishes, plus $f(t=0)=0$, then the energy at stroboscopic times is conserved (notice that, at stroboscopic times, the expectation value of the full Hamiltonian does not need to be equal to the expectation value of the Floquet Hamitonian). When f is periodic, but its integral on a time–period is non-vanishing, then the energy at stroboscopic times is in general not conserved.

For a periodic driving, we have analysed in detail the dynamics of the systems. In this case we have employed the Floquet approach and written down the Floquet Hamiltonian and the micro-motion operator, describing the time evolution of the system at stroboscopic times and generic intermediate times, respectively. Our results, as discussed in Section 5.5.3.1, are valid when the two-body interaction terms depend only on the relative distance between the particles so that the total momentum commutes with the undriven Hamiltonian. If the undriven Hamiltonian is integrable, and obeys such conditions, then, when $\int_0^T f(\tau)\,d\tau = 0$, the Floquet Hamiltonian is integrable too. Therefore, our results are valid for any one–dimensional integrable Hamiltonian on the continuum including the Gaudin–Yang model for one–dimensional Fermi gases, integrable Bose-Fermi mixtures, integrable multi-component Lieb–Liniger Bose gases and Calogero–Sutherland models (in absence of external one-body harmonic potential). It would be of interest to study the integrablity of the Floquet Hamiltonian and the micro-motion operator for undriven integrable lattice Hamiltonians subjected to time–periodic linear potentials (or magnetic fields) suitably extending the method presented here.

If the integral of the driving function on a period of oscillation is, on the contrary, non-vanishing, then the Floquet Hamiltonian can be shown to be time–independent and it contains a linear, constant in time, external potential. In this case, such term can be eliminated using the same recipe of a gauge transformation and a translation over the position variables. The study whether such Floquet Hamiltonians are in general formally integrable is a very interesting topic of future research.

We finally obtained expressions for the Floquet states for one-, two- and many-body cases with contact interactions, where it has been observed that they essentially retains the form of the eigenfunctions of the original undriven Hamiltonian with a time dependent translation over the momenta (or pseudo-momenta). Our approaches can be applied to any many-body system where the particles interact with a two-body potential which depends on the difference between particles positions and are translationally invariant. It would be very interesting to consider the effects of different boundary conditions on the problem

in finite-size systems, and employing a Floquet engineering approach to study ac–Stark shifts and multiphoton resonances [45] for single and many-particles systems.

In the last part of Chapter 5 we have extended these results to the case of a free falling many–body quantum system. There we proved that the quantum description of the free fall motion in a gravitational field can be nicely simplified making use of a gauge transformation of the wavefunction, which corresponds to a change of the reference frame for the system, from the laboratory reference frame to the one that moves within the falling body. We have also discussed the time evolution relative to a generic three–dimensional quantum many–body system subject to a gravitational potential and we have shown that it can be described in terms of the free time evolution, as we knew already from the one–dimensional time varying linear potential.

BIBLIOGRAPHY

[1] A. Colcelli, G. Mussardo, and A. Trombettoni, Europhys. Lett. **122**, 50006 (2018).

[2] A. Colcelli, J. Viti, G. Mussardo, and A. Trombettoni, Phys. Rev. A **98**, 063633 (2018).

[3] A. Colcelli, G. Mussardo, G. Sierra, and A. Trombettoni, Phys. Rev. Lett. **123**, 130401 (2019).

[4] A. Colcelli, G. Mussardo, G. Sierra, and A. Trombettoni, Phys. Rev. A **102**, 033310 (2020).

[5] A. Colcelli, N. Defenu, G. Mussardo, and A. Trombettoni, `arXiv:2007.01403`, accepted for publication in Phys. Rev. B.

[6] A. Colcelli, G. Mussardo, G. Sierra, and A. Trombettoni, `arXiv:2009.03744`, submitted to Am. J. Phys.

[7] O. Penrose and L. Onsager, Phys. Rev. **104**, 576 (1956).

[8] P. W. Anderson Rev. Mod. Phys. **38**, 298 (1966.

[9] K. Huang, *Bose-Einstein Condensation and Superfluidity*, in [10], p. 31.

[10] A. Griffin, D. W. Snoke, and S. Stringari, *Bose–Einstein Condensation* (Cambridge University Press, Cambridge, UK) 1995.

[11] M. H. Anderson, J. R. Ensher, M. R. Matthews, C. E. Wieman, and E. A. Cornell, Science **269**, 198 (1995).

[12] N. D. Mermin and H. Wagner, Phys. Rev. Lett. **17**, 1307 (1966).

[13] P. C. Hohenberg, Phys. Rev. **158**, 383 (1967).

[14] N. Defenu, A. Trombettoni, S. Ruffo, Phys. Rev. B **94**, 224411 (2016).

[15] N. Defenu, A. Trombettoni, S. Ruffo, Phys. Rev. B **96**, 104432 (2017).

[16] G. Gori, M. Michelangeli, N. Defenu, A. Trombettoni, Phys. Rev. E **96**, 012108 (2017).

[17] U. R. Fischer, Phys. Rev. Lett. **89**, 280402 (2002); J. Low Temp. Phys. **138**, 723 (2005).

[18] L.P. Pitaevskii and S. Stringari, *Bose-Einstein Condensation and Superfluidity* (Oxford University Press, Oxford, UK) 2016.

[19] C. N. Yang, Rev. Mod. Phys. **34**, 694 (1962).

[20] S. Stringari, *Sum Rules and Bose-Einstein Condensation*, in [10], p. 86.

[21] A. J. Coleman and V. I. Yukalov, Mod. Phys. Lett. B **5**, 1679 (1991).

[22] A. J. Coleman and V. I. Yukalov, Nuovo Cimento **107**, 535 (1992).

[23] V. I. Yukalov, Physica A **310**, 413 (2002).

[24] V. I. Yukalov, Entropy, **22**(5), 565 (2020).

[25] D.H. Dunlap and V.M. Kenkre, Phys. Rev. B **34**, 3625 (1986).

[26] C.E. Creffield, Phys. Rev. B **67**, 165301 (2003).

[27] A. Eckardt, C. Weiss, and M. Holthaus, Phys. Rev. Lett. **95**, 260404 (2005).

[28] H. Lignier, C. Sias, D. Ciampini, Y. Singh, A. Zenesini, O. Morsch, and E. Arimondo, Phys. Rev. Lett. **99**, 220403 (2007).

[29] E. Kierig, U. Schnorrberger, A. Schietinger, J. Tomkovic, and M.K. Oberthaler, Phys. Rev. Lett. **100**, 190405 (2008).

[30] A. Eckardt, M. Holthaus, H. Lignier, A. Zenesini, D. Ciampini, O. Morsch, and E. Arimondo, Phys. Rev. A **79**, 013611 (2009).

[31] C.E. Creffield and G. Sierra, Phys. Rev. A **91**, 063608 (2015).

[32] R. He, M.-Z. Ai, J.-M. Cui, Y.-F. Huang, Y.-J. Han, C.-F. Li, and G.-C. Guo, Phys. Rev. A **101**, 043402 (2020).

[33] A. Eckardt, Rev. Mod. Phys. **89**, 011004 (2017).

[34] T. Kitagawa, E. Berg, M. Rudner, and E. Demler, Phys. Rev. B **82**, 235114 (2010).

[35] N. Lindner, G. Refael, and V. Galitski, Nat. Phys. **7**, 490 (2011).

[36] F. Wilczek, Phys. Rev. Lett. **111**, 250402 (2013).

[37] H. Watanabe and M. Oshikawa, Phys. Rev. Lett. **114**, 251603 (2015).

[38] S. Choi *et al.*, Nature **543**, 221 (2017).

[39] J. Zhang *et al.*, Nature **543**, 217 (2017).

[40] A. Russomanno, F. Iemini, M. Dalmonte, and R. Fazio, Phys. Rev. B **95**, 214307 (2017).

[41] N.Y. Yao, A.C. Potter, I.-D. Potirniche, and A. Vishwanath, Phys. Rev. Lett. **118**, 030401 (2017).

[42] K. Sacha and J. Zakrzewski, Rep. Prog. Phys. **81**, 016401 (2018).

[43] K. Giergiel, A. Kosior, P. Hannaford, and K. Sacha, Phys. Rev. A **98**, 013613 (2018).

[44] N. Goldman and J. Dalibard, Phys. Rev. X **4**, 031027 (2014).

[45] M. Holthaus, J. Phys. B **49**, 013001 (2016).

[46] A. Russomanno, A. Silva, and G.E. Santoro, Phys. Rev. Lett. **109**, 257201 (2012).

[47] S.A. Weidinger and M. Knap, Sci. Rep. **7**, 45382 (2017).

[48] A. Herrmann, Y. Murakami, M. Eckstein, and P. Werner, Europhys. Lett. **120**, 57001 (2018).

[49] T. Oka and S. Kitamura, Annu. Rev. Condens. Matter Phys. **10**, 387 (2019).

[50] G. Floquet, Ann. de l'Ecole Norm. Suppl. **12**, 47 (1883).

[51] J.H. Shirley, Phys. Rev. B **138**, 979 (1965).

[52] M. Grifoni and P. Hänggi, Phys. Rep. **304**, 229 (1998).

[53] E. H. Lieb and W. Liniger, Phys. Rev. **130**, 1605 (1963).

[54] E.A. Yuzbashyan, Ann. Phys. **392**, 323 (2018).

[55] N.A. Sinitsyn, E.A. Yuzbashyan, V.Y. Chernyak, A. Patra, and C. Sun, Phys. Rev. Lett. **120**, 190402 (2018).

[56] A. Komnik and M. Thorwart, Eur. Phys. J. B **89**, 244 (2016).

[57] C. N. Yang and C. P. Yang, J. Math. Phys. **10**, 1115 (1969).

[58] V.E. Korepin, N.M. Bogoliubov, and A.G. Izergin, *Quantum inverse scattering method and correlation functions* (Cambridge University Press, Cambridge, UK) 1993.

[59] G. Mussardo, *Statistical Field Theory: An Introduction to Exactly Solved Models in Statistical Physics* (Oxford University Press, Oxford, UK) 2010.

[60] M. Kormos, G. Mussardo, A. Trombettoni, Phys. Rev. A **81**, 043606 (2010).

[61] V. A. Yurovsky, M. Olshanii, and D. S. Weiss, Adv. At. Mol. Opt. Phys. **55**, 61 (2008).

[62] I. Bouchoule, N. J. van Druten, and C. I. Westbrook, `arXiv:0901.3303`.

[63] M.A. Cazalilla, R. Citro, T. Giamarchi, E. Orignac, and M. Rigol, Rev. Mod. Phys. **83**, 1405 (2011).

[64] O. I. Patu, V. E. Korepin, and D.V. Averin, J. Phys. A **40**, 14963 (2007).

[65] M. T. Batchelor, X. W. Guan, and J.D. He, J. Stat. Mech. **2007**, P03007 (2007).

[66] M. Olshanii, Phys. Rev. Lett. **81**, 938 (1998).

[67] M. Girardeau, J. Math. Phys. **1**, 516 (1960).

[68] F. Franchini, *An Introduction to Integrable Tech- niques for One-Dimensional Quantum Systems* (Springer, Cham) 2017.

[69] M. Gaudin and J.-S. Caux, *The Bethe Wavefunction* (Cambridge University Press, Cambridge, UK) 2014.

[70] C. J. Pethick and H. Smith, *Bose–Einstein Condensation in Dilute Gases* (Cambridge University Press, Cambridge, UK) 2008.

[71] F.D.M. Haldane, Phys. Rev. Lett. **47**, 1840 (1981).

[72] T. Giamarchi, *Quantum Physics in One Dimension* (Oxford University Press, Oxford, UK) 2003.

[73] E.R. Love, Quart. Journ. Mech. and Applied Math., Vol. II, Pt. 4 (1949).

[74] M. Gaudin, Phys. Lett. **A24**, 55 (1967).

[75] B. U. Felderhof, `arXiv:1309.3662`.

[76] A. Imambekov and E. Demler, Phys. Rev. A **73**, 021602(R) (2006).

[77] O. I. Patu, V. E. Korepin, and D. V. Averin, J. Phys. A **40**, 14963 (2007).

[78] X.-W. Guen, M. T. Batchelor, and C. Lee, Rev. Mod. Phys. **85**, 1633 (2013).

[79] T. Iida and M. Wadati, J. Phys. Soc. Jpn. **74**, 1724 (2005).

[80] M. Wadati and T. Iida, Phys. Lett. A **360**, 423 (2007).

[81] Hutson V., Proc. Camb. Phil. Soc., **59**, 211 (1963).

[82] G. Lang, F. Hekking, and A. Minguzzi, SciPost Phys. **3**, 003 (2017).

[83] L. M. Delves and J. L. Mohamed, *Computational Methods for Integral Equations* (Cambridge University Press, Cambridge, UK) 1985.

[84] D. Levy, *Introduction to numerical analysis* (Department of Mathematics and Center for Scientific Computation and Mathematical Modeling, CSCAMM, University of Maryland, USA) 2010.

[85] M. Wadati, J. Phys. Soc. Jpn. **71**, 2657 (2002).

[86] M. Marino and T. Reis, J. Stat. Phys. **177**, 1148 (2019).

[87] M. Olshanii and V. Dunjko, Phys. Rev. Lett. **91**, 090401 (2003).

[88] U. Schollwöck, Rev. Mod. Phys. **77**, 259 (2005).

[89] J. -S. Caux and P. Calabrese, Phys. Rev. A **74**, 031605 (2006).

[90] M. Panfil and J. -S.Caux, Phys. Rev. A **89**, 033605 (2014).

[91] J.-S. Caux, P. Calabrese, and N. A. Slavnov, J. Stat. Mech. **2007**, P01008 (2007).

[92] A. Shashi, M. Panfil, J.-S. Caux, and A. Imambekov, Phys. Rev. B **84**, 045408 (2011).

[93] A. Shashi, M. Panfil, J.-S. Caux, and A. Imambekov, Phys. Rev. B **85**, 155136 (2012).

[94] M. Jimbo and T. Miwa, Phys. Rev. D **24**, 3169 (1981).

[95] C. Mora and Y. Castin, Phys. Rev. A **67**, 053615 (2003).

[96] D. M. Gangardt and G. V. Shlyapnikov, New J. Phys. **5**, 79 (2003).

[97] P. J. Forrester, N. E. Frankel, and M. I. Makin, Phys. Rev. A **74**, 043614 (2006).

[98] A. Imambekov, I. E. Mazets, D. S. Petrov, V. Gritsev, S. Manz, S. Hofferberth, T. Schumm, E. Demler, and J. Schmiedmayer, Phys. Rev. A **80**, 033604 (2009).

[99] A. Lenard, J. Math. Phys. **5**, 930 (1964).

[100] P. J. Forrester, N. E. Frankel, T. M. Garoni, and N. S. Witte, Phys. Rev. A **67**, 043607 (2003).

[101] D. S. Petrov, G. V. Shlyapnikov and J. T. M. Walraven, Phys. Rev. Lett. **85**, 3745 (2000).

[102] D. S. Petrov, D. M. Gangardt, and G. V. Shlyapnikov, J. Phys. IV France **116**, 3 (2004), in [104].

[103] Y. Castin, J. Phys. IV France **116**, 89 (2004), in [104].

[104] M. Olshanii, H. Perrin, and L. Pricoupenko, *Lecture notes of Les Houches school on low dimensional quantum gases* (Journal de Physique IV Colloque, Quantum Gases in Low Dimensions) 2004.

[105] A. Kundu, Phys. Rev. Lett. **83**, 1275 (1999).

[106] M. T. Batchelor, X. W. Guan, and N. Oelkers, Phys. Rev. Lett. **96**, 210402 (2006).

[107] R. Santachiara, F. Stauffer and D. Cabra, J. Stat. Mech. **2007**, L05003 (2007).

[108] R. Santachiara and P. Calabrese, J. Stat. Mech. **2008**, P06005 (2008).

[109] M.D. Girardeau, Phys. Rev. Lett. **97**, 210401 (2006).

[110] P. Calabrese and R. Santachiara, J. Stat. Mech. **2009**, P03002 (2009).

[111] P. Calabrese and M. Mintchev, Phys. Rev. B **75**, 233104 (2007).

[112] S. Scopa, L. Piroli, and P. Calabrese, J. Stat. Mech. **2020**, 093103 (2020).

[113] B. Sutherland, Phys. Rev. A **4**, 2019 (1971).

[114] B. Sutherland, Phys. Rev. A **5**, 1372 (1971).

[115] B. Sutherland, *Beautiful models* (World Scientific, Singapore) 2004.

[116] F. Calogero, J. Math. Phys. **10**, 2191 (1969).

[117] F. Calogero, J. Math. Phys. **10**, 2197 (1969).

[118] B. Sutherland, J. Math. Phys. **12**, 246 (1971).

[119] B. Sutherland, J. Math. Phys. **5**, 251 (1971).

[120] B. Paredes, A. Widera, V. Murg, O. Mandel, S. Fölling, I. Cirac, G. V. Shlyapnikov, T. W. Hänsch, and I. Bloch, Nature **429**, 277 (2004).

[121] T. Kinoshita, T. Wenger, and D. S. Weiss, Science **305**, 1125 (2004).

[122] E. Haller, M. Gustavsson, M. J. Mark, J. G. Danzl, R. Hart, G. Pupillo, and H.-C. Nägerl, Science **325**, 1224 (2009).

[123] E. Haller, R. Hart, M. J. Mark, J. G. Danzl, L. ReichsÏlner, M. Gustavsson, M. Dalmonte, G. Pupillo, and H.-C. Nägerl, Nature **29**, 597 (2010).

[124] G. Boéris, L. Gori, M. D. Hoogerland, A. Kumar, E. Lucioni, L. Tanzi, M. Inguscio, T. Giamarchi, C. D'Errico, G. Carleo, G. Modugno, and L. Sanchez-Palencia, Phys. Rev. A **93**, 011601 (2016).

[125] M. D. Girardeau, Phys. Rev. Lett. **97**, 210401 (2006).

[126] M. D. Girardeau and E. M. Wright, Phys. Rev. Lett. **84**, 5691 (2000).

[127] R. Pezer and H. Buljan, Phys. Rev. Lett. **98**, 240403 (2007).

[128] G. J. Lapeyre, M. D. Girardeau, and E.M. Wright Phys. Rev. A **66**, 023606 (2002).

[129] A. Minguzzi and D. M. Gangardt, Phys. Rev. Lett. **94**, 240404 (2005).

[130] P. Vignolo and A. Minguzzi, Phys. Rev. Lett. **110**, 020403 (2013).

[131] M. Collura, S. Sotiriadis, and P. Calabrese, Phys. Rev. Lett. **110**, 245301 (2013).

[132] G. Lang, P. Vignolo, and Anna Minguzzi, Eur. Phys. J. Special Topics **226**, 1583 (2017).

[133] M. Rizzi, C. Miniatura, A. Minguzzi, and P. Vignolo, Phys. Rev. A **98**, 043607 (2018).

[134] M. Rigol and A. Muramatsu, Phys. Rev. A **70**, 031603 (2004).

[135] B.-B. Wei, S.-J. Gu, and H.-Q. Lin, Phys. Rev. A **79**, 063627 (2009).

[136] K. Lelas, T. Ševa, H. Buljan, and J. Goold, Phys. Rev. A **86**, 033620 (2012).

[137] Z.-L. Wang, A.-M. Wang, and X.-C. Li, `arXiv:1201.6019v2`.

[138] F. Cartarius, E. Kawasaki, and A. Minguzzi, Phys. Rev. A **92**, 063605 (2015).

[139] G. E. Astrakharchik, K. V. Krutitsky, M. Lewenstein, and F. Mazzanti, Phys. Rev. A **93**, 021605 (2016).

[140] G. E. Astrakharchik, K. V. Krutitsky, M. Lewenstein, F. Mazzanti, and J. Boronat, Phys. Rev. A **96**, 033606 (2017).

[141] J. Radić, V. Bačić, D. Jukić, M. Segev, and H. Buljan, Phys. Rev. A **81**, 063639 (2010).

[142] R. Seiringer and S. Warzel, New J. Phys. **18**, 035002 (2016).

[143] J. Settino, N. Lo Gullo, A. Sindona, J. Goold, and F. Plastina, Phys. Rev. A **95**, 033605 (2017).

[144] G. E. Astrakharchik, J. Boronat, J. Casulleras, and S. Giorgini, Phys. Rev. Lett. **95**, 190407 (2005).

[145] M. T. Batchelor, M. Bortz, X. W, Guan, and N. Oelkers, J. Stat. Mech. **2005**, L10001 (2005).

[146] M. Kormos, G. Mussardo, and A. Trombettoni, Phys. Rev. A **83**, 013617 (2011).

[147] M. D. Girardeau and G. E. Astrakharchik, Phys. Rev. Lett. **109**, 235305 (2012).

[148] M. Panfil, J. De Nardis, and J.-S. Caux, Phys. Rev. Lett. **110**, 125302 (2013).

[149] P. J. Forrester, N. E. Frankel, T. M. Garoni, and N. S. Witte, Comm. Math. Phys. **238**, 257 (2003).

[150] G. Marmorini, M. Pepe, and P. Calabrese, J. Stat. Mech. **2016**, 073106 (2016).

[151] Y. Hao, Phys. Rev. A **93**, 063627 (2016).

[152] M. Campostrini and E. Vicari, Phys. Rev. Lett. **102**, 240601 (2009).

[153] M. Campostrini and E. Vicari, Phys. Rev. A **81**, 023606 (2010); *ibid.* **81**, 063614 (2010).

[154] M. D. Girardeau, E. M. Wright, and J. M. Triscari, Phys. Rev. A **63**, 033601 (2001).

[155] P. Forrester, *Meet Andréief, Bordeaux 1886, and Andreev, Kharkov 1882-1883.*, `arXiv: 1806.10411`.

[156] Y. Brun and J. Dubail, SciPost Phys. **2**, 012 (2017).

[157] J. Dubail, J. M. Stéphan, J. Viti and P. Calabrese, SciPost Phys. **2**, 002 (2017).

[158] Y. Brun and J. Dubail, SciPost Phys. **4**, 037 (2018).

[159] C. M. Bender and S. A. Orszag, *Advanced mathematical methods for scientists and engineers* (Springer-Verlag New York, USA) 1999.

[160] *Chebfun Guide*, T. A. Driscoll, N. Hale, and L. N. Trefethen eds. (Oxford, Pafnuty Publications) 2014.

[161] *Handbook of mathematical functions: with formulas, graphs, and mathematical tables*, M. Abramowitz and I. A. Stegun eds. (Dover) 1972.

[162] P. J. Forrester, N. E. Frankel, and T. M. Garoni, J. Math. Phys. **44**, 4157 (2003).

[163] M. D. Girardeau, Phys. Rev. Lett. **97**, 100402 (2006).

[164] L. Yang and H. Pu, Phys. Rev. A **95**, 051602(R) (2017).

[165] F. J. Dyson, J. Math. Phys. **3**, 140 (1962).

[166] F. J. Dyson, J. Math. Phys. **3**, 157 (1962).

[167] G. Livan, M. Novaes, and P. Vivo, *Introduction to Random Matrices – Theory and Practice* (Springer, New York, USA) 2018.

[168] B. D. Simons, P. A. Lee, and B. L. Altshuler, Phys. Rev. Lett. **70**, 4122 (1993).

[169] B. D. Simons, P. A. Lee, and B. L. Altshuler, Nucl. Phys. B **409**, 487 (1993).

[170] B. Sutherland, Phys. Rev. B **45**, 907 (1992).

[171] F. D. M. Haldane and M. R. Zirnbauer, Phys. Rev. Lett. **71**, 4055 (1993).

[172] P. J. Forrester, Nucl. Phys. B **388**, 671 (1992).

[173] P. J. Forrester, Phys. Lett. A **179**, 127 (1993).

[174] Z. N. C. Ha, Phys. Rev. Lett. **73**, 1574 (1994).

[175] P. J. Forrester and J. A. Zuk, Nucl. Phys. B **473**, 616 (1996).

[176] D. Serban, F. Lesage, and V. Pasquier, Nucl. Phys. B **466**, 499 (1996).

[177] D. M. Gangardt and A. Kamenev, Nucl. Phys. B **610**, 578 (2001).

[178] G. E. Astrakharchik, D. M. Gangardt, Yu. E. Lozovik, and I. A. Sorokin, Phys. Rev. E **74**, 021105 (2006).

[179] P. Nozières, *Some comments on Bose-Einstein Condensation*, in [10], p. 15.

[180] G. D. Mahan, *Many-particles physics* (Plenum Press, New York, USA), Chap. 10, 1990.

[181] B. Capogrosso-Sansone, S. Giorgini, S. Pilati, L. Pollet, N. Prokof'ev, B. Svistunov, and M Troyer, New J. Phys. **12**, 043010 (2010).

[182] G. E. Astrakharchik and S. Giorgini, J. Phys. B: At. Mol. Opt. Phys. **39**, S1 (2006).

[183] A. Minguzzi, P. Vignolo and M. P. Tosi, Phys. Lett. A **294**, 222 (2002).

[184] M. Olshanii and V. Dunjko, New J. Phys. **5**, 98 (2003).

[185] S. Tan, Ann. Phys. **323**, 2971 (2008).

[186] H. Yao, D. Clément, A. Minguzzi, P. Vignolo, and L. Sanchez-Palencia, Phys. Rev. Lett. **121**, 220402 (2018).

[187] M. A. Cazalilla, J. Phys. B **37**, S1 (2004).

[188] B. Schmidt and M. Fleischhauer, Phys. Rev. A **75**, 021601(R) (2007).

[189] A. R. Its, A. G. Izergin, and V. E. Korepin, Phys. Lett. **141A**, 121 (1989); Comm. Math. Phys. **130**, 471 (1990); Physica D **53**, 187 (1991);

[190] A. R. Its, A. G. Izergin, V. E. Korepin, and G. G. Varzugin, Physica D **54**, 351 (1992).

[191] O. I. Patu and A. Klumper, Phys. Rev. A **88**, 033623 (2013).

[192] V. L. Berezinskii, Sov. Phys. JETP **32**, 493 (1971).

[193] J. M. Kosterlitz and D. J. Thouless, J. Phys. C **6**, 1181 (1973).

[194] J. M. Kosterlitz, J. Phys. C **7**, 1046 (1974).

[195] M. Le Bellac, *Quantum and Statistical Field Theory* (Oxford University Press, Oxford, UK) 1991.

[196] E. Simanek, *Inhomogeneous Superconductors* (Oxford University Press, Oxford, UK) 1994.

[197] H. Nishimori and G. Ortiz, *Elements of Phase Transitions and Critical Phenomena* (Oxford University Press, Oxford, UK) 2010.

[198] J. Villain, J. Phys. (Paris) **36**, 581 (1975).

[199] H. Kleinert, *Gauge Fields in Condensed Matter - Vol. 1: Superflow and Vortex Lines* (World Scientific, Singapore) 1989.

[200] D. R. Nelson and J. M. Kosterlitz, Phys. Rev. Lett. **39**, 1201 (1977).

[201] N. V. Prokof'ev and B. V. Svistunov, Phys. Rev. B **61**, 11282 (2000).

[202] M. Hasenbusch, J. Phys. A **38**, 5869 (2005).

[203] W. Janke and K. Nather, Phys. Rev. B **48**, 7419 (1993).

[204] R. Gupta, J. DeLapp, G. G. Batrouni, G. C. Fox, C. F. Baillie, and J. Apostolakis, Phys. Rev. Lett. **61**, 1996 (1988).

[205] R. Gupta, and C. F. Baillie, Phys. Rev. B **45**, 2883 (1992).

[206] N. Schultka and E. Manousakis, Phys. Rev. B **49**, 12071 (1994).

[207] Y. Komura and Y. Okabe, J. Phys. Soc. Japan **81**, 113001 (2012).

[208] N. Defenu, A. Trombettoni, I. Nándori, and T. Enss, Phys. Rev. B **96**, 174505 (2017).

[209] I. Maccari, L. Benfatto, and C. Castellani, Phys. Rev. B **96**, 060508(R) (2017).

[210] A. S. T. Pires, Phys. Rev. B **53**, 235 (1996).

[211] M. Hasenbusch (private communication).

[212] N. Prokof'ev, O. Ruebenacker, and B. Svistunov, Phys. Rev. Lett. **87**, 270402 (2001).

[213] N. Prokof'ev and B. Svistunov, Phys. Rev. A **66**, 043608 (2002).

[214] A. Trombettoni, A. Smerzi, and P. Sodano New J. Phys. **7**, 57 (2005).

[215] Z. Hadzibabic and J. Dalibard, Rivista Del Nuovo Cimento **34**, 389 (2011).

[216] J. W. Kane and L. P. Kadanoff, Phys. Rev. **155**, 80 (1967).

[217] V. N. Popov, Theor. Math. Phys. **11**, 565 (1972).

[218] E. Gross, Nuovo Cimento **20**, 454 (1961).

[219] L. P. Pitaevskii, Sov. Phys. JETP **13**, 451 (1961).

[220] P. Öhberg and L. Santos, Phys. Rev. Lett. **89**, 240402 (2002).

[221] S. Choi, V. Dunjko, Z. D. Zhang, and M. Olshanii, Phys. Rev. Lett. **115**, 115302 (2015).

[222] E. Madelüng, Z. Phys. **40**, 322 (1926).

[223] V. Dunjko, V. Lorent, and M. Olshanii, Phys. Rev. Lett. **86**, 5413 (2001).

[224] P. G. Drazin and R. S. Johnson, *Solitons: An Introduction* (Cambridge University Press, Cambridge, UK) 1989.

[225] O. A. Castro-Alvaredo, B. Doyon, and T. Yoshimura, Phys. Rev. X **6**, 041065 (2016).

[226] B. Bertini, M. Collura, J. De Nardis, and M. Fagotti, Phys. Rev. Lett. **117**, 207201 (2016).

[227] A. Polkovnikov, K. Sengupta, A. Silva, and M. Vengalattore, Rev. Mod. Phys. **83**, 863 (2011).

[228] J. Eisert, M. Friesdorf, and C. Gogolin, Nature Phys. **11**, 124 (2015).

[229] C. Gogolin and J. Eisert, Rep. Prog. Phys. **79**, 056001 (2016).

[230] F. Essler and M. Fagotti, J. Stat. Mech. **2016**, 064002 (2016).

[231] L. Vidmar and M. Rigol, J. Stat. Mech. **2016**, 064007 (2016).

[232] V. B. Bulchandani, R. Vasseur, C. Karrasch, and J. E. Moore, Phys. Rev. Lett. **119**, 220604 (2017).

[233] B. Doyon, T. Yoshimura, and J.-S. Caux, Phys. Rev. Lett. **120**, 045301 (2018).

[234] B. Bertini, M. Fagotti, L. Piroli, and P. Calabrese, J. Phys. A: Math. Theor. **51**(39), 39LT01 (2018).

[235] B. Doyon, J. Dubail, R. Konik, and T. Yoshimura, Phys. Rev. Lett. **119**, 195301 (2017).

[236] G. Baym and C. Pethick, Phys. Rev. Lett. **76**, 6 (1996).

[237] A. Minguzzi, S. Succi, F. Toschi, M. P. Tosi, and P. Vignolo, Phys. Rep. **395**, 223 (2004).

[238] C. F. Barenghi and N. G. Parker, *A Primer in Quantum Fluids* (Springer, Berlin, Germany) 2016.

[239] J. Javanainen and J. Ruostekoski, J. Phys. A **39**, L179 (2006).

[240] V. Gritsev and A. Polkovnikov SciPost Phys. **2**, 021 (2017).

[241] H.H. Chen and C.S. Liu, Phys. Rev. Lett. **37**, 693 (1976).

[242] See Appendix D in M.J. Ablowitz, B. Prinari, and A.D. Trubatch, *Discrete and Continuous Nonlinear Schrödinger Systems* (Cambridge, Cambridge University Press, UK) 2004.

[243] A. Kundu, Phys. Rev. E **79**, 015601(R) (2009).

[244] M.V. Berry and N.L. Balazs, Am. J. Phys. **47**, 264 (1979).

[245] A.R.P. Rau and K. Unnikrishnan, Phys. Lett. A **222**, 304 (1996).

[246] I. Guedes, Phys. Rev. A **63**, 034102 (2001).

[247] M. Feng, Phys. Rev. A **64**, 034101 (2001).

[248] L. D. Landau and E. M. Lifshitz, *Quantum Mechanics Non-Relativistic Theory* (Pergamon Press, Oxford, UK) 1965.

[249] D. Bauch, Nuovo Cimento B **85**, 118 (1985).

[250] M.A. Andreata and V. V. Dodonov, J. Phys. A **37**, 2423 (2004); J. Rus. Las. Res. **35**, 39 (2014).

[251] S. Pandey, H. Mas, G. Drougakis, P. Thekkeppatt, V. Bolpasi, G. Vasilakis, K. Poulios, and W. von Klitzing, Nature **570**, 205 (2019).

[252] S. Zöllner, H.-D. Meyer, and P. Schmelcher, Phys. Rev. A **78**, 013629 (2008).

[253] D. Jukić, S. Galić, R. Pezer, and H. Buljan, Phys. Rev. A **82**, 023606 (2010).

[254] T. Tsurumi and M. Wadati, J. Phys. Soc. Jpn. **71**, 1044 (2002).

[255] T. Timberlake, *Regular and chaotic quantum dynamics in the driven square well* (2004).

[256] S. Weigert, Found. Phys. **29**, 1785 (1999).

[257] E. Eisenberg, N. Shnerb, R. Avigur, `arXiv:cond-mat/9512003`.

[258] Z. Huang and S. Kais, Phys. Rev. A **73**, 022339 (2006).

[259] J. Lancaster and A. Mitra, Phys. Rev. E **81**, 061134 (2010).

[260] G. Genovese, PhD Thesis entitled *Quantum Dynamics of Integrable Spin Chains* (2010).

[261] V. Eisler and D. Bauernfeind, Phys. Rev. B **96**, 174301 (2017).

[262] H. J. Shan, C. M. Dai, H. Z. Shen, and X. X. Yi, Sci. Rep. **8**, 13565 (2018).

[263] M. Nauenberg, Am. J. Phys. **84**, 879 (2016).

[264] M. Wadati, J. Phys. Soc. Jpn. **68**, 2543 (1999).

[265] T. Tsurumi and M. Wadati, J. Phys. Soc. Jpn. **70**, 60 (2001).

[266] S. Sen and A.R. Chowdhurry, J. Phys. Soc. Jpn. **57**, 1511 (1988).

[267] N. Defenu, A. Codello, S. Ruffo, and A. Trombettoni, J. Phys. A **53**, 143001 (2020).

[268] R. Seiringer, J. Yngvason, and V. A. Zagrebnov, J. Stat. Mech. **2012**, P11007 (2012).

[269] M. Könenberg, T. Moser, R. Seiringer, and J. Yngvason, New J. Phys. **17**, 013022 (2015).

[270] A. Khare, *Fractional Statistics and Quantum Theory* (World Scientific, Singapore) 2005.

[271] F. Mancarella, A. Trombettoni, and G. Mussardo, Nucl. Phys. B **867**, 950 (2013); *ibid.* **887**, 216 (2014).

[272] D. Lundholm and J. P. Solovej, Commun. Math. Phys. **322**, 883 (2013).

[273] S. Ouvry and A. Polychronakos, Nucl.Phys. B **936**, 189 (2018); *ibid.* **949**, 114797 (2019).

[274] P. A. Murthy, N. Defenu, L. Bayha, M. Holten, P. M. Preiss, T. Enss, and S. Jochim, *Science* **365**, 268-272 (2019).

[275] T. Enss, Phys. Rev. Lett. **123**, 205301 (2019).

[276] P. M. Preiss, J. H. Becher, R. Klemt, V. Klinkhamer, A. Bergschneider, N. Defenu, and S. Jochim, Phys. Rev. Lett. **122**, 143602 (2020).

[277] D. Vodola, L. Lepori, E. Ercolessi, A. V. Gorshkov, and G. Pupillo, Phys. Rev. Lett. **113**, 156402 (2014).

[278] M. Heyl, Rep. Prog. Phys. **81**, 054001 (2018).

[279] D. T. Liu, J. Shabani, and A. Mitra Phys. Rev. B **97**, 235114 (2018).

[280] N. Defenu, T. Enss, and J. C. Halimeh, Phys. Rev. B **100**, 014434 (2019).

[281] N. Defenu, G. Morigi, L. Dell'Anna, and T. Enss, Phys. Rev. B **100**, 184306 (2019).

COLOPHON

This document was typeset using the typographical look-and-feel `classicthesis` developed by André Miede. The style was inspired by Robert Bringhurst's seminal book on typography "*The Elements of Typographic Style*". `classicthesis` is available for both LaTeX and LyX:

http://code.google.com/p/classicthesis/

Happy users of `classicthesis` usually send a real postcard to the author, a collection of postcards received so far is featured here:

http://postcards.miede.de/

Final Version as of October 5, 2020 (`classicthesis` version 1.0).